BỘ GIÁO DỤC VÀ ĐÀO TẠO

TRƯỜNG ĐẠI HỌC SƯ PHẠM KỸ THUẬT

THÀNH PHỐ HỒ CHÍ MINH

DANH MỤC CÔNG TRÌNH CÔNG BỐ

NGHIÊN CỨU SINH: BÙI VĂN HIỀN

LUẬN ÁN TIẾN SĨ

NGÀNH: KỸ THUẬT ĐIỆN

TÊN ĐỀ TÀI:

NÂNG CAO HIỆU SUẤT HỆ THỐNG PIN QUANG ĐIỆN

DANH MỤC CÔNG TRÌNH ĐÃ CÔNG BỐ

STT	Tác giả	Năm xuất bản	Tên bài báo	Tên tạp chí/kỷ yếu, số/tập, số ISSN/ISBN	ISSN/ ISBN	Link/Doi	Ghi chú
I.		**Tạp chí khoa học trong danh mục WoS (SCIE, SSCI, AHCI, ESCI)**					
1	Bui Van Hien, Truong Viet Anh, Nguyen Tung Linh, Pham Quoc Khanh	8/2023	Rapidly Determine the Maximum Power Point in the Parallel Configuration of the Photovoltaic System	Sensors	1424-8220	https://doi.org/10.3390/s23177503	
2	Van Hien Bui, Viet Anh Truong, Vu Lan Nguyen, Thanh Long Duong	1/2024	Estimating the potential maximum power point based on the calculation of short-circuit current and open-circuit voltage	IET Power Electronics	1755-4535 / 1755-4543	https://doi.org/10.1049/pel2.12651	
3	Truong Viet Anh, Ton Ngoc Trieu, Pham Vo Hong Nghi, Bui Van Hien	9/2024	Fast and Accurate GMPPT Based on Modified P&O Algorithm	IEEE Access	2169-3536	10.1109/ACCESS.2024.3457825	
II		**Tạp chí khoa học trong danh mục Scopus**					
III		**Tạp chí khoa học quốc tế có ISSN, có phản biện nhưng chưa xếp hạng WoS/Sopus**					
4	Bùi Văn Hiền, Trương Việt Anh, Quách Thanh Hải	3/2020	Tối ưu điểm phát công suất cực đại của pin quang điện làm việc trong điều kiện bóng che	VNUHCM journal of engineering and technology	1859-0128	https://doi.org/10.32508/stdjet.v3i1.544	
5	Bùi Văn Hiền, Nguyễn Tùng Linh, Nguyễn Vũ Lân, Trương Việt Anh, Nguyễn Hồng Nguyên	4/2022	Truy Xuất Điểm Phát Công Suất Cực Đại Của Hệ Thống Pin Quang Điện Trong Các Thiết Bị Di Chuyển	Tạp chí Khoa học và Công nghệ Đại học Thái Nguyên	1859-2171, 2374-9098	https://doi.org/10.34238/tnu-jst.5471	
6	Trương Việt Anh, Bùi Văn Hiền, Nguyễn Tùng Linh, Nguyễn	7/2022	Đề Xuất Giải Pháp Tìm Điểm Phát Công Suất Cực Đại	Tạp chí Khoa học và Công	1859-2171,	https://doi.org/10.34238/tn	

	Vũ Lân, Quách Thanh Hải		Của Hệ Thống PV Dựa Vào Dự Đoán Giá Trị I_{sc} Và V_{oc}	nghệ Đại học Thái Nguyên	2374-9098	u-jst.6088	
IV		**Kỷ yếu hội nghị khoa học quốc tế có phản biện và có ISBN**					
7	X. T. Luong, V. H. Bui, D. T. Do, T. H. Quach and V. A. Truong	10/2020	An Improvement of Maximum Power Point Tracking Algorithm Based on Particle Swarm Optimization Method for Photovoltaic System	5th International Conference on Green Technology and Sustainable Development (GTSD)	978-1-7281-9982-5	10.1109/GTSD50082.2020.9303110	
8	Trinh Trong Chuong, Nguyen Duc Minh, Bui Van Hien, Fan Yang, Truong Viet Anh	11/2021	Optimizing the Performance of the Photovoltaic System using the Micro DC-DC Converter	3rd International Conference on Smart Power & Internet Energy Systems (SPIES)	978-0-7381-4632-4	10.1109/SPIES52282.2021.9633791	
9	Bui Van Hien, Truong Viet Anh, Nguyen Duc Minh, Trinh Trong Chuong, Y Do Nhu, Trieu Viet Phuong	12/2022	Module Integrated Converters and Independent MPPT Technique.	International Conference on Engineering Research and Applications	978-3-031-22200-9	https://doi.org/10.1007/978-3-031-22200-9_73	

Bài báo số 1: SCIE Q2 – IF 3.9

Bui Van Hien, Truong Viet Anh, Nguyen Tung Linh, and Pham Quoc Khanh, *"Rapidly Determine the Maximum Power Point in the Parallel Configuration of the Photovoltaic System,"* Sensors, 2023, 23, 7503. https://doi.org/10.3390/s23177503.

sensors

MDPI

Article

Rapidly Determine the Maximum Power Point in the Parallel Configuration of the Photovoltaic System

Bui Van Hien [1,2], Truong Viet Anh [2], Nguyen Tung Linh [3] and Pham Quoc Khanh [4,*]

[1] Faculty of Mechanical-Electrical and Computer Engineering, School of Technology, Van Lang University, Ho Chi Minh City 700000, Vietnam; hien.bv@vlu.edu.vn
[2] Faculty of Electrical and Electronics Engineering, HCMC University of Technology and Education, Ho Chi Minh City 700000, Vietnam; anhtv@hcmute.edu.vn
[3] Faculty of Control and Automation, Electric Power University, Hanoi 100000, Vietnam; linhnt@epu.edu.vn
[4] Faculty of Electrical Engineering Technology, Industrial University of Ho Chi Minh City (IUH), Ho Chi Minh City 700000, Vietnam
* Correspondence: phamquockhanh@iuh.edu.vn

Abstract: The maximum power point tracking (MPPT) solutions improve power generation efficiency, quickly stabilizing the output waveform of photovoltaic (PV) systems under variable operating conditions. Along with new algorithms, improved and adjusted methods to exploit energy from PV systems are increasingly being researched and proposed. However, the proposed solutions based on the traditional algorithms and their improvements have poor performance, while the advanced algorithms or hybrid methods bring high performance but need to be simplified, and the response speed is higher. Moreover, a suitable PV configuration makes choosing a simple but highly efficient algorithm, especially in low-power PV system applications such as rooftop solar power, traffic lights, and moving vehicles. . .where the number of PV panels is insufficient to implement flexible configurations. This paper proposes a modified version of the Perturb and Observe (MPO) algorithm to improve MPPT performance and increase convergence speed in the parallel structure of PV panels. The Short-Circuit Current (I_{sc}) and Open-Circuit Voltage (V_{oc}) are calculated directly at specific operating conditions to quickly determine the potential maximum power point (MPP) that will reduce power interruptions and increase power generation efficiency compared to periodic updates. Therefore, the proposed solution converges faster, with higher efficiency, and the output signal in static and dynamic MPPT situations is more stable. The results show that the highest efficiency in simulation and experiment is 99.99% and 99.93%, respectively, while the convergence speed is 0.01 s and 0.03 s, respectively. They are better than the traditional Perturb and Observe (P&O) algorithm, the Variable Step Size Perturb and Observe (VSSP&O) method, and the Particle Swarm Optimization (PSO) technique under the same operating conditions. In addition, its performance and convergence speed are also compared with the latest introduced algorithms. The results show that it is valuable and reliable for parallel PV configuration.

Keywords: modified P&O algorithm; parallel PV configuration; fill factor; MPPT

Citation: Hien, B.V.; Anh, T.V.; Linh, N.T.; Khanh, P.Q. Rapidly Determine the Maximum Power Point in the Parallel Configuration of the Photovoltaic System. *Sensors* **2023**, *23*, 7503. https://doi.org/10.3390/s23177503

Academic Editor: Marco Pisco

Received: 27 July 2023
Revised: 15 August 2023
Accepted: 25 August 2023
Published: 29 August 2023

1. Introduction

Rooftop photovoltaic systems are essential for apartments-integrated centralized generation, especially in high mountains or islands. Their advantages can be considered in some critical points as follows [1]: First, utilizing available space can generate electricity near where needed, reducing transmission and distribution losses associated with traditional centralized power generation. Secondly, they contribute to sustainable energy development by reducing reliance on conventional fossil fuel-based electricity, significantly reducing greenhouse gas emissions and environmental impact. Finally, they can result in significant cost savings over time due to low maintenance requirements and can generate

electricity for a long time. Additionally, depending on local regulations and policies, excess electricity can be fed back into the grid.

However, in low-power PV system applications, due to the limitation of PV quantity, it is less efficient to implement complex configurations such as total-cross-tied, bridge-link, honeycomb, etc. . . Meanwhile, the parallel structure has outstanding advantages such as high power generation efficiency, low loss, and less variable I(V) and P(V) characteristic curves. Even under partial shading conditions, the observed characteristics consistently display a singular peak, and the maximum power remains unaffected by the bypass diodes present in this configuration [2]. Therefore, applying MPPT algorithms to efficiently improve the performance and convergence speed and quickly stabilize under the environment changes continuously is simple.

Further, along with the continuous development of PV systems globally due to the rapid energy demand growth, solutions to determine the MPP of PV systems are also proposed, adjusted, and improved continuously. They can be classified into conventional, intelligent, optimization, and hybrid methods [3,4]. The classical algorithms are simple and low-cost, but the convergence speed and efficiency must improve.

In contrast, advanced methods have high efficiency and speed but are complicated and expensive. As a result, hybrid or improved methods are proposed to optimize the strengths of individual algorithms. However, finding a solution that achieves high efficiency, fast tracking speed, low cost, and less complexity is challenging.

To solve the above problem, many studies have been introduced in different approaches and treatments. Recent publications concentrate on the traditional techniques combined with the I(V) characteristic curve of PV systems to improve efficiency and speed due to simplicity and low cost. By using the FF value to determine the power loss between the MPP under standard conditions and when shaded, document [5] has provided a solution to continuously compare actual working parameters with standard conditions to adjust the working position. While the authors in [6–8] proposed a solution to approximate the current at MPP ($I_{mp} = k_i I_{sc}$) to improve MPPT efficiency, convergence rate, and output stability. The PV module's I_{sc} value is measured by interrupting the system's regular operation with a particular frequency, storing the calculated value. However, speed and performance have yet to be significantly improved. Further, some studies focus on the V_{oc} value to determine MPP ($V_{mp} = k_v V_{oc}$) [8–10].

In the same way, the V_{oc} is also achieved by disconnecting the regular operation of the system. The significant advantages of these approaches are simple and low price. Yet, its drawback is that the interrupted system operation yields power losses when scanning the entire control range. If the sampling period of these two parameters is small, the accuracy of MPPT will increase, but it also increases the supply interruption time between source and load. Conversely, if they are not regularly updated, the calculated values may not be the optimal MPP of the PV system because I_{sc} and V_{oc} values are affected by operating conditions and aging.

To overcome this drawback, in the reference [11], the authors introduced an enhanced approach to improve the conventional P&O and INC methods. This method aims to optimize the maximum output power of the PV system and identify the most suitable design variable for regulating the step size in conventional algorithms. This solution can achieve a convergence speed of 0.0434 s and an efficiency of 99.07%. In [12], the Low Burden Narrow Search (LBNS), a reduced search space exploration metaheuristic algorithm for MPPT, is proposed. The main goal of this solution is to confine the search space around the actual optimum to minimize the number of update equations needed, effectively avoiding the exploration of irrelevant regions and decreasing computational steps. The simulation efficiency of this solution is 99.98% at 0.038 s. The document [13] introduces a variety of intelligent algorithms, such as Modified Incremental Conductance (MIC), the Cuckoo Search Algorithm (CSA), Gray Wolf Optimization (GWO), and PSO. Their efficiency ranges from 78.42% to 99.99% depending on operating conditions, and the fastest convergence speed is 0.14 s. The convergence speed is slightly improved in [14],

about 0.0375 s, but its performance is only 99.54%. This paper presents a novel GMPPT algorithm that combines the Measurement Cells (MC) algorithm and the P&O method. Firstly, it utilizes the fast dynamic MC algorithm to identify and evaluate the local maximum power points. Then, the P&O method is employed to approximate and adjust the voltage to approach the MPP determined in the previous step. Overall, the proposed GMPPT algorithm offers an innovative approach by combining the strengths of the MC algorithm and the P&O method to efficiently track and maintain the maximum power point of the photovoltaic system. Most recently, the [15] document mentions an entirely new algorithm. The authors introduced the musical chairs algorithm (MCA), inspired by the game of musical chairs. Its outstanding advantage is that there is only one tuning parameter and variable swarm size, which makes it much easier to tune than other algorithms. Then, the adjusted version (BMCA) introduced in [16] can reduce error and convergence speed by 40% compared to different optimization algorithms while maintaining a zero failure rate. Therefore, the convergence speed of the MCA of 0.3 s has been improved up to 0.096 s in the BMCA version. Although it is more straightforward than other optimization algorithms, it is quite complex compared to traditional algorithms. In [17], a hybrid approach between the Fuzzy Logic Controller and the Cuckoo Optimization Algorithm (COA-FLC) to increase convergence speed, improve performance, and reduce oscillations around MPP is proposed. This combination increases the convergence speed of the solution to 0.016 s, and the efficiency is about 99.83%. A hybrid solution in [1] applies a hybrid MPPT control algorithm between PSO and P&O to ensure the system's effectiveness even under various irradiance conditions. However, it only achieves simulation and experimental efficiency of about 92% and 90%, respectively.

The above analysis shows that there are many criteria to evaluate the effectiveness of an MPPT solution. However, have yet to find a solution that satisfies all evaluation criteria. This study introduces a simple MPPT method, low cost, high performance, and fast convergence speed, and can be widely applied in different operating conditions. The proposed solution is based on a modified P&O algorithm to quickly determine the potential MPP of the photovoltaic system. It is a simple, robust algorithm with high MPPT performance under standard conditions [4]. Further, the characteristic curves of parallel configuration always show the same under all operating conditions. Therefore, applying a modified P&O algorithm to this configuration will be helpful in low-voltage solar power applications due to its simplicity and low cost.

The outstanding contributions of this study include:

- Investigate some typical PV modules' I(V) characteristics to determine the linear region where the I_{sc} value can be calculated directly. This data can be helpful for further research on photovoltaic systems;
- Suggest a cut-off point of 0.4 V_{oc} to directly calculate the I_{sc} value within this limit;
- Propose a method to directly determine I_{sc} and V_{oc} according to operating conditions using linear extrapolation from two random points.
- Quickly determine the duty cycle value at the potential MPP (d_{mp}), which is then used as the starting point for the MPO algorithm.
- Improve convergence speed and MPPT performance of parallel PV panels under different operating conditions.

The simulation and experimental results show that the proposed method's convergence speed and MPPT efficiency are better than other methods. It can effectively be applied in parallel PV systems with low voltage and power.

The paper is organized as follows: Section 2 presents the characteristics of PV systems under different operating conditions, and Section 3 details the principle of the Boost converter. The I(V) characteristic curves of some typical PV modules and methods to determine I_{sc}, V_{oc} are presented in this section. In Section 4, simulation and experimental results are shown and discussed. Finally, Section 5 draws conclusions from the study.

2. Effects of Working Conditions on PV System

Equation (1) presents the relationship between the output current and voltage of a typical PV cell that is introduced in Figure 1 [18–20].

$$I_{pv} = I_{ph} - I_0\left\{e^{\frac{q(V_{pv}+I_{pv}R_s)}{nKT_c}} - 1\right\} - \frac{V_{pv}+I_{pv}R_s}{R_{sh}} \quad (1)$$

where V_{pv} and I_{pv} are the output voltage (V) and current (A) of PV, respectively; I_{ph} is the light current (A); I_0 is the reverse saturation current of the diode (A); q is the electron charge (1.602×10^{-19} C); K is the Boltzmann constant (1.381×10^{-23} J/K); Tc is the cell temperature (K); R_s, R_{sh} are series and shunt resistance, respectively (Ω); n is diode ideality factor (dimensionless).

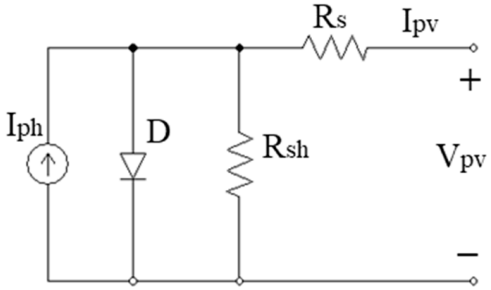

Figure 1. Equivalent circuit of PV cell.

In which the light current I_{ph} depends on the solar irradiation and the working temperature of the PV cell, as stated in (2) [20,21].

$$I_{ph} = [I_{sc} + \alpha_i(T_c - T_{ref})]\frac{W}{W_{ref}} \quad (2)$$

where I_{sc} is short circuit current (A); T_{ref} is the temperature at standard condition (K); W is the solar irradiance level (W/m^2); W_{ref} is the irradiance level at standard state (W/m^2); α_i is the temperature coefficient of I_{sc} ($mA/^\circ C$).

At any operating condition, the component currents of the PV cell are introduced as in (3).

$$I_{pv} = I_{sc} - I_D - I_{R_{sh}} \quad (3)$$

where I_D and I_{Rsh} are the diode-current and the shunt-resistance-current, respectively. Their values are determined according to Equations (4) and (5).

$$I_D = I_0\left\{e^{\frac{q(V_{pv}+I_{pv}R_s)}{nKT_c}} - 1\right\} \quad (4)$$

$$I_{R_{sh}} = \frac{V_{pv}+I_{pv}R_s}{R_{sh}} \quad (5)$$

The graphs of Equations (3)–(5) are shown in Figure 2. In which the nonlinear region on the I(V) curve is caused by the I_D current. In contrast, the slope in this area is mainly due to the I_{Rsh} current. However, these operating zones are affected by radiation and temperature (Figure 3). Furthermore, under the same operating conditions, its slope depends on the R_{sh} value (Figure 4). Therefore, surveying the working regions of PV modules under different operating conditions will simplify calculating their parameters.

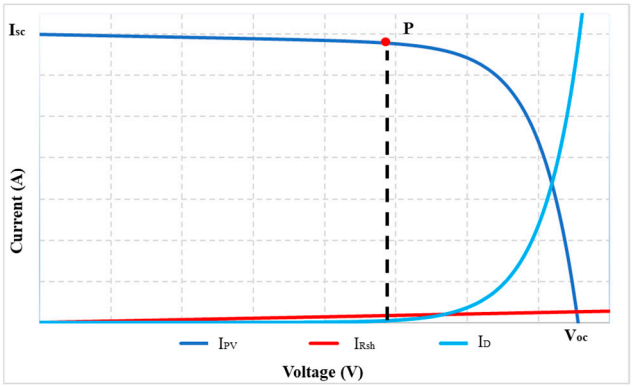

Figure 2. The I(V) characteristics under standard working conditions.

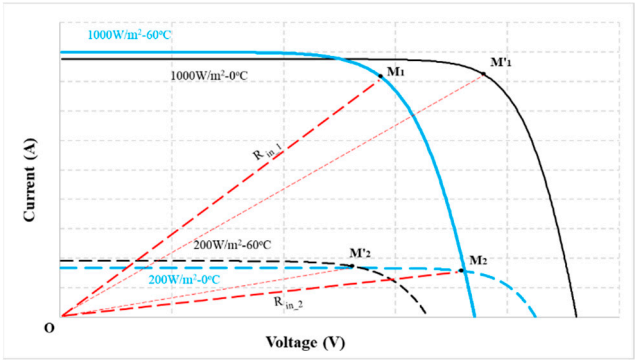

Figure 3. The I(V) characteristics under different working conditions.

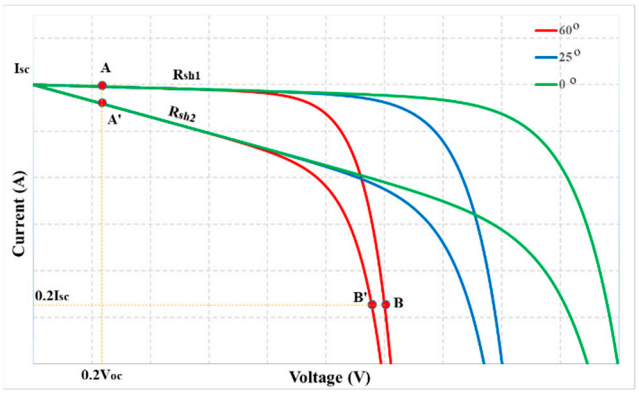

Figure 4. The I(V) characteristics under different conditions of temperature and R_{sh}.

3. The Duty Cycle of the PV Control System

3.1. The Relationship between Duty Cycles of the Boost Converter

The boost converter in Figure 5 provides maximum power to the load. The MPPT block controls the DC/DC converter to keep the system working at the highest PV efficiency by adjusting the output voltage (V_{out}) according to the input voltage (V_{in}) through a duty cycle (d) value ($0 < d < 1$). The relationship between the input and output voltages is presented in (6) [22,23].

$$\frac{V_{out}}{V_{in}} = \frac{1}{1-d} \quad (6)$$

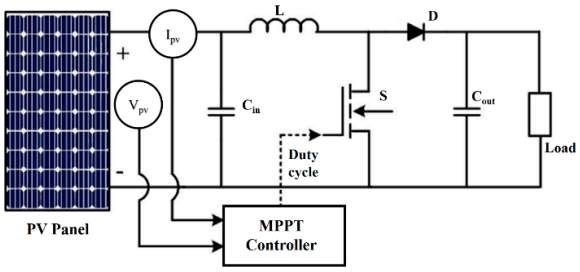

Figure 5. Schematic diagram of the PV control system in this research.

If the losses on the DC/DC circuit are negligible, the V_{pv} and I_{pv} values are determined based on a random d value, and the relationships between them and resistive load (R_L) can be introduced as in Equation (7).

$$\frac{V_{pv}}{I_{pv}} = R_L(1-d)^2 \tag{7}$$

In the range $0 < d < 1$, only one duty cycle value achieves the maximum output power under the input power changes, and the load R_L remains constant. However, as the operating conditions change, the potential MPP ($P_{mp} = V_{mp} \times I_{mp}$) will also change. Therefore, the corresponding estimated duty cycle (d_{mp}) must also be recalculated. The relationship between them is shown in (8) [23].

$$\frac{V_{mp}}{I_{mp}} = R_L(1-d_{mp})^2 \tag{8}$$

Combine Equations (7) and (8) to determine d_{mp} at MPP, as shown in (9).

$$d_{mp} = 1-(1-d)\sqrt{\frac{V_{mp}}{I_{mp}}\frac{I_{pv}}{V_{pv}}} \tag{9}$$

The I_{pv} and V_{pv} values are measured and stored at any value of d. When the working environment changes, it is difficult to directly determine the d_{mp} value. However, the stability of the characteristic curve of the parallel configuration under all operating conditions makes it simpler to calculate the V_{mp} and Imp values according to FF. In other words, if the I_{sc} and V_{oc} values are known, the MPP(V_{mp}, I_{mp}) will be estimated following (10) [5–10], and then calculate d_{mp} following (9).

$$V_{mp} = k_v V_{oc} \quad \text{and} \quad I_{mp} = \frac{FF}{k_v} I_{sc} = k_i I_{sc} \tag{10}$$

As analyzed above, if the I_{sc} and V_{oc} values are updated periodically, the solution will be less accurate because they are affected and changed continuously by the environment. On the contrary, when measured under actual conditions, it will increase convergence speed and reduce error. Therefore, it is necessary to investigate the different working conditions of PV modules to find a solution to quickly calculate these parameters.

3.2. The Relationship between Duty Cycles at the MPP

To propose a solution to quickly calculate Isc and V_{oc} in real time, in this study, radiation and temperature were adjusted from $W_1 = 200\ W/m^2$ to $W_2 = 1000\ W/m^2$ and $T_1 = 0\ ^\circ C$ to $T_2 = 60\ ^\circ C$, respectively (Figure 3). At these limits, the resistance value of the

PV system is from R_{in_1} at $M_1(W_1, T_1)$ to R_{in_2} at $M_2(W_2, T_2)$. The relationship between the parameters at these two points is shown in (11).

$$\frac{V_{mp1}}{I_{mp1}(1-d_{mp1})^2} = \frac{V_{mp2}}{I_{mp2}(1-d_{mp2})^2} \tag{11}$$

Solve Equation (11) to get Equation (12) as follows.

$$\frac{(1-d_{mp2})^2}{(1-d_{mp1})^2} = \frac{V_{mp2}I_{mp1}}{I_{mp2}V_{mp1}} \tag{12}$$

Combine Equations (10) and (12), the relationship between duty cycles at MPP (d_{mp}), as shown in (13).

$$\frac{(1-d_{mp2})^2}{(1-d_{mp1})^2} = \frac{k_v V_{oc2} k_i I_{sc1}}{k_i I_{sc2} k_v V_{oc1}} = \frac{V_{oc2} I_{sc1}}{I_{sc2} V_{oc1}} \tag{13}$$

Since M_1 and M_2 operate differently from the standard conditions, Equation (13) is rewritten as in (14). Where α_v is the temperature coefficient on V_{oc} (mV/°C), and α_i is the temperature coefficient of I_{sc} (mA/°C).

$$\frac{(1-d_{mp2})^2}{(1-d_{mp1})^2} = \frac{(V_{oc}-\alpha_v(T_2-25))}{W_2(I_{sc}+\alpha_i(T_2-25))} \frac{W_1(I_{sc}+\alpha_i(T_1-25))}{(V_{oc}-\alpha_v(T_1-25))} \tag{14}$$

Substitute the data in Table 1 [24] into Equation (14) to calculate the relationship between duty cycles at M_1 and M_2, as shown in (15).

$$\frac{(1-d_{mp2})^2}{(1-d_{mp1})^2} = 1.65 \tag{15}$$

Table 1. Specifications of the PV panel MSX-60.

Parameters	Value
Number of cells	36
Series Resistance	0.2 (Ω)
Shunt Resistance	304.83 (Ω)
Short Circuit Current	3.8 (A)
Open Circuit Voltage	21.1 (V)
Maximum Power Point Voltage	17.1 (V)
Maximum Power Point Current	3.5 (A)
The diode reverse saturation current	9.094×10^{-8} (A)
Temperature coefficient of I_{sc}	3 (mA/°C)
Temperature coefficient on V_{oc}	−80 (mV/°C)

Equation (15) shows that the relationship between d_{mp1} and d_{mp2} under the best and worst operating conditions is established based on the technical characteristics of the PV module. To reduce the pressure on the DC/DC converters switches, the d_{mp} values should be around 0.5 [25,26]. To satisfy all operating conditions within this survey limit, duty cycle values must be satisfied as in (16).

$$0.5 - d_{mp1} = d_{mp2} - 0.5 \tag{16}$$

Combine Equations (15) and (16) to get the d_{mp1} = 0.29 and d_{mp2} = 0.71.

In the same way, the survey results for the remaining PV modules [24] are also collected and detailed in Table 2.

Table 2. The best region of d.

Type of PV Module	d_{mp1}	d_{mp2}
MSC-60	0.86	0.80
Shell SP75	0.82	0.75
Shell SQ150	0.84	0.78
SSt 230-60P	0.83	0.77
Shell S70	0.83	0.75
GxB-340	0.85	0.79
Shell ST40	0.81	0.72

3.3. The Linear Region on the I(V) Curve

The working areas of the I(V) curve in Figure 3 show that the d_{mp2} value (at M_2) is suitable for calculating I_{sc} under all operating conditions. Because the resistance value of the PV system at 1000 W/m^2—60 °C (R_{in_2}) belongs to line OM_2, it always intersects the linear region of the curves. In contrast, d_{mp1} was chosen as the reference limit to calculate the V_{oc} value of the PV system.

According to reference [27], the authors have proposed a working point A(0.2 V_{oc}; I_{sc}) on the I(V) curve to calculate I_{sc}. That is, at a particular operating condition, the relationship between the parameters at A and MPP(V_{mp}; I_{mp}) is presented as in (17) after combining Equations (9) and (10).

$$d_A = 1 - (1 - d_{mp2})\sqrt{\frac{0.2V_{oc}}{I_{sc}}\frac{0.93I_{sc}}{0.8V_{oc}}} = 0.86 \quad (17)$$

With d_{mp2} = 0.71, the limit for calculating the I_{sc} of PV module MSX-60. The values of k_v and k_i are chosen as 0.80 and 0.93, respectively, because they satisfy all PV modules surveyed in Table 2. The duty cycle at 0.2 V_{oc} is d_A = 0.86, which the I_{sc} can be calculated directly without interrupting the power supply for periodic updates.

However, the PV module's R_{sh} value causes the characteristic curve slope in the linear region. Therefore, the calculation of the I_{sc} value at A (corresponding to R_{sh1}) can be accurate, but the error increases significantly when calculating at A′ (corresponding to R_{sh2}) (Figure 4). The larger this resistance fluctuates, the greater the calculation error. It causes a decrease in the MPPT efficiency of the PV system. The analysis shows that calculating I_{sc} at A(0.2 V_{oc}, I_{sc}) is less accurate in actual operating conditions. An extrapolation method is proposed from two points in the linear region to solve these problems. It is necessary to define the linear part on the I(V) curve corresponding to its d parameters. With a significant d value, the measured voltage and current are in the linear region but will pressure the DC/DC converter switches. On the contrary, the output signals may fall into the nonlinear zone, causing I_{sc} calculation error.

To analyze the active regions on the PV modules' I(V) curve, their parameters are investigated according to V_{oc}. If $I_{pv}R_s << V_{pv}$, the output voltage of the PV module will be considered in Equation (18) with $0 \leq x \leq 1$.

$$V_{pv} = xV_{oc} \quad (18)$$

Then, Equations (4) and (5) are rewritten as in (19) and (20). Where k = 0.1 to 1.0 means survey shunt-resistor-current from 0.1 I_{Rsh} to I_{Rsh} to compare with I_D.

$$I_D = \left| I_0 \left\{ e^{\frac{qxV_{oc}}{nKT_c}} - 1 \right\} \right| \quad (19)$$

$$I_{Rsh} = k\left|\frac{xV_{oc}}{R_{sh}}\right| \quad (20)$$

The 5-parameter model of the PV module MSX-60 is used to investigate according to Equations (19) and (20) under different temperatures and R_{sh}. In which the I_{pv} is determined by Equation (3). The current waveforms in Figure 6 show that the linear region is limited in $V_{pv} < 0.4\ V_{oc}$. Then, the remaining PV modules were similarly surveyed. The survey results in Figure 7 show that their linear areas are in the voltage range of less than $0.4\ V_{oc}$. In particular, the PV modules such as GxB-340 and Shell SQ150 have linear regions in $V_{pv} < 0.5\ V_{oc}$. Therefore, $V_{pv} = 0.4\ V_{oc}$ is the reference point for determining the d limit to calculate I_{sc} in this study.

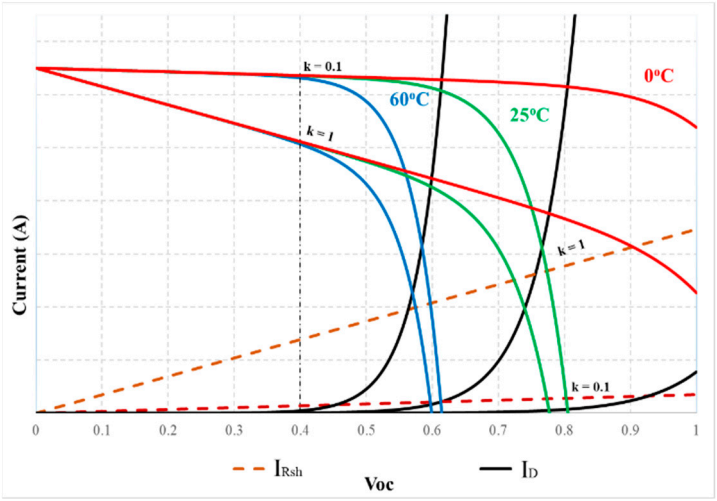

Figure 6. The I(V) characteristic curve of the PV module MSX-60.

However, output parameters are measured and stored based on the duty cycle value at specific times. It is necessary to determine the value of d at $0.4\ V_{oc}$ of PV modules according to Equation (21).

$$d_A = 1 - (1 - d_{mp2}) \sqrt{\frac{0.4V_{oc}}{I_{sc}} \frac{0.93I_{sc}}{0.8V_{oc}}} = 0.80 \quad (21)$$

Equation (21) shows that the linear range is $d \geq 0.80$ for PV module MSX-60. This value ensures that the measured current and voltage are always in the linear region of all operating conditions.

Similarly, the d_{mp2} values in Table 2 are used to calculate the duty cycle at $0.4\ V_{oc}$ for the remaining PV modules. The results listed in Table 3 show that, within the survey range, the d value at $0.4\ V_{oc}$ is from 0.72 to 0.80. Therefore, using any two points within this range to establish the equation of the line through I_{sc} will limit the disadvantage mentioned above. In this survey, $d_1 = 0.8$ and $d_2 = 0.75$ were chosen as the reference data to survey all PV modules.

Table 3. The duty cycle d_A at $0.2\ V_{oc}$ and $0.4\ V_{oc}$.

Type of PV Module	0.2 V_{oc}	0.4 V_{oc}
MSX-60	0.29	0.71
Shell SP75	0.36	0.64
Shell SQ150	0.33	0.67
SSt 230-60P	0.34	0.66
Shell S70	0.36	0.64
GxB-340	0.31	0.69
Shell ST40	0.41	0.60

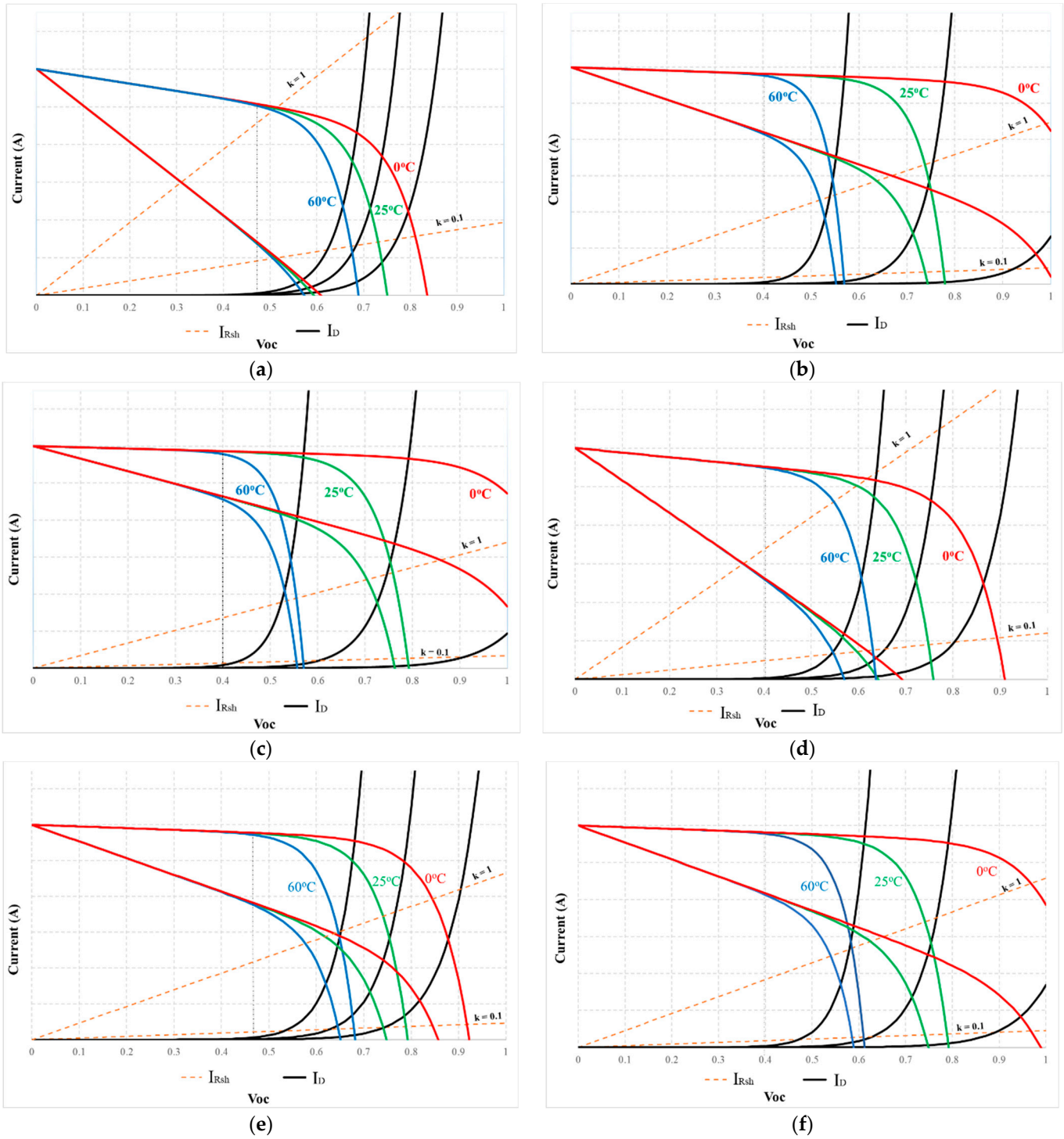

Figure 7. The I(V) characteristic curve of some typical PV modules: (**a**) GxB-340; (**b**) Shell ST40; (**c**) Shell S70; (**d**) SSt 230-60P; (**e**) Shell SQ150; and (**f**) Shell SP75.

3.4. Identifying the Value of the Isc

With two points [$P_1(V_1, I_1)$ and $P_2(V_2, I_2)$] in the linear area of the I(V) curve corresponding to d_1 và d_2, the equation of the line through P_1 and P_2 is shown in (22).

$$I = \frac{I_2 - I_1}{V_2 - V_1}V + \left[I_1 - \frac{I_2 - I_1}{V_2 - V_1}V_1\right] \quad (22)$$

Accordingly, the value of I_{sc} is inferred by (23) when substituting V = 0 into (22) as follows.

$$I_{sc} = I_1 - \frac{I_2 - I_1}{V_2 - V_1} V_1 \quad (23)$$

Applying Equation (23) calculates the I_{sc_cal} value of PV modules under different temperature and radiation conditions. The current deviation (ΔI%) between this result and the actual value (I_{sc}) of PV modules is determined using Equation (24).

$$\Delta I\% = \frac{|I_{sc} - I_{sc\_cal}|}{I_{sc}} 100\% \quad (24)$$

The summary of the survey, calculation, and comparison results in Tables 4 and 5 shows that the maximum deviation is 3.79% when operating conditions are 1000 W/m^2 and 60 °C (PV module Shell SQ150), and the minimum error is 0.00% in some cases. The maximum average deviation is 1.14% (PV module Shell SQ150), while the lowest difference is 0.04% (PV module SSt 230-60P). The results show that the proposed method can accurately estimate the I_{sc} value of the PV system.

Table 4. The ΔI% under different radiations.

Type of PV Module		Radiation (W/m^2)						
		200	**350**	**500**	**650**	**800**	**900**	**1000**
MSX-60	I_{sc}	1.48	2.59	3.7	4.81	5.92	6.66	7.41
	I_{sc_cal}	1.5	2.63	3.75	4.89	6.01	6.76	7.51
	ΔI%	1.35	1.54	1.35	1.66	1.52	1.5	1.35
Shell SP75	I_{sc}	1.89	3.32	4.74	6.17	7.6	8.56	9.4
	I_{sc_cal}	1.9	3.33	4.75	6.18	7.6	8.55	9.5
	ΔI%	0.53	0.3	0.21	0.16	0	0.12	1.06
Shell SQ150	I_{sc}	1.89	3.32	4.73	6.16	7.58	8.54	10
	I_{sc_cal}	1.89	3.32	4.74	6.16	7.58	8.53	9.9
	ΔI%	0	0	0.21	0	0	0.12	1
SSt 230-60P	I_{sc}	3.36	5.88	8.41	10.93	13.45	15.14	16.83
	I_{sc_cal}	3.36	5.88	8.41	10.94	13.45	15.13	16.81
	ΔI%	0	0	0	0.09	0	0.07	0.12
Shell S70	I_{sc}	1.77	3.1	4.43	5.76	7.08	7.97	8.86
	I_{sc_cal}	1.77	3.12	4.42	5.76	7.08	7.97	8.85
	ΔI%	0	0.65	0.23	0	0	0	0.11
GxB-340	I_{sc}	3.66	6.41	9.15	11.91	14.65	16.49	18.33
	I_{sc_cal}	3.66	6.41	9.15	11.91	14.6	16.48	18.3
	ΔI%	0	0	0	0	0.34	0.06	0.16
Shell ST40	I_{sc}	1.05	1.85	2.63	3.43	4.22	4.76	5.32
	I_{sc_cal}	1.05	1.85	2.64	3.43	4.22	4.75	5.28
	ΔI%	0	0	0.38	0	0	0.21	0.75

Table 5. The ΔI% under different temperatures.

Type of PV Module		Temperature (°C)						
		0	**10**	**20**	**30**	**40**	**50**	**60**
MSX-60	I_{sc}	7.28	7.33	7.39	7.47	7.59	7.59	7.6
	I_{sc_cal}	7.39	7.44	7.49	7.54	7.59	7.64	7.69
	ΔI%	1.51	1.5	1.35	0.94	0	0.66	1.18
Shell SP75	I_{sc}	9.35	9.41	9.48	9.57	9.68	9.85	10.1
	I_{sc_cal}	9.35	9.41	9.47	9.53	9.58	9.65	9.75
	ΔI%	0	0	0.11	0.42	1.03	2.03	3.47

Table 5. *Cont.*

Type of PV Module		Temperature (°C)						
		0	**10**	**20**	**30**	**40**	**50**	**60**
Shell SQ150	I_{sc}	9.41	9.45	9.5	9.58	9.71	9.94	10.3
	I_{sc_cal}	9.41	9.44	9.48	9.53	9.6	9.72	9.91
	ΔI%	0	0.11	0.21	0.52	1.13	2.21	3.79
SSt 230-60P	I_{sc}	16.63	16.7	16.79	16.88	16.99	17.14	17.37
	I_{sc_cal}	16.62	16.7	16.78	16.85	16.93	17.01	17.08
	ΔI%	0.06	0	0.06	0.18	0.35	0.76	1.67
Shell S70	I_{sc}	8.76	8.8	8.84	8.88	8.93	9	9.08
	I_{sc_cal}	8.75	8.79	8.83	8.87	8.91	8.95	8.99
	ΔI%	0.11	0.11	0.11	0.11	0.22	0.56	0.99
GxB-340	I_{sc}	18.01	18.14	18.27	18.4	18.55	18.72	18.93
	I_{sc_cal}	18.01	18.13	18.2	18.3	18.5	18.6	18.74
	ΔI%	0	0.06	0.38	0.54	0.27	0.64	1.00
Shell ST40	I_{sc}	5.26	5.28	5.3	5.34	5.41	5.53	5.72
	I_{sc_cal}	5.27	5.29	5.33	5.4	5.5	5.6	5.84
	ΔI%	0.19	0.19	0.57	1.12	1.66	1.27	2.1

3.5. Identifying the Value of the Voc

As analyzed above, the I_{sc} value is determined based on d_{mp2}, while V_{oc} depends on d_{mp1} (Table 2). To calculate V_{oc} in all operating conditions, point B(V_B, I_B) must satisfy $d_B \leq d_{mp1}$, as shown in Equation (25).

$$d_B = 1 - (1 - d_{mp1}) \sqrt{\frac{0.93 I_{sc}}{0.8 V_{oc}} \frac{V_B}{I_B}} \tag{25}$$

In reference [20], the authors proposed calculating V_{oc} at I_B = 0.2 I_{sc}. That is, the coordinates of point B(V_{oc}, 0.2 I_{sc}) are substituted into Equation (25) as follows.

In the worst operating condition (d_{mp1}), the d_B value calculated from Equation (25) (PV MSX-60) is $d_B = -0.71$. In contrast, at best operating condition (d_{mp2}), this value is 0.30. It shows that choosing $V_{oc} = V_B$ at 0.2 I_{sc} cannot satisfy all operational requirements. The results of the same survey for the remaining PV modules are presented in Table 6.

Table 6. The d_B values at 0.2 I_{sc} under different conditions.

Type of PV Module	M_1	M_2
MSC-60	−0.71	0.3
Shell SP75	−0.54	0.13
Shell SQ150	−0.61	0.22
SSt 230-60P	−0.59	0.19
Shell S70	−0.54	0.14
GxB-340	−0.66	0.25
Shell ST40	−0.42	0.03

The calculation results in Table 6 are suitable only within a narrow range of operating conditions. They do not represent PV modules under the operating conditions proposed in this study. Therefore, if V_{oc} is calculated at B, the error increases, and the convergence rate decreases significantly. Furthermore, if this value is calculated at d = 0, it will pressure the diode. In the same way, V_{oc} is also calculated from two points to limit the above defects. In this study, the values d_3 = 0.1 and d_4 = 0.05 were chosen as representatives for calculating V_{oc}. The equation of the line passing through two points $P_3(V_3, I_3)$ and $P_4(V_4, I_4)$ is presented in Equation (26).

$$I = \frac{I_4 - I_3}{V_4 - V_3} V + \left[I_3 - \frac{I_4 - I_3}{V_4 - V_3} V_3 \right] \tag{26}$$

Accordingly, the value of V_{oc} is inferred by (27) when substituting I = 0 into (26).

$$V_{oc} = V_3 - \frac{V_4 - V_3}{I_4 - I_3} I_3 \quad (27)$$

Applying Equation (27) calculates the V_{oc_cal} value of PV modules under different temperature and radiation conditions. The voltage error (ΔV%) between this result and the actual value (V_{oc}) of PV modules is determined using Equation (28).

$$\Delta V\% = \frac{|V_{oc} - V_{oc\_cal}|}{V_{oc}} 100\% \quad (28)$$

The summary results in Tables 7 and 8 show that the most significant deviation is 4.69% (PV module Shell ST40) at 200 W/m^2 and 25 °C. The minimum error is 0.02% (PV module MSX-60) at 900 W/m^2 and 25 °C. Meanwhile, the maximum average difference is 2.18% (PV module Shell ST40). The minimum average error is 0.07% (PV module MSX-60).

Table 7. The ΔV% under different radiations.

Type of PV Module		Radiation (W/m^2)						
		200	**350**	**500**	**650**	**800**	**900**	**1000**
MSX-60	V_{oc}	37.24	39.17	40.29	41.03	41.61	41.93	42.21
	V_{oc_cal}	38.29	39.62	40.5	41.13	41.63	41.92	42.17
	ΔV%	2.82	1.15	0.52	0.24	0.05	0.02	0.09
Shell SP75	V_{oc}	38.62	40.52	41.63	42.36	42.93	43.25	43.53
	V_{oc_cal}	39.77	41.1	41.98	42.61	43.11	43.4	43.65
	ΔV%	2.98	1.43	0.84	0.59	0.42	0.35	0.28
Shell SQ150	V_{oc}	76.06	80.82	82.99	84.43	85.57	86.2	86.75
	V_{oc_cal}	79.09	81.75	83.51	84.76	85.87	86.34	86.85
	ΔV%	3.98	1.15	0.63	0.39	0.35	0.16	0.12
SSt 230-60P	V_{oc}	65.05	68.29	70.17	71.41	72.38	72.91	73.38
	V_{oc_cal}	66.98	69.19	70.67	71.71	72.56	73.03	73.45
	ΔV%	2.97	1.32	0.71	0.42	0.25	0.16	0.1
Shell S70	V_{oc}	37.21	39.24	40.39	41.15	41.74	42.06	42.35
	V_{oc_cal}	38.54	39.87	40.75	41.38	41.88	42.17	42.42
	ΔV%	3.57	1.61	0.89	0.56	0.34	0.26	0.17
GxB-340	V_{oc}	90.52	95.18	97.81	99.53	100.88	102.62	102.8
	V_{oc_cal}	93.75	96.81	98.85	100.3	101.47	102.12	102.71
	ΔV%	3.57	1.71	1.06	0.77	0.58	0.49	0.09
Shell ST40	V_{oc}	40.76	42.88	44.01	44.75	45.33	45.65	45.93
	V_{oc_cal}	42.67	44	44.88	45.51	46.01	46.3	46.55
	ΔV%	4.69	2.61	1.98	1.7	1.5	1.42	1.35

Table 8. The ΔV% under different temperatures.

Type of PV Module		Temperature (°C)						
		0	**10**	**20**	**30**	**40**	**50**	**60**
MSX-60	V_{oc}	45.99	44.49	42.97	41.44	39.91	38.38	36.83
	V_{oc_cal}	45.94	44.44	42.93	41.41	39.89	38.36	36.82
	ΔV%	0.11	0.11	0.09	0.07	0.05	0.05	0.03
Shell SP75	V_{oc}	47.18	45.73	44.26	42.79	41.32	39.84	38.35
	V_{oc_cal}	47.3	45.84	44.38	42.92	41.44	39.96	38.47
	ΔV%	0.25	0.24	0.27	0.3	0.29	0.3	0.31
Shell SQ150	V_{oc}	94.15	91.2	88.24	85.27	82.28	79.27	76.26
	V_{oc_cal}	94.22	91.28	88.33	85.37	82.38	79.39	76.38
	ΔV%	0.07	0.09	0.1	0.12	0.12	0.15	0.16

Table 8. *Cont.*

Type of PV Module		Temperature (°C)						
		0	**10**	**20**	**30**	**40**	**50**	**60**
SSt 230-60P	V_{oc}	79.44	77.02	74.6	72.16	69.71	67.25	64.78
	V_{oc_cal}	79.49	77.08	74.66	72.24	69.79	67.34	64.87
	ΔV%	0.06	0.08	0.08	0.11	0.11	0.13	0.14
Shell S70	V_{oc}	46.12	44.62	43.16	41.59	40.06	38.53	36.99
	V_{oc_cal}	46.18	44.68	43.18	41.66	40.14	38.61	37.08
	ΔV%	0.13	0.13	0.05	0.17	0.2	0.21	0.24
GxB-340	V_{oc}	108.45	105.99	103.51	101.02	98.52	95.99	93.46
	V_{oc_cal}	108.87	106.42	103.95	101.46	98.96	96.44	93.91
	ΔV%	0.39	0.41	0.43	0.44	0.45	0.47	0.48
Shell ST40	V_{oc}	49.45	48.09	46.73	45.35	43.97	42.58	41.14
	V_{oc_cal}	50	48.63	47.26	45.88	44.48	43.09	41.68
	ΔV%	1.11	1.12	1.13	1.17	1.16	1.2	1.31

In conclusion, the I_{sc} and V_{oc} values of PV modules under different operating conditions can be measured using the linear extrapolation method with an average error of less than 2.2% for V_{oc} and 1.2% for I_{sc}.

3.6. Identifying the Potential MPP

To implement the proposed method, the I(V) characteristic curves of PV modules are investigated to determine the linear region as part of the study. After that, the I_{sc} and V_{oc} are determined based on the d value of the DC/DC converter by extrapolating from two random points in this limit. This solution not only reduces the disconnection time between the source and the load but also increases the calculation accuracy of I_{sc} and V_{oc} compared to updating them periodically. Finally, the Perturbation and Observation algorithm will verify the calculated MPP coordinates based on FF [18,28]. It ensures that the optimal operating point of the PV system is determined correctly if there is an error in the calculation of I_{sc} and V_{oc}. The detailed sequence of steps is as follows:

Step 1. Calculate I_{sc} and I_{mp}: Select the values of d_1, d_2, d_3, and d_4 to calculate I_{sc} according to (23) and calculate the I_{mp} according to (10), respectively.
Step 2. Calculate V_{oc} and V_{mp}: Determine V_{oc} according to (27) and calculate the V_{mp} according to (10), respectively.
Step 3. Estimate P_{mp}: Calculate the potential P_{mp} of the PV system based on I_{sc} and V_{oc} according to (29).

$$P_{mp} = I_{mp}V_{mp} = k_v V_{oc} k_i I_{sc} \tag{29}$$

Step 4. Calculate d_{mp}: Calculate d_{mp} at potential MPP according to (9), which is later chosen as the starting reference point for the P&O method to find the actual duty cycle at the optimal MPP (d_{opt}). It is the obtained duty cycle value when the solution converges.
Step 5. Calculate the power at the optimal MPP (P_{opt}): Change the Δd value to observe the output power and voltage. Then, compare them to the respective reference values to locate the optimal MPP. The algorithm converges when Equation (30) is satisfied.

$$|\Delta P| = \frac{P_{i+1} - P_i}{P_i} \times 100\% \leq \varepsilon \tag{30}$$

If the constraint is not satisfied, the algorithm double-checks the voltage error ΔV according to (31) to adjust accordingly.

$$\Delta V = \frac{V_{i+1} - V_i}{V_i} \times 100\% \tag{31}$$

If $\Delta V \times \Delta P > 0$, reduce d to increase V; if $\Delta V \times \Delta P < 0$, increase d to reduce V.

Conversely, if expression (30) is satisfied, the algorithm converges and simultaneously checks the current deviation between two consecutive measurements to detect sudden changes in operating conditions according to (32). If the working environment is stable, the algorithm will continue to check the power deviation according to (30). Otherwise, the system restarts from the beginning.

$$|\Delta I| = \frac{I_{i+1} - I_i}{I_i} \times 100\% \leq \varepsilon \quad (32)$$

As a result, Figure 8 presents the flowchart of the proposed method.

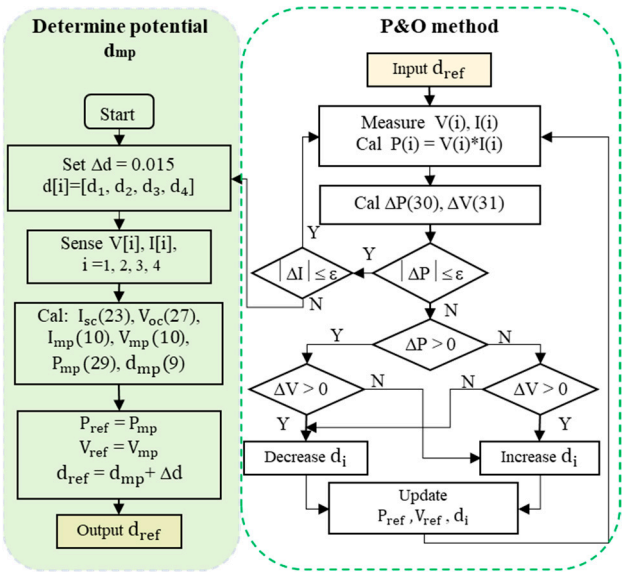

Figure 8. Algorithm flowchart of the proposed method.

4. Results and Discussion

The proposed solution is simulated and experimented with, evaluating its effectiveness in the following situations:

- Compare the d_{mp} value with the d_{opt} to highlight the effectiveness of quickly calculating the starting value compared to scanning the entire I(V) curve. Check the error power ($\Delta P\%$) between the initially estimated power (P_{mp}) and the P_{max} of each case. Further, the optimal convergence time (T_{opt}) and simulation efficiency (η_{opt}) between P_{opt} and P_{max} are also collected under different radiation and temperature conditions.
- Compare the T_{opt} and η_{opt} of the proposed solution with those of the traditional P&O [29], the VSSP&O [18], and the PSO [13] in the same operating conditions. This work demonstrates that the starting point of the proposed method plays an essential role in improving the speed and performance of the algorithm.
- Combine the Boost converter with the Chroma 62050H-600S PV simulator, which meets the PV parameters shown in Table 1, to experiment under the recommended operating conditions. The comparison results of the experiment convergence time (T_e) and MPPT efficiency (η_e) between output power (P_e) and P_{max} are also investigated and collected.

To collect evaluation data for the above proposals, simulation and test scenarios under different operating conditions are proposed in Table 9. Further, additional simulation and experiment cases are also tested, such as radiation and temperature increase or decrease together, or one parameter increasing and the other decreasing. This evaluates the proposed solution's response speed when working conditions change suddenly. Figure 9 shows the structure diagram of the proposed method in the PSIM environment.

Table 9. The proposed simulation and experimental cases.

No.	Radiation (W/m^2)	Temperature (°C)	P_{max} (W)
1	250	25	60.29
2	500	25	122.31
3	750	25	182.52
4	1000	25	240.2
5	1000	20	245.73
6	1000	30	234.77
7	1000	40	223.69
8	1000	50	212.57
9	1000	60	201.42
10	200	0	48.32
11	300	20	73.94
12	400	35	94.01
13	600	45	134.23
14	800	55	168.37
15	900	60	182.88

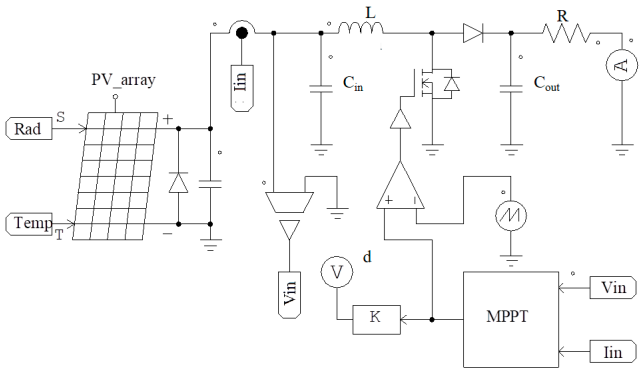

Figure 9. Schematic diagram of the proposed method.

4.1. Evaluate the Dmp and Pmp Values of the Proposed Algorithm

Figure 10 shows the output parameters under standard conditions, while Figure 11 compares the deviance between d_{mp} and d_{opt} in all proposed working conditions. The data pointed out that.

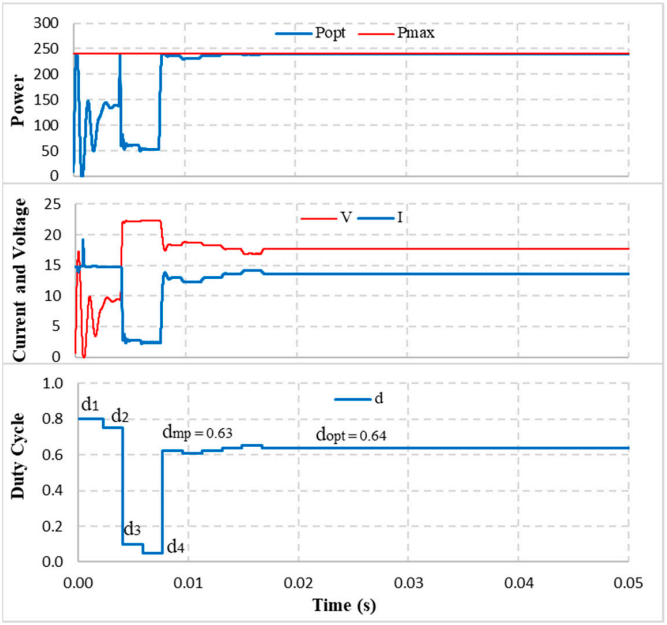

Figure 10. MPPT simulation under standard condition.

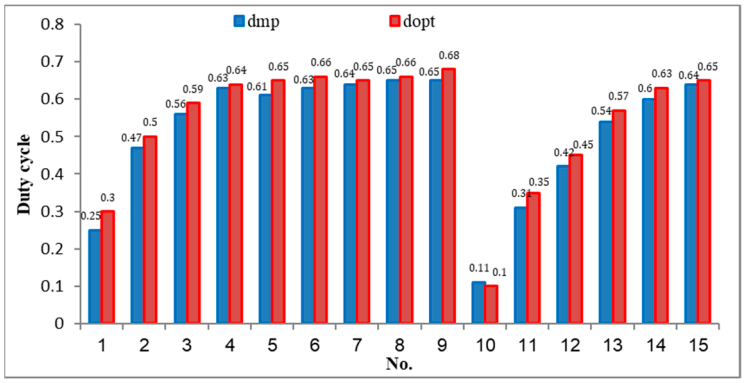

Figure 11. Compare the d_{mp} values with d_{opt}.

The calculated d_{mp} value at standard condition is 0.63 compared with 0.64 of the d_{opt}. Therefore, the solution only undergoes 5 adjustment steps to converge at d_{opt}. Further, the current and voltage waveforms are also stable at 0.0175 s after the d_{opt} value stops at 0.0168 s (Figure 10). The estimated power at d_{mp} is P_{mp} = 237.04 W compared to the P_{max} = 240.20 W, reaching 98.68%. The most significant calculation error is the No.1 because d_{mp} = 0.25 compared to d_{opt} = 0.3. Therefore, it undergoes eight adjustment steps to reach the convergence value. The most minor calculation error is in No.10. It takes only two adjustment steps to stabilize the system. This is also the case with the most significant power error (ΔP% = 2.9%). The minimum error is 1.03% (No.8). The average deviation for all tested cases is 1.83% (Table 10). The results show that d_{mp} always approximates the d_{opt} of the PV system under all proposed simulation conditions. Therefore, the adjustment iterations can be significantly reduced to reach the convergence value.

Table 10. Simulation results with the proposed solution.

No.	Number of Δd	P_{mp} (W)	ΔP%	P_{opt} (W)	η_{opt} (%)	T_{opt} (s)
1	8	58.78	2.5	60.01	99.54	0.022
2	6	119.9	1.97	122.3	99.99	0.019
3	6	178.91	1.98	182.39	99.93	0.019
4	5	237.04	1.32	240.19	99.99	0.019
5	6	239.98	2.34	245.45	99.89	0.019
6	6	229.91	2.07	234.15	99.74	0.019
7	5	219.85	1.72	223.46	99.9	0.017
8	5	210.39	1.03	212.5	99.97	0.017
9	6	197.66	1.87	201.29	99.94	0.019
10	2	46.92	2.9	48.28	99.91	0.01
11	5	72.79	1.69	73.7	99.68	0.017
12	6	92.28	1.81	94	99.99	0.018
13	4	132.78	1.08	134.18	99.96	0.015
14	6	164.61	2.12	168.27	99.94	0.019
15	5	180.94	1.06	182.86	99.99	0.016

4.2. Evaluate the Convergence Speed and Performance of the Proposed Algorithm

The output power under standard conditions is P_{opt} = 240.19 W compared to P_{max} = 240.20 W (MPPT efficiency is about η_{opt} = 99.99%). This is also the maximum performance, and that of the minimum is 99.54% (No.1). The output powers at the optimal MPP are always approximately P_{max}, the average efficiency being over 99.86% (Table 10).

Because the potential MPP is determined quickly, the solution has significantly reduced the number of iterations to increase the convergence speed to the optimal MPP. Specifically, the fastest speed is 0.01 s (No.10) due to only two adjustment steps. The slowest time is 0.022 s (No.1) with eight iterations, and the average speed is 0.018 s (Table 10).

Further, the proposed method's MPPT performance, convergence speed, and iterations are compared with classic P&O, VSSP&O, and PSO algorithms in the same operating conditions and initial starting position. That means the starting value of P&O and VSSP&O is d = 0.1, and that of the proposed solution is from the lowest (d = 0.05) to the highest (d = 0.8). Because it has to calculate starting point (d_{mp}) according to (9), this parameter ensures objectivity when comparing the convergence speed and performance of solutions. The adjustment step size of VSSP&O is $\Delta d = 0.4(dP/dV)$. It allows the duty cycle's step size to adjust automatically without setting the maximum and minimum values [12]. It is explained that if the initial searching point is far from the actual MPP location, the deviation dP/dV is large, so Δd increases. In contrast, when the searching position is close to MPP, this value is small, and Δd is automatically adjusted to decrease. The correction factor is 0.4 to ensure minimal error at the stable position. Because of the significant step size, converging at the MPP point will be challenging. Conversely, a small step size increases the search time. The step size for the remaining two solutions is Δd = 0.015. Finally, the main parameters of the PSO algorithm include the population size (N = 3), inertia weight (w = 0.25), cognitive coefficient (c_1 = 0.02), and social coefficient (c_2 = 0.5). In summary, the results show that:

Under standard operating conditions, the proposed solution only needs five adjustment steps from d_{mp} to converge. Meanwhile, the traditional P&O requires 36 iterations to scan the entire P(V) curve. Although the step size is adjusted, the VSSP&O also needs 16 adjustment steps to achieve the optimal MPP. With five adjustment steps for each individual, the PSO algorithm needs 15 calculations for all populations (Figure 12). In this case, the proposed solution has reduced the number of iterations compared to traditional P&O, VSSP&O, and PSO by 86%, 69%, and 67%, respectively. Therefore, the proposed method has the fastest convergence speed of 0.019 s. The traditional P&O takes 0.090 s, the VSSP&O is 0.020 s, and the PSO needs 0.037 s to reach the optimal position. This outstanding advantage helps the proposed solution get a fast convergence speed and is far ahead of the remaining algorithms.

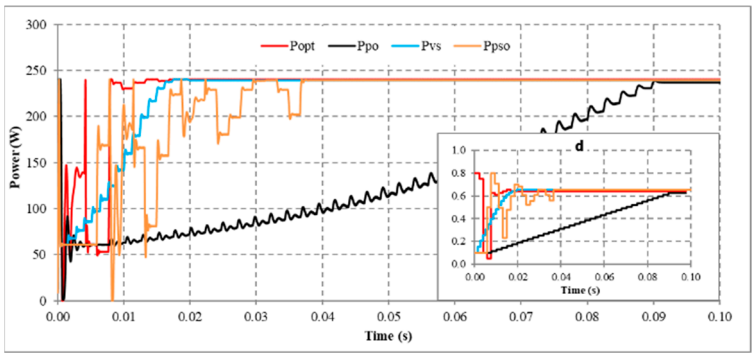

Figure 12. Output waveform under standard operating conditions (No.4).

The combined results in Table 11 show that the slowest convergence rate is the P&O algorithm. Which usually has a convergence time of more than 0.09 s. Its fastest speed in case of 10 is also 0.037 s. In contrast, the proposed solution is consistently outperforming in search speed. Although the convergence speed of VSSP&O and PSO is faster than that of P&O, it is still slower than that of the proposed solution in all survey cases. The average convergence speed of the proposed solution is 0.017 s. In contrast, that of P&O, VSSP&O, and PSO are 0.079 s, 0.022 s, and 0.38 s, respectively. Although the search times of the solutions are different, their MPPT performance is not significantly different. The average efficiency of MPO, P&O, VSSP&O, and PSO are 99.89%, 98.04%, 98.68%, and 99.26%, respectively (Table 11). The results show that the proposed solution always has better performance and convergence speed than the remaining solutions.

Table 11. Comparison between MPPT algorithms.

No.	Convergence Speed (ms)				Efficiency (η%)			
	MPO	P&O	VSSP&O	PSO	MPO	P&O	VSSP&O	PSO
1	22	51	22	38.0	99.54	99.39	99.57	99.83
2	19	80	21	37.0	99.99	99.58	98.98	99.99
3	19	88	20	36.8	99.93	99.61	99.31	99.93
4	19	90	20	37.7	99.99	98.33	99.65	99.29
5	19	91	19	37.5	99.89	99.19	98.96	99.29
6	19	91	22	37.0	99.74	98.12	99.97	98.28
7	17	92	25	37.1	99.90	96.98	97.49	98.69
8	17	91	25	37.2	99.97	94.87	97.43	99.85
9	19	91	25	37.3	99.94	93.41	97.34	99.24
10	10	37	16	38.0	99.91	99.96	98.99	99.75
11	17	52	24	35.6	99.68	96.16	96.70	99.43
12	18	67	25	37.3	99.99	98.62	99.70	99.95
13	15	86	25	37.1	99.96	99.69	99.89	99.02
14	19	91	25	53.6	99.94	99.59	99.60	98.98
15	16	91	24	37.5	99.99	97.03	96.73	97.50

Another scenario is proposed to simulate and compare the dynamic response between the proposed method and other algorithms. Assuming the system is working stably, the operating conditions change suddenly, and the proposed solution needs to redefine the parameters I_{sc} and V_{oc} to find d_{mp} again. During the survey and research, the authors found that the current value is affected more than the voltage value under changing operating conditions. Therefore, this study uses expression (32) to detect sudden changes in radiation and temperature. If the current difference between two consecutive measurements is insignificant, the system performs P&O iterations around the operating point. However, if there is a significant current error, the solution will immediately reset the search method from the first step. The simulation results are presented in Figures 13–16, while Figures 17–24 show the experimental scheme and the results obtained under the proposed operating conditions.

First, the system operates stably with a sudden increase in radiation and temperature at 0.20 s (Figure 13). The results show that P&O has the worst response when it only reaches 188.15 W (about 93.41%) compared to the maximum power of 201.42 W at 0.091 s. Further, VSSP&O can improve the speed significantly (0.025 s), but the efficiency is only 97.34% (about 196.06 W). The proposed solution responds the fastest to fluctuations in operating conditions and reaches approximately 99.94% at 0.017 s. While the PSO algorithm's efficiency is 99.24%, and the convergence time is 0.037 s.

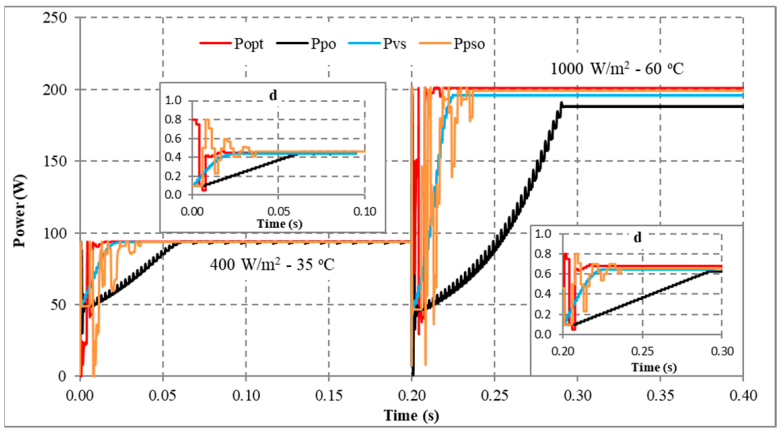

Figure 13. MPPT when solar irradiation and temperature increased.

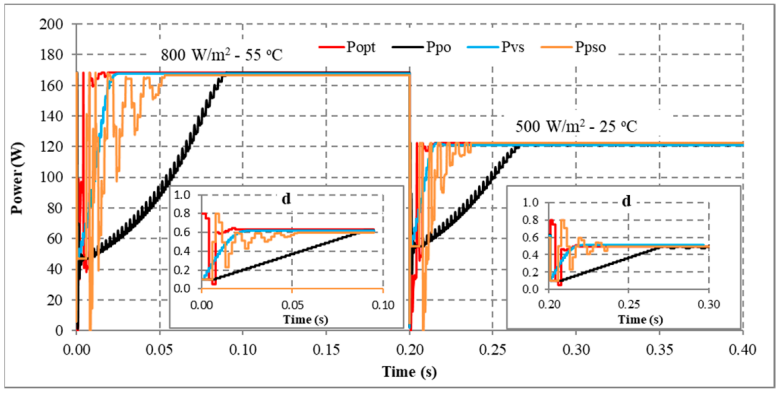

Figure 14. MPPT when solar irradiation and temperature decreased.

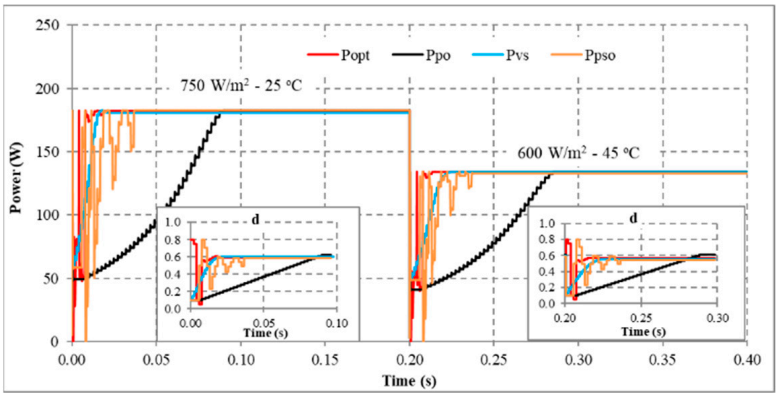

Figure 15. MPPT under the operating conditions from No. 03 to No. 13.

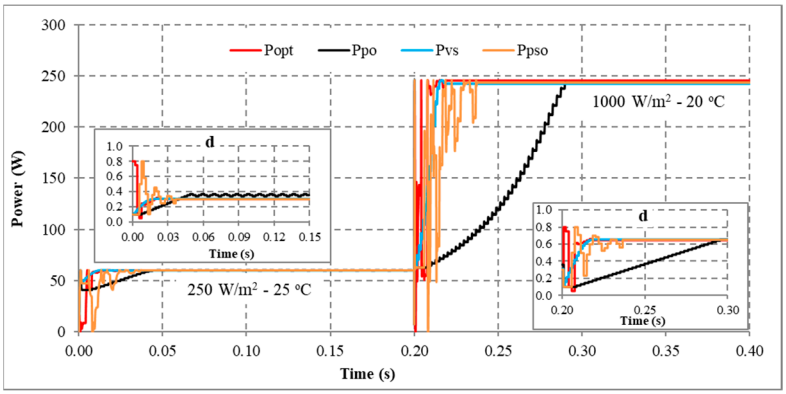

Figure 16. MPPT under the operating conditions from No. 01 to No. 05.

Second, when there is a sudden decrease in radiation and temperature in the system, the MPPT capabilities of the solutions are presented in Figure 14. The convergence speed of the proposed solution is an outstanding advantage. As soon as the operating condition changed at 0.20 s, it converged after 0.019 s. Meanwhile, P&O, PSO, and VSSP&O spent 0.080 s, 0.037 s, and 0.021 s, respectively. Although their performance is similar, the power and duty cycle waveforms of the traditional P&O algorithm are less stable than other solutions.

Third, the system works under stable conditions with dropped irradiation but increases temperature immediately at 0.2 s (Figure 15). The proposed solution responds fastest when converging at 0.015 s, and VSSP&O stops at 0.025 s. The P&O method has the slowest convergence speed of 0.086 s. While the PSO algorithm needs 0.0371 s. The efficiency of the solutions is the same at over 99%.

Finally, the system operates stably, then the radiation increases, and the temperature decreases at 0.2 s (Figure 16). The comparison results show that P&O responds the worst. Its convergence speed is 0.091 s compared to 0.017 s of the proposed method, 0.018 s of the VSSP&O, and 0.0375 s of the PSO.

In conclusion, the proposed solution always has a superior convergence speed compared to the remaining methods in the testing conditions. This advantage is due to an accurate prediction of the d_{mp} value. Furthermore, changing operating conditions makes the convergence speed less affected. Because the start point of the search loops (d_{mp}) always approximates the optimal value (d_{opt}). The average MPPT speed is about 0.017 s. Although VSSP&O has step size adjustment to increase MPPT speed, the average time is about 0.022 s. Further, the search time of the PSO algorithm is about 0.038 s. Finally, the traditional P&O method needs more time when the average convergence speed is about 0.079 s. The testing results show that the proposed solution has a high MPPT efficiency, stability in continuously changing operating conditions, and superior convergence speed compared to other algorithms.

4.3. Experiment with the Proposed Algorithm

The proposed solution has been experimented with on a PV Chroma 62050H-600S simulator (Figure 17). It is connected to the resistive load by a boost converter. The main parameters of the DC/DC converter can be calculated according to reference [30] and are listed in Table 12. The system is tested based on the operating conditions as previously simulated. The results under conditions such as attenuated radiation (Figure 18) and increased temperature (Figure 19), and both parameters differ from standard conditions (Figure 20), showing the most excellent MPPT efficiency can reach 99.38%. The lowest efficiency value is 92.87%, and the average efficiency value is over 96.56%. The fastest MPPT speed is 0.03 s, the slowest is 0.31 s, and the average time is about 0.14 s. Further, the duty cycle ranges from 0.26 to 0.74 when the operating environment changes with a wide fluctuation (Table 13). It is asymptotic from both sides of d = 0.5 to ensure there is not too much pressure on the switches compared to working at extremes.

Table 12. Specification of the boost converter.

Parameters	Value
Input voltage	20 V
Output voltage	70 V
Output power	300 W
Ripple voltage	5%
Ripple current	5%
Electrolytic capacitor C_{in}	1000 µF
Electrolytic capacitor C_{out}	100 µF
Inductor L	0.17 mH
Diode D	MUR3060PT
MOSFET	FDA50N50
Switching frequency	40 kHz
Sampling time	1.5 µs

Table 13. The experimental MPPT performance.

No.	Output Power P_e (W)	Experimental Performance η_e(%)	Duty Cycle	Convergence Speed T_e (s)
1	59.61	99.38	0.35	0.05
2	117.8	98.24	0.55	0.05
3	169.2	94.02	0.64	0.06
4	226.7	94.5	0.7	0.14
5	237.3	96.9	0.71	0.31
6	225	95.76	0.72	0.1
7	213.6	94.95	0.73	0.15
8	207	96.26	0.73	0.35
9	190.4	92.87	0.74	0.15
10	48.27	98.75	0.26	0.12
11	68.88	97.74	0.42	0.12
12	90.59	98.49	0.47	0.21
13	126.4	95.75	0.62	0.16
14	163.4	97.21	0.7	0.15
15	175.9	97.66	0.72	0.03

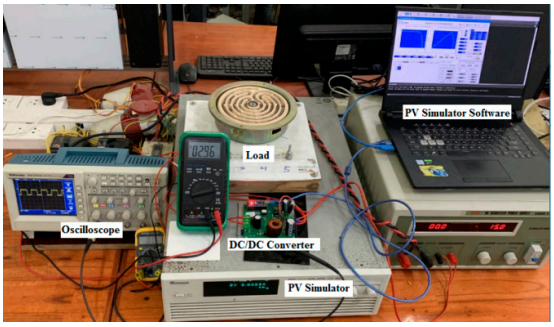

Figure 17. Experimental system setup.

Meanwhile, Table 14 shows that the proposed solution has superior convergence speed and performance compared to the latest studies. Its respective values are 0.010 s and 99.99%, respectively. Hybrid solutions can significantly reduce the search time, 0.016 s for the COA-FLC algorithm, but the performance is low, 99.83%. In contrast, intelligent algorithms can improve the performance to 99.99% (GWO), but its disadvantage is slow convergence, 0.190 s.

To test the dynamic response of the proposed solution when operating conditions change continuously, experimental scenarios are deployed, including a sudden increase in radiation and temperature (Figure 21), a decrease in radiation and temperature (Figure 22), a reduction in radiation but increase in working temperature (Figure 23), and finally increase in radiation but decrease in temperature (Figure 24). The time axis from 0 to 100 in Figures 21–24 represents a total simulation time of 20 s. While the system operates stably, the temperature and radiation parameters suddenly change at 10 s. The power waveform shows that when the radiation increases, the new MPP search time is about 1.0 s (Figure 21), and the efficiency is 94.68%. Meanwhile, stable speed and MPPT performance increase significantly in cases of radiation reduction. After only 0.7 s, the system stabilized and achieved an efficiency of 99.58% (Figure 22).

Table 14. Comparison of the algorithms.

Algorithms	Convergence Speed (s)	MPPT Efficiency (%)
MPO	0.01	99.99
PSO+INC [11]	0.0434	99.40
PSO+P&O [11]	0.0495	99.00
LBNS [12]	0.038	99.98
CSA [13]	0.48	99.90
GWO [13]	0.19	99.99
MIC [13]	0.14	99.90
PSO [13]	0.92	99.96
MC-P&O [14]	0.0375	99.54
BMCA [16]	0.096	96.70
COA-FLC [17]	0.016	99.83

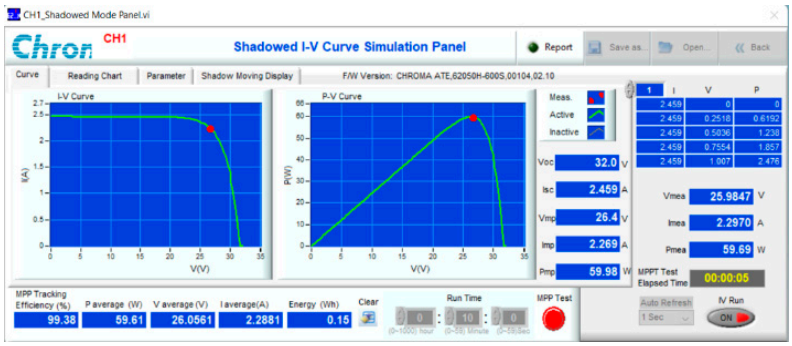

Figure 18. Experiment MPPT for No. 01.

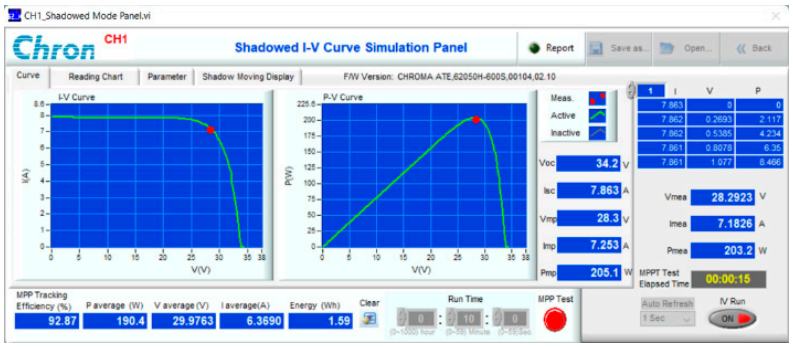

Figure 19. Experiment MPPT for No. 09.

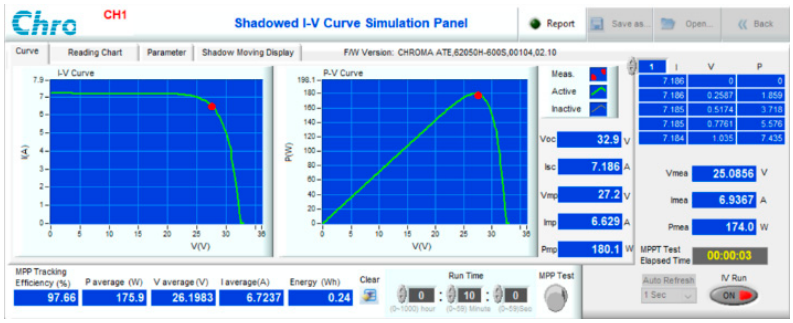

Figure 20. Experiment MPPT for No. 15.

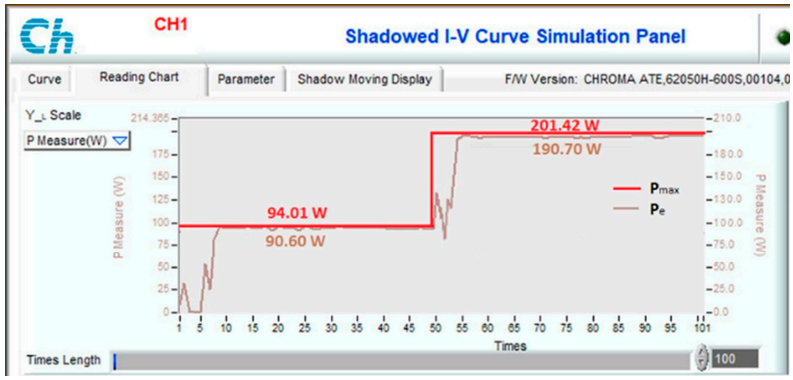

Figure 21. MPPT under the operating conditions from No. 12 to No. 09.

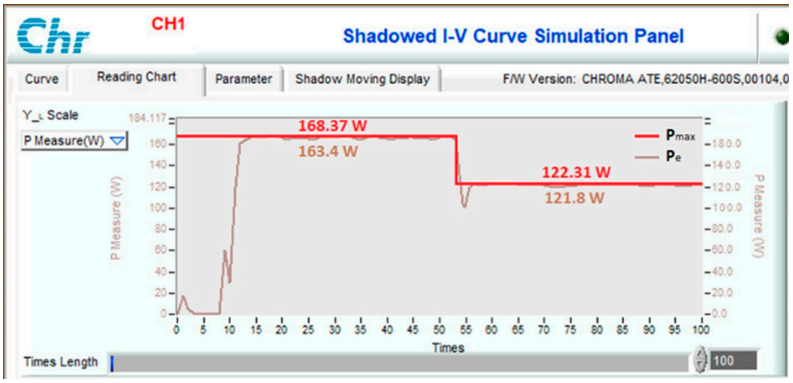

Figure 22. MPPT under the operating conditions from No. 14 to No. 02.

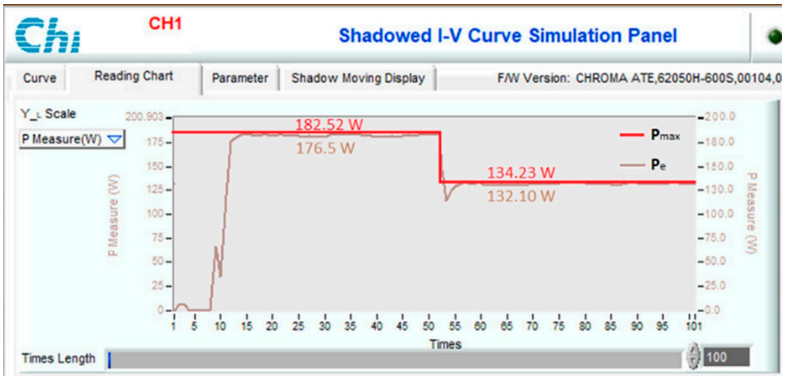

Figure 23. The power waveform under experimental conditions varies from No. 03 to No. 13.

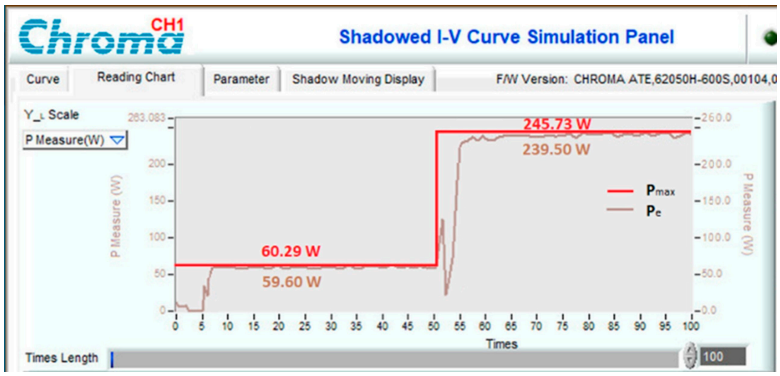

Figure 24. The power waveform under experimental conditions varies from No. 01 to No. 05.

The above results and discussions show that the proposed solution promises to bring convenient applications in a parallel configuration, where medium and small capacity power is used.

5. Conclusions

The paper presents an MPPT method for the photovoltaic system based on an MPO algorithm. The V_{oc} and I_{sc} are calculated directly based on the d value to quickly determine the starting point for the proposed solution. A comprehensive set of studies was conducted under standard test conditions and variations in irradiance and temperature. These studies aimed to thoroughly examine the system's performance under different scenarios. Both simulation results in the PSIM environment and experiment results on the Chroma model show that the proposed method's MPPT speed is always superior to other algorithms in the same testing conditions. It also has a faster dynamic response and more stability when PV systems operate in changing conditions (about 0.01 s). Further, the quick determination of the potential MPP value significantly limits the search space, reduces the computational burden, and improves performance. The comparison results show that the MPO solution has the highest dynamic rendition (approximately 100%). It has a high potential to be widely and reliably applied in applications with low voltage and power requirements. In addition, the article also presents the survey data of the I(V) characteristic curves of some typical PV modules, which can be used as a reference for further research on photovoltaic systems. The limitation of this study is that the proposed solution only applies to the parallel configuration of PV panels, which has only one extreme in all operating conditions. Therefore, the applied research to determine the global maximum power point in partial shade conditions with many local extremes will be the goal of the following studies by the authors.

Author Contributions: Writing—original draft, B.V.H. and N.T.L.; writing—review and editing, B.V.H. and T.V.A.; experiments, simulations, and surveys, B.V.H. and P.Q.K. All authors have read and agreed to the published version of the manuscript.

Funding: This research received no external funding.

Institutional Review Board Statement: Not applicable.

Informed Consent Statement: Not applicable.

Data Availability Statement: The data presented in this study is available on request from the corresponding author.

Conflicts of Interest: The authors declare no conflict of interest.

References

1. Iam, I.W.; Ding, Z.; Huang, Z.; Lam, C.S.; Martins, R.P.; Mak, P.I. A Flexible Rooftop Photovoltaic-Inductive Wireless Power Transfer System for Low Voltage DC Grid. *IEEE Access* **2023**, *11*, 51117–51132. [CrossRef]
2. Belhachat, F.; Larbes, C. Modeling, analysis and comparison of solar photovoltaic array configurations under partial shading conditions. *Sol. Energy* **2015**, *120*, 399–428. [CrossRef]
3. Pachauri, R.; Mahela, O.P.; Sharma, A.; Bai, J.; Chauhan, Y.K.; Khan, B.; Alhelou, H.H. Impact of Partial Shading on Various PV Array Configurations and Different Modeling Approaches: A Comprehensive Review. *IEEE Access* **2020**, *8*, 3028473. [CrossRef]
4. Kumar, M.; Panda, K.P.; Rosas-Caro, J.C.; Gonzalez, A.V.; Panda, G. Comprehensive Review of Conventional and Emerging Maximum Power Point Tracking Algorithms for Uniformly and Partially Shaded Solar Photovoltaic Systems. *IEEE Access* **2023**, *11*, 31778–31812. [CrossRef]
5. Pachauri, R.K.; Alhelou, H.H.; Bai, J.; Golshan, M.E.H. Adaptive Switch Matrix for PV Module Connections to Avoid Permanent Cross-Tied Link in PV Array System Under Non-Uniform Irradiations. *IEEE Access* **2021**, *9*, 45978–45992. [CrossRef]
6. Belhachat, F.; Larbes, C. A review of global maximum power point tracking techniques of the photovoltaic system under partial shading conditions. *Renew. Sustain. Energy Rev.* **2018**, *92*, 513–553. [CrossRef]
7. Sher, H.A.; Murtaza, A.F.; Noman, A.; Addoweesh, K.E.; Chiaberge, M. An intelligent control strategy of fractional short circuit current maximum power point tracking technique for photovoltaic applications. *J. Renew. Sustain. Energy* **2015**, *7*, 013114. [CrossRef]
8. Husain, M.A.; Jain, A.; Tariq, A.; Iqbal, A. Fast and precise global maximum power point tracking techniques for photovoltaic system. *IET Renew. Power Gener.* **2019**, *14*, 2569–2579. [CrossRef]
9. Baba, A.O.; Liu, G.; Chen, X. Classification and Evaluation Review of Maximum Power Point Tracking Methods. *Renew. Sustain. Energy Rev.* **2020**, *2*, 433–443. [CrossRef]
10. Başoğlu, M.E.; Çakır, B. Hybrid global maximum power point tracking approach for photovoltaic power optimizers. *IET Renew. Power Gener.* **2018**, *12*, 875–882. [CrossRef]
11. Ibrahim, M.H.; Ang, S.P.; Dani, M.N.; Rahman, M.I.; Petra, R.; Sulthan, S.M. Optimizing Step-Size of Perturb & Observe and Incremental Conductance MPPT Techniques. *IEEE Access* **2023**, *11*, 13079–13090.
12. Pervez, I.; Antoniadis, C.; Masound, Y. A Reduced Search Space Exploration Metaheuristic Algorithm for MPPT. *IEEE Access* **2022**, *10*, 26090–26100. [CrossRef]
13. Pamuk, N. Performance Analysis of Different Optimization Algorithms for MPPT Control Techniques under Complex Partial Shading Conditions in PV Systems. *Energies* **2023**, *16*, 3358. [CrossRef]
14. Morales, R.H.; Rohten, J.A.; Garbarino, M.N.; Muñoz, J.A.; Silva, J.J.; Pulido, E.S.; Espinoza, J.R.; Andreu, M.L. A Novel Global MPPT Method Based on Measurement Cells. *IEEE Access* **2022**, *10*, 97481–97494. [CrossRef]
15. Eltamaly, A.M. A novel musical chairs algorithm applied for MPPT of PV systems. *Renew. Sustain. Energy Rev.* **2021**, *146*, 111135. [CrossRef]
16. Eltamaly, A.M.; Rabie, A.H. A Novel Musical Chairs Optimization Algorithm. *Arab. J. Sci. Eng.* **2023**, *48*, 10371–10403. [CrossRef]
17. Zand, S.J.; Mobayen, S.; Gul, H.Z.; Molashahi, H.; Nasiri, M.; Fekih, A. Optimized Fuzzy Controller Based on Cuckoo Optimization Algorithm for Maximum Power-Point Tracking of Photovoltaic Systems. *IEEE Access* **2022**, *10*, 71699–71716. [CrossRef]
18. John, R.; Mohammed, S.S.; Zachariah, R. Variable step size Perturb and observe MPPT algorithm for standalone solar photovoltaic system. In Proceedings of the IEEE International Conference on Intelligent Techniques in Control, Srivilliputtur, India, 23–25 March 2017.
19. Abdulmawjood, K.; Alsadi, S.; Refaat, S.S.; Morsi, W.G. Characteristic Study of Solar PV Array Under Different Partial Shading Conditions. *IEEE Access* **2022**, *10*, 6856–6866. [CrossRef]
20. Angadi, S.; Yaragatti, U.R.; Suresh, Y.; Raju, A.B. System Parameter Based Performance Optimization of Solar PV Systems with Perturbation Based MPPT Algorithms. *Energies* **2021**, *14*, 2007. [CrossRef]
21. Al-Hussain, H.M.A.; Yasin, N. Modeling and simulation of a solar PV module for comparison of two MPPT algorithms (P&O & INC) in MATLAB/Simulink. *Indones. J. Electr. Eng. Comput. Sci.* **2020**, *18*, 666–677.

22. Motahhir, S.; Ghzizal, A.E.; Sebti, S.; Derouich, A. Proposal and Implementation of a Novel Perturb and Observe Algorithm using Embedded Software. In Proceedings of the 3rd International Renewable and Sustainable Energy Conference (IRSEC), Marrakech, Morocco, 10–13 December 2015.
23. Wang, Y.; Zhao, C.M.; Zhang, L. Adaptive High-Power Laser-Based Simultaneous Wireless Information and Power Transfer System with Current-Fed Boost MPPT Converter. *IEEE Photonics J.* **2021**, *13*, 8400111. [CrossRef]
24. Khezzar, R.; Zereg, M.; Khezzar, A. Modeling improvement of the four-parameter model for photovoltaic modules. *Sol. Energy* **2014**, *110*, 452–462. [CrossRef]
25. Lee, S.; Kim, P.; Choi, S. High Step-Up Soft-Switched Converters Using Voltage Multiplier Cells. *IEEE Trans. Power Electron.* **2013**, *28*, 3379–3387. [CrossRef]
26. Li, W.; He, X. Review of Nonisolated High-Step-Up DC/DC Converters in Photovoltaic Grid-Connected Applications. *IEEE Trans. Ind. Electron.* **2011**, *58*, 1239–1250. [CrossRef]
27. Orioli, A.; Gangi, A.D. A procedure to calculate the five-parameter model of crystalline silicon photovoltaic modules based on the tabular performance data. *Appl. Energy* **2013**, *102*, 1160–1177. [CrossRef]
28. Kota, V.R.; Bhukya, M.N. A novel linear tangents based P&O scheme for MPPT of a PV system. *Renew. Sustain. Energy Rev.* **2017**, *71*, 257–267.
29. Jusoh, A.; Sutikno, T.; Guan, T.K.; Mekhilef, S. A Review on Favourable Maximum Power Point Tracking Systems in Solar Energy Application. *Telecommun. Comput. Electron. Control* **2014**, *12*, 622.
30. Pendem, S.R.; Mikkili, S. Assessment of Cross-coupling Effects in PV String-integrated-converters with P&O MPPT Algorithm Under Various Partial Shading Patterns. *CSEE J. Power Energy Syst.* **2022**, *8*, 1013–1028.

Bài báo số 2: SCIE Q2 – IF 2.0

Van Hien Bui, Viet Anh Truong, Vu Lan Nguyen, Thanh Long Duong, *"Estimating the potential maximum power point based on the calculation of short-circuit current and open-circuit voltage,"* IET Power Electronics, 2024, pp: 1-20. https://doi.org/10.1049/pel2.12651

Received: 22 February 2023 | Revised: 21 December 2023 | Accepted: 31 December 2023

IET Power Electronics

DOI: 10.1049/pel2.12651

The Institution of Engineering and Technology WILEY

ORIGINAL RESEARCH

Estimating the potential maximum power point based on the calculation of short-circuit current and open-circuit voltage

Van Hien Bui[1,2] | Viet Anh Truong[2] | Vu Lan Nguyen[3] | Thanh Long Duong[4]

[1]Faculty of Mechanical – Electrical and Computer Engineering, School of Technology, Van Lang University, Ho Chi Minh City, Vietnam

[2]Faculty of Electrical and Electronics Engineering, HCMC University of Technology and Education, Ho Chi Minh City, Vietnam

[3]Department of International Relations, Nguyen Tat Thanh University, Ho Chi Minh City, Vietnam

[4]Faculty of Electrical Engineering Technology, Industrial University of Ho Chi Minh City, Ho Chi Minh City, Vietnam

Correspondence
Viet Anh Truong, Faculty of Electrical and Electronics Engineering, HCMC University of Technology and Education, Ho Chi Minh City 7000, Vietnam.
Email: anhtv@hcmute.edu.vn

Abstract

This paper presents a technique to quickly determine the potential maximum power point (MPP) of a photovoltaic system using the duty cycle (D) of the DC/DC converter. The proposed method depends on estimating the open-circuit voltage (V_{oc}) and short-circuit current (I_{sc}) values under different operating conditions. It is an adapted version derived from the conventional Perturb and Observe (P&O) algorithm, designed to restrict the search area for the MPP. The working conditions, including temperature variations, irradiance, or both, are simulated in the PSIM environment and experimented with a simulator with parameters satisfied according to the proposed operating conditions. The research objective of this study also involves operating under partially shaded conditions. When comparing the results of this research with those obtained from the traditional P&O method and the Variable Step Size Perturb and Observe (VSSP&O) approach, it becomes evident that the proposed solution excels in terms of both convergence speed and performance, particularly when operating under partial shade conditions. In addition, this study's methods of determining I_{sc}, V_{oc}, and D_{mp} can be widely applied in low-voltage and power systems.

1 | INTRODUCTION

Low voltage and power systems using solar energy rapidly increase in roof solar power, agriculture, traffic applications, electric vehicles, and even fashion, where the converters can extract the highest power from the photovoltaic (PV) system to charge electrical devices [1, 2]. Because of the limited installation area, they almost work under uniform or full shade conditions [3]. However, the operating conditions of the PV system change continuously and suddenly. Meanwhile, the PV systems must operate at the maximum power point (MPP), affected by operating conditions, to enhance power generation efficiency. Therefore, many techniques have been introduced to track the MPP of PV systems, from simple traditional methods to advanced solutions based on swarm optimization and hybrid approaches, which can combine the advantages of many algorithms.

For the traditional solution based on the $I(V)$ characteristic curve, the authors referenced in [4–7] have presented a method for approximating the maximum operating current, $I_{mp} = k_i I_{sc}$. This approach aims to enhance the performance of MPPT, reduce search times, and improve output stability. Nevertheless, the highest efficiency was 99.75% and did not indicate the convergence speed. Besides, some studies focus on the relation between the voltage at MPP (V_{mp}) and V_{oc} ($V_{mp} = k_v V_{oc}$) to obtain an efficiency of 97.39%, but the convergence speed is slow (about 5 s) [7, 9]. Generally, in these previous researches, I_{sc} and V_{oc} are constant under all operating conditions, which makes the results less accurate because they are directly affected by radiation and temperature. In the literature [7, 10], the authors used both parameters to improve the effectiveness of the proposed solution. However, the disadvantage of these solutions is that they have to sweep almost the entire characteristics curves of the PV system. Therefore, the convergence speed of the solution is limited; the fastest time is 1.35 s, and the average efficiency is about 99.5%.

For advanced solutions based on swarm optimization, a series of intelligent algorithms are mentioned in the literature [11], including the Cuckoo Search Algorithm (CSA), Particle Swarm Optimization (PSO), and Grey Wolf Optimization (GWO).

The highest convergence speed and efficiency belong to GWO, which are 0.19 s and 99.99%, respectively. The authors in [12] proposed a novel metaheuristic algorithm based on the Driving Training-Based Optimization (DTBO) algorithm for MPPT in the PV system. It has superior performance and convergence speed compared to other algorithms under the same operating conditions. However, the average convergence speed is about 1.11 s, and the mean efficiency is 98.22%. Most recently, a solution was introduced for the first time based on a game show called the musical chairs algorithm [13]. This algorithm can reduce errors by 40%, and search time is significantly reduced compared to other optimization algorithms. However, its adjusted version only achieved a best speed of 0.096 s. The outstanding effectiveness of these innovative solutions cannot be denied, but their disadvantages are that the process is complicated, high cost, and search speed needs to be significantly improved.

Meanwhile, the reference [14] introduces an innovative method based on the Cuckoo Optimization Algorithm and the Fuzzy Logic Controller (COA-FLC). This hybrid approach is designed to enhance the convergence speed, increase MPPT performance, and reduce fluctuations around the stable position. As a result of this synergy, the solution target is significantly improved, achieving an impressive 0.016 s, and the overall efficiency is 99.83%. Another hybrid solution employs a mixed MPPT method combining PSO and Perturb and Observe (P&O) [1]. This approach is tailored to improve system performance under varying irradiance conditions. However, while this hybrid solution achieves a commendable simulation efficiency of approximately 92%, the corresponding experimental efficiency is somewhat lower, at around 90%. With the hybrid MPPT algorithm, Monte–Carlo and Artificial Neural Network, the reference [15] introduced a new enhanced MPPT method achieves high efficiency and is robust to rapid irradiance change. This algorithm's MPPT performs is 95% and takes 0.28 s of tracking time under testing conditions. Also, in document [11], a solution combining Measurement cells with the traditional P&O algorithm has brought unexpected results. Although the efficiency is about 99.54%, the convergence speed can reach 0.0375 s. It shows that simple algorithms can also improve performance significantly based on appropriate improvements. However, increasing performance and convergence speed is challenging for all proposed algorithms.

To overcome the shortcomings of the previous solutions, this paper introduces a solution to quickly identify potential MPP locations to limit the search scope. Thereby not only increasing the convergence speed but also improving MPPT performance. Besides, some surveys related to the contributions of this study are also proposed to be included:

i Proposing a method to determine the I_{sc} according to operating conditions.
ii Proposing limits and methods for calculating I_{sc} values to limit calculation errors and reduce pressure on switches.
iii Calculate I_{sc} and V_{oc} based on duty cycle D within the survey range. Then, quickly determine the potential MPP location based on these parameters.

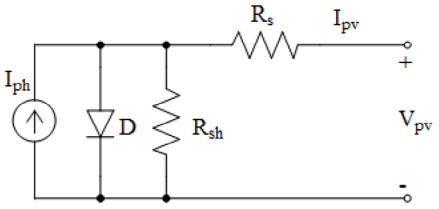

FIGURE 1 Single-diode model for PV cell. PV, photovoltaic.

iv Traditional P&O modification is based on adjusting the starting point position to increase convergence speed, reduce fluctuations around the stable operating point, and improve MPPT performance.

The findings indicate that in simulation, the maximum MPPT efficiency could achieve 100%, while in practical experimentation, it reached 99.95%. The convergence speed is also much higher than the other methods, which means that the MPP prediction can significantly reduce the search range in the proposed solution. Moreover, the kernel of this method is that instead of using the fixed input parameters, the solution uses actual I_{sc} and V_{oc} parameters according to operating conditions. It helps this method become more efficient and faster than other solutions.

2 | THE CHARACTERISTICS OF THE PV SYSTEM

A schematic diagram equivalent circuit, Figure 1, represents a standard PV cell [16, 17]. The correlation between its output parameters at the working point, described in Equation (1), while Equation (2), establishes the dependency of the light current (I_{ph}) on both the PV module surface temperature and solar radiation [16–22].

$$I_{pv} = I_{ph} - I_0 \left\{ e^{\frac{q\left(V_{pv}+I_{pv}R_s\right)}{AkT_c}} - 1 \right\} - \frac{V_{pv} + I_{pv}R_s}{R_{sh}} \quad (1)$$

$$I_{ph} = [I_{sc} + \alpha_i (T_c - T_{ref})] \frac{W}{W_{ref}} \quad (2)$$

At a homogeneous working condition, the output characteristics of the whole PV system and those of all PV cells are the same. Because the output power of a PV cell is relatively low, linking more PV cells into one PV module is necessary. In the same way, a PV system consists of multiple modules connected to achieve the required output voltage and power values. The relation between the PV system's output current and output voltage consists of N_s panels in series and N_p string in parallel, as in Equation (3) [21].

$$I = N_p I_{sc} - N_p I_0 \left\{ e^{\frac{q(V+N_s I R_s)}{N_s AkT}} - 1 \right\} - \frac{V + N_s I R_s}{N_s R_{sh}} \quad (3)$$

The operating conditions decide the MPP value of a PV system, which is lower than the MPP at the standard working condition (1000 W/m^2 and 25°C) [1, 18]. Under the actual

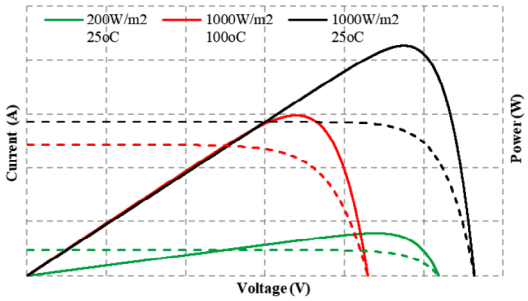

FIGURE 2 The characteristic curve changes according to the environment.

working environment, the increase of solar irradiation leads to its temperature increase, and vice versa, causing the MPP to depend on both parameters. However, the temperature change rate due to partial shading is slow, so the temperature of the PV system is considered uniform. Therefore, the I_{sc} and V_{oc} of the PV system depend more on radiation than temperature [7, 23] (Figure 2). In other words, the MPP coordinates depend on radiation and temperature parameters under uniform conditions but fluctuate more with radiation under partial shading conditions.

3 | THE PROPOSED METHOD

The P&O is a traditional algorithm that can operate effectively under uniform conditions. Its main rules depend on the perturbation of voltage. It means that an increase in voltage causes an increase in power, and the operating point will move towards the MPP. Otherwise, the PV system will move in the opposite direction. Change the duty cycle factor (ΔD) to control the voltage of the PV system to achieve the MPP. Each value of D corresponds to a power level (P) and voltage value (V). Figure 3 describes the flowchart of the traditional P&O algorithm [24]. However, its speed and performance depend on the starting position of the loops. If this point is far from the MPP, more iterations and more time are required to converge. Its other drawback is poor stability at the convergence point. The ΔD must be reduced to decrease this disadvantage, but the convergence speed is slow. That means if the starting point of the algorithm is close to the MPP, the number of iterations will reduce, so the MPPT speed is faster while increasing performance.

In conclusion, the starting position of the solution plays a core role in increasing the convergence speed and MPPT performance. On the other hand, P&O is ineffective under partially shaded conditions due to local extreme traps. Therefore, a suitable PV configuration for low voltage and power applications is needed to overcome this drawback.

3.1 | PV system configuration

Low-voltage power PV systems mainly operate under uniform conditions because of their small installation areas. Therefore,

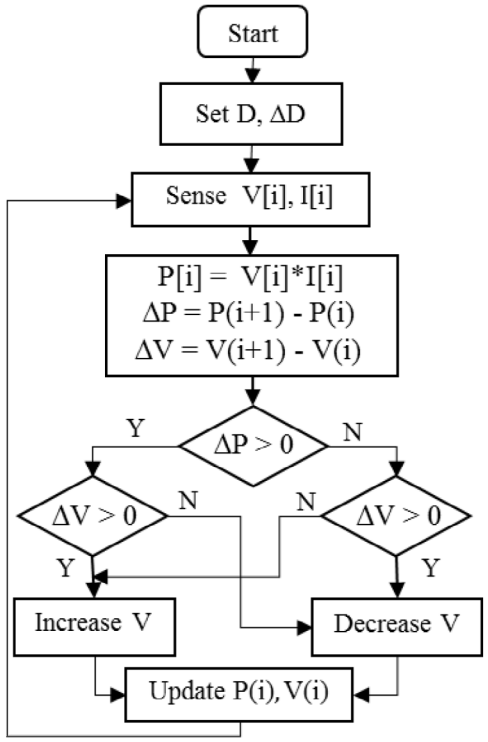

FIGURE 3 Flowchart of conventional P&O algorithm. P&O, perturb and observe.

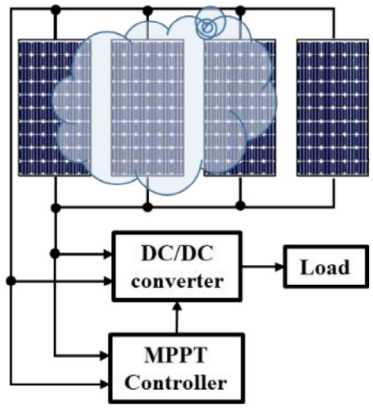

FIGURE 4 Schematic diagram of the PV control system in this research. PV, photovoltaic.

it is possible to exploit the advantages of the traditional P&O algorithm as analyzed above. However, partial shadows may still occur. To limit the disadvantages of the local MPP, the proposed PV system in this research has the configuration shown in Figure 4. The DC/DC converter connects the PV panel array to the load and is controlled by the MPPT to obtain maximum power. Parameters of PV module type MSX-60 given in Table 1 [25] are used for survey and research in the following proposed cases: In the first three cases, the system operates under uniform conditions with temperature or radiation different from standard conditions. The remaining were tested under partial shade conditions without the influence of temperature (Table 2). The

TABLE 1 Parameters of PV modules in this study [25].

	Monocrystalline		Polycrystalline			Thin-film	
Type of PV panel	**Shell SP77**	**Shell SQ150**	**SST 230–60P**	**Shell S70**	**MSX-60**	**GxB-340**	**Shell ST40**
I_{sc} (A)	4.8	4.8	8.52	4.5	3.8	9.3	2.68
V_{oc} (V)	21.7	43.4	36.7	21.2	21.1	51.4	23.3
I_{mp} (A)	4.4	4.4	7.83	4.12	3.5	8.5	2.41
V_{mp} (V)	17	34	29.4	17	17.1	40	16.6
μ_{Isc} (mA/°C)	2	1.4	3.83	2	3	0.06	0.35
μ_{Voc} (mV/°C)	−76	−161	−128	−76	−80	−0.27	−100
N_s	36	72	60	36	36	72	36
A	1.3	1.3	1.3	1.3	1.3	1.5	1.3
R_s	0.33	0.67	0.2	0.25	0.2	0.37	1.52
R_{sh}	236.7684	466.46	152.6382	311.8126	304.83	132.5701	284.1
I_0 (A)	6.957×10^{-8}	6.975×10^{-8}	9.4629×10^{-8}	9.8886×10^{-8}	9.094×10^{-8}	8.3667×10^{-8}	1.0264×10^{-8}

Abbreviation: PV, photovoltaic.

TABLE 2 The proposed cases for study.

	PV1		PV2		PV3		PV4	
No.	**W/m²**	**°C**	**W/m²**	**°C**	**W/m²**	**°C**	**W/m²**	**°C**
1	250	25	250	25	250	25	250	25
2	1000	60	1000	60	1000	60	1000	60
3	200	0	200	0	200	0	200	0
4	900	25	750	25	500	25	200	25
5	400	25	600	25	400	25	800	25
6	300	25	1000	25	300	25	1000	25
7	200	25	500	25	100	25	800	25
8	500	25	400	25	600	25	200	25

Abbreviation: PV, photovoltaic.

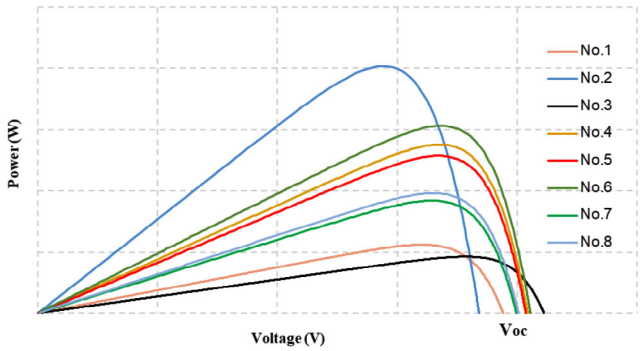

FIGURE 5 The $P(V)$ curves of some proposed operating cases.

proposed configuration' advantage is that it is only one extreme under all operating conditions. This is shown in Figure 5, which shows the $P(V)$ waveforms of some proposed operate cases.

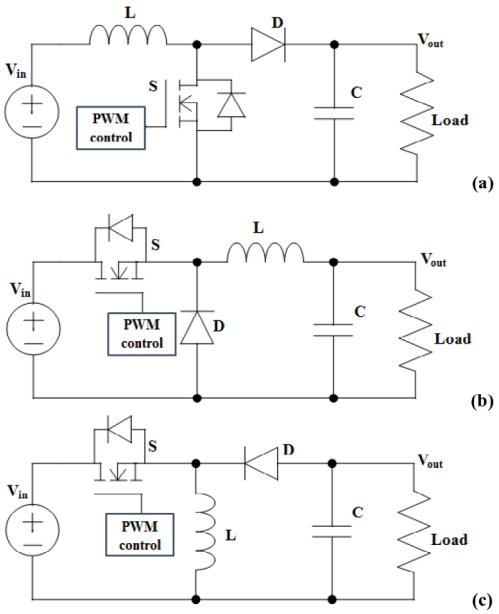

FIGURE 6 DC/DC converters: (a) Boost; (b) Buck; (c) Buck-boost.

3.2 | The DC/DC converter

The DC/DC converter is controlled by a pulse width modulator provided by the MPPT block to control the output voltage (V_{out}) according to the input voltage (V_{in}). Each pulse width value, called duty cycle D between 0 and 1, corresponds to an output voltage level. Equation (4) represents the relationship between D and the input and output voltages of the Boost converter, as in Figure 6a [26, 27].

$$\frac{V_{out}}{V_{in}} = \frac{1}{1-D} = K_{boost} \tag{4}$$

Conversely, the Buck converter can reduce output voltage with minimal power loss. Equation (5) demonstrates the connection between the input and output voltages in the Buck converter, depicted in Figure 6b [28].

$$\frac{V_{out}}{V_{in}} = D = K_{buck} \tag{5}$$

If there is a high fluctuation in the input voltage, the Buck-boost converter is an effective solution. It has both the buck function and the boost function. Its schematic is in Figure 6c, and the input and output voltage ratio is in Equation (6) [29].

$$\frac{V_{out}}{V_{in}} = \frac{D}{1-D} = K_{buck\text{-}boost} \tag{6}$$

If $D < 0.5$, then $V_{in} > V_{out}$; if $D > 0.5$, then $V_{in} < V_{out}$; and if $D = 0.5$, then $V_{in} = V_{out}$.

3.3 | The proposed method

The above analysis shows that a quick estimate of the potential MPP location is needed to improve the performance and MPPT speed in low voltage and power PV systems. This work helps the algorithm reduce step size without increasing search time. In other words, estimate the starting point for the MPPT process to minimize the number of iterations. This issue is considered based on the relationship between the load resistance (R_L), the operating resistance of the PV (R_{in}), and the ratio between the output (V_{out}) and input (V_{in}) voltage (K) of the DC/DC converter. Under simulation conditions, the input (P_{in}) and output (P_{out}) powers of the DC/DC converter can be considered constant when its losses are ignored. Then, the relationship between V_{in} and V_{out} is stated in Equation (7).

$$P_{in} = P_{out} \Rightarrow \frac{V_{in}^2}{R_{in}} = \frac{V_{out}^2}{R_L} \tag{7}$$

$$\Rightarrow R_L = K^2 R_{in} \tag{8}$$

The changing operating conditions affect the PV system's MPP position (Figure 2). However, at any point on the $I(V)$ characteristic curve, there will be a D value ($0 < D < 1$) corresponding to the output and input parameters of the DC/DC converter. Therefore, the input resistance at the MPP (R_{in_mp}) depends on the R_L and the working position of the DC/DC converter as Equation (9)

$$\begin{cases} R_{in\_mp} = \frac{V_{in\_mp}}{I_{in\_mp}} \\ R_L = K_{mp}^2 R_{in\_mp} \end{cases} \tag{9}$$

Besides, the fill factor (FF) of the PV system is determined according to Equation (10) [6, 8, 9].

$$FF = \frac{V_{mp} I_{mp}}{V_{oc} I_{sc}} = \frac{V_{mp}}{V_{oc}} \frac{I_{mp}}{I_{sc}} = k_v k_i \tag{10}$$

TABLE 3 The parameters of MSX-60 under survey conditions.

No.	V_{oc} (V)	I_{sc} (A)	V_{mp} (V)	I_{mp} (A)	k_v	k_i	P_{mp} (W)
1	19.41	3.76	16.06	3.52	0.83	0.94	56.54
2	18.41	15.38	14.19	14.19	0.77	0.92	201.36
3	21.12	2.76	17.80	2.60	0.84	0.94	46.28
4	20.36	8.83	16.79	8.38	0.82	0.95	140.90
5	20.36	8.27	16.75	7.68	0.82	0.93	128.69
6	20.55	9.73	16.88	9.06	0.82	0.93	153.03
7	19.97	6.01	16.48	5.58	0.83	0.93	91.98
8	20.05	6.39	16.47	5.96	0.82	0.93	98.15

FF value depends on PV type and operating conditions. Therefore, the proposed cases in Table 2 were used to determine the FF for PV module type MSX-60 to investigate the MPP location. The results are listed in Table 3.

The k_i values vary from 0.92 to 0.95, while k_v varies from 0.77 to 0.84. Therefore, the $k_i = 0.93$ and $k_v = 0.80$ are chosen in this study, respectively.

At any available D value, the measured values from this location are used to calculate the R_{in} and the K ratio according to Equation (11).

$$K^2 = \frac{R_L}{R_{in}}, \text{ with } R_{in} = \frac{V_{in}}{I_{in}} \tag{11}$$

Combining (9) and (11) gives the relationship between the ratio at MPP (K_{mp}) and K, as in (12)

$$K_{mp}^2 R_{in\_mp} = K^2 R_{in} \tag{12}$$

$$\Rightarrow K_{mp} = K\sqrt{\frac{V_{in}}{I_{in}}\frac{I_{in\_mp}}{V_{in\_mp}}} = K\sqrt{\frac{V_{in}}{I_{in}}\frac{0.93 I_{sc}}{0.8 V_{oc}}} \tag{13}$$

From Equation (13), the K_{mp} value can be determined based on the measured current and voltage parameters of any duty cycle D. Then, the value of D_{mp} will be calculated depending on the DC/DC converters according to Equations (4) to (6). Therefore, to estimate the potential MPP location, it is necessary to accurately calculate the I_{sc} and V_{oc} values for Equation (13).

In conclusion, calculating D_{mp} following FF will quickly locate the potential P_{mp} position. However, to increase the performance and stability around the working point of the algorithm, several iterations of the P&O algorithm should be used to determine the convergence value (D_{con}) according to the operating conditions.

3.3.1 | Identifying I_{sc} of PV module

In conventional DC/DC converters, if duty cycle D is the time the current operates across the switches, then $(1-D)$ is the time to act on the diode. The extreme duty cycle stresses the switches in high-output voltage applications, increasing the current ripple

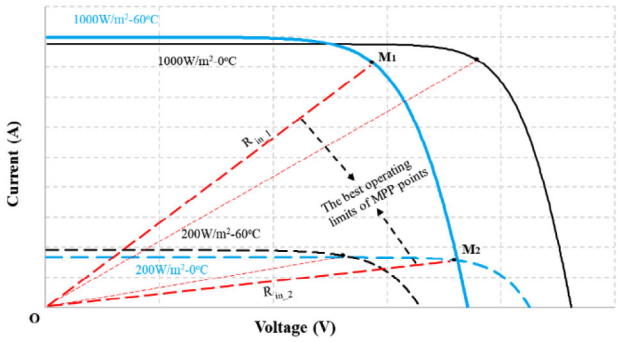

FIGURE 7 The $I(V)$ curves in the operating limit of PV. PV, photovoltaic.

and reducing the system's stability. In these cases, the high step-up topologies or step-down structure are applied to limit stress on switches, reduce ripple continuous input current, smooth switching of diodes, substantial voltage gain at a low duty cycle, low cost, and improve power efficiency [30–32]. Alternatively, the converters should be designed to operate stably around the value $D = 0.5$.

Relationship between K_{mp} *under various working conditions*

Investigate the parameters of the PV module MSX-60 under operating conditions where the PV system can generate power, as shown in Figure 7. The limit resistance values from $R_{\text{in-1}}$ to $R_{\text{in-2}}$ correspond to the working range from best to worst conditions. That is, within the experiment conditions, the operating resistance of the PV system is $R_{\text{in-1}} < R_{\text{pv}} < R_{\text{in-2}}$. In other words, the D value changes from D_{mp1} to D_{mp2} at the MPPs from M_1 to M_2. Therefore, the K_{mp} ratios also vary from K_{mp1} to K_{mp2}, respectively, and depend on the DC/DC converter. The above analysis shows that the duty cycles are preferably equal to or near 0.5. That means the values of D_{mp1} and D_{mp2} should differ from 0 or 1 at a steady working state [23]. To determine the safe working range of D_{mp} values, the relationship between the load resistance R_{L} and the K ratio at these MPPs is based on Equation (9) as follows:

$$R_L = \frac{V_{\text{in\_mp1}}}{I_{\text{in\_mp1}}} K_{\text{mp1}}^2 = \frac{V_{\text{in\_mp2}}}{I_{\text{in\_mp2}}} K_{\text{mp2}}^2 \tag{14}$$

Combining (10) and (14) gives (15) as follows:

$$\frac{k_{\text{v}} V_{\text{oc\_1}}}{k_i I_{\text{sc\_1}}} K_{\text{mp1}}^2 = \frac{k_{\text{v}} V_{\text{oc\_2}}}{k_{\text{i}} I_{\text{sc\_2}}} K_{\text{mp2}}^2 \tag{15}$$

Because of the PV system's characteristic curves being affected by radiation and temperature, Equation (15) can be rewritten as Equation (16)

$$\frac{K_{\text{mp1}}}{K_{\text{mp2}}} = \sqrt{\frac{\left(V_{\text{oc}_o} - \alpha_{\text{v}}(T_2 - 25)\right)}{W_2\left(I_{\text{sc}_o} + \alpha_{\text{i}}(T_2 - 25)\right)} \frac{W_1\left(I_{\text{sc}_o} + \alpha_{\text{i}}(T_1 - 25)\right)}{\left(V_{\text{oc}_o} - \alpha_{\text{v}}(T_1 - 25)\right)}} \tag{16}$$

Substitute the PV module MSX-60 parameters into Equation (16) to figure out the relationship between K_{mp} ratios. In particular, radiation and temperature in the survey range are from $W_1 = 1000$ W/m^2 to $W_2 = 200$ W/m^2 and $T_1 = 60°$C to $T_2 = 0°$C, respectively. The I_{sc0} and V_{oc0} are short-circuit current and open-circuit voltage in standard conditions.

TABLE 4 The best region of D.

	Boost		Buck		Buck-boost	
Type of PV panel	D_{mp1}	D_{mp2}	D_{mp1}	D_{mp2}	D_{mp1}	D_{mp2}
MSX-60	0.29	0.71	0.29	0.71	0.39	0.61
Shell SP75	0.36	0.64	0.36	0.64	0.43	0.57
Shell SQ150	0.33	0.67	0.33	0.71	0.41	0.59
SSt 230–60P	0.34	0.66	0.34	0.67	0.42	0.58
Shell S70	0.36	0.64	0.36	0.64	0.43	0.57
GxB-340	0.31	0.69	0.31	0.69	0.40	0.66
Shell ST40	0.41	0.60	0.41	0.60	0.45	0.54

Abbreviation: PV, photovoltaic.

$$K_{\text{mp2}} = 2.46 K_{\text{mp1}} \tag{17}$$

Equation (17) shows that under the testing conditions, the K_{mp} values at the lowest radiation and temperature conditions are 2.46 times higher than those at the highest. That means, within this range, the D_{mp} values will ensure the best operating modes of the DC/DC converters.

The operating range of the D_{MP}

The relationship between K_{mp1}, K_{mp2}, and D_{mp1}, D_{mp2} depends on the DC/DC converters, as shown in Equations (4) to (6). As discussed above, the DC/DC converters operate most efficiently when they satisfy the Equation (18)

$$D_{\text{mp1}} - 0.5 = 0.5 - D_{\text{mp2}} \tag{18}$$

From (4), (17), and (18), one may get the values of D_{mp1} and D_{mp2} as in (19) for the Boost converter.

$$\begin{cases} D_{\text{mp2}} - 0.5 = 0.5 - D_{\text{mp1}} \\ \dfrac{1}{1 - D_{\text{mp2}}} = 2.46 \dfrac{1}{1 - D_{\text{mp1}}} \end{cases} \tag{19}$$

Solve (19) to get $D_{\text{mp1}} = 0.29$ and $D_{\text{mp2}} = 0.71$, respectively. This range [0.29; 0.71] is the best operating limit for the PV module MSX-60 when connected to the Boost converter. In the same way, when this PV links to the Buck and Buck-boost converters, the achieved limit is [0.29; 0.71] and [0.39; 0.61], respectively (Table 4).

Similarly, determine the best operating limit of D for all the PV modules suggested in Table 1. Each PV module associated with a DC/DC converter type has a different operating limit range. Thus, the working variation from M_1 to M_2 corresponds to the change from D_{mp1} to D_{mp2}. Summarize the data presented in Table 4. The data shows that, within the survey scope, each PV module operating with a different DC/DC converter

will have the best operating range of duty cycle D. It ensures the best performance and safest for switches.

Parameters at 0.2V$_{oc}$

Assume that MPPs that operate in the D_{mp} region, listed in Table 4, are the best for the PV system. To determine the I_{sc} value, the authors in [33] have proposed a working point A(V_A, I_A) on the characteristic $I(V)$. Here, the voltage at A is $V_A = 0.2V_{oc}$, and the short-circuit current is $I_{sc} = I_A$. By substituting the coordinates of A($0.2V_{oc}$, I_{sc}) and MPP($0.8V_{oc}$, $0.93I_{sc}$) into (13), the relationship between K_A and K_{mp} is presented as in (20)

$$K_A = 2.074K_{mp} \tag{20}$$

Substitute (4) into (20) to determine the relationship between D_A and D_{mp}, as shown in (21)

$$\frac{1}{1-D_A} = 2.074\frac{1}{1-D_{mp}} \tag{21}$$

For PV module MSX-60 linked to Boost converter, the D_{mp} value ranges from $D_{mp1} = 0.29$ to $D_{mp2} = 0.71$ (Table 4), and the D_A calculated from Equation (21) is $D_{A1} = 0.65$ and $D_{A2} = 0.86$, respectively. Similarly, Table 5 summarizes of the calculation results of the D_A value at $0.2V_{oc}$ for the Buck and Buck-boost converters.

The D_{A1} and D_{A2} are the duty cycles at $0.2V_{oc}$ on the $I(V)$ curve under the operating states from M_1 to M_2, respectively (Figure 7). Due to solar radiation and temperature changes, D_A should be the maximum of D_{A1} and D_{A2} to ensure an accurate I_{sc} measurement under all testing conditions. For example, for the PV module MSX-60 connected to the Boost converter, since $D_{A1} = 0.65$, $D_{A2} = 0.86$, the $D_A = \max(D_{A1}, D_{A2}) = 0.86$ is used to measure I_{sc}. Meanwhile, for the Buck and the Buck-boost converters, D_A should be 1.48 and 0.76, respectively. These parameters represent the following problems:

- For Boost and Buck-boost converters, the D value is used to measure I_{sc} is within the operating limit ($0 < D < 1$), which can be used to calculate I_{sc} from a position with a voltage that approximates $0.2V_{oc}$.
- However, the Buck converter has no compatible operating range of D ($D > 1$). So, it is hard to calculate I_{sc} exactly from this value.
- A more immense value of D will put more pressure on the converter switches. Furthermore, finding a suitable D value for the Buck converter to reduce error I_{sc} calculation at the voltage of $0.2V_{oc}$ is challenging.

In contrast, the slope of the $I(V)$ characteristic relies on the currents passing through the diode and the resistance R_{sh}, as indicated in Equation (1). Analyzing these parameters aids in identifying the boundary point between the linear and non-linear segments on the $I(V)$ curve of the PV system. This boundary range facilitates a more precise calculation of I_{sc} value while lowering the D value to alleviate stress on the controller switches.

TABLE 5 The duty cycle at $0.2V_{OC}$ and $0.4V_{OC}$.

	$0.2V_{oc}$		$0.4V_{oc}$	
Types of PV panel	D_{A1}	D_{A2}	D_{A1}	D_{A2}
Boost converter				
MSX60	0.65	0.86	0.51	0.80
Shell SP-75	0.69	0.82	0.56	0.75
Shell SQ-150	0.67	0.84	0.54	0.78
SST 230–60P	0.68	0.83	0.55	0.77
Shell S70	0.69	0.83	0.56	0.75
GxB-340	0.66	0.85	0.52	0.79
Shell ST40	0.71	0.81	0.59	0.72
Buck converter				
MSX60	0.60	1.48	0.42	1.04
Shell SP-75	0.74	1.33	0.52	0.94
Shell SQ150	0.68	1.42	0.48	1.00
SST 230–60P	0.70	1.39	0.49	0.98
Shell S70	0.74	1.34	0.52	0.95
GxB-340	0.64	1.44	0.45	1.01
Shell ST40	0.85	1.25	0.60	0.88
Buck-boost converter				
MSX60	0.57	0.76	0.48	0.69
Shell SP-75	0.61	0.73	0.52	0.66
Shell SQ150	0.59	0.75	0.50	0.68
SST 230–60P	0.60	0.75	0.51	0.67
Shell S70	0.61	0.74	0.52	0.66
GxB-340	0.58	0.75	0.49	0.68
Shell ST40	0.63	0.71	0.54	0.64

Proposed operating point 0.4V$_{oc}$

The equivalent circuit (Figure 1) and the above analysis show that the calculating I_{sc} at $0.2V_{oc}$ will increase error as the currents on the diode and R_{sh} rise. To assess accurately their effect on the calculated I_{sc} value, it is necessary to consider the PV output voltage varying from 0 to V_{oc} as follows:

$$V_{pv} = x \times V_{oc}, \text{where } 0 \le x \le 1. \tag{22}$$

Substitute Equation (22) into (1) to obtain Equation (23)

$$I_{pv} = I_{sc} - I_0\left\{e^{\frac{q\left(xV_{oc}+I_{pv}R_s\right)}{AkT_c}} - 1\right\} - \frac{xV_{oc} + I_{pv}R_s}{R_{sh}} \tag{23}$$

Considering that $I_{pv}R_s << V = x \times V_{oc}$, then the current across the diode and the current on the resistor R_{sh} are expressed by (24) and (25), respectively.

$$I_D = I_0\left\{e^{\frac{qxV_{oc}}{AkT_c}} - 1\right\} \tag{24}$$

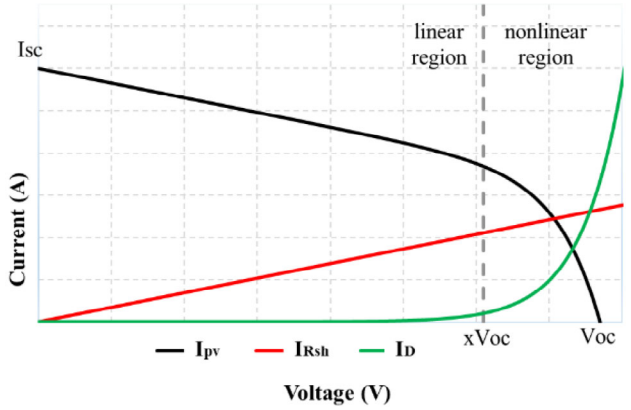

FIGURE 8 Working regions of PV module characteristic curves. PV, photovoltaic.

$$I_{Rsh} = \frac{xV_{oc}}{R_{sh}} \tag{25}$$

Equations (24) and (25) vary with V_{oc}, but the non-linearity of I_{pv} depends on I_D (Figure 8). In the range from 0 to V_{oc}, a value $V_{pv} = x \times V_{oc}$ ($x = 0$ to 1) causes the I_D and I_{pv} currents to begin to be non-linear. It is also the position where the difference between I_{Rsh} and I_D reaches its maximum value.

Thus, to determine the linear zone, it is necessary to calculate the x value so that expression (26) reaches its maximum value.

$$f(x) = I_{Rsh} - I_D = \frac{xV_{oc}}{R_{sh}} - I_0\left\{e^{\frac{qxV_{oc}}{AkT_c}} - 1\right\} \tag{26}$$

$$=> f(x) = ax - b(e^{cx} - 1) \tag{27}$$

where $a = \frac{V_{oc}}{R_{sh}}$; $b = I_0$; $c = \frac{qV_{oc}}{AkT_c}$

$$\frac{f(x)}{dx} = 0 => a - bce^{cx} = 0 => x = \frac{1}{c}\ln\left(\frac{a}{bc}\right) \tag{28}$$

Due to $\frac{f(x)}{(dx)^2} = -bc^2e^{cx} < 0$
So $f(x) = f(\max)$ at

$$x = \frac{1}{c}\ln\left(\frac{a}{bc}\right) \tag{29}$$

The $I(V)$ curve is considered linear when the operating point has a voltage $V_{pv} = [0 \text{ to } x]$. Linearity is higher when this point moves towards 0 and vice versa. Therefore, to eliminate the non-linear regions within the calculation range, the V_{pv} should be smaller than λ*x ($\lambda = 0$ to 1). To ensure safety and accuracy, the λ value is 0.6 in this research. Because of the enormous value of λ, the survey section may not be linear; while λ is small, the output current is large, causing pressure on the switches. That means the linear zone is determined when expression (30) is satisfied.

$$x = 0.6\frac{1}{c}\ln\left(\frac{a}{bc}\right) \tag{30}$$

TABLE 6 The x, k_i, and k_v values of the PV modules.

Types of PV panel	λ*x	k_i	k_v
MSX-60	0.47	0.93	0.8
Shell SP75	0.46	0.91	0.79
Shell SQ150	0.48	0.91	0.78
SSt 230–60P	0.49	0.92	0.8
Shell S70	0.48	0.94	0.79
GxB-340	0.49	0.92	0.78
Shell ST40	0.5	0.91	0.75

Abbreviation: PV, photovoltaic.

Table 3 shows that the k_v value in case No. 2 is the smallest, so its linear limit ratio is the smallest. Therefore, it was chosen to investigate the limit point between the linear and non-linear areas on the graph, as shown in Figure 8. Substituting the values of MSX-60 into Equation (30), the calculated x value is 0.47.

A similar survey was conducted for the PV modules listed in Table 1 to determine the linear range. The investigation results are presented in Table 6. Besides, their k_i and k_v values were also investigated under the same proposed operating conditions.

These data show that $V_{pv} \leq 0.47V_{oc}$ (for MSX-60), the slope of the $I(V)$ characteristic curve only depends on the value of the current across R_{sh}, and it is always linear. So, $V_{pv} = 0.4V_{oc}$ is used as the linear region limit point for all PV modules in this study. Where the effect of current on the diode is negligible, and Equation (1) will become Equation (31)

$$I_{pv} = I_{sc} - \frac{V_{pv} + I_{pv}R_s}{R_{sh}} \text{ or } I_{pv} = I_{sc} - \frac{V_{pv}}{R_{sh}} \tag{31}$$

The coordinates of point A($0.4V_{oc}$, I_{sc}) are substituted into Equation (12) to get the relationship between the K_A and K_{mp}, as presented in Equation (32).

$$K_A = 1.46K_{mp} \tag{32}$$

Thus, if $i_A = 2.074\ K_{mp}$ at $0.2V_{oc}$, as in Equation (20), then at $0.4V_{oc}$, its value is $i_A = 1.46K_{mp}$.

Substitute Equation (4) into Equation (32) to calculate the relationship between D_A and D_{mp} at $0.4V_{oc}$ for PV module MSX-60; the results are $D_{A1} = 0.51$ to $D_{A2} = 0.8$, respectively. This value is smaller than $D_{A1} = 0.65$ to $D_{A2} = 0.86$ at $0.2V_{oc}$. Similarly, calculate K_A and D_A for all PV modules and converters at A($0.4V_{oc}$, I_{sc}). A summary of survey data for the PV modules in this study, as presented in Table 5, indicates that:

- At $0.4V_{oc}$, its D value is smaller than at $0.2V_{oc}$ in all cases.
- For Boost and Buck-boost converters, the D value at $0.4V_{oc}$ is within the allowable operating limits of the DC/DC converters. Thus, the output current (I_{pv}) and I_{sc} can be measured based on these regions.

If R_{sh} is determined and kept constant, the I_{sc} can be calculated based on the schematic diagram (Figure 1) as shown in

TABLE 7 The I_{sc} and V_{oc} of PV modules under proposed survey cases.

		Cases study							
Types of PV panel		**1**	**2**	**3**	**4**	**5**	**6**	**7**	**8**
MSX-60	I_{sc} (A)	3.76	15.4	2.76	8.83	8.27	9.73	6.01	6.39
	V_{oc} (V)	19.41	18.4	21.1	20.36	20.36	20.55	19.97	20.05
Shell SP-75	I_{sc} (A)	20.15	19.2	21.8	21.16	21.1	21.26	20.68	20.78
	V_{oc} (V)	4.75	19.4	3.5	11.16	10.44	12.35	7.6	8.07
Shell SQ-150	I_{sc} (A)	40.08	38.2	43.5	42.09	41.96	42.31	41.14	41.34
	V_{oc} (V)	4.74	19.2	3.65	11.13	10.43	12.32	7.58	8.06
SST 230–60P	I_{sc} (A)	33.94	32.4	36.7	35.63	35.52	35.82	34.85	35
	V_{oc} (V)	8.41	34.2	6.34	19.76	18.49	21.86	13.45	14.29
Shell S70	I_{sc} (A)	19.54	18.5	21.3	20.55	20.48	20.67	20.08	20.17
	V_{oc} (V)	4.43	17.8	3.34	10.41	9.74	11.51	7.08	7.53
GxB-340	I_{sc} (A)	47.5	47	50.2	49.81	49.67	50.05	48.71	48.95
	V_{oc} (V)	9.16	37.5	6.72	21.52	20.15	23.81	14.65	15.57
Shell ST40	I_{sc} (A)	21.61	20.8	23.2	22.58	22.53	22.67	22.08	22.22
	V_{oc} (V)	2.64	10.6	2.07	6.2	5.8	6.86	4.22	4.48

Abbreviation: PV, photovoltaic.

Equation (33)

$$I_{sc} = I_{pv} + \frac{V_{pv}}{R_{sh}} \tag{33}$$

However, the R_{sh} value can be affected by temperature, and its current increases as V_{pv} moves towards V_{oc}. This means that the slope of the I_{Rsh} curve increases. It is the cause of increased deviance in calculating the I_{sc} value at $0.4V_{oc}$ or $0.2V_{oc}$. Thus, if applying $V_A = 0.2V_{oc}$ to calculate I_{sc}, the error is small, but D is large (the DC/DC converters' performance quality is affected). Conversely, at $V_A = 0.4V_{oc}$, the D value is small, but the error increases.

To overcome this drawback, the coordinates of two points in the linear region (with voltage less than $0.4V_{oc}$) are used to determine the I_{sc}. This will ensure a more accurate calculation of I_{sc} because it is determined by linear extrapolation from the equation of the line containing the I_{sc}. Besides, the D values in the $0.4V_{oc}$ limit are smaller (Table 5). It will put less pressure on the switches of the converters than the $0.2V_{oc}$. Moreover, Table 5 also shows that applying the $0.4V_{oc}$ parameter will ensure that the D values of the converters are within the allowable range of the DC/DC converters.

This method considers two arbitrary operating points within the voltage limit of less than $0.4V_{oc}$, denoted as $P_1(V_1, I_1)$ and $P_2(V_2, I_2)$, the equation of the line passing through these points, as expressed in Equation (34)

$$I = \frac{I_2 - I_1}{V_2 - V_1}V + \left[I_1 - \frac{I_2 - I_1}{V_2 - V_1}V_1\right] \tag{34}$$

From Equation (34), the I_{sc} value is calculated as follows:

$$I_{sc} = I_1 - \frac{I_2 - I_1}{V_2 - V_1}V_1 \tag{35}$$

To calculate I_{sc} at $0.2V_{oc}$ for a Buck converter, the duty cycle value is 1.48, which is impossible. Therefore, the proposed solution calculated at $0.4V_{oc}$ is 1.04. Surveys for all PV modules in Table 5 show that the calculation range is from 0.88 to 1.04 for Buck converter, so choose $D = 1$ to determine I_{sc}.

Meanwhile, the remaining two converters are about 0.72 to 0.8 for the Boost converter and 0.64 to 0.69 for the Buck-boost converter (Table 5). Therefore, we should use the linear extrapolation method from two random points in the voltage range less than $0.4V_{oc}$ to calculate I_{sc} according to expression 35.

To evaluate the calculated short-circuit current error $\Delta I\%$, the I_{sc} and V_{oc} parameters of PV modules are surveyed and listed in Table 7.

The I_{cal} calculation error compared to their actual values under varying conditions is summarized in Table 8. The results show that:

- In the case of the Boost converter, under working conditions of 1000 W/m^2 and a temperature of 60°C, the Shell SP-75 has a maximum error of about 2.63%, with a minimum error of 0.00%. Additionally, Shell SP-75 and Shell S70 have the highest average mistake, 0.34%, while Shell ST40 has the smallest spread at 0.00%.
- For the Buck converter, the maximum difference is 5.85% at 1000 W/m^2 and 60°C for SST 230–60P. It is also the PV module with the most significant average error (0.77%). Shell SQ-150′s calculation parameters are more accurate, with the

TABLE 8 The calculated current error ΔI% compared to I_{sc}.

Types of PV panel		Cases study								Average error ΔI%
		1	2	3	4	5	6	7	8	
Boost converter										
MSX-60	I_{cal} (A)	3.76	15.44	2.76	8.83	8.27	9.77	6.02	6.39	
	ΔI%	0	0.39	0	0	0	0.41	0.17	0	0.12
Shell SP-75	I_{cal} (A)	4.75	19.92	3.5	11.2	10.45	12.4	7.6	8.07	
	ΔI%	0	2.63	0	0	0.1	0	0	0	0.34
Shell SQ-150	I_{cal} (A)	4.74	19.2	3.65	11.1	10.43	12.32	7.58	8.06	
	ΔI%	0	0.05	0	0.09	0	0	0	0	0.017
SST 230–60P	I_{cal} (A)	8.41	35.01	6.34	19.76	18.5	21.9	13.45	14.3	
	ΔI%	0	2.46	0	0	0.05	0	0	0	0.31
Shell S70	I_{cal} (A)	4.43	18.3	3.34	10.41	9.75	11.52	7.08	7.53	
	ΔI%	0	2.53	0	0	0.1	0.09	0	0	0.34
GxB-340	I_{cal} (A)	9.16	37.59	6.72	21.52	20.15	23.81	14.65	15.57	
	ΔI%	0	0.29	0	0	0	0	0	0	0.036
Shell ST40	I_{cal} (A)	2.64	10.61	2.07	6.2	5.8	6.86	4.22	4.48	
	ΔI%	0	0	0	0	0	0	0	0	0.00
Buck converter										
MSX-60	I_{cal} (A)	3.76	15.73	2.76	8.84	8.27	9.78	6.02	6.39	
	ΔI%	0	2.28	0	0.11	0	0.51	0.17	0	0.38
Shell SP-75	I_{cal} (A)	4.75	20.1	3.5	11.16	10.45	12.35	7.6	8.07	
	ΔI%	0	3.55	0	0	0.1	0	0	0	0.46
Shell SQ-150	I_{cal} (A)	4.74	19.16	3.65	11.14	10.43	12.32	7.58	8.06	
	ΔI%	0	0.05	0	0.09	0	0	0	0	0.02
SST 230–60P	I_{cal} (A)	8.41	36.17	6.34	19.77	18.51	21.88	13.46	14.29	
	ΔI%	0	5.85	0	0.05	0.11	0.09	0.07	0	0.77
Shell S70	I_{cal} (A)	4.43	18.57	3.34	10.41	9.75	11.52	7.08	7.53	
	ΔI%	0	4.33	0	0	0.1	0.09	0	0	0.56
GxB-340	I_{cal} (A)	9.16	37.84	6.72	21.51	20.15	23.81	14.65	15.57	
	ΔI%	0	0.96	0	0.05	0	0	0	0	0.13
Shell ST40	I_{cal} (A)	2.64	10.64	2.07	6.2	5.81	6.86	4.22	4.49	
	ΔI%	0	0.28	0	0	0.17	0	0	0.22	0.08
Buck-boost converter										
MSX-60	I_{cal} (A)	3.76	15.39	2.76	8.84	8.27	9.77	6.02	6.39	
	ΔI%	0	0.07	0	0.11	0	0.41	0.17	0	0.1
Shell SP-75	I_{cal} (A)	4.75	19.42	3.5	11.2	10.5	12.35	7.6	8.07	
	ΔI%	0	0.05	0	0	0.1	0	0	0	0.02
Shell SQ-150	I_{cal} (A)	4.74	19.15	3.65	11.1	10.4	12.32	7.58	8.06	
	ΔI%	0	0	0	0.09	0	0	0	0	0.01
SST 230–60P	I_{cal} (A)	8.41	34.19	6.35	19.8	18.5	21.86	13.5	14.3	
	ΔI%	0	0.06	0.16	0	0.05	0	0.07	0.07	0.05
Shell S70	I_{cal} (A)	4.43	18	3.34	10.4	9.75	11.52	7.09	7.53	
	ΔI%	0	1.12	0	0	0.1	0.09	0.14	0	0.18
GxB-340	I_{cal} (A)	9.16	37	6.72	21.52	20.15	23.8	14.66	15.57	
	ΔI%	0	0	0	0	0	0.04	0.07	0	0.02
Shell ST40	I_{cal} (A)	2.64	10.61	2.07	6.2	5.81	6.86	4.22	4.49	
	ΔI%	0	0	0	0	0.17	0	0	0.22	0.05

Abbreviation: PV, photovoltaic.

TABLE 9 The D value at $0.2I_{sc}$.

	Boost		Buck		Buck-boost	
Types of PV panel	D_{B1}	D_{B2}	D_{B1}	D_{B2}	D_{B1}	D_{B2}
MSX60	−0.71	0.3	0.12	0.29	0.21	0.39
Shell SP75	−0.54	0.13	0.15	0.26	0.23	0.35
Shell SQ150	−0.61	0.22	0.13	0.28	0.22	0.37
SSt 230–60P	−0.59	0.19	0.14	0.28	0.23	0.37
Shell S70	−0.54	0.14	0.15	0.26	0.24	0.36
GxB-340	−0.66	0.25	0.12	0.29	0.21	0.38
Shell ST40	−0.42	0.03	0.17	0.25	0.25	0.33

slightest average error being only 0.02% and a minor mistake being 0.00%.

- For Buck-boost converter: The maximum error is 1.12% (PV module Shell S70) at case No.2. The highest median error of 0.18% also belongs to this PV module. Like the Buck converter, Shell SQ150 is accurate, with a minor mean error of 0.01%. In some cases, all modules can achieve this with the smallest deviation of 0.00%.

The findings indicate that the most prominent errors often occur under maximum radiation and temperature (case No. 2). However, the suggested approach demonstrates a commendable ability to precisely estimate the I_{sc} value of the PV system, with an average error of about 0.2% for the entire survey data.

3.3.2 | Identifying V_{oc} of PV module

Determining V_{oc} based on duty cycle D is more complicated than setting the V_{oc} value as a constant for entire operating periods. However, it ensures more flexibility and accuracy under different operating conditions. Replace the coordinate of B(V_{oc}, $0.2I_{sc}$) [33] into Equation (13) to calculate the D value at V_{oc} as follows:

$$K_B = 0.415K_{mp} \tag{36}$$

The output voltage will approach V_{oc} when R_{in} exceeds R_{in_2} (Figure 7). Therefore, each value of D in Table 4 is used to determine K_B according to Equation (36). Combine Equation (4) with Equation (36) to get the relationship between the duty cycle at $0.2I_{sc}$ versus MPPs as Equation (37).

$$\frac{1}{1-D_B} = 0.415\frac{1}{1-D_{mp}} \tag{37}$$

The best operating range of PV module MSX-60 is $D_{mp1} = 0.29$ to $D_{mp2} = 0.71$. Substitute these parameters into Equation (37) to calculate $D_{B1} = -0.71$ and $D_{B2} = 0.3$.

Do the same for the remaining PV modules and DC/DC converters; the results are presented in Table 9. The data pointed that

- For Buck and Buck-boost converters. The D value to determine V_{oc} is always in the operating range ($0 < D < 1$). Therefore, the calculated open-circuit voltage (V_{cal}) corresponds to $D = 0.1$.
- For the boost converter. The data in Table 9 show that $D < 0$ at $0.2I_{sc}$, so the minimum value of D to measure V_{oc} is $D = 0$. Therefore, checking the difference between the voltage at $D = 0$ (V_{cal}) and the V_{oc} of the PV modules under different operating conditions is necessary.

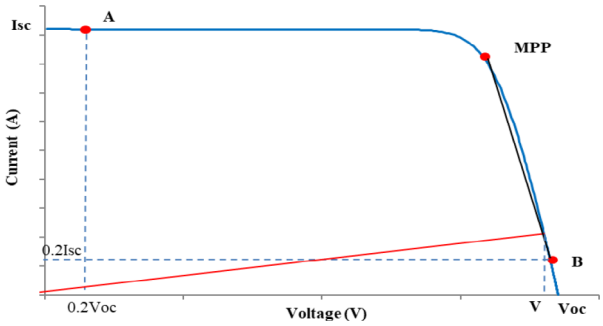

FIGURE 9 The location determines V_{oc} and I_{sc}.

Figure 9 shows that the resistance value (R_L) at B increases significantly when the radiation and temperature decrease. Since the K_B ratio is small, the D_B value must satisfy Equation (38) as follows:

$$R_L = K_B^2\frac{V_{oc}}{0.2I_{sc}} = K_B^2\frac{5V_{oc}}{I_{sc}} \tag{38}$$

Meanwhile, the relationship between R_L and parameters at MPP(V_{mp}, I_{mp}) follows Equation (39):

$$R_L = K_{mp}^2\frac{V_{mp}}{I_{mp}} \tag{39}$$

Equation (40) presents the dependence of load resistance on voltage and current as shown in Figure 9. Meanwhile, expression (41) represents the equation of the straight line connecting B and MPP.

$$I = \frac{I_{mp}}{K_{mp}^2 V_{mp}}V \tag{40}$$

$$I = \frac{I_{mp}-I_B}{V_{mp}-V_B}V + I_{mp} - \frac{(I_{mp}-I_B)}{V_{mp}-V_B}V_{mp} \tag{41}$$

Combine Equations (40) and (41) to have the relationship as in Equation (42).

$$\frac{I_{mp}}{K_{mp}^2 V_{mp}}V = \frac{I_{mp}-I_B}{V_{mp}-V_B}V + I_{mp} - \frac{(I_{mp}-I_B)}{V_{mp}-V_B}V_{mp} \tag{42}$$

Substitute B(V_{oc}, $0.2I_{sc}$) and MPP(V_{mp}, I_{mp}) into Equation (42) to get the correspondence between V and V_{oc} as in Equation (43).

$$V = \frac{3.85K_{mp}^2}{3.65K_{mp}^2 + 1.16}V_{OC} \tag{43}$$

Table 4 shows that each PV module has a specific active range between D_{mp1} and D_{mp2} related to the K_{mp1} and K_{mp2} values. Substitute Equation (4) and the D_{mp} parameters of the PV module MSX-60 into Equation (43) to get $V_1 = 0.91V_{oc}$ and $V_2 = 1.02V_{oc}$. Thus, the voltage V_{oc} is approximately V according to Equation (44) with $D = 0$.

$$V = \frac{V_1 + V_2}{2} = \frac{0.91V_{OC} + 1.02V_{OC}}{2} = 0.96V_{OC} \quad (44)$$

In summary, a duty cycle value, $D = 0.1$, is selected to calculate the open-circuit voltage (V_{cal}) for buck and buck-boost converters, whereas $D = 0$ is opted for Boost converters. The calculation results are compiled and compared with the V_{oc} of PV modules listed in Table 10. The data shows that

- For the Boost converter, Shell ST40 has the largest deviation when operating at 200 W/m^2 and 0°C, 11.9%. It is also the module with the most significant mean error, 7.64%. The SST 230–60T has the highest accuracy with a standard mistake of about 1.72% and a minor difference of 0.35% at 250 W/m^2 and 25°C.
- For the Buck converter, the maximum deviation is 2.31% under conditions of 250 W/m^2 and 25°C for GxB340, and the MSX-60 has the slightest difference of 0.00%. The highest average difference and the smallest are of 1.2% and 0.48% for Shell ST40 and SST 230–60P, respectively.
- In the case of using the Buck-boost converter, Shell ST40 has the most significant difference, 0.42%, at 200 W/m^2 and 25°C. The highest mean deviation and the lowest are 0.32% and 0.09% for Shell ST40 and PV Shell S70, respectively. Meanwhile, some cases have the lowest calculation error of 0.05%.

The PV module's V_{oc} value calculation error ($\Delta V\%$) is more significant than the current ($\Delta I\%$) due to reference from one point. However, the average error of all survey cases is 1.52%. This result is very reliable for determining the V_{oc} of the PV system under actual operating conditions.

3.3.3 | Identifying the potential MPP position

The sequence of potential MPP determination solutions is as follows:

Step 1. Calculate I_{sc}

Select the values of D_1, D_2, and D_3, as shown in Table 11, to calculate I_{sc}.

Step 2. Calculate V_{oc}

Determine V_{oc} according to D_3, as shown in Table 11.

Step 3. Estimate P_{mp}

Calculate the $I_{in\_mp} = k_i I_{sc}$ and $V_{in\_mp} = k_v V_{oc}$.

Estimate the power at MPP based on the previously calculated parameters according to Equation (45)

$$P_{mp} = I_{in\_mp} V_{in\_mp} = k_v V_{oc} k_i I_{sc} \quad (45)$$

Step 4. Calculate K_{mp} and R_{in_mp}.

Calculate the K_{mp} and R_{in_mp} according to Equation (9).

Step 5. Calculate D_{mp}

+ For the Boost converter:

Combine Equations (4) with (9) to calculate D_{mp} at potential MPP as in Equation (46)

$$K_{mp} = \frac{1}{1 - D_{mp}} = \sqrt{\frac{R_L}{R_{in\_mp}}} \quad \Rightarrow \quad D_{mp} = 1 - \sqrt{\frac{R_{in\_mp}}{R_L}} \quad (46)$$

+ For the Buck converter:

Combine Equations (5) with (9) to calculate D_{mp} at potential MPP as in Equation (47)

$$K_{mp} = D_{mp} = \sqrt{\frac{R_L}{R_{in\_mp}}} \quad (47)$$

+ For the Buck-boost converter:

Combine Equations (6) with (9) to calculate D_{mp} at potential MPP as in Equation (48)

$$K_{mp} = \frac{D_{mp}}{1 - D_{mp}} = \sqrt{\frac{R_L}{R_{in\_mp}}} \quad \Rightarrow \quad D_{mp} = \frac{\sqrt{\frac{R_L}{R_{in\_mp}}}}{1 + \sqrt{\frac{R_L}{R_{in\_mp}}}} \quad (48)$$

3.3.4 | Determine the convergence MPP

Table 11 summarizes the parameters and equations to calculate the D_{mp} value at MPP in this study. To improve the performance of the proposed solution, the P&O method is initialized based on this D_{mp} value to search for the optimal convergence location (D_{con}). The solution stops searching when the allowable error from Equation (49) is reached, or the number of iterations is exhausted. Conversely, a ΔD value is added to adjust the output power move towards the

$$|\Delta P| = \frac{P_{i+1} - P_i}{P_i} \times 100\% \leq \varepsilon \quad (49)$$

To reduce the power calculation error, Equation (50) is used to check the operating point position to adjust towards the MPP. If $\Delta V \times \Delta P > 0$, increase V based on D and vice versa. The algorithm flow chart of the proposed method is presented in Figure 10.

TABLE 10 The calculated voltage error $\Delta V\%$ compared to V_{oc}.

Types of PV panel		Cases study								Average error $\Delta V\%$
		1	2	3	4	5	6	7	8	
Boost converter										
MSX-60	V_{cal} (V)	19.24	18.9	20.4	20.81	20.7	20.97	20.17	20.28	
	$\Delta V\%$	0.88	2.5	3.36	2.21	1.77	2.04	1	1.15	1.86
Shell SP-75	V_{cal} (V)	19.34	18.9	20.6	20.71	20.6	20.83	20.11	20.25	
	$\Delta V\%$	4	1.67	5.42	2.13	2.21	2	2.75	2.57	2.84
Shell SQ-150	V_{cal} (V)	43.21	36.6	41.4	42.41	40.1	40.6	38.71	39.05	
	$\Delta V\%$	7.81	4.29	4.92	0.76	4.48	4.04	5.91	5.54	4.72
SST 230–60P	V_{cal} (V)	34.06	33.3	36.4	36.42	36.3	36.65	35.4	35.6	
	$\Delta V\%$	0.35	2.65	0.79	2.22	2.11	2.32	1.58	1.71	1.72
Shell S70	V_{cal} (V)	18.76	18.3	20.1	20.17	20.1	20.31	19.57	19.69	
	ΔV%	3.99	1.4	5.36	1.85	1.95	1.74	2.54	2.38	2.65
GxB-340	V_{cal} (V)	45.08	46	46.58	48.51	48.32	48.81	47.05	47.37	
	$\Delta V\%$	5.09	2.04	7.14	2.61	2.72	2.48	3.41	3.23	3.59
Shell ST40	V_{cal} (V)	22.14	22.76	20.43	24.4	24.33	24.54	23.47	23.75	
	$\Delta V\%$	2.45	9.27	11.9	8.06	7.99	8.25	6.3	6.89	7.64
Buck converter										
MSX-60	V_{cal} (V)	19.2	18.35	20.8	20.36	20.28	20.48	19.85	19.94	
	$\Delta V\%$	0.93	0.33	1.37	0	0.39	0.34	0.6	0.55	0.56
Shell SP-75	V_{cal} (V)	20	19.16	21.5	21.08	21.01	21.19	20.57	20.68	
	ΔV%	0.84	0.42	1.19	0.38	0.43	0.33	0.53	0.48	0.58
Shell SQ-150	V_{cal} (V)	39.3	37.97	42.7	41.7	41.55	41.94	40.6	40.83	
	$\Delta V\%$	1.9	0.58	1.91	0.93	0.98	0.87	1.31	1.23	1.21
SST 230–60P	V_{cal} (V)	33.7	32.33	36.3	35.52	35.4	35.71	34.7	34.86	
	$\Delta V\%$	0.74	0.34	0.95	0.31	0.34	0.31	0.43	0.4	0.48
Shell S70	V_{cal} (V)	19.4	18.48	21	20.49	20.42	20.6	19.98	20.08	
	$\Delta V\%$	0.82	0.32	1.13	0.29	0.29	0.34	0.5	0.45	0.52
GxB-340	V_{cal} (V)	46.96	46.75	49.43	49.57	49.41	49.8	48.36	48.6	
	$\Delta V\%$	1.14	0.45	1.46	0.48	0.52	0.44	0.72	0.67	0.74
Shell ST40	V_{cal} (V)	21.11	20.63	22.68	22.27	22.22	22.4	21.69	21.9	
	$\Delta V\%$	2.31	0.96	2.2	1.37	1.38	1.28	1.77	1.67	1.62
Buck-boost converter										
MSX-60	V_{cal} (V)	19.38	18.4	21.07	20.4	20.3	20.53	20	20.03	
	$\Delta V\%$	0.15	0.05	0.24	0.29	0.1	0.1	0.1	0.1	0.14
Shell SP-75	V_{cal} (V)	20.12	19.22	21.76	21.1	21.1	21.25	20.7	20.76	
	$\Delta V\%$	0.15	0.1	0.18	0.09	0.14	0.05	0.1	0.1	0.11
Shell SQ-150	V_{cal} (V)	39.95	38.13	43.32	42	41.9	42.23	41.1	41.25	
	$\Delta V\%$	0.32	0.16	0.39	0.17	0.19	0.19	0.22	0.22	0.23
SST 230–60P	V_{cal} (V)	33.89	32.42	36.63	35.6	35.5	35.79	34.8	34.96	
	$\Delta V\%$	0.15	0.06	0.16	0.08	0.08	0.08	0.11	0.11	0.10
Shell S70	V_{cal} (V)	19.51	18.53	21.22	20.5	20.5	20.65	20.1	20.15	
	$\Delta V\%$	0.15	0.05	0.19	0.05	0.05	0.1	0.05	0.1	0.09
GxB-340	V_{cal} (V)	47.4	47	50.03	49.75	49.61	50	48.64	48.88	
	$\Delta V\%$	0.21	0.1	0.26	0.12	0.12	0.1	0.14	0.14	0.15
Shell ST40	V_{cal} (V)	21.52	21	23.09	22.51	22.47	22.6	22.01	22.15	
	$\Delta V\%$	0.42	0.2	0.43	0.31	0.27	0.26	0.32	0.32	0.32

Abbreviation: PV, photovoltaic.

TABLE 11 The setting parameters to calculate MPP.

Type	Boost	Buck	Buck-boost
D_1	0.82	1	0.82
D_2	0.80	–	0.80
D_3	0	0.1	0.1
I_{sc}	Equation (35)	$I_{sc} = I_{D1}$	Equation (35)
K_{mp}	Equation (9)	Equation (9)	Equation (9)
V_{oc}	$0.96V_{D3}$	V_{D3}	V_{D3}
$R_{in\text{-}mp}$	Equation (9)	Equation (9)	Equation (9)
D_{mp}	Equation (46)	Equation (47)	Equation (48)

Abbreviation: MPP, maximum power point.

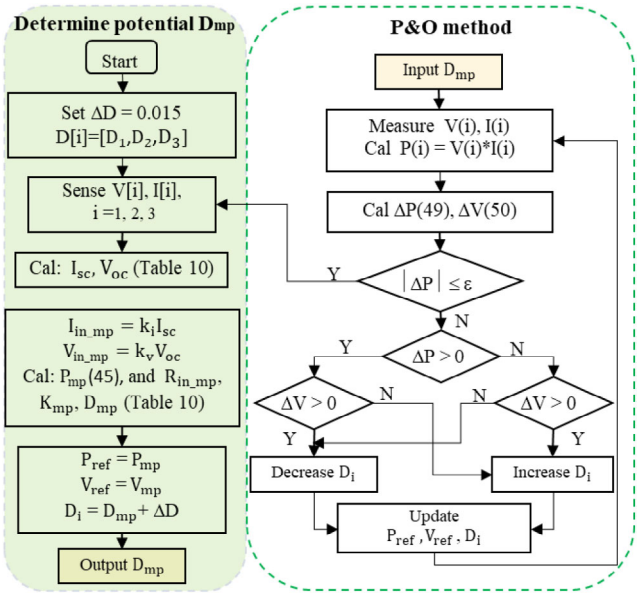

FIGURE 10 Flowchart of the proposed algorithm.

$$\Delta V = \frac{V_{i+1} - V_i}{V_i} \times 100\% \quad (50)$$

4 | RESULTS AND DISCUSSIONS

The simulation and testing scenarios on the Buck, Boost, and Buck-boost converters measure and evaluate the efficiency under the following situations:

- Check the error between the initial estimated D_{mp} and P_{mp} values with the D_{con} and P_{con} at the convergence position of the proposed solution under operating conditions. Besides, the convergence speed (T_s) and simulation efficiency (η_s) between P_{con} and maximum power (P_{max}) of the system are also collected.
- The number of iterations of this algorithm is compared with those of the Variable Step Size (VSS) P&O approach and the standard P&O method [17, 34] under identical working environments. Furthermore, the data collected and compared

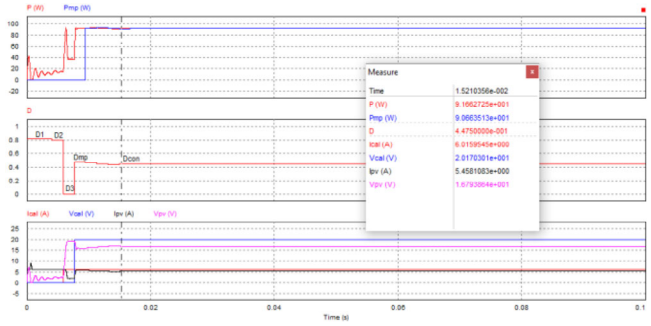

FIGURE 11 The output waveform under partial shade conditions (No. 7).

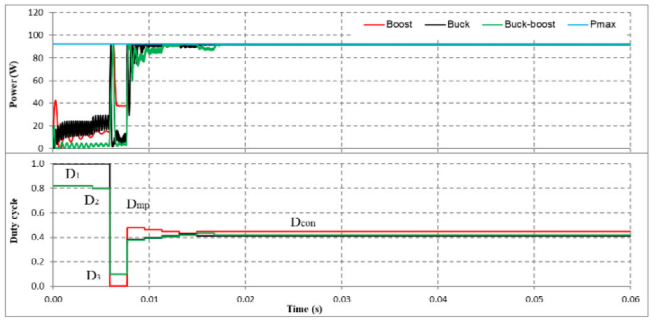

FIGURE 12 MPPT simulation for case No. 7.

demonstrate that this algorithm's performance and rate are significantly improved based on determining the searching zone's starting point.
- Experiment under the same simulation conditions using the Boost, Buck, and Buck-boost converters. The PV simulator, Chroma 62050H-600S, emulates the data of PV modules in this study. The testing's MPPT performance (η_e) and convergence speed (T_e) were also surveyed and evaluated.

4.1 | Evaluate potential MPP positions

The proposed solution's MPP parameters are evaluated based on the operating conditions listed in Table 2. Reduce the calculation deviation between D_{mp} and D_{con} to reduce the number of iterations, thus speeding up the search process. Figure 11 shows the output waveform of the proposed solution simulated using the Boost converter under partial shade conditions (No. 7). Meanwhile, Figure 12 summarizes the waveforms of the Boost, Buck, and Buck-boost converters, and Table 12 points out that.

For the Boost converter, the calculated D_{mp} value (No. 7) is 0.4775 compared with D_{con}, which converges at 0.4475 with a deviation of about 0.07% (Figure 11). This is also the case with the slightest error. The maximum difference is 0.26% (No. 1), and the mean difference is 0.18% for the entire data. That means the calculated D_{mp} value is accurate compared to the optimal values of the three MPPT solutions. Besides, the computed power corresponding to D_{mp} is P_{mp} = 90.66 W, reaching

TABLE 12 Simulation results with the proposed solution.

No.	D_{mp}	D_{con}	$\Delta D\%$	P_{mp} (W)	P_{con} (W)	$\Delta P\%$	η_s (%)
Boost converter							
1	0.25	0.34	0.26	48.58	55.22	87.98	97.67
2	0.74	0.68	0.09	172.30	201.08	85.69	99.86
3	0.21	0.15	0.40	46.04	46.07	99.93	99.55
4	0.62	0.55	0.13	112.64	137.79	81.75	97.79
5	0.62	0.53	0.17	111.95	128.69	86.99	100.00
6	0.64	0.56	0.14	129.72	152.61	85.00	99.73
7	0.47	0.44	0.07	90.66	91.65	98.92	99.64
8	0.57	0.47	0.21	78.90	98.10	80.43	99.95
Buck converter							
1	0.31	0.34	0.09	51.12	55.87	91.50	98.81
2	0.63	0.69	0.09	194.30	201.20	96.53	99.94
3	0.25	0.27	0.07	45.31	46.29	97.88	100.00
4	0.46	0.5	0.08	128.30	136.70	93.85	97.03
5	0.45	0.47	0.04	117.30	128.20	91.50	99.60
6	0.48	0.53	0.09	142.20	151.90	93.65	99.24
7	0.38	0.41	0.07	91.79	91.95	99.83	99.97
8	0.40	0.43	0.07	92.69	98.07	94.51	99.92
Buck-boost converter							
1	0.33	0.37	0.12	49.76	55.27	90.03	97.75
2	0.50	0.55	0.08	180.20	201.20	89.59	99.90
3	0.29	0.32	0.10	42.81	46.20	92.66	99.83
4	0.42	0.47	0.10	130.70	137.50	95.04	97.59
5	0.41	0.46	0.10	122.50	128.10	95.68	99.52
6	0.43	0.48	0.09	143.00	153.00	93.51	99.96
7	0.38	0.42	0.11	89.79	91.80	97.81	99.80
8	0.38	0.43	0.11	90.42	97.93	92.33	99.78

about 98.92% compared to the power at the convergence point $P_{con} = 91.65$ W. The estimated capacity at potential MPP value can get the highest level of 99.93% (No. 3), while the lowest accuracy is 80.43% (No. 8). The average value for this case is 88.34%. In addition, the calculated short-circuit current (I_{cal}) and open-circuit voltage (V_{cal}) values are 6.02 A and 21.72 V, with the corresponding calculation errors of 0.17% and 1%, respectively. These values coincide with the $\Delta I\%$ and $\Delta V\%$ calculation results in Tables 8 and 10. They are used to determine the PV system's output current (I_{pv}) and voltage (V_{pv}) values.

The calculated D_{mp} value (No. 7) for the Buck converter is 0.38, then converges at $D_{con} = 0.41$ with about 0.07% deviation. In some cases, the maximum error when using this converter is 0.09%, and the most minor mistake is 0.04% (No. 5). For the entire survey, the standard difference is 0.075%. The results of calculating the D_{mp} value under operating conditions with the Buck converter are listed in Table 12.

The data show that the estimated power at the MPP, $P_{mp} = 91.79$ W, compared to the optimal value, $P_{con} = 91.95$ W, is 99.83% (No. 7). This is also the most accurate estimated value. At the same time, the lowest accuracy is 91.5% (No. 1 and 5). The mean value is about 94.91%.

For the Buck-boost converter, the calculated D_{mp} value (No. 7) is 0.38, and then the D_{con} converges at 0.42 with a deviation of about 0.11%. The maximum difference is 0.12% (No. 1), and the slightest fault is 0.08% (No. 2). The mean value is 0.10%.

This case's estimated power at MPP is $P_{mp} = 89.79$ W compared to $P_{con} = 91.80$ W (about 97.81% in No. 7), the most enormous estimated power for the Buck-boost converter. Case No. 2 has the lowest value (89.59%), while 93.33% is the average difference for this DC/DC converter.

In summary, potential MPP locations are swiftly identified by accurately computing D_{mp} values, achieving an accuracy rate exceeding 92%. These values are reference points for the P&O algorithm to pinpoint the optimal MPP. Consequently, the algorithm's convergence speed and the MPPT performance are notably enhanced. When applying the proposed solution to the DC/DC converters, the power waveforms and duty cycle in Figure 12 show that all achieve an efficiency of over 99% and a speed of less than 0.02 s.

4.2 | Evaluate the search rate

Table 13 presents the results of the MPPT performance, convergence rate, and the number of iterations of the proposed method under operating conditions.

For the Boost converter, four tuning steps are the best case for the algorithm to converge with a time of 0.015 s (No. 7). The slowest search time is 0.026 s (No. 1), while the average speed is about 0.021 s. In this case, the most excellent simulation MPPT performance is $\eta_s = 100\%$ (No. 5), and the minimum efficiency is 97.67% (No. 1). Average value is over 99.27%.

For the Buck converter, 0.0165 s is the mean search time. The slowest search time is 0.018 s, while the fastest search time is 0.015 s. The simulated MPPT efficiency at No. 7 reaches 99.97%, equivalent to the power $P_{con} = 91.95$ W compared to $P_{max} = 91.98$ W. The best efficiency is 100% (No. 3), the slightest efficiency level is 97.03%, and 99.31% is the standard value.

Finally, the Buck-boost converter operates stably in all shading situations. They mainly require five adjustment steps to reach the optimal position. In this case, the convergence speed does not change significantly (about 0.017 s). Therefore, the performance does not fluctuate greatly, reaching an average of 99.27%. The lowest efficiency is 97.59% in No. 4, and the maximum efficiency is about 99.96% in No. 6. Figure 12 and Table 12 show that the MPPT performance in this case is 99.80 %, which reaches about $P_{con} = 91.80$ W compared to $P_{max} = 91.98$ W.

The output power at the convergence point (P_{con}) remains nearly constant in the simulation scenarios, with an average efficiency exceeding 99.00%. Despite minor discrepancies in the average calculation deviations when applying different converters, these differences are negligible. This phenomenon aids in minimizing the iterations required to identify the optimal MPP.

The proposed solution's convergence rate and MPPT performance were also compared with two algorithms, P&O and

TABLE 13 The MPPT performance and convergence speed.

No.	Number of adjustment steps	Convergence speed (s)	Simulation performance η_s (%)
Boost converter			
1	10	0.026	97.67
2	6	0.019	99.86
3	4	0.016	99.55
4	7	0.021	97.79
5	8	0.023	100.00
6	7	0.021	99.73
7	4	0.015	99.64
8	9	0.024	99.95
Buck converter			
1	4	0.017	98.81
2	6	0.018	99.94
3	5	0.017	100.00
4	5	0.017	97.03
5	4	0.015	99.60
6	5	0.017	99.24
7	4	0.016	99.97
8	4	0.015	99.92
Buck-boost converter			
1	5	0.018	97.75
2	5	0.017	99.90
3	5	0.016	99.83
4	5	0.017	97.59
5	5	0.017	99.52
6	5	0.017	99.96
7	5	0.018	99.80
8	5	0.017	99.78

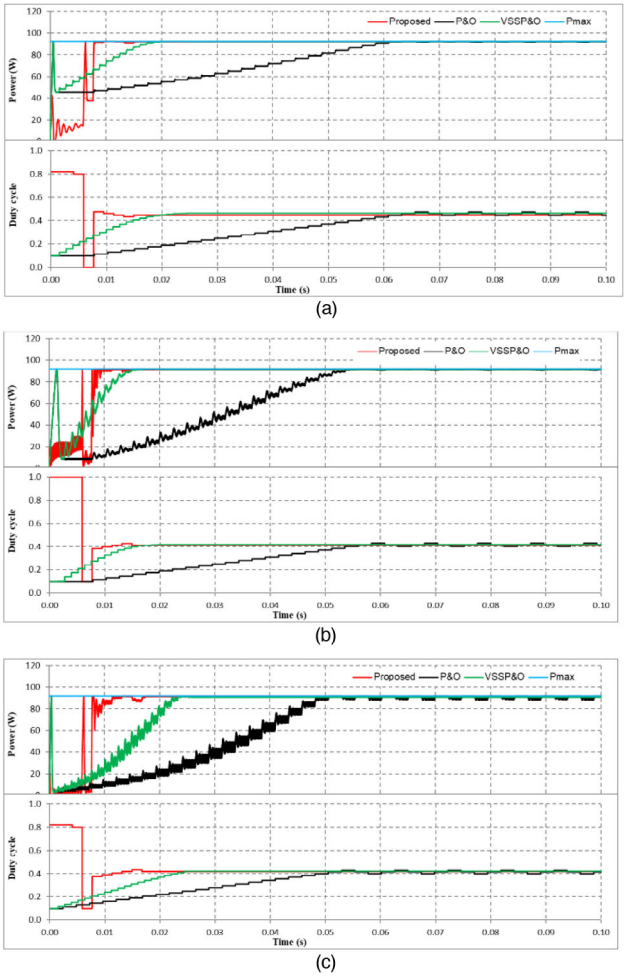

FIGURE 13 Compare the convergence speed of the three solutions using (a) Boost converter, (b) Buck converter, and (c) Buck-boost converter.

VSSP&O, under the same operating conditions (Figure 13). The proposed solution uses the data according to Table 11 to start, while those of other methods are $D = 0.1$. The lowest starting value is $D = 0$ for a Boost converter and $D = 0.1$ for other converters. It is crucial to ensure objectivity when comparing their convergence speed and performance. The $\Delta D = 0.4(\mathrm{dP/dV})$ is the step size of the VSSP&O algorithm. This value enables it to adapt automatically without requiring predefined maximum and minimum limits [16]. This value indicates that when the reference point is distant from the MPP, the error in dP/dV is significant, resulting in an increase in ΔD and vice versa. Meanwhile, this value for the remaining methods is $\Delta D = 0.015$. In summary, the search rate depends not only on the starting position but also on the adjustment step size. Figure 13 depicts the P and D waveforms of the solutions under partial shade conditions (No. 7), while Table 14 summarizes data on the search time and number of iterations of the methods under proposed operating conditions. The results show that:

For the Boost converter, under partial shade conditions (No. 7). The proposed solution demonstrates remarkable efficiency by converging in just four adjustment steps from D_{mp}, as depicted in Figure 13a. In contrast, the conventional P&O method necessitates a significant iteration number to cover the entire $P(V)$ curve, 26 steps. VSSP&O still needs 20 tuning steps to converge, even though the step size has been adjusted. In this context, it is evident that the proposed method has significantly reduced the number of iterations required compared to other methods, achieving an 85% and 80% reduction, respectively.

The MPPT performance of the solutions under case No. 7 is similar, but the convergence speed differs. For the proposed solution, 0.015 s is the rapidest search time, while the search times of P&O and VSSP&O are 0.070 and 0.025 s, respectively.

The proposed algorithm exhibits a rapid search time, ranging from 0.015 s (fastest) to 0.026 s (slowest), with a standard value of approximately 0.021 s. The average convergence speed for the P&O and VSSP&O methods is 0.069 and 0.023 s, respectively (refer to Table 14). Although the number of adjustment steps of VSSP&O is significant because the step size changes flexibly, the convergence time is relatively fast. While the other two solutions use fixed adjustment steps, the speed

TABLE 14 Compare the convergence speed of the solutions.

	Number of adjustment steps			Convergence speed (s)		
No.	**Proposed**	**P&O**	**VSSP&O**	**Proposed**	**P&O**	**VSSP&O**
Boost converter						
1	10	17	20	0.026	0.048	0.025
2	6	36	19	0.019	0.091	0.024
3	4	5	13	0.016	0.020	0.018
4	7	32	19	0.021	0.080	0.023
5	8	32	19	0.023	0.081	0.023
6	7	34	19	0.021	0.087	0.023
7	4	26	20	0.015	0.071	0.025
8	9	28	20	0.024	0.073	0.025
Buck converter						
1	4	17	13	0.017	0.048	0.018
2	6	35	20	0.018	0.091	0.026
3	5	14	12	0.017	0.040	0.018
4	5	28	17	0.017	0.075	0.021
5	4	27	16	0.015	0.073	0.020
6	5	31	19	0.017	0.080	0.023
7	4	23	15	0.016	0.064	0.019
8	4	24	16	0.015	0.066	0.020
Buck-boost converter						
1	5	33	18	0.018	0.087	0.027
2	5	29	20	0.017	0.077	0.028
3	5	11	14	0.016	0.035	0.022
4	5	15	19	0.017	0.044	0.027
5	5	14	19	0.017	0.042	0.027
6	5	16	20	0.017	0.047	0.025
7	5	23	20	0.018	0.058	0.025
8	5	14	19	0.017	0.039	0.024

Abbreviations: P&O, perturb and observe; VSS, variable step size.

depends on the number of adjustment steps. Case 3 shows this when VSSP&O needs 13 adjustment steps in about 0.018 s while P&O needs five adjustment steps but takes 0.020 s. The proposed method has the fewest iterations, so the fastest convergence speed is at 0.016 s.

After four adjustment steps, the proposed solution converges at 0.016 s for the Buck converter. Traditional P&O takes 23 iterations to stop at 0.064 s. Meanwhile, VSSP&O takes 0.191 s after 15 step size adjustments (Figure 13b). Although the performance is similar, the output power waveform of the P&O method is more oscillating than the remaining methods. The results show that the number of iterations is reduced by 83% and 73%, respectively, compared with the other methods. The average convergence speed is 0.016 s faster than the remaining algorithms, P&O (0.067 s) and VSSP&O (0.021 s).

The Buck-boost converter, like the other converters, only takes five adjustment steps to converge from D_{mp} to D_{con} in about 0.018 s. Meanwhile, VSSP&O needs 20 adjustment steps

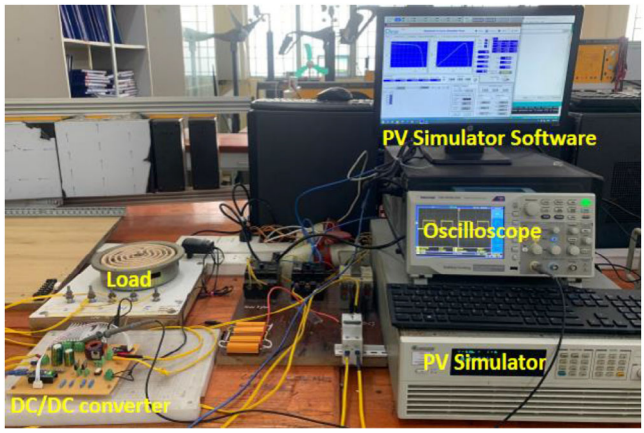

FIGURE 14 Experimental system setup.

to stabilize at 0.0251 s. Finally, the traditional P&O has a convergence speed of 0.058 s (about 23 iterations). In this case, the P&O method has another disadvantage. Its output power is less stable due to the fluctuation of D_{con} (Figure 13c). Although all the solutions have similar MPPT performance, the convergence speed of the proposed method is the fastest due to the number of iterations reduced by 75% compared to VSSP&O and 82% compared to P&O, respectively.

The mean MPPT time of the proposed algorithm, P&O, and VSSP&O is 0.017, 0.054, and 0.026 s, respectively. It has the shortest searching time in all simulation cases (Table 14).

In summary, outstanding convergence speed and stable output waveform are the advantages of this research. In changing operating environments, the MPPT rate is less affected due to the ability to estimate the D_{mp} value accurately. The average search time of this algorithm is about 0.017 s compared to 0.021 s for VSSP&O and 0.07 s for P&O. When simulated under the same partial shade conditions, the MPPT performance and convergence rate of the proposed solution is also outstanding to the remaining algorithms

4.3 | Evaluate experimental results

Similar to the simulation conditions, the experiments with Boost, Buck, and Buck-boost converters were carried out through the PV simulator. The experimental system setup is shown in Figure 14. The parameters of the DC/DC converters are listed in Table 15. The experimental MPPT performance under the testing conditions is presented in Table 16, while Figure 15 shows the results of the partial shading condition (No. 7). The experimental results show that the performance of the proposed solution for the Boost, Buck, and Buck-boost converters is 99.07%, 99.22%, and 99.51%, respectively. Its current and voltage waveforms are presented in Figure 16a. The duty cycle value of the Buck converter is 0.51 (Figure 16b), while the remaining converters are 0.68 and 0.64, respectively. The maximum efficiency is $\eta_e = 99.95\%$ (No. 1), the lowest efficiency value is 98.33% (No. 3) of the Boost converter, and the mean performance is about 99%. The fastest convergence rate is 1.0 s,

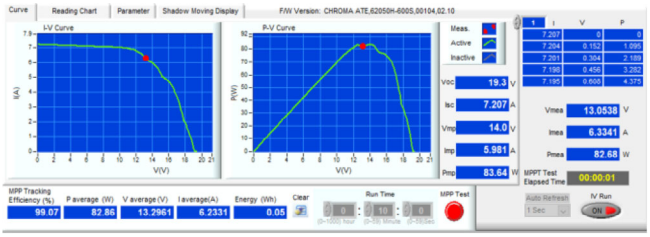

(a)

(b)

(c)

FIGURE 15 Experiment MPPT for case No. 7 with (a) Boost converter, (b) Buck converter, and (c) Buck-boost converter.

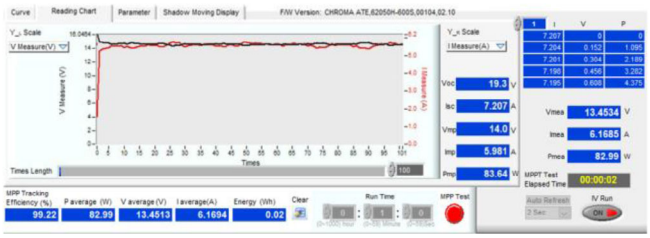

(a)

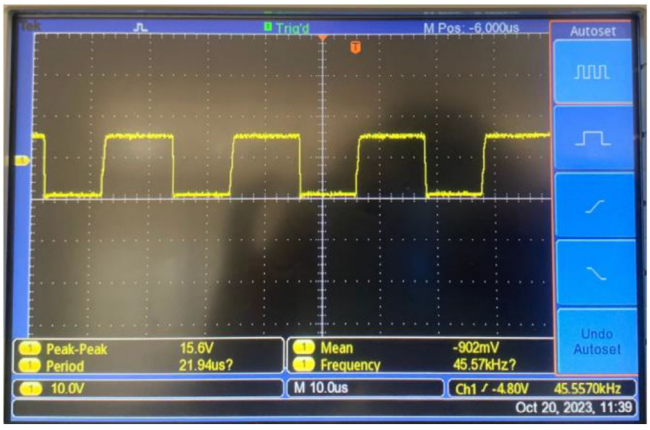

(b)

FIGURE 16 The output waveform when experimenting with Buck converter for case No.7, (a) current and voltage, (b) duty cycle.

TABLE 15 Specification of the DC/DC converters.

Parameter	Values
Electrolytic capacitor C_{in}	47 uF
Electrolytic capacitor C_{out}	47 uF
Inductor L	0.4 mH
Diode D	MUR3060PT
MOSFET	FGA_25N120
Switching frequency	45 kHz

TABLE 16 The testing performance.

No.	P_{max} (W)	Testing power P_e (W)	Testing effectiveness η_e (%)	D	Search time T_e (s)
Boost converter					
1	56.53	56.50	99.95	0.56	3
2	198.05	196.72	99.33	0.81	1
3	45.42	44.66	98.33	0.46	2
4	132.2	130.89	99.01	0.75	1
5	129.2	127.60	98.76	0.73	1
6	146.7	144.52	98.51	0.76	2
7	83.64	82.86	99.07	0.68	1
8	96.41	96.13	99.71	0.72	2
Buck converter					
1	56.53	55.78	98.67	0.47	3
2	198.05	195.50	98.71	0.73	2
3	45.42	45.35	99.85	0.41	2
4	132.2	131.18	99.23	0.63	1
5	129.2	128.10	99.15	0.57	2
6	146.7	145.07	98.89	0.65	1
7	83.64	82.99	99.22	0.51	2
8	96.41	95.08	98.62	0.53	1
Buck-boost converter					
1	56.53	56.46	99.88	0.54	5
2	198.05	196.85	99.39	0.73	2
3	45.42	44.76	98.55	0.46	2
4	132.2	130.94	99.05	0.68	1
5	129.2	127.52	98.70	0.65	3
6	146.7	146.05	99.56	0.70	1
7	83.64	83.36	99.67	0.64	1
8	96.41	96.06	99.64	0.67	2

while the slowest search time is 5 s. The average value for all proposed test cases is 1.83 s.

Table 16 shows that the value of D varied from 0.41 to 0.81 under the conditions in this study. It ensures no position difference of $D = 0.5$ to achieve the best efficiency for DC/DC converters. With fast convergence speed and high MPPT

efficiency, this study's results have the potential to be widely applied in medium- and small-power systems.

5 | CONCLUSION

This article presents a method to quickly determine potential MPP locations by calculating two parameters (V_{oc} and I_{sc}) according to operating conditions. Its D value serves as the search area limit point for the proposed algorithm. The results demonstrate that its convergence speed and MPPT performance are always superior to other algorithms under the same working cases. The output power waveform is also more stable when the PV system operates in partial shade conditions. It also shows that there is no need to update the PV module's instant specifications (which undoubtedly vary after a long time) because of the ability to calculate V_{oc} and I_{sc} based on D. Moreover, the highest MPPT performance is approximately 100%. It has a significant search rate of 0.015 s. Hence, this method is promising for extensive and dependable deployment in low-voltage applications and modest power demands.

NOMENCLATURE

I_{pv}	The output current of PV (A)
V_{pv}	The output voltage of PV (V)
I_{ph}	The light current (A)
I_0	The diode reverse saturation current (A)
q	An electron charge 1.602×10^{-19} (C)
k	The Boltzmann's constant 1.381×10^{-23} (J/K)
T_c	The cell temperature (K)
A	The diode ideality factor (dimensionless)
R_s	The series resistance (Ω)
R_{sh}	The shunt resistance (Ω)
I_{sc}	Short circuit current (A)
T_{ref}	The temperature at standard condition (K)
K	The ratio between V_{out} and V_{in} of DC/DC converters
W	Solar radiation under normal conditions W/m^2
W_{ref}	Solar radiation under at standard condition W/m^2
N_p	The number of panels in parallel
N_s	The number of panels in series
k_i	The current proportionality constant
k_v	The voltage proportionality constant
V_{in}	The input voltage of the DC/DC converter (V)
V_{out}	The output voltage of the DC/DC converter (V)
I_{in}	The input current of DC/DC converter (A)
I_{out}	The output current of DC/DC converter (A)
I_{mp}	The current at the estimated maximum power point (A)
V_{mp}	The voltage at the estimated maximum power point (V)
P_{mp}	The Power at the estimated maximum power point (W)
D_{mp}	Duty cycle at the P_{mp}.
D_{con}	Duty cycle at convergence point of the proposed algorithm
α_i	Temperature coefficient of I_{sc} (mA/°C)
α_v	Temperature coefficient on V_{oc} (mV/°C)
R_L	Resistance load (Ω)
FF	The fill factor of photovoltaic

AUTHOR CONTRIBUTIONS

Van Hien Bui: Data curation; formal analysis; software; writing—original draft. **Viet Anh Truong**: Methodology; supervision. **Vu Lan Nguyen**: Investigation; writing—review & editing. **Thanh Long Duong**: Investigation; writing—review & editing.

CONFLICT OF INTEREST STATEMENT

The authors declare no conflict of interest.

DATA AVAILABILITY STATEMENT

The data presented in this study is available on request from the corresponding author.

ORCID

Van Hien Bui https://orcid.org/0000-0003-4835-1726

REFERENCES

1. Kota, V.R., Bhukya, M.N.: A novel linear tangents based P&O scheme for MPPT of a PV system. Renew. Sustain. Energy Rev. 71, 257–267 (2017)
2. Pathak, P.K., Yadav, A.K., Padmanaban, S., Twala, B.: Innocent Kamwa: Design of smart battery charging circuit via photovoltaic for hybridelectric vehicle. IET Renew. Power Gener. 1–13 (2023). https://doi.org/10.1049/rpg2.12656
3. Gao, L., Dougal, R.A., Liu, S., Iotova, A.P.: Parallel-connected solar PV system to address partial and rapidly fluctuating shadow conditions. IEEE Trans. Ind. Electron. 56(5), 1548–1556 (2009)
4. Huang, Y.-P., Hsu, S.-Y.: A performance evaluation model of a high concentration photovoltaic module with a fractional open circuit voltage-based maximum power point tracking algorithm. Comput. Electr. Eng. 51, 331–342 (2016)
5. Belhachat, F., Larbes, C.: A review of global maximum power point tracking techniques of the photovoltaic system under partial shading conditions. Renew. Sustain. Energy Rev. 92, 513–553 (2018)
6. Sher, H.A., Murtaza, A.F., Noman, A., Addoweesh, K.E., Chiaberge, M.: An intelligent control strategy of fractional short circuit current maximum power point tracking technique for photovoltaic applications. J. Renew. Sustain. Energy 7, 013114 (2015). https://doi.org/10.1063/1.4906982
7. Husain, M.A., Jain, A., Tariq, A., Iqbal, A.: Fast and precise global maximum power point tracking techniques for photovoltaic system. IET Renew. Power Gener. 13(14), 2569–2579 (2019)
8. Baba, A.O., Liu, G., Chen, X.: Classification and evaluation review of maximum power point tracking methods. Renew. Sustain. Energy Rev. 19(4), 433–443(2013)
9. Başoğlu, M.E., Çakır, B.: Hybrid global maximum power point tracking approach for photovoltaic power optimizers. IET Renew. Power Gener. 12(8), 875–882 (2018)
10. Wang, Y., Li, Y., Ruan, X.: High accuracy and fast speed MPPT methods for PV string under partially shaded conditions. IEEE Trans. Ind. Electron. 63(1), 235–245 (2016)
11. Pamuk, N.: Performance: Analysis of different optimization algorithms for MPPT control techniques under complex partial shading conditions in PV systems. Energies 16, 3358 (2023)
12. Rehman, H., Sajid, I., Sarwar, A., Tariq, M., Bakhsh, F.I., Ahmad, S., Mahmoud, H.A., Aziz, A.: Driving training-based optimization (DTBO) for global maximum power point tracking for a photovoltaic system under partial shading condition. IET Renew. Power Gener. 17, 2542–2562 (2023)
13. Eltamaly, A.M., Rabie, A.H.: A novel musical chairs optimization algorithm. Arab. J. Sci. Eng. 48, 10371–10403 (2023)
14. Zand, S.J.; Mobayen, S.; Gul, H.Z.; Molashahi, H.; Nasiri, M.; Fekih, A.: Optimized fuzzy controller based on cuckoo optimization algorithm for maximum power-point tracking of photovoltaic systems. IEEE Access 10, 71699–71716 (2022)

15. Chen, L., Wang, X.: Enhanced MPPT method based on ANN assisted sequential Monte–Carlo and quickest change detection. IET Smart Grid 2(4), 635–644 (2019)
16. Pathak, P.K., Padmanaban, S., Yadav, A.K., Alvi, P.A., Khan, B.: Modified incremental conductance MPPT algorithm for SPV-based grid-tied and stand-alone systems. IET Gener. Transm. Distrib. 16, 776–791 (2022)
17. Priyadarshi, N., Maroti, P.K., Azam, F., Hussien, M.G.: An improved Z-source inverter-based sensorless induction motor-driven photovoltaic water pumping with Takagi—Sugeno fuzzy MPPT. IET Renew. Power Gener. 1–14 (2022)
18. John, R., Sheik Mohammed, S., Zachariah, R.: Variable step size Perturb and observe MPPT algorithm for standalone solar photovoltaic system. In: IEEE International Conference on Intelligent Techniques in Control, Srivilliputtur, India (2017)
19. Abdulmawjood, K., et al.: Characteristic study of solar PV array under different partial shading conditions. IEEE Access 10, 6856–6866 (2022)
20. Angadi, S., Yaragatti, U.R., Suresh, Y., Raju, A.B.: System parameter based performance optimization of solar PV systems with perturbation based MPPT algorithms. Energies 14(7), 2007 (2021)
21. Al-Hussain, H.M.A., Yasin, N.: Modeling and simulation of a solar PV module for comparison of two MPPT algorithms (P&O & INC) in MATLAB/Simulink. Indones. J. Electr. Eng. Comput. Sci. 18(2), 666–677 (2020)
22. Batzelis, E.I., Anagnostou, G., Cole, I.R., Betts, T.R., Pal, B.C.: A state-space dynamic model for photovoltaic systems with full ancillary services support. IEEE Trans. Sustain. Energy 10(3), 1399–1409 (2019)
23. Husain, M.A., Tariq, A.: Transient analysis and selection of perturbation parameter for PV-MPPT implementation. Int. J. Ambient Energy 41(10), 1176–1182 (2018)
24. Ballaji, A., et al.: Design & development of MPPT using PSO with pre-defined search space based on FFPS. IEEE Access 10, 80764–80783 (2022)
25. Khezzar, R., Zereg, M., Khezzar, A.: Modeling improvement of the four-parameter model for photovoltaic modules. Sol. Energy 110, 452–462 (2014)
26. Motahhir, S., El Ghzizal, A., Sebti, S., Derouich, A.: Proposal and implementation of a novel perturb and observe algorithm using embedded software. In: The 3rd International Renewable and Sustainable Energy Conference (IRSEC), Marrakech, Morocco (2015)
27. Bataineh, K.: Improved hybrid algorithms-based MPPT algorithm for PV system operating under severe weather conditions. IET Power Electron. 12(4), 703–711 (2019)
28. Saadat, S.A., Ghamari, S.M., Mollaee, H.: Adaptive backstepping controller design on Buck converter with a novel improved identification method. IET Control Theory Appl. 16, 485–495 (2022). https://doi.org/10.1049/cth2.12241
29. Martina, A.D., Vazquez, J.R., Cano, J.M.: MPPT in PV systems under partial shading conditions using artificial vision. Electr. Power Syst. Res. 162, 89–98 (2018)
30. Li, W., He, X.: Review of nonisolated high-step-up DC/DC converters in photovoltaic grid-connected applications. IEEE Trans. Ind. Electron. 58(4), 1239–1250 (2011)
31. Truong, V.A., Luong, X.T., Nguyen, P.T., Quach, T.H.: The improvement switching technique for high step-up DC-DC boost converter. Electronics 9, 981 (2020). https://doi.org/10.3390/electronics9060981
32. Hashemzadeh, S.M., Hosseini, S.H., Babaei, E., Sabahi, M.: A soft switched high step-up DC-DC converter based on VMC and coupled inductor for photovoltaic energy applications. IET Renew. Power Gener. 17, 1583–1596 (2023)
33. Orioli, A., Di Gangi, A.: A procedure to calculate the five-parameter model of crystalline silicon photovoltaic modules based on the tabular performance data. Appl. Energy 102, 1160–1177 (2013)
34. Jusoh, A., Sutikno, T., Guan, T.K., Mekhilef, S.: A review on favourable maximum power point tracking systems in solar energy application. Telecomm. Comput. Electron. Control 12(1), 622 (2014)

How to cite this article: Bui, V.H., Truong, V.A., Nguyen, V.L., Duong, T.L.: Estimating the potential maximum power point based on the calculation of short-circuit current and open-circuit voltage. IET Power Electron. 1–20 (2024). https://doi.org/10.1049/pel2.12651

Bài báo số 3: SCIE Q1 – IF 3.4

Truong Viet Anh, Ton Ngoc Trieu, Pham Vo Hong Nghi, **Bui Van Hien.** "Fast and Accurate GMPPT Based on Modified P&O Algorithm". *IEEE Access*, Vol 12, 2024, pp: 29588-129600, doi: 10.1109/ACCESS.2024.3457825.

IEEE Access
Multidisciplinary | Rapid Review | Open Access Journal

Received 25 July 2024, accepted 5 September 2024, date of publication 11 September 2024, date of current version 20 September 2024.

Digital Object Identifier 10.1109/ACCESS.2024.3457825

RESEARCH ARTICLE

Fast and Accurate GMPPT Based on Modified P&O Algorithm

TRUONG VIET ANH[1], TON NGOC TRIEU[2], PHAM VO HONG NGHI[1], AND BUI VAN HIEN[3]
[1]Faculty of Electrical and Electronics Engineering, Ho Chi Minh City University of Technology and Education, Ho Chi Minh City 700000, Vietnam
[2]Thu Duc College of Technology, Ho Chi Minh City 721400, Vietnam
[3]Faculty of Mechanical–Electrical and Computer Engineering, School of Technology, Van Lang University, Ho Chi Minh City 700000, Vietnam

Corresponding author: Bui Van Hien (hien.bv@vlu.edu.vn)

This work was supported by Ho Chi Minh City University of Technology and Education, Vietnam, under Grant T2023-58.

ABSTRACT The most significant challenge the maximum power point tracking (MPPT) algorithms face is reaching the global MPPT under partial shading conditions (PSC). In this case, the power-voltage (P-V) and current-voltage (I-V) characteristic curves of the photovoltaic (PV) system produce many maximum power points, which is the reason that the algorithms often trapped in local maximum power point (LMPP). The Perturbation and Observation (P&O) algorithm is simple and effective for finding MPP on a mono-extreme graph. Under PSC with many extremes, it is necessary to limit the range of potential GMPP so that this algorithm can avoid the LMPP trap. This paper introduces a global MPPT (GMPPT) method based on the combination of modified P&O and simulates the behavior of the I-V curve under PSC. In particular, the starting parameters of the algorithm are adjusted in the potential GMPP region to exploit simplicity and efficiency to increase performance and convergence speed. The proposed method determines the area where the GMPP is potentially found more accurately, and this contribution is crucial for increasing the efficiency of the strings of PV arrays under partial shading conditions. By comparing results with other algorithms, such as Modified P&O, Adaptive Jaya (Ajaya), and Jaya, the proposed algorithm has verified its outstanding advantages in MPPT performance and search time under the same test conditions.

INDEX TERMS P&O algorithm, partial shade conditions, photovoltaic system, GMPPT, open-circuit voltage, short-circuit current.

I. INTRODUCTION

Under PSC, the advantage of the parallel configuration (PC) is that it reduces losses due to non-uniform radiation and produces only one extreme in all shading conditions. However, this connection can generate high currents under uniform conditions that cause resistive losses and stress the switching devices. Therefore, it is often applied in low-power systems [1], [2]. Meanwhile, the series configuration (SC) has high output voltage and low working current. It is suitable for large power systems, but its disadvantage is that it creates more local extremes and significant power losses in PSC. Even the "hot-spot" effect can interrupt the power supply or destroy the PV string if it is not protected under non-uniform conditions [3]. The series-parallel configuration (S-PC) combines two basic connection types to achieve the required output current and voltage limits. Besides the advantages inherited from the two kinds of single linkage, its biggest disadvantage is determining the GMPP among many LMPPs under PSC. By adding connects to address the effects of non-uniform irradiation to avoid power loss in S-PC configuration, Bridge Linked (BL), Honey-Comb (HC), and Total-Cross-Tied (TCT) configurations have significantly reduced power loss compared to S-PC. However, they share common drawbacks: increased costs due to too many links in the array and they have more redundant connections cause power loss under uniform irradiation.

Furthermore, these configurations require many modules and a large installation area to achieve the effect of the additional connections. The above analysis shows that the S-PC

The associate editor coordinating the review of this manuscript and approving it for publication was Zhilei Yao.

configuration is more straightforward to deploy because of its flexibility in structural changes. It would be best if the multi-extreme problem under PSC is solved [4], [5]. As a result, MPPT techniques are increasingly being introduced to GMPPT. They are classified depending on the point of view and perspective, but generally, they fall into three basic types: traditional techniques, optimal and intelligent algorithms, and hybrid solutions.

The traditional techniques groups include P&O, Incremental Conductance (InC), Constant Voltage (CV), or Constant Current (CC)…The common advantage of this class is that the algorithm is simple and effective under uniform irradiation conditions. However, the output signal fluctuates around the MPP, leading to energy loss, poor stability, and trapping into the LMPP under PSC. To overcome this drawback, the recently published document [6] introduced the P&O and InC algorithms based on modified variable step sizes (M-VSS-P&O). The solution relies on the power difference between two measurements to adjust the step size. This solution can achieve the largest convergence speed and efficiency of 16.34 ms and 99.37%, respectively. Unfortunately, it has not been tested under PSC, which directly affects the performance and feasibility of MPPT solutions. An improved version of the CV method introduced in [7] uses a single dynamic tuning parameter to increase MPPT efficiency. Although the convergence speed is improved by 38.75% compared to the original version, the best value is 0.15 s, with an efficiency of about 99.8%.

Meanwhile, the intelligent algorithm group can be mentioned as PSO, Artificial Bee Colony (ABC), Ant Colony Optimization (ACO), Gray Wolf Optimization (GWO), GA…The outstanding advantages of this class include high MPPT efficiency and an excellent ability to avoid LMPP traps. However, their disadvantages are that the objective function and calculation method are complex, expensive, challenging to implement, and have a slow convergence speed [8]. One of the recent publications in this class based on improving the PSO algorithm introduced in the document [9] is a novel metaheuristic MPPT technique based on an Enhanced Autonomous Group PSO. It is introduced as the best-enhanced version of PSO and can be stable around the working point with an error of about 2.03%. However, this solution's performance and convergence speed are 98.6% and 2.6 s, respectively, and there are better solutions than this. Another modified version was proposed in the literature [10], which can increase the performance and reduce the search time by 75% compared to the traditional version by reducing the swarm size. Although the convergence speed was reduced to 0.258 s, the MPPT performance needed to be clearly shown, and the limited number of case studies was a disadvantage of this solution. In the document [11], the authors introduced an improved GWO algorithm that allows the speed to be adjusted automatically to the objective function after each iteration. Compared to regular GWO, this enhanced version can improve performance by up to 1.4% and reduce search time by up to 82%. However, with the highest efficiency of about 99.57% and convergence speed of 72 s, the effectiveness of this solution is far lower than that of other optimal algorithms.

Finally, the hybrid solution group. Nowadays, research and proposals in this group are introduced and applied more and more from a combination of two traditional algorithms, between a conventional algorithm and a smart algorithm, or a hybrid between two optimal solutions. Their advantage is that they can inherit the strengths of each individual algorithm to improve MPPT efficiency. However, it is difficult for any solution to simultaneously achieve the set standards such as performance, speed, complexity, and applicability. In the document [12], an improved ABC algorithm (IABC) combined with a Simultaneous Heat Transfer Search (SHTS) for MPPT under PSC was proposed. In this case, IABC quickly limits the GMPP region and then increases the convergence rate by SHTS. This way, the solution can reach a peak efficiency of 99.55% in 0.13 s. A combination of the P&O with PSO in the literature [13] produces a two-stage solution. In particular, the first stage uses the PSO method to optimize the step size for the traditional algorithms in the remaining stages. In this way, the proposed solution can achieve a speed of 49.5 ms with an efficiency of about 98.73%. Meanwhile, paper [14] introduces a new hybrid method that combines GA with fractional OCV, allowing it to use a single decision variable to simplify the calculation and increase convergence speed and MPPT performance. This solution has achieved some achievements, such as an average tracking efficiency of about 99.96%, an increase of 3% compared to conventional FOCV, and a search time of about 0.07 s. It also increases energy efficiency because there is no need to interrupt the power supply to measure the reference open-circuit voltage (V_{oc}) value. Although the solution is simple, using a separate voltage sensor to measure the V_{oc} of a pilot PV module increases costs. There may be errors when using a reference voltage from an independent system.

Document [15] presents a solution to determine GMPP divided into 2 stages; stage 1 determines the I_{sc} of PV panels in a string by using an amount of ΔD to evaluate the position of the I_{sc} of the panel ($dI \leq \varepsilon_i$) then indicates the location of the GMPP using the current and voltage ratio method. Phase 2 uses P&O to accurately determine the GMPP point in the previously designated GMPP area. If phase 1 is handled well, the GMPP point can be accurately determined in the shortest time possible. However, in this study, the area with GMPP was found, but it was not accurate. In paper [16], a modified InC method is introduced for GMPPT under PSC and variable load. This solution also relies on I-V and P-V characteristic curves to adjust the step size. However, because the potential GMPP region cannot be quickly determined, its fastest convergence speed is only 0.5 s. A recently introduced modified P&O version initially set up a significant ΔD value, which then diminishes to zero as it tracks the MPP to accelerate convergence during tracking and minimize oscillations [17]. Although it has improved convergence speed by 50% compared to the traditional method and is introduced as better

than previous modified P&O versions, its disadvantage is that it does not mention the PSC. The average convergence speed and MPPT efficiency are 0.5 s and 99.8%, respectively. Therefore, this study introduces an improved GMPPT solution for PV systems under PSC to overcome this drawback. Its outstanding performance and convergence speed are built on the following specific recommendations.

1) Determine the potential GMPP more accurately by adding the lacking BB' segment to calculate the voltage V_{mp} with the slightest error. Furthermore, the predicted MPP is close to the actual value of MPP, so it shortens the time to adjust D to move to the MPP position.

2) Quickly determine I_{sc} under shaded and unshaded operating conditions. This reduces the PSC checking time because the entire I-V curve is not required to be scanned and thus can increase the convergence speed.

The remainder of the paper is organized as follows: Section II introduces the materials and operating principles under PSC. Section III presents the proposed solution while Section IV shows simulation results and discussion. Finally, Section V is the conclusion of the article.

II. MATERIALS AND METHODOLOGY

The PV system consists of multiple parallel strings connected to the load via a DC/DC converter, as in Figure 1. The MPPT block provides a pulse width value to the Buck-boost converter to control the system so that it works efficiently at GMPP. Meanwhile, the PV array consists of many parallel strings with 4 PV panels per string. The parameters of the PWX200 model can be found in Table 1.

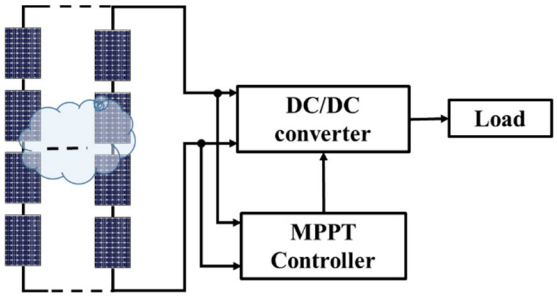

FIGURE 1. Schematic diagram of the proposed PV system.

TABLE 1. The proposed simulation and experimental cases.

Model	PWX200
Open circuit voltage (V_{oc})	20.20 V
Short circuit current (I_{sc})	1.4 A
Voltage at MPP (V_{mp})	16.00 V
Current at MPP (I_{mp})	1.28 A

A. THE OPEN CIRCUIT VOLTAGE OF THE PV SYSTEM UNDER PSC

In the string consisting of N modules operating under PSC, its I-V characteristic will have N steps, and the P-V curve will be separated into N intervals, each area has an extreme.

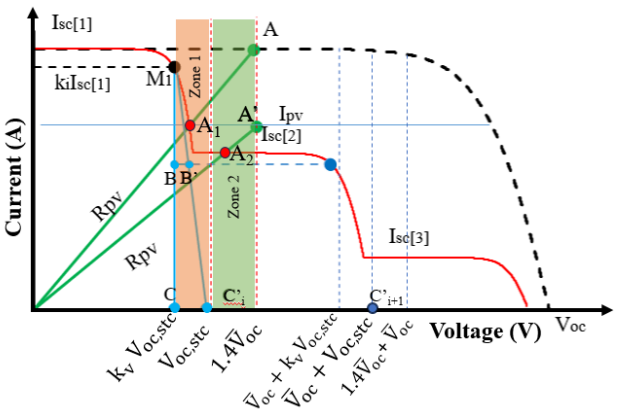

FIGURE 2. Determine MPPs on the I-V curve under PSC.

The relationship between the average open circuit voltage of a single module ($\bar{V}_{oc}$) and the open circuit voltage of the system ($V_{oc,sys}$) is presented as in (1) [15].

$$\overline{V}_{oc} = \frac{V_{oc,\mathrm{sys}}}{N} \tag{1}$$

The voltage at the MPP approximates the V_{oc} in each interval by a factor of k_v. Therefore, the voltage value at the first extreme (M_1 in Figure 2) can be determined according to the following (2).

$$V_{\mathrm{mp}[1]} = k_v \frac{V_{oc,\mathrm{sys}}}{N} \tag{2}$$

Applying this relationship, the document [16] used the InC algorithm to detect the first MPP and then adjust the ΔD jump to the next MPP by an interval of $0.8V_{oc}$. If PSC occurs, the operating point will belong to the nonlinear from $V_{mp[1]}$ to $V_{oc[1]}$. A current error value (dI) is proposed to be checked. If $dI \leq dI_{min}$, deploy InC to find MPP in the next region; otherwise, increase ΔD to escape the nonlinear region. In summary, this solution proposes a voltage step of $0.8V_{oc}$ to calculate the D value at the start point, then checks the dI to ensure it has moved to the new MPP region. However, its disadvantage is that it must scan the entire I – V curve to find the MPPs. Using the same ΔD value for the two goals of shadow checking and MPP search causes the solution to have a slow convergence speed. Furthermore, when the radiation drops deeply, the $I_{sc[2]}$ value drops sharply, causing the segment BB' in Figure 2 to increase. Therefore, the calculation $V_{mp[2]} = k_v V_{mp[1]}$ will have a significant error. The more PVs in the string, the more cumulative error increases, so more search time is needed. Document [18] proposes a solution to test PSC by comparing the current at the first MPP ($0.8V_{oc}$) and the last MPP in the string ($0.8V_{oc,sys}$). This solution assumes that V_{mp} is known and $V_{oc,sys}$ is estimated according to the relationship $V_{mp} = 0.8\ V_{oc,sys}$. This means that at initialization, it is considered to be in uniform condition, and the currents at all MPPs are the same. If they are different, it means a shadow appears. It also has the disadvantage that scanning the entire I-V curve from the first $0.8V_{oc}$ to

$0.8V_{oc,sys}$ using the PSO algorithm is necessary. Therefore, its simulated MPPT speed under PSC conditions is about 0.32 s, and not mentioning MPPT performance is also a disadvantage of this method. Document [19] also assumes that the V_{oc} of PV panels in the string is the same. A PV's maximum and minimum V_{oc} are surveyed to limit the search area for the MPPs. The algorithm is divided into several stages. Initially, a large ΔD is applied to quickly move to the MPP. Then, variable steps are used to improve performance. The PSC is checked after the GMPP has been determined by comparing the V_{mp} with other points. A new peak appears if there is another point with the same P_{mp} value. Then, the algorithm will look for the direction of increasing or decreasing the voltage compared to the current position. Although much more efficient than the traditional P&O algorithm is achieved, if the current position is the lowest among the extremes, many points with the same capacity will lead to increased processing time. The result is the fastest convergence speed of 1.35 s and no mention of MPPT performance. Recently, document [20] proposed a strategy for checking capacity at LMPP locations. In their study, with 4 PVs in series, the proposed solution to test at 4 locations are $\{0.25; 0.5; 0.75; 1.0\}V_{oc,sys}$. This solution is quite simple and effective when the number of PVs in the chain is small. If the number of PVs in the string increases, the initial starting position also increases, making it more time-consuming to check the entire curve. Therefore, the time to search for GMPP with 4 extremes is about 0.17 s, an efficiency of approximately 99.7%. Under uniform conditions, the efficiency can reach 99.99%, but the speed of 0.121 s also needs further improvement. In summary, previous studies consider the V_{oc} of the panels to be constant, $\bar{V}_{oc} = V_{oc,sys}/N$, and determining the V_{mp} of PV panels is based on the relationship $V_{mp[i]} = V_{mp[i-1]} + k_v\bar{V}_{oc}$ [20]. This study combines a constant V_{oc} value with a method to determine the V_{mp} of a multi-string parallel system by adding the lacking voltage segment BB' to overcome the disadvantages of previous solutions. The process for determining the BB' segment is presented in detail in Section III. Besides, the $V_{oc,sys}$ value is determined based on a convenient location at D = 0.1 without interrupting the power supply [21]. This work will help increase the accuracy of calculating voltage values at $V_{mp[i]}$ locations, then increase convergence speed and improve MPPT performance.

B. THE SHORT CIRCUIT CURRENT OF THE PV SYSTEM UNDER PSC.

Determining the two parameters, I_{sc} and V_{oc}, for the PV systems is very important because the MPP can be predicted quite accurately based on the voltage and current factors according to the CC or CV method with $P_{mp} = k_v V_{oc} k_i I_{sc}$ [7], [22]. Obviously, determining V_{oc} is extremely simple, based on $\bar{V}_{oc}$ [15], but determination is relatively more difficult for short-circuit current under PSC, determination is relatively more complex. Based on the I-V characteristics of photovoltaic cells, this study proposes a checking region where the measured current value is approximately I_{sc} under PSC conditions. However, the disadvantage of solutions based on CV and CC techniques is that the power supply must be interrupted to measure the I_{sc} and V_{oc} parameters, reducing the power generation efficiency during the PV system's operational interruption [8]. To solve this problem, the short circuit current of the PV system $I_{sc,sys}$ is quickly determined at D = 0.8 based on some previous research [17], [21].

Figure 2 can be divided into 2 regions. In zone 1, the V_{pv} value, $k_v V_{oc,stc} < V_{pv} < V_{oc,stc}$, is the working area belonging to the characteristic curve of the first PV panel. Region 2, $V_{oc,stc} < V_{pv} < \bar{V}_{oc} + 0.4\bar{V}_{oc}$, is the linear area where the I_{sc} of the second photovoltaic panel can be determined. Based on the literature [23], the $0.4\bar{V}_{oc}$ position is used to determine I_{sc}. When the working point is located in zone 1 (point A_1), deciding whether the PV strings are being shaded will be challenging. Therefore, the operating conditions in zone 2 are proposed to check and determine the I_{sc} of the next PV panel. To change from working point A_1 to A_2 to satisfy the condition of zone 2 is to increase R_{pv} based on its previous value according to the following (3).

$$R_{pv} = \frac{\overline{V}_{\mathrm{oc}} + 0.4\overline{V}_{\mathrm{oc}}}{I_{\mathrm{pv}}} \tag{3}$$

Updating R_{pv} according to (3) to ensure that the checkpoint is always within region 2, $V_{oc,stc} < V_{pv} < \bar{V}_{oc} + 0.4\bar{V}_{oc}$, (point A_2) to determine the fastest I_{sc} value. Furthermore, continuously updating R_{pv} according to the operating current and voltage values at $1.4\bar{V}_{oc}$ will significantly reduce the time needed to determine GMPP, compared to scanning the entire I–V curve, according to the document [16]. In a system with many PV strings connected in parallel, the V_{oc} (point C_i') of the i^{th} step in the shaded I–V characteristic will be near position $i\bar{V}_{oc}$. To ensure that region 2 does not overlap with region 1, the voltage at C_i' can be determined as $(i\text{-}2)\bar{V}_{oc} + V_{oc,stc}$, where i is the panel being tested. Equation (3) will be repeated until A_2 belongs to zone 2 and all panels in the string have been tested.

When operating conditions are uniform (black dashed line), the current in regions 1 and 2 is almost unchanged, so the location where I_{sc} of the next photovoltaic panel can be determined is at $1.4\bar{V}_{oc}$ (point A). One limitation of this solution is that when determining the I_{sc} value for the last panel in the string, there will be a slight error due to falling into the nonlinear region. However, this error is insignificant because the voltage in the last panel is much larger than the remaining panels, so it does not significantly affect the power prediction results.

In summary, the shading condition will be checked for a system consisting of N PV panels in a string, and the LMPP will be generally estimated as follows.

Check the working area of the current PV panel according to (4), where i is the panel being tested

$$k_v V_{oc,stc} + \bar{V}_{oc}\,(i-2) < V_{pv} < V_{oc,stc} + \bar{V}_{oc}\,(i-2) \tag{4}$$

Determine the I_{sc} value of the next PV panel according to (5)

$$V_{oc,stc} + \bar{V}_{oc}\,(i-2) < V_{pv} < 1.4\bar{V}_{oc}\,(i-1) \tag{5}$$

Update R_{pv} to move to the linear region that can determine the I_{sc} of the next PV panel as in (6).

$$R_{pv} = \frac{1.4\overline{V}_{\mathrm{oc}}\,(i-1)}{I_{\mathrm{pv}}} \tag{6}$$

C. DETERMINE DUTY CYCLE

Suppose there are always values V_{pv} and I_{pv} at any working point. The resistance value of PV at the working point (R_{pv}) is determined according to (7). Meanwhile, the D value of the Buck-boost converter determines the output voltage value (V_{out}) according to the input voltage (V_{in}) as in (8) [24].

$$R_{pv} = \frac{V_{pv}}{I_{pv}} \tag{7}$$

$$\frac{V_{out}}{V_{in}} = K = \frac{D}{1-D} \tag{8}$$

The duty cycle of any operating point can be calculated according to (9) [21].

$$D = 1 - \frac{1}{1+\sqrt{R_L/R_{pv}}} \tag{9}$$

III. PROPOSED GMPPT METHOD

A. DETERMINE THE PARAMETERS AT THE FIRST MPP

Based on CC and CV techniques, it is possible to determine the short-circuit current and open-circuit voltage of the first photovoltaic panel ($I_{sc[1]}$ and $V_{oc[1]}$) in the string. Then, calculate $V_{mp[1]}$ and $I_{mp[1]}$ based on the ratio of open circuit voltage and short circuit current [20].

$$V_{mp[1]} = k_v V_{oc[1]} = k_v \frac{V_{oc,\mathrm{sys}}}{N} \tag{10}$$

$$I_{mp[1]} = k_i I_{sc[1]} \tag{11}$$

$$P_{mp[1]} = V_{mp[1]} I_{mp[1]} \tag{12}$$

$$R_{mp[1]} = \frac{V_{mp[1]}}{I_{mp[1]}} \tag{13}$$

$$D_{mp[1]} = 1 - \frac{1}{1+\sqrt{R_L/R_{mp[1]}}} \tag{14}$$

If the V_{oc} of the panels is considered the same ($\bar{V}_{oc}$), then the V_{mp} of the next panel can be determined as in (15) [20]:

$$V_{mp[2]} = V_{mp[1]} + k_v \frac{V_{oc,\mathrm{sys}}}{N} = 2k_v \frac{V_{oc,\mathrm{sys}}}{N} \tag{15}$$

Figure 3 shows that if the voltage is determined as documented [20], $V_{mp[2]} = V_{mp[1]} + k_v V_{oc}$, point F is considered the second MPP, but in reality, it must be at position MPP_2. As a result, MPP will be incorrectly determined because there is a missing voltage segment from F to MPP_2. Assuming the power at MPP_1 and MPP_2 is the approximation, $P_{mp1} = k_v \bar{V}_{oc} k_i I_{sc[1]}$ and $P_{mp2} = (V_{mp[1]} + BB' + k_v \bar{V}_{oc}) k_i I_{sc[2]}$, adding fragment BB' will determine P_{mp2} more accurately.

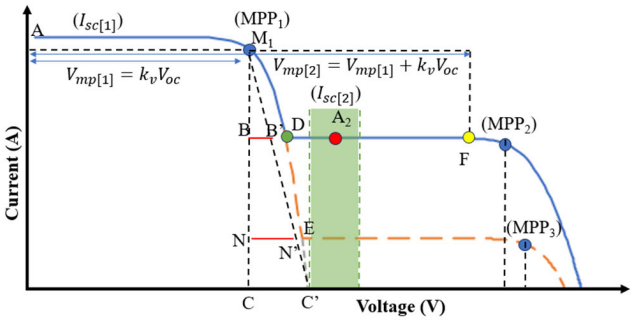

FIGURE 3. Determinethe lack voltage under PSC.

This increases the rate of correctly determining GMPP if there are many approximate power peaks.

Figure 3 also illustrates that if point D (the point where shadowing begins) can be accurately determined, the voltage $V_{mp[2]}$ will be determined more accurately, but this is a significant challenge. Meanwhile, determining point A_2 is much simpler, so this study proposes to use a similar triangle method to determine the approximate lack of voltage after determining the $I_{sc[1]}$ and $I_{sc[2]}$ values based on the ratio of BB' and CC' segments. Calculating this voltage shortfall is very important because when the shadow on the PV panel is little, this missing voltage is relatively small and may not have a significant impact. But when there is a lot of shading, this voltage deficit is very large (segment NN').

Although this method only determines an approximate value because there is still an unknown range of B'D or N'E voltages, this problem can be improved using more similar triangles. However, the experimental and simulation results in cases with many MPPs are the same; this method can still accurately determine GMPP.

B. DETERMINE THE REMAINING MPPs

Determine the $V_{mp[i]}$: The potential difference between two points, M_1 and B', is segment BB' depending on the level of shading (Figure 2). When the radiation decreases significantly, the BB' distance increases, and the equal division method in previous studies becomes less accurate. In this case, the voltage at B' is approximately calculated when considering two similar triangles, M_1 BB' and M_1 CC', as in (16):

$$BB' = V_{B'} - V_{mp[1]} = (1-k_v)\overline{V}_{oc} \frac{k_i \left(I_{sc[1]} - I_{sc[2]}\right)}{k_i I_{sc[1]}} \tag{16}$$

Point MPP_2 has a voltage $V_{mp[2]}$, and the distance from point B' has a voltage value of approximately $k_v \bar{V}_{oc}$, so $V_{mp[2]} = V_{B'} + k_v \bar{V}_{oc}$ is calculated according to (17)

$$V_{mp[2]} = V_{\mathrm{mp}[1]} + \overline{V}_{oc} \left[(1-k_v) \frac{I_{sc[1]} - I_{sc[2]}}{I_{sc[1]}} + k_v \right] \tag{17}$$

Using the proposed method, determining the value of $V_{mp[2]}$ according to (19) is more accurate than calculating $V_{mp[2]} = V_{mp[1]} + k_v V_{oc[1]}$ in previous studies [16]. In general,

the voltage value at any MPP ($V_{mp[i]}$) in a string under PSC is calculated as in (18) to (20) (i = 2 to N).

$$\begin{aligned} BB' &= V_{B'} - V_{mp[i]} \\ &= (1-k_v)\overline{V}_{oc}\,(i-1)\,\frac{k_i\left(I_{sc[i-1]} - I_{sc[i]}\right)}{k_i I_{sc[i-1]}} \end{aligned} \tag{18}$$

$$V_{mp[i]} = V_{\mathrm{mp}[i-1]} + BB' + k_v\overline{V}_{oc} \tag{19}$$

$$V_{mp[i]} = V_{\mathrm{mp}[i-1]} + \overline{V}_{\mathrm{oc}}\left[(1-k_v)\frac{I_{sc[i-1]} - I_{sc[i]}}{I_{sc[i-1]}} + k_v\right] \tag{20}$$

Determine the $I_{mp[i]}$: As stated in Section II, subsection II, to determine I_{mp}, it is necessary to first determine the I_{sc} of the panels when a shadow appears. After determining the first MPP point, the solution needs to output a value D to move to the region $V_{oc,stc} + \bar{V}_{oc}(i-2) < V_{pv} < 1.4\bar{V}_{oc}(i-1)$ (with i from 2 to N panels in the string). This is done by holding the desired voltage constant at $1.4\bar{V}_{oc}(i-1)$ and measuring the current to calculate the R_{pv} value. Then, send a D value to the point with the specified R_{pv} and check the condition following (4). If (4) is satisfied, the system works at point A_1 (Figure 2). Therefore, it is necessary to increase R_{pv} according to (6) to update the new D value according to (9) enough to move to the desired region $V_{oc,stc} + \bar{V}_{oc}(i-2) < V_{pv} < 1.4\bar{V}_{oc}(i-1)$. After determining $I_{sc[i]}$, $I_{mp[i]}$ can be easily determined according to (21)

$$I_{mp[i]} = k_i I_{sc[i]} \tag{21}$$

Check all remaining PVs in the string by following the same steps. The most enormous power among the stored $P_{mp[i]}$ is selected to test the GMPP. After checking all the panels in the string, select the GMPP point and move to the GMPP point using D_{mp} with P_{max} just determined. Then apply P&O to detect the most accurate GMPP point.

C. PROPOSED GMPPT METHOD

Based on the analysis above, to determine the GMPP of the PV system under PSC, Figure 4 introduces the proposed algorithm flow chart, including the following steps:

Step 1. Set value $D_{[i]} = [0.1; 0.8]$ and step size $\Delta D = 0.015$ to measure $V_{oc,sys}$ and $I_{sc,sys}$ of the PV system consisting of N modules in the SC. Set the open circuit voltage of the PV modules under standard conditions, such as $V_{oc,stc}$.

Step 2. Calculate $V_{oc[1]}$ of a the first PV module in the system according to (2) and select the value $I_{sc[1]} = I_{sc,sys}$ is the short-circuit current of the first PV module with the largest radiation. Increase counter variable i by 1 unit.

Step 3. Estimating the parameters at the first MPP point, including $V_{mp[1]}$, $I_{mp[1]}$, $P_{mp[1]}$ and $D_{mp[1]}$ according to (10), (11), (12) and (14), respectively. Then, the measured values at $D_{mp[1]}$ are updated and stored. Increase counter variable i by 1 unit.

Step 4. Determine the working resistance (R_{pv}) to find I_{sc} in the next zone. At i^{th} MPP points (i = 2 to N) according to (22) as follows

$$R_{pv} = \frac{\overline{V}_{\mathrm{oc}}\,(i-1) + 0.4\overline{V}_{\mathrm{oc}}}{I_{\mathrm{sc}[i-1]}} \tag{22}$$

Step 5. Calculate the $D_{[i]}$ value at the R_{pv} according to (23).

$$D_{[i]} = 1 - \frac{1}{1+\sqrt{R_L/R_{pv}}} \tag{23}$$

Step 6. Measure the parameters $I_{pv[i]}$ and $V_{pv[i]}$ corresponding to the $D_{[i]}$ value.

Step 7. Check the working position in shaded areas.

If $k_v V_{oc,stc} + \bar{V}_{oc}(i-2) < V_{pv} < V_{oc,stc} + \bar{V}_{oc}(i-2)$, then $I_{vp[i]} \neq I_{sc[i]}$, so the controller must increase the R_{pv} value according to (24) to jump next zone in the I-V curve. After that, return to step 5.

$$R_{pv} = \frac{1.4\overline{V}_{\mathrm{oc}}\,(i-1)}{I_{\mathrm{pv}}} \tag{24}$$

Step 8. If $V_{oc,stc} + \bar{V}_{oc}(i-2) < V_{pv} < 1.4\bar{V}_{oc}(i-1)$, then $\mathrm{I_{sc[i]}} = \mathrm{I_{pv}}$. Check whether all N modules have been scanned. If $i < N+1$, then calculate BB', $V_{mp[i]}$, $I_{mp[i]}$, $P_{mp[i]}$, and $D_{mp[i]}$ following (18), (19), (25), (26), and (27), respectively. Do the same for the remaining PVs until $i > N+1$, which means the shade is gone. Then, move to the next step, calculate $V_{mp[i]}$, $I_{mp[i]}$, $P_{mp[i]}$, and $D_{mp[i]}$ following (19), (25), (26), and (27), respectively.

$$I_{mp[i]} = k_i I_{sc[i]} = k_i I_{pv[i]} \tag{25}$$

$$P_{mp[i]} = V_{mp[i]} I_{mp[i]} \tag{26}$$

$$D_{mp[i]} = 1 - \frac{1}{1+\sqrt{R_L/R_{mp[i]}}} \tag{27}$$

Otherwise, $V_{pv} > 1.4\bar{V}_{oc}(i-1)$, the PV system operates under homogeneous conditions, and $I_{sc[i]} = I_{pv[i]}$. Recalculate the parameters at MPP according to (19), (25) to (27), and return to step 5 until $i > N+1$.

Step 9. Find the maximum power point and select the reference power (P_{ref}) corresponding to the largest $P_{mp[i]}$ value. At the same time, select the D_{ref} corresponding to P_{ref} as reference values for the next steps.

Step 10. Measure the I_{pv} and V_{pv} at the D_{ref} in step 9.

Step 11. Run P&O algorithm. Check the convergence condition. Modify the ΔD parameter to track the optimal MPP. The algorithm reaches convergence upon satisfying the constraint outlined in (28).

$$|\Delta P| = \frac{P_{[i]} - P_{[i-1]}}{P_{[i]}} 100\% \leq \varepsilon_P \tag{28}$$

Step 12. Check for sudden radiation changes based on calculating power loss (P_{loss}). If (29) is satisfied, go back to step 10. Otherwise, do it again from the beginning

$$|P_{loss}| = P_{[i]} - P_{[i-1]} \leq \beta_p \tag{29}$$

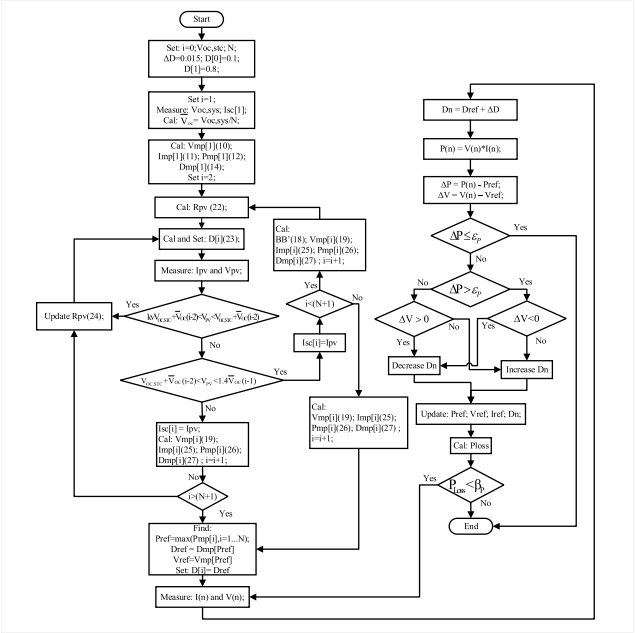

FIGURE 4. Algorithm flowchart of the proposed method.

IV. RESULTS AND DISCUSSIONS

The GMPPT algorithm is validated using simulation in the PSIM environment and experiments with the Chroma Simulator. The case studies are based on the scenarios listed in Table 2, including the number of LMPPs varying from 1 to 4 and the GMPP location being random at vertices 1, 2, 3, and 4 on the entire operating voltage range. Details of the location of the MPPs of the PV system in these cases are presented in Figure 5. The MPPT block provides an optimal D value to control the DC/DC converter to operate at the maximum power delivery to the load $R_L = 20\ \Omega$. The input and the output capacitance of the converter are $C_{in} = 100\ \mu$F and $C_{out} = 47\ \mu$F respectively, inductance is 0.4 mH, The simulation results focus on highlighting the merits of the proposed solution, including

1) Validate the ability to accurately position GMPP among LMPPs on the PV system's I-V characteristic curve.

2) Confirming the effectiveness of the proposed solution in improving MPPT performance and speed under PSC.

3) Demonstrate the proposed method's superior convergence speed and MPPT performance compared to other optimization algorithms under the same operating conditions.

Table 3 shows the voltage deviation at GMPP when using the method as documented [20] and the proposed solution. These data indicate that the proposed solution can calculate V_{mp} values more accurately in PSC. When the GMPP point is in the first position from the left (case 4), their calculation errors are the same because segment BB' has no impact. However, cases 2, 3, and 5 have apparent differences in V_{mpp} prediction due to the influence of the BB', and the proposed solution always gives more accurate results. Furthermore, if segment BB' is not added, the probability of misidentifying the extreme point will be higher (case 3) due to sensor noise

TABLE 2. The proposed simulation and experimental cases.

String 1	String 2
1000	1000
1000	1000
1000	1000
1000	1000

P_{max} = 166.75 W

String 1	String 2
1000	800
900	450
400	1000
750	500

P_{max} = 89.21 W

String 1	String 2
500	1000
1000	700
700	1000
1000	500

P_{max} = 103.12 W

String 1	String 2
1000	400
1000	400
400	1000
400	1000

P_{max} = 83.18 W

String 1	String 2	String 3
1000	200	900
900	700	200
450	450	400
200	900	1000

P_{max} = 109.80 W

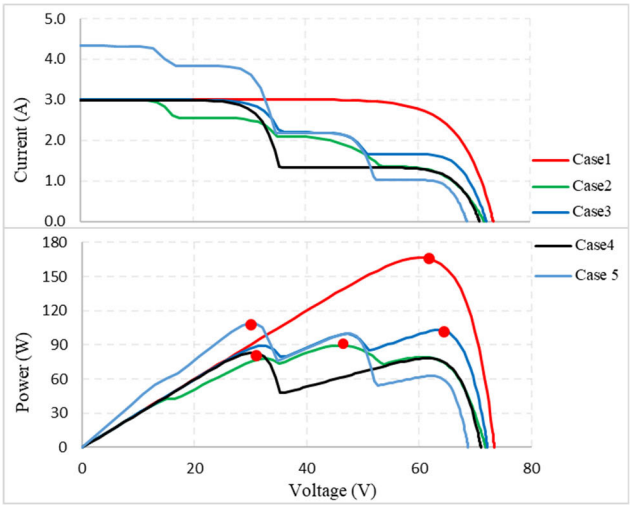

FIGURE 5. Characteristic curves of PV system under PSC.

TABLE 3. Compare the voltage error at GMPP between solutions.

Case	V_{mp}^{GMPP} (V)[20]	Proposed V_{mp}^{GMPP} (V)	Actual V_{mp}^{GMPP} (V)	ΔV (%) [20]	Proposed ΔV(%)
1	58.61	60.05	59.85	2.07	0.33
2	43.10	44.71	46.35	7.01	3.54
3	57.73	57.99	63.52	9.12	8.71
4	28.38	28.38	29.72	4.51	4.51
5	27.48	27.87	30.30	9.31	8.02

Note: k_V = 0.8 in this study.

errors. If the noise in the two cases shown in Figure 6 is considered the same, the addition of segment BB' ensures that the point $P_3 > P_2$ is always determined due to segment BB's additional impact. Uniform conditions (case 1) is a special case mentioned in Table 2. Experiments show that the error in determining the $I_{sc[4]}$ value is small, so it does not significantly affect the GMPP calculation results.

A. SIMULATION RESULTS

Figures 7 and 8 show the output parameters under standard conditions and PSC, respectively. The data pointed out that:

Under uniform conditions, after determining the basic parameters from $D_1 = 0.1$ and $D_2 = 0.8$, four D values

are calculated without adjustment because the current I_{sc} at the estimated positions is the same. The solution quickly determines GMPP stops before 0.075 s and achieves MPPT efficiency of about 99.94%, corresponding to an output power of 166.65 W compared to a maximum power of 166.75 W.

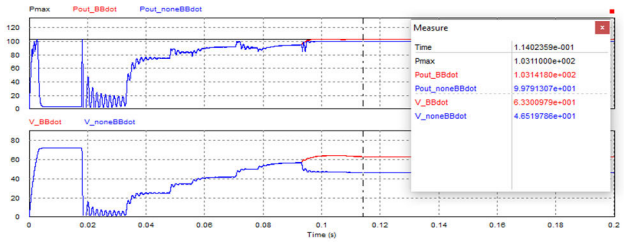

FIGURE 6. Compare waveforms with and without BB'.

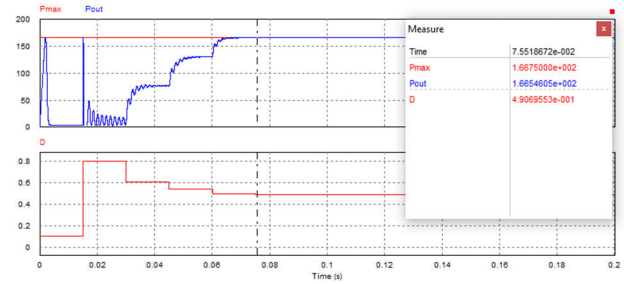

FIGURE 7. MPPT simulation under standard condition.

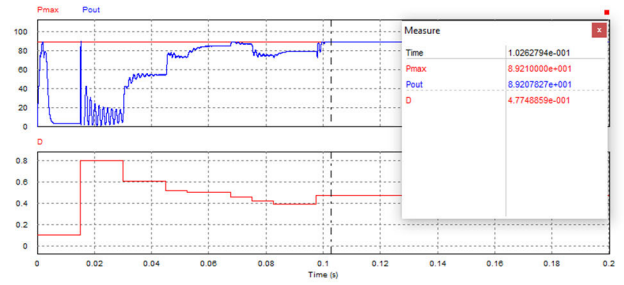

FIGURE 8. MPPT simulation under PSC.

When PSC occurs, waveform graph D in Figure 8 shows the adjustment steps in the LMPP region to find the optimal limit. Specifically, the solution needs to adjust D by changing the R value once in zone 2, while in zone 3, it requires two updates. After 0.102 s, the algorithm can converge and extract energy equivalent to 89.20 W compared to the maximum value of 89.21 W, achieving MPPT efficiency of about 99.99%. In the remaining cases, MPPT efficiency is above 99.9%. Simulation results for the proposed cases are summarized in the following Table 4.

For case 3, the values at the LMPPs are almost the same ($P_3 = 99.7.18$ W, $P_4 = 103.12$ W). A scenario is investigated to compare the results of using segment BB' and not in determining GMPP under PSC. This work aims to validate the proposed solution's potential GMPP precise positioning ability compared to previous versions. Figure 6 presents the simulation process of the proposed algorithm when using

TABLE 4. Simulation results with the proposed solution.

Cases	1	2	3	4	5
P_{max} (W)	166.75	89.21	103.12	83.18	109.80
P_{out} (W)	166.65	89.20	103.10	83.13	109.78
Efficiency (%)	99.94	99.99	99.98	99.94	99.98
Time (s)	0.075	0.102	0.108	0.112	0.146

BB's value and without to calculate the voltage V_{mp}. The results show that without BB's value, the voltage V_{mp} lacks a large amount of cumulative voltage from PV panel 2 to PV panel 4, causing a power difference. This deviation is significantly more significant when the number of PVs in the string increases. As a result, the power comparator misidentifies the potential GMPP (the correct point is at position 4). The simulated power and voltage waveforms in Figures 6 show that when the BB' segment is used, the GMPP point is located precisely at P_3 ($V_{mp} = 63.40$ V). Meanwhile, GMPP is incorrectly located at P_2 with $V_{mp} = 47.50$ V without BB'. In reality, operating conditions are not as optimal as simulated, so the error is much larger due to sensor signal interference. Therefore, segment BB' should be used to improve reliability.

In addition, a simulation scenario under changing operating conditions is also investigated. When the PV system operates at standard conditions with a single MPP of 166.75 W, partial shading suddenly occurs at 0.15 s. The power value and GMPP position change from case 1 to case 2. This condition generates four peaks, and the proposed solution has to find a new GMPP. The resulting simulation output waveform for this scenario is shown in Figure 9, which shows that, after the working conditions change, the proposed solution repeats the entire calculation process in 1 s. A new stable position is determined at 0.25 s with an efficiency of over 99.94%.

In general, for simulation results under uniform conditions, PSC, or continuously changing radiation, the proposed algorithm still demonstrates the ability to accurately GMPPT at high speed.

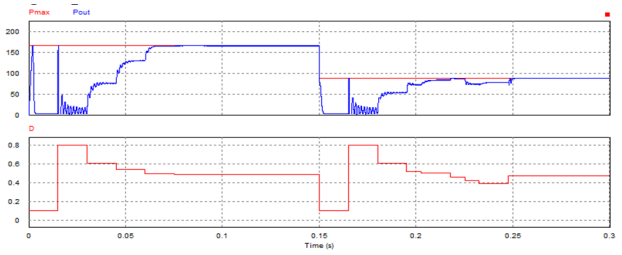

FIGURE 9. MPPT under variable operating conditions.

B. EXPERIMENT WITH THE PROPOSED ALGORITHM

The proposed solution has been experimented with on a PV Chroma 62050H-600S simulator (Figure 10). The system is tested based on the operating conditions as previously simulated. The results under standard conditions (Figure 11a)

show the most excellent MPPT efficiency can reach 99.97% with an average power of 166.5 W. The current and voltage waveforms in Figure 11b also show how the algorithm determines the LMPP in different zones to find the potential MPP region (with zones 1, 2, 3, 4 being the determining regions $I_{sc[1]}$, $I_{sc[2]}$, $I_{sc[3]}$, $I_{sc[4]}$, respectively). The search speed, in this case, is about 0.70 s.

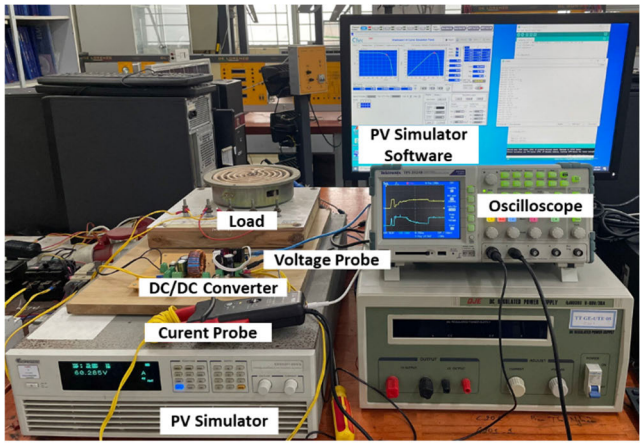

FIGURE 10. Experimental system setup.

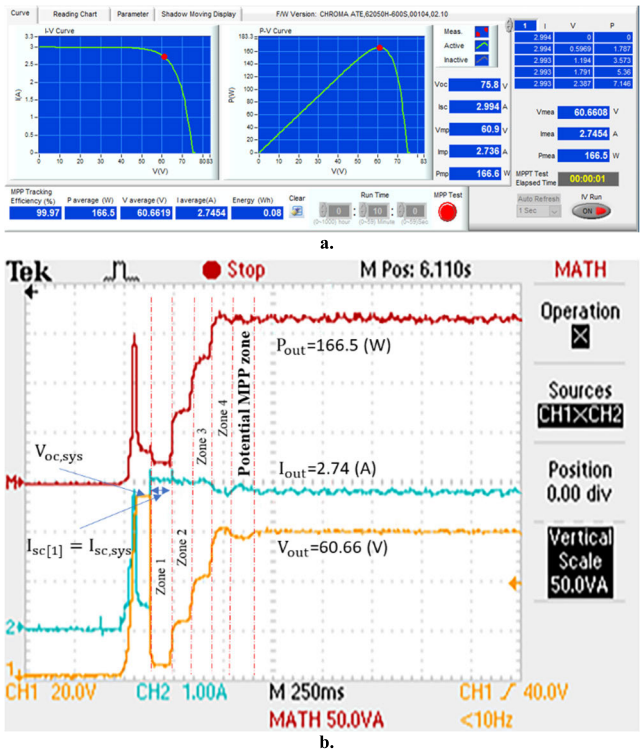

FIGURE 11. Experiment MPPT for No.01 with a. efficiency, and b. waveforms.

Meanwhile, Figure 12 presents the ability to exploit energy under PSC. The average output power is 88.82 W, reaching 99.46%. The convergence speed is also significantly improved when the total search time is about 0.9 s. This is also the case with the lowest experimental performance. The average efficiency for all cases is 99.78%.

Experimental scenarios under changing working conditions are similarly investigated. The output waveform results in Figure 13 show that it can re-stabilize quickly after a disturbance in less than 0.75 s. When operating under standard conditions, the I-V characteristic curve has a single extreme, so the $I_{mp[i]}$ values are the same and equal to $k_i I_{sc,sys}$. The power at the LMPPs is differentiated based on the $V_{mp[i]}$. When the radiation fluctuates from case 1 to 2, the proposed solution needs 1.5 s to stabilize at the new GMPP position (Figure 13). Due to the appearance of many steps on the I-V curve, the $I_{mp[i]}$ and $V_{mp[i]}$ values are redefined based on the ability to update R_{pv}. In which, $V^{I_{sc[1]}}$ to $V^{I_{sc[4]}}$ are the voltage at the corresponding I_{sc} determination region. The solution significantly reduced search time by updating ΔR to adjust to a new search space compared to using a fixed ΔD value. Therefore, the convergence speed is improved, and the GMPPT efficiency is enhanced. The above experiment was performed based on the popular Arduino Nano microcontroller, so noise handling and relatively significant signal transmission delay also significantly reduced convergence time.

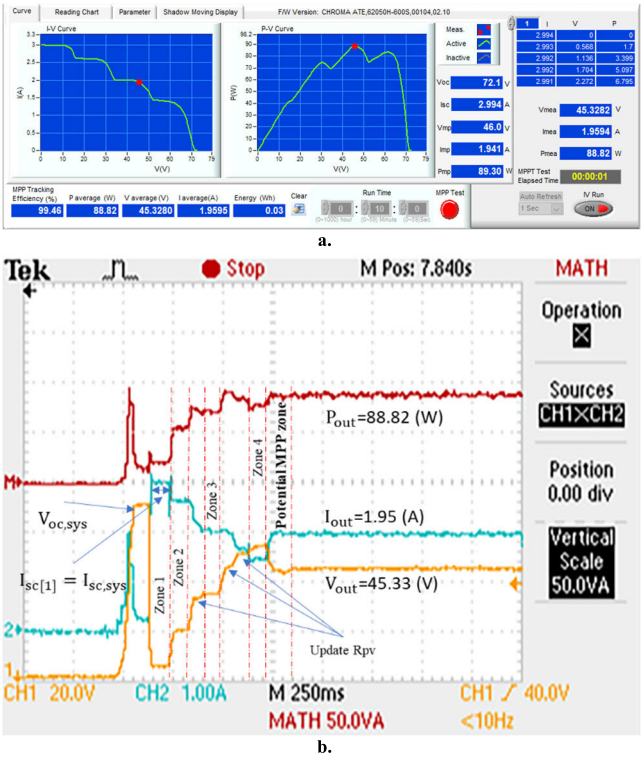

FIGURE 12. Experiment MPPT for No.02 with a. efficiency, and b. waveforms.

To ensure the algorithm works effectively with a system of multiple strings connected in parallel, Figure 14 shows the current, voltage, and output power waveforms when experimenting with 3 parallel strings (case 5). Obviously, for systems with many strings, the algorithm still works well, but it takes more time to locate the GMPP value. This depends on the degree of shading of the PV panels. In this case, the convergence speed is about 1.125 s.

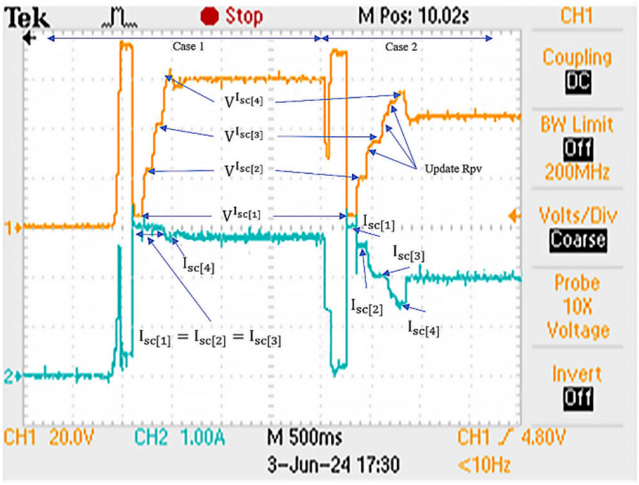

FIGURE 13. Experiment with MPPT under variable conditions.

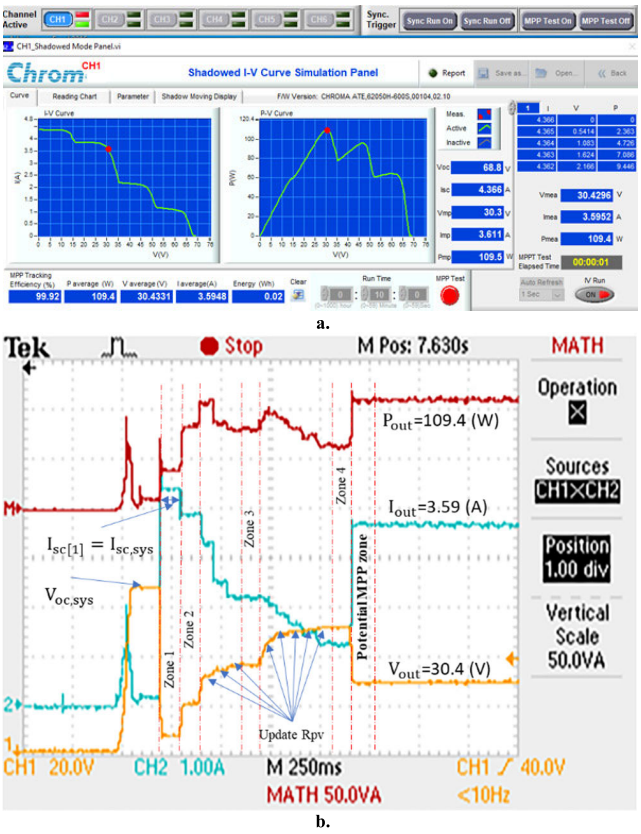

FIGURE 14. Experimental results with three parallel strings a. efficiency, and b. waveforms.

To confirm the validity of the proposed solution compared to previous studies, a simulation scenario under PSC using four modules, S36 in Table 5 to 7, and KC85T in Table 8, are compared with previous research results in the literature [25], and [16]. The simulation results are summarized in Tables 5 to 7 shown that:

In the first scenario when operating conditions are uniform (Table 5), the proposed solution exploits an output power of 142.9488 W compared to the maximum value of 142.97 W, achieving an efficiency of about 99.98%. The MPPT performance of the algorithms is quite similar but the convergence speed significantly differs. Compared to the search time of the proposed algorithm, which is 0.079 s, the Ajaya, Jaya, and PSO algorithms have speeds of 0.602 s, 1.174 s, and 1.177 s, respectively [25]. This result shows that the proposed solution can reduce search time by up to approximately 93.30% compared to PSO and Jaya. It also saves 86.88% processing time compared to Ajaya's improved version.

TABLE 5. Comparison based on convergence speed and GMPPT efficiency under uniform condition using S36 PV module [25].

The radiation (W/m^2)			
PV1	PV2	PV3	PV4
1000	1000	1000	1000

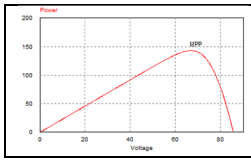

MPPT algorithm	Time (s)	Eff (%)
Proposed	0.079	99.98
Ajaya [25]	0.602	99.93
Jaya [25]	1.174	99.98
PSO [25]	1.177	99.98

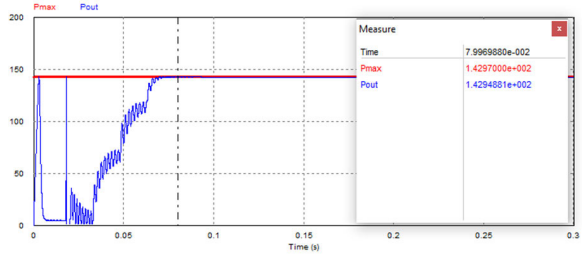

TABLE 6. Comparison of convergence speed and GMPPT performance under PSC when the extrema is on the left.

The radiation (W/m^2)			
PV1	PV2	PV3	PV4
1000	1000	300	300

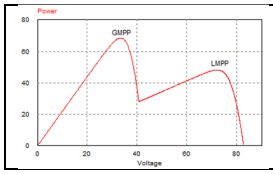

MPPT algorithm	Time (s)	Eff (%)
Proposed	0.136	99.99
Ajaya [25]	0.844	99.93
Jaya [25]	1.771	99.96
PSO [25]	1.627	99.97

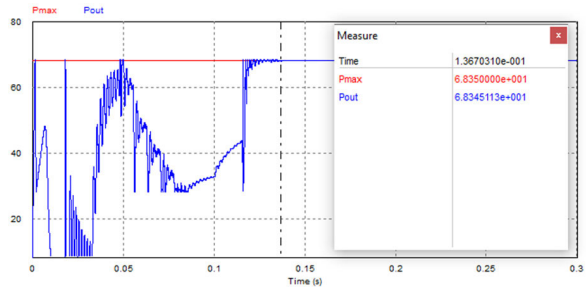

In the following scenario under PSC, with two extreme peaks and GMPP shifted to the left – low voltage region (Table 6). The MPPT speed of the proposed algorithm is

0.136 s, while the search times of the PSO, Jaya, and Ajaya methods are 1.627 s, 1.771 s, and 0.844 s, respectively. In this scenario, the proposed solution reduced the search time by a maximum of 92.32% compared to Jaya. The average processing time has been reduced by 89.28%. The Ajaya algorithm has the lowest MPPT efficiency, 99.93%. This means it improves speed but is less efficient than the unmodified version and PSO. Meanwhile, the proposed algorithm not only increases the convergence speed but can also achieve the best performance, about 99.99%.

For the final shading scenario using S36 PV panels, the GMPP is in the middle position on the P-V characteristic curve (Table 7). The proposed algorithm stabilizes the output power at 0.125 s while PSO needs 1.473 s, Jaya converges after 1.17 s, and Ajaya stops at 0.694 s. That means it can save 91.51% of the time compared to PSO, 89.31% to Jaya, and 81.99% to Ajaya. The proposed algorithm and PSO have an efficiency equivalent to 99.99%, while the lowest efficiency is 99.90% for Ajaya and that of Jaya is 99.94%.

TABLE 7. Comparison of convergence speed and GMPPT performance under PSC when the extrema is in the middle.

The radiation (W/m^2)			
PV1	**PV2**	**PV3**	**PV4**
1000	**700**	**500**	**300**

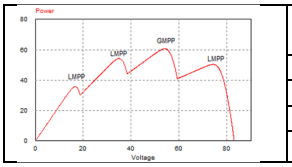

MPPT algorithm	Time (s)	Eff (%)
Proposed	0.125	99.99
Ajaya [25]	0.694	99.90
Jaya [25]	1.17	99.94
PSO [25]	1.473	99.99

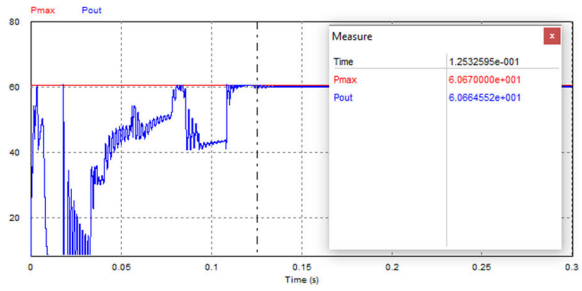

It can be concluded from these results that the proposed algorithm tracked the MPP in the least amount of time spent. The proposed algorithm's average search time reduction percentage compared with PSO, Jaya, and Ajaya is 92.15%, 91.64%, and 84.25%, respectively. Furthermore, the proposed algorithm has outstanding performance in all test scenarios.

Besides, the ability of the proposed algorithm to improve GMPPT speed is also compared with the InC-Cond algorithm in the document [16]. With four KC85T PV panels, two shading patterns generate the four LMPPs in Table 8.

In the first pattern, the extreme peak is on the right – the high voltage region. The search speed of the proposed algorithm is 0.102 s compared to InC-Cond, which is 1.010 s. Thereby, processing time can be reduced by 86.04%. Meanwhile, with pattern 2, the GMPP position is in the middle of the characteristic curve. The proposed algorithm also quickly locates and stabilizes after 0.133 s. Meanwhile, the InC-Cond algorithm requires 1.5 s. Under this condition, the proposed solution reduced the search time by about 91.47%. It not only has outstanding convergence speed but also has significantly better MPPT performance in shading states.

TABLE 8. Comparison of convergence speed and GMPPT performance under PSC when the extrema is on the right, using KC85T PV module [16].

The radiation (W/m^2)			
PV1	**PV2**	**PV3**	**PV4**
1000	**600**	**400**	**300**

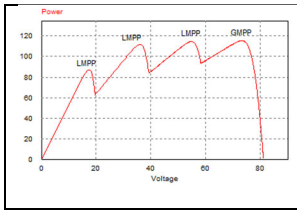

MPPT algorithm	Time (s)	Eff (%)
Proposed	0.102	99.96
Inc-Cond [16]	1.010	99.23

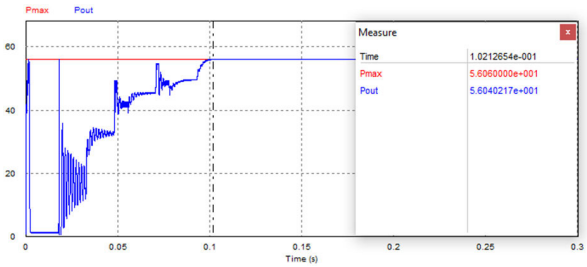

1000	**500**	**400**	**200**

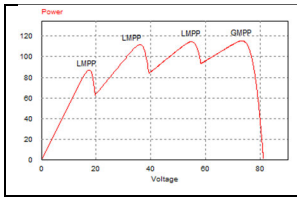

MPPT algorithm	Time (s)	Eff (%)
Proposed	0.133	99.98
Inc-Cond [16]	1.500	99.30

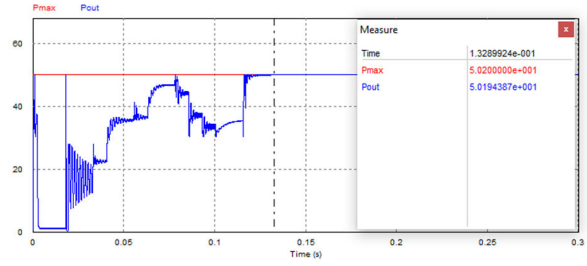

In summary, in any PSC scenario, the proposed algorithm always has outstanding GMPP speed. These results accurately reflect how the solution performs based on the ability to regulate ΔR within the $1.4V_{oc}$ control limit. It allows broad jump adjustments to overcome new shade areas. This solution is more effective than using the same ΔD value to scan the entire I-V curve applied in the literature [16]. Simulation

and experimental results show that the proposed solution promises to bring convenient applications in series and series - parallel configuration.

Research results in reference documents have proven them to be the best versions compared to previous adjusted or modified versions in all operating conditions. Therefore, to demonstrate the outstanding GMPPT ability of the proposed solution, this study only focuses on comparing the results obtained with the group of algorithms considered the best published previously. The comparison results are summarized in Table 8 show that the two solutions, M-VSS-P&O [6] and PSO+P&O [13], require less search time but do not mention PSC. The algorithms to solve the PSC problem require more time but the proposed solution is still superior in terms of convergence speed and MPPT performance. Moreover, it is better than M-P&O proposed in [17].

TABLE 9. Comparison of convergence speed and GMPPT performance some MPPT solutions.

MPPT methods	Efficiency (%)	Convergence speed (s)	Tested for PSC
Proposed	99.99	0.115	Yes
EAGPSO [9]	98.60	2.6	Yes
Ajaya [25]	99.93	0.602	Yes
I-GWO [11]	99.57	72	Yes
M-VSS-P&O [6]	99.37	0.01634	NA
PSO+P&O [13]	98.73	0.0495	NA
M-P&O [17]	99.80	0.50	NA

V. CONCLUSION

The article proposed a GMPPT method for PV systems under PSC based on the combination of the behavior of the I-V characteristic curve with the traditional P&O algorithm. By calculating the voltage deviation between two consecutive extreme peaks when shading occurs, this method can position the LMPP more accurately to increase the convergence speed and improve the GMPPT performance. The average convergence speed, about 0.115 s, was reduced by 92.14% compared to PSO and an average decrease of 90.63% compared to other algorithms under the same operating conditions. In a solution, achieving both goals, such as fast search time and high GMPPT performance, is challenge. However, the proposed algorithm is outstanding in convergence speed and has higher GMPPT performance than the other algorithms under the same operating conditions. The results have shown that this method is simple, easy to implement, and more reliable than the previous algorithms under PSC. It is a piece that completes the picture of GMPPT techniques and helps visualize in more detail the behavior of the PV system's I-V and P-V characteristic curves under PSC. Therefore, it has many potential applications in PV systems operating under different conditions.

REFERENCES

[1] A. Calcabrini, M. Muttillo, R. Weegink, P. Manganiello, M. Zeman, and O. Isabella, "A fully reconfigurable series-parallel photovoltaic module for higher energy yields in urban environments," *Renew. Energy*, vol. 179, pp. 1–11, Dec. 2021.

[2] L. Gao, R. A. Dougal, S. Liu, and A. P. Iotova, "Parallel-connected solar PV system to address partial and rapidly fluctuating shadow conditions," *IEEE Trans. Ind. Electron.*, vol. 56, no. 5, pp. 1548–1556, May 2009, doi: 10.1109/TIE.2008.2011296.

[3] Z. Bi, J. Ma, K. Wang, K. L. Man, J. S. Smith, and Y. Yue, "Identification of partial shading conditions for photovoltaic strings," *IEEE Access*, vol. 8, pp. 75491–75502, 2020, doi: 10.1109/ACCESS.2020.2988017.

[4] A. S. Yadav, R. K. Pachauri, Y. K. Chauhan, S. Choudhury, and R. Singh, "Performance enhancement of partially shaded PV array using novel shade dispersion effect on magic-square puzzle configuration," *Sol. Energy*, vol. 144, pp. 780–797, Mar. 2017.

[5] S. Malathy and R. Ramaprabha, "Comprehensive analysis on the role of array size and configuration on energy yield of photovoltaic systems under shaded conditions," *Renew. Sustain. Energy Rev.*, vol. 49, pp. 672–679, Sep. 2015.

[6] D. Khodair, S. Motahhir, H. Mostafa, A. Shaker, H. Munim, M. Abouelatta, and A. Saeed, "Modeling and simulation of modified MPPT techniques under varying operating climatic conditions," *Energies*, vol. 16, no. 1, p. 549, Jan. 2023.

[7] I. Shams, S. Mekhilef, and K. S. Tey, "Improved social ski driver-based MPPT for partial shading conditions hybridized with constant voltage method for fast response to load variations," *IEEE Trans. Sustain. Energy*, vol. 12, no. 4, pp. 2255–2267, Oct. 2021.

[8] M. L. Katche, A. B. Makokha, S. O. Zachary, and M. S. Adaramola, "A comprehensive review of maximum power point tracking (MPPT) techniques used in solar PV systems," *Energies*, vol. 16, no. 5, p. 2206, Feb. 2023.

[9] A. Refaat, A.-E. Khalifa, M. M. Elsakka, Y. Elhenawy, A. Kalas, and M. H. Elfar, "A novel metaheuristic MPPT technique based on enhanced autonomous group particle swarm optimization algorithm to track the GMPP under partial shading conditions—Experimental validation," *Energy Convers. Manage.*, vol. 287, Jul. 2023, Art. no. 117124.

[10] A. O. Baatiah, A. M. Eltamaly, and M. A. Alotaibi, "Improving photovoltaic MPPT performance through PSO dynamic swarm size reduction," *Energies*, vol. 16, no. 18, p. 6433, Sep. 2023.

[11] H. Gundogdu, A. Demirci, S. M. Tercan, and U. Cali, "A novel improved grey wolf algorithm based global maximum power point tracker method considering partial shading," *IEEE Access*, vol. 12, pp. 6148–6159, 2024.

[12] L. Gong, G. Hou, and C. Huang, "A two-stage MPPT controller for PV system based on the improved artificial bee colony and simultaneous heat transfer search algorithm," *ISA Trans.*, vol. 132, pp. 428–443, Jan. 2023.

[13] M. H. Ibrahim, S. P. Ang, M. N. Dani, M. I. Rahman, R. Petra, and S. M. Sulthan, "Optimizing step-size of perturb & observe and incremental conductance MPPT techniques using PSO for grid-tied PV system," *IEEE Access*, vol. 11, pp. 13079–13090, 2023.

[14] A. Hassan, O. Bass, and M. A. S. Masoum, "An improved genetic algorithm based fractional open circuit voltage MPPT for solar PV systems," *Energy Rep.*, vol. 9, pp. 1535–1548, Dec. 2023.

[15] J. Ahmed and Z. Salam, "An accurate method for MPPT to detect the partial shading occurrence in a PV system," *IEEE Trans. Ind. Informat.*, vol. 13, no. 5, pp. 2151–2161, Oct. 2017.

[16] K. S. Tey and S. Mekhilef, "Modified incremental conductance algorithm for photovoltaic system under partial shading conditions and load variation," *IEEE Trans. Ind. Electron.*, vol. 61, no. 10, pp. 5384–5392, Oct. 2014.

[17] R. I. Jabbar, S. Mekhilef, M. Mubin, and K. K. Mohammed, "A modified perturb and observe MPPT for a fast and accurate tracking of MPP under varying weather conditions," *IEEE Access*, vol. 11, pp. 76166–76176, 2023.

[18] Y. Wang, Y. Li, and X. Ruan, "High-accuracy and fast-speed MPPT methods for PV string under partially shaded conditions," *IEEE Trans. Ind. Electron.*, vol. 63, no. 1, pp. 235–245, Jan. 2016.

[19] M. A. Husain, A. Jain, A. Tariq, and A. Iqbal, "Fast and precise global maximum power point tracking techniques for photovoltaic system," *IET Renew. Power Gener.*, vol. 13, no. 14, pp. 2569–2579, Aug. 2019.

[20] L. Li, Y. Chen, H. Liu, W. Tang, M. Liu, J. Wu, and Z. Li, "A multi-producer group-search-optimization method-based maximum-power-point-tracking for uniform and partial shading condition," *IEEE Access*, vol. 8, pp. 184688–184696, 2020.

[21] V. H. Bui, V. A. Truong, V. L. Nguyen, and T. L. Duong, "Estimating the potential maximum power point based on the calculation of short-circuit current and open-circuit voltage," *IET Power Electron.*, vol. 17, no. 3, pp. 402–421, Jan. 2024.

[22] M. Kumar, K. P. Panda, J. C. Rosas-Caro, A. Valderrabano-Gonzalez, and G. Panda, "Comprehensive review of conventional and emerging maximum power point tracking algorithms for uniformly and partially shaded solar photovoltaic systems," *IEEE Access*, vol. 11, pp. 31778–31812, 2023.
[23] B. V. Hien, T. V. Anh, N. T. Linh, and P. Q. Khanh, "Rapidly determine the maximum power point in the parallel configuration of the photovoltaic system," *Sensors*, vol. 23, no. 17, p. 7503, Aug. 2023.
[24] A. Ba, C. O. Ehssein, M. E. M. O. M. Mahmoud, O. Hamdoun, and A. Elhassen, "Comparative study of different DC/DC power converter for optimal PV system using MPPT (P&O) method," *Appl. Sol. Energy*, vol. 54, no. 4, pp. 235–245, Nov. 2018.
[25] I. Pervez, A. Pervez, M. Tariq, A. Sarwar, R. K. Chakrabortty, and M. J. Ryan, "Rapid and robust adaptive Jaya (Ajaya) based maximum power point tracking of a PV-based generation system," *IEEE Access*, vol. 9, pp. 48679–48703, 2021.

TRUONG VIET ANH was born in Hanoi, Vietnam, in 1971. He received the B.Eng., M.Eng., and Ph.D. degrees in electrical engineering from Ho Chi Minh City University of Technology (HCMUT), Vietnam National University Ho Chi Minh City (VNU-HCM), Vietnam, in 1994, 1999, and 2004, respectively.

He is currently with the Faculty of Electrical-Electronic Engineering and the Power System and Renewable Energy Laboratory (C201), Ho Chi Minh City University of Technology and Education, Thu Duc, Ho Chi Minh City, Vietnam.

TON NGOC TRIEU was born in Quang Ngai, Vietnam, in 1981. He received the B.Eng., M.Eng., and Ph.D. degrees in electrical engineering from Ho Chi Minh City University of Technology and Education, Ho Chi Minh City, Vietnam, in 2005, 2009, and 2023, respectively.

He works with the Training Department, Thu Duc College of Technology, Ho Chi Minh City.

PHAM VO HONG NGHI received the B.Eng. degree in electrical and electronic engineering from Ho Chi Minh City University of Technology and Education, Thu Duc, Ho Chi Minh City, Vietnam, in 2022, where he is currently pursuing the master's degree in electrical engineering.

He is with the Laboratory (C201), Ho Chi Minh City University of Technology and Education.

BUI VAN HIEN received the bachelor's and master's degrees in electrical engineering from Ho Chi Minh City University of Technology and Education, Ho Chi Minh City, Vietnam, in 2005 and 2009, respectively, where he is currently pursuing the Ph.D. degree with the Faculty of Electrical-Electronic Engineering.

He is a Lecturer with the Faculty of Mechanical–Electrical and Computer Engineering, School of Technology, Van Lang University, Ho Chi Minh City.

Bài báo số 4:

Bùi Văn Hiền, Trương Việt Anh, Quách Thanh Hải (2020). *"Tối ưu điểm phát công suất cực đại của pin quang điện làm việc trong điều kiện bóng che".* Tạp chí Phát triển Khoa học và Công nghệ – Kĩ thuật và Công nghệ, 73(1), pp: 326-338, https://doi.org/10.32508/stdjet.v3i1.544.

Tạp chí Phát triển Khoa học và Công nghệ – Kĩ thuật và Công nghệ, 3(1):326-338

Open Access Full Text Article

Bài Nghiên cứu

Tối ưu điểm phát công suất cực đại của pin quang điện làm việc trong điều kiện bóng che

Bùi Văn Hiền[1], Trương Việt Anh[2,*], Quách Thanh Hải[2]

Use your smartphone to scan this QR code and download this article

TÓM TẮT

Pin quang điện (PV) được dùng để biến đổi điện năng từ bức xạ mặt trời. Đặc tính làm việc của nó phụ thuộc vào điều kiện môi trường như nhiệt độ, cường độ bức xạ mặt trời và môi trường xung quanh. Trong quá trình hoạt động, hệ thống PV có thể bị che một phần hoặc toàn bộ do các hiện tượng tự nhiên như: đám mây, tòa nhà, bụi, động vật, cột điện, cây cối… làm thay đổi đặc tính công suất phát của nó. Bài báo này đề xuất một giải thuật dò tìm điểm phát công suất cực đại (MPPT) của hệ thống PV vận hành trong điều kiện bóng che một phần dựa trên thuật toán tối ưu hóa phần tử bày đàn (PSO) và một mô hình gồm 3 modul PV loại PHM60W36 được sử dụng để mô phỏng bằng phần mềm PSIM. Nghiên cứu tập trung vào sự thay đổi đặc tính làm việc của hệ thống khi thay đổi các yếu tố như: mức độ, vị trí che phủ pin quang điện. Tính hiệu quả của giải pháp đề xuất không những được so sánh với phương pháp nhiễu loạn và quan sát (P&O) mà còn được so sánh với các giải thuật tối ưu trước đó trong cùng điều kiện vận hành. Bên cạnh đó, một mô hình thực nghiệm được phát triển để khảo sát đáp ứng của giải pháp đề xuất trong môi trường thực với bộ mô phỏng pin quang điện Chroma-62050H cũng được xem xét thảo luận. Những kết quả thu được cho thấy sự vượt trội của giải pháp đề xuất trong việc nâng cao hiệu suất và tốc độ MPPT của hệ thống trong điều kiện vận hành phức tạp.

Từ khoá: Bóng che một phần, pin quang điện, dãy pin năng lượng mặt trời, đặc tính P-V

GIỚI THIỆU

Trong khi vấn đề ấm lên toàn cầu do sử dụng năng lượng từ các nguồn hóa thạch phát thải khí nhà kính đang được quan tâm trên toàn thế giới thì việc các nhà máy năng lượng xanh, sạch, bền vững phát triển một cách nhanh chóng như ngày nay là một tất yếu. Điện mặt trời đã, đang và sẽ đóng góp một phần không nhỏ vào việc duy trì ổn định nguồn cung cấp điện do sự thiếu hụt các nguồn năng lượng truyền thống và nhu cầu sử dụng ngày một tăng cao của con người [1,2]. Tuy nhiên, các module PV khi làm việc với tổng trở tải không thích hợp vẫn có hiệu suất chuyển đổi thấp, mặt khác, nó cũng bị ảnh hưởng không nhỏ bởi các điều kiện vận hành như bóng che một phần. Do đó, dò tìm MPPT là điều cần thiết trong một hệ thống PV. Điện năng tạo ra của một modul PV phụ thuộc vào dòng điện và điện áp hoạt động của nó. Trên đặc tuyến V-I và P-V của PV tồn tại duy nhất một điểm mà ở đó công suất phát đạt cực đại, điểm này thay đổi phụ thuộc vào bức xạ và nhiệt độ môi trường. Nhiệm vụ của bộ MPPT là xác định và duy trì chế độ làm việc hiệu quả nhất. Tuy nhiên, công suất đạt được bị dao động lớn và dễ rơi vào cực trị địa phương (LMPP) khi bức xạ của các module không đồng đều. Vì vậy, ngoài phương pháp truyền thống là P&O và điện dẫn gia tăng (Incremental Conductance-INC), gần đây nhiều giải thuật tối ưu khác cũng đã được đề xuất để cải thiện nhược điểm của giải thuật truyền thống như: Modified PSO (M-PSO), Bat Algorithm (BA), Whale Optimization Algorithm (WOA), Firework Algorithm (FWA), Grey Wolf Optimization (GWO), Ant Colony Optimization (ACO), Firefly Algorithm (FFA), hay sự kết hợp giữa các giải thuật với nhau như PSO-P&O, INC-FFA, FWA-P&O [3–13]. Hiệu suất, tốc độ hội tụ, độ phức tạp và chi phí nói lên tính khả thi của giải pháp. Việc duy trì độ chính xác tối đa với thời gian nhỏ nhất trong nghiên cứu của Ram and Rajasekar (2017) [3] tỏ ra hiệu quả hơn M-PSO trong nghiên cứu của Chao *et al.* [4]. Ngay cả khi kết hợp PSO và P&O [13] giúp giảm không gian tìm kiếm nên giảm đáng kể thời gian hội tụ nhưng tính hiệu quả không được đề cập [14]. Bài viết này đề xuất sử dụng giải thuật PSO với sự cải tiến bộ lọc, giới hạn độ rộng xung D và phân bố hợp lý các tham số điều khiển để xác định GMPPT trong điều kiện bức xạ thay đổi khi bị bóng che. Tính hiệu quả của giải thuật đề xuất được kiểm chứng với P&O truyền thống và các giải thuật tối ưu khác trình bày trong phần Kết quả và Thảo luận.

[1]*Trường ĐH Công nghiệp Thực phẩm Thành Phố Hồ Chí Minh, Việt Nam*

[2]*Trường ĐH Sư phạm Kỹ thuật TP.HCM, Việt Nam*

Liên hệ

Trương Việt Anh, Trường ĐH Sư phạm Kỹ thuật TP.HCM, Việt Nam

Email: anhtv@hcmute.edu.vn

Lịch sử

- Ngày nhận: 13-08-2019
- Ngày chấp nhận: 10-12-2019
- Ngày đăng: 31-3-2020

DOI : 10.32508/stdjet.v3i1.544

Check for updates

Trích dẫn bài báo này: Hiền B V, Anh T V, Hải Q T. **Tối ưu điểm phát công suất cực đại của pin quang điện làm việc trong điều kiện bóng che**. *Sci. Tech. Dev. J. - Eng. Tech.;* 3(1):326-338.

CƠ SỞ LÝ THUYẾT VÀ PHƯƠNG PHÁP GIẢI QUYẾT

Pin quang điện

Mô hình toán của tế bào quang điện được giới thiệu trong **Hình 1** bao gồm một diode song song với một nguồn dòng được điều khiển bởi ánh sáng và hai điện trở nối tiếp và song song là R_S, R_P [15–18].

Hai thông số quan trọng của PV là dòng ngắn mạch I_{SC} và điện áp hở mạch V_{OC} liên quan đến biểu thức tính dòng ngõ ra (2), (3). Dòng qua diode:

$$I_d = I_0\left(e^{\frac{qV_d}{kT}} - 1\right) \qquad (1)$$

Mà $I_{SC} - I_d - I - I_P = 0$

$\Rightarrow I = I_{SC} - I_d - I_P$

Với $I_P = \frac{V_d}{R_P}$ và $V_d = V + I.R_S$

$$\Rightarrow I = I_{SC} - I_0\left\{e^{\frac{q(V+I.R_S)}{kT}} - 1\right\} - \frac{V+I.R_S}{R_P} \qquad (2)$$

Điện áp hở mạch

$$V_{OC} = \frac{kT}{q}\ln\left(\frac{I_{SC}}{I_0} + 1\right) \qquad (3)$$

Trong đó:

V_d - điện áp diode (V);

V – điện áp ra của PV (V)

I – dòng điện ra của PV (A).

I_P – dòng qua điện trở R_P (A)

I_{SC} – dòng điện ngắn mạch của PV (A)

I_0 – dòng điện bão hòa của diode (A);

q - điện tích của electron ($1{,}602.10^{-19}$C);

k - hằng số Boltzman ($1{,}381.10^{-23}$J/K);

T - nhiệt độ lớp tiếp xúc (K);

R_S, R_P – điện trở nối tiếp và song song (W)

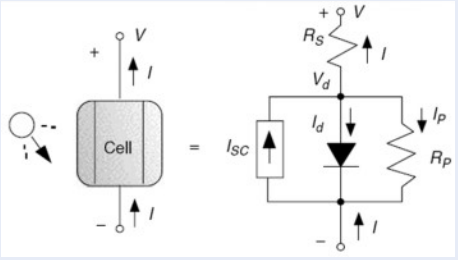

Hình 1: **Sơ đồ thay thế tế bào quang điện.**

Ảnh hưởng của bóng che.

Từ (1), (2) và (3), một mô hình gồm 3 modul PV có thông số như **Bảng 1** được sử dụng để mô phỏng và thực nghiệm.

Trong điều kiện vận hành tiêu chuẩn (1000 W/m^2 tại 25^{o}C), thông thường công suất của một PV khá nhỏ được xác định dựa vào đường đặc tuyến I-V như **Hình 2**. Do đó, để có được hệ thống với dòng điện lớn thì cần mắc song song các modul PV, ngược lại muốn có một điện áp ngõ ra cao cần phải liên kết nối tiếp chúng với nhau. Khi cần một điện áp cao và dòng cũng phải đủ lớn thì cấu hình nối tiếp – song song thường được sử dụng [19,20].

Bảng 1: Thông số module PV

Tên module PV	PHM60W36
Số lượng cell	36
Công suất cực đại	60 W
Dòng điện tại Pmax	3,33 A
Điện áp tại Pmax	18 V
Dòng điện ngắn mạch Isc	3,99 A
Điện áp hở mạch Voc	21,6 V
Hiệu suất module	14,2 %
Điện áp cực đại hệ thống	165 V
Kích thước	780 x 675 x 35 mm

Các nghiên cứu trước đây cũng chỉ ra rằng, trong cùng điều kiện vận hành với mức độ bức xạ của các module là như nhau, đường đặc tuyến P-V và I-V của hệ thống không thay đổi hình dạng (**Hình 2**). Nhưng khi mức độ bức xạ không đồng đều, số lượng MPP tăng lên gây khó khăn cho việc xác định MPP toàn cục ảnh hưởng đến công suất ra của toàn hệ thống. Theo đó, việc sử dụng các giải thuật MPPT là cần thiết trong trường hợp này (**Hình 3**).

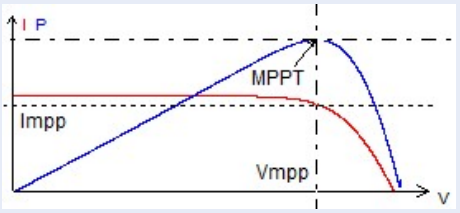

Hình 2: **Đặc tuyến I-V và P-V của PV.**

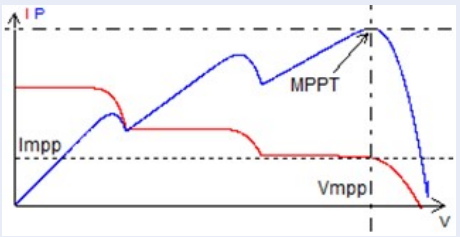

Hình 3: **Đặc tuyến I-V và P-V khi bị bóng che.**

Bộ chuyển đổi DC – DC

Như đã trình bày trong mục Ảnh hưởng của bóng che, điện áp của hệ thống PV tương đối thấp so với nhu cầu của thiết bị dùng điện. Ngoài việc thay đổi cách liên kết PV, các bộ chuyển đổi điện áp DC-DC cũng được nghiên cứu ứng dụng để nâng cao điện áp.

Bộ tăng áp Boost

Boost là bộ biến đổi nguồn DC-DC có điện áp đầu ra lớn hơn điện áp đầu vào. Nó chứa ít nhất hai chuyển mạch bán dẫn và ít nhất một phần tử tích lũy năng lượng, một tụ điện, một cuộn dây hoặc cả hai (**Hình 4**a). Điện áp ngõ ra được xác định theo biểu thức (4):

$$V_{out} = \frac{v_{in}}{1-\frac{T_{on}}{T_{on}+T_{off}}} = \frac{V_{in}}{1-D} \qquad (4)$$

Trong đó: D là tỷ số đóng điện,

T_{on}: thời gian khóa đóng,

T_{off}: thời gian khóa mở.

$T=T_{on}+T_{off}$: chu kỳ

Với nguồn Boost để có điện áp ra lớn thì công suất vào phải lớn, khi đó công suất thu được phụ thuộc vào cuộn cảm L. Hiệu suất của bộ nguồn Boost đã được chứng minh là hiệu quả và được sử dụng rộng rãi. Tuy nhiên, khi công suất vào không đủ lớn do điều kiện vận hành hoặc sự cố trên hệ thống, cần giảm áp thì nguồn này không thể đáp ứng.

Bộ giảm áp Buck

Ngược lại với nguồn Boost thì Buck là bộ giảm áp hiệu quả được thiết kế như bộ chuyển đổi step up và giống bộ Boost converter, sử dụng hai khóa chuyển mạch như **Hình 4**b. Điện áp ngõ ra của nguồn Buck được tính theo biểu thức (5).

$$V_{out} = \frac{T_{on}}{T_{on+T_{off}}}.V_{in} = D.V_{in} \qquad (5)$$

Với điện áp thu được thấp hơn ngõ vào nên công suất ra rất lớn so với công suất cung cấp. Nó phù hợp cho các trường hợp giảm áp nguồn DC với tổn hao công suất thấp.

Phương pháp giải quyết

PSO là thuật toán được phát triển bởi Eberhart và Kennedy năm 1995. Đây là kỹ thuật tính toán tìm ra vị trí tối ưu cho một cá thể dựa vào hành vi và kinh nghiệm của số đông [21]. Trong đó, mỗi cá thể được đặc trưng bởi thông số vị trí "x_i" và tốc độ "v_i". Do đó, vị trí sau mỗi lần tìm kiếm bị thay đổi và phụ thuộc vào tốc độ cũng như vị trí trước đó theo biểu thức (6):

$$x_i^{k+1} = x_i^k + v_i^{k+1} \qquad (6)$$

Trong quá trình tìm kiếm luôn tồn tại những vị trí tốt nhất mà mỗi cá thể đã xác định $P_{best,i}$ và vị trí tốt nhất của đám đông $G_{best,i}$. Do đó, tốc độ của mỗi cá thể bị ảnh hưởng bởi đám đông và được xác định theo biểu thức (7).

$$v_i^{k+1} = w_i v_i^k + c_1 r_1 (P_{best,i} - x_i^k) + c_2 r_2 (G_{best} - x_i^k) \qquad (7)$$

Trong đó: c_1, c_2 là các hằng số gia tốc cá thể và xã hội r_1, r_2 là hai số ngẫu nhiên phân bố điều trong khoảng [0,1].

k: số lần lặp

w_i: trọng số quán tính xác định theo (8)

$$w_i = 0,9 - 0,8\frac{iter-1}{max\_iter-1} \qquad (8)$$

iter: số lần lặp

max_iter: số lần lặp tối đa

Để áp dụng PSO vào việc dò tìm GMPPT thì x = D và v = DD trong (7) với D được phân bố đều từ [0,2 ÷ 0,8] trong giới hạn điều khiển của mạch Boost.

Lưu đồ giải thuật PSO được trình bày như **Hình 5** có các tham số trong **Bảng 2** dùng để xác định tỷ số D tốt nhất cho cá thể (P_{best}) và toàn cục (G_{best}) dựa vào điều kiện hội tụ của hàm mục tiêu (9).

$$P\left(d_i^k\right) \geq P\left(d_i^{k-1}\right) \qquad (9)$$

Mặc dù giảm w, c_1, c_2 trong (7) có thể làm tăng thời gian xử lý nhưng cùng với việc giới hạn độ rộng xung $|\triangle D| \leq D_0$ (D_0=0,15 – để đảm bảo không bỏ qua bất cứ điểm cực trị nào) và phân bố vị trí cho các cá thể $D \in [0,2 \div 0,8]$ để mọi điểm trên đặc tuyến P-V đều được xem xét sẽ tránh được LMPP khi bước nhảy không quá lớn, gia tăng xác suất tìm được GMPPT. Hơn nữa, việc chủ động dừng lấy mẫu khi hai thông số dòng điện và điện áp đạt các sai số giới hạn là sự cải tiến bộ lọc giúp tăng tốc độ hội tụ, thể hiện ưu điểm nổi bật so với các giải pháp trước đây.

$$\bar{V}_I = \frac{\sum_{j=1}^{i} V_j}{i}; \; \bar{I}_I = \frac{\sum_{j=1}^{i} I_j}{i} \qquad (10)$$

Bảng 2: Tham số của giải thuật PSO

Thuộc tính PSO	Giá trị
Kích cỡ của bầy đàn (n)	4
Số lần lập cực đại (k_{max})	100
Hằng số gia tốc c_1; c_2	0,1; 0,5
Trọng số quán tính w_i	0,07
Hệ số ngẫu nhiên r_1, r_2	[0 1]
Chu kỳ tính toán	$2*10^{-6}$(s)
Số lượng mẫu	350

Để đánh giá tính khách quan về hiệu quả của PSO đã đề xuất trong mục ***Phương pháp giải quyết***, phương pháp P&O được dùng để mô phỏng nhằm so sánh kết quả thu được trong cùng điều kiện vận hành. P&O là giải thuật truyền thống có ưu điểm: chi phí thấp, thực

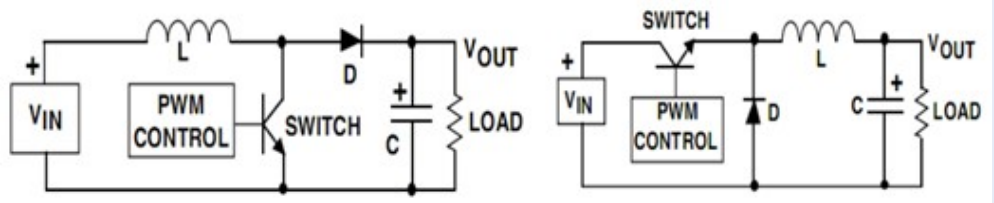

Hình 4: Bộ chuyển đổi: **a**. Boost và **b**. Buck.

hiện đơn giản, ít bảo trì và giám sát. Lưu đồ giải thuật P&O được trình bày trong **Hình 6** với thông số nhiễu loạn DV để quan sát DP như sau:

- Nếu $\triangle P>0$ và $\triangle V>0$ hoặc $\triangle P<0$ và $\triangle V<0$ thì cần tăng điện áp để đạt điểm MPP
- Nếu $\triangle P>0$ và $\triangle V<0$ hoặc $\triangle P<0$ và $\triangle V>0$ thì cần giảm điện áp để đạt điểm MPP.

KẾT QUẢ VÀ THẢO LUẬN

Mô phỏng bằng phần mềm PSIM

Các nghiên cứu trước đây đã chỉ ra rằng, hình dạng đặc tuyến P-V mắc song song không bị ảnh hưởng bởi điều kiện vận hành. Do đó, cấu hình mắc nối tiếp được đề xuất để khảo sát ứng với các trường hợp (TH) trong **Bảng 3**.

Từ kết quả mô phỏng bằng phần mềm về mối quan hệ giữa các đại lượng dòng điện, điện áp và công suất của hệ thống PV khi sử dụng hai giải thuật P&O và PSO để xác định MPPT cho thấy:

Bảng 3: Các trường hợp nghiên cứu PV

TH	Cường độ bức xạ trên các modul (W/m^2)
1	1000-1000-1000
2	1000-700-500
3	800-300-200
4	800-400-200

- Khi không có bóng che, đường cong đặc tuyến I-V và P-V của hệ thống có dạng như **Hình 2**, chỉ có một MPP duy nhất. Khi đó kết quả tìm kiếm bằng cả hai giải thuật đều xác định chính xác được MPPT như nhau trong khoảng 185W (**Hình 7**).
- Khi có bóng che, đường cong đặc tuyến của PV bị thay đổi phụ thuộc vào số lượng modul bị bóng che và có dạng như **Hình 3**. Kết quả trong **Hình 7** và **Hình 8** đã cho thấy PSO luôn tìm được gần đúng giá trị GMPP hơn so với P&O trong cùng điều kiện vận hành.
- Khi thay đổi trật tự của các modul trong **Bảng 3** thì kết quả thu được không bị thay đổi.

Thực nghiệm trên mô hình

Để khảo sát đáp ứng của giải thuật với mô hình đề xuất, bộ mô phỏng pin quang điện Chroma 62050H được dùng thay cho các tấm PV. Nó có ưu điểm là có thể tùy chỉnh thông số của tấm pin với nhiều điều kiện khác nhau như mức độ bức xạ, nhiệt độ, hiện tượng bóng che,… đồng thời có thể ghi lại dữ liệu và kiểm tra hiệu suất của giải thuật MPPT. Tất cả dữ liệu đều có thể giám sát trên máy tính thông qua phần mềm giao tiếp Chroma Array Simulation.

Các trường hợp khảo sát đề xuất trong **Bảng 3** cũng được thực nghiệm tương tự trên mô hình trong cùng điều kiện vận hành với sơ đồ khối được trình bày trong **Hình 9**.

Kết quả thực nghiệm bằng mô hình thể hiện trong các **Hình 10, 11 và 12** cũng cho thấy: ở điều kiện vận hành tiêu chuẩn và khi các modul nhận được bức xạ như nhau thì hệ thống cũng chỉ có một MPP. Do đó, cả hai giải thuật đều xác định tương đối chính xác giá trị công suất ngõ ra ở mức 97,69% và 98,19% tương ứng với P&O và PSO so với công suất cực đại của hệ thống.

Nhưng khi xuất hiện bóng che, các modul nhận được mức độ bức xạ không đồng đều, hai giải thuật cho kết quả khác nhau trong cùng điều kiện vận hành. Cụ thể, PSO luôn xác định đúng GMPP trong mọi trường hợp còn P&O kém chính xác hơn khi bị bẫy vào LMPP như trong **Hình 10 và 12**.

Các số liệu thu được từ mô phỏng bằng PSIM và thực nghiệm trên mô hình được thống kê và so sánh trong **Bảng 4** cho thấy: giải thuật PSO đề xuất luôn có hiệu suất lớn hơn so với phương pháp truyền thống. Bên cạnh đó, việc mô phỏng với 5 modul PV cũng được thực hiện để so sánh độ chính xác, hiệu suất và tốc độ hội tụ của giải thuật đề xuất với các thuật toán tối ưu khác. Bức xạ trên các modul được điều khiển

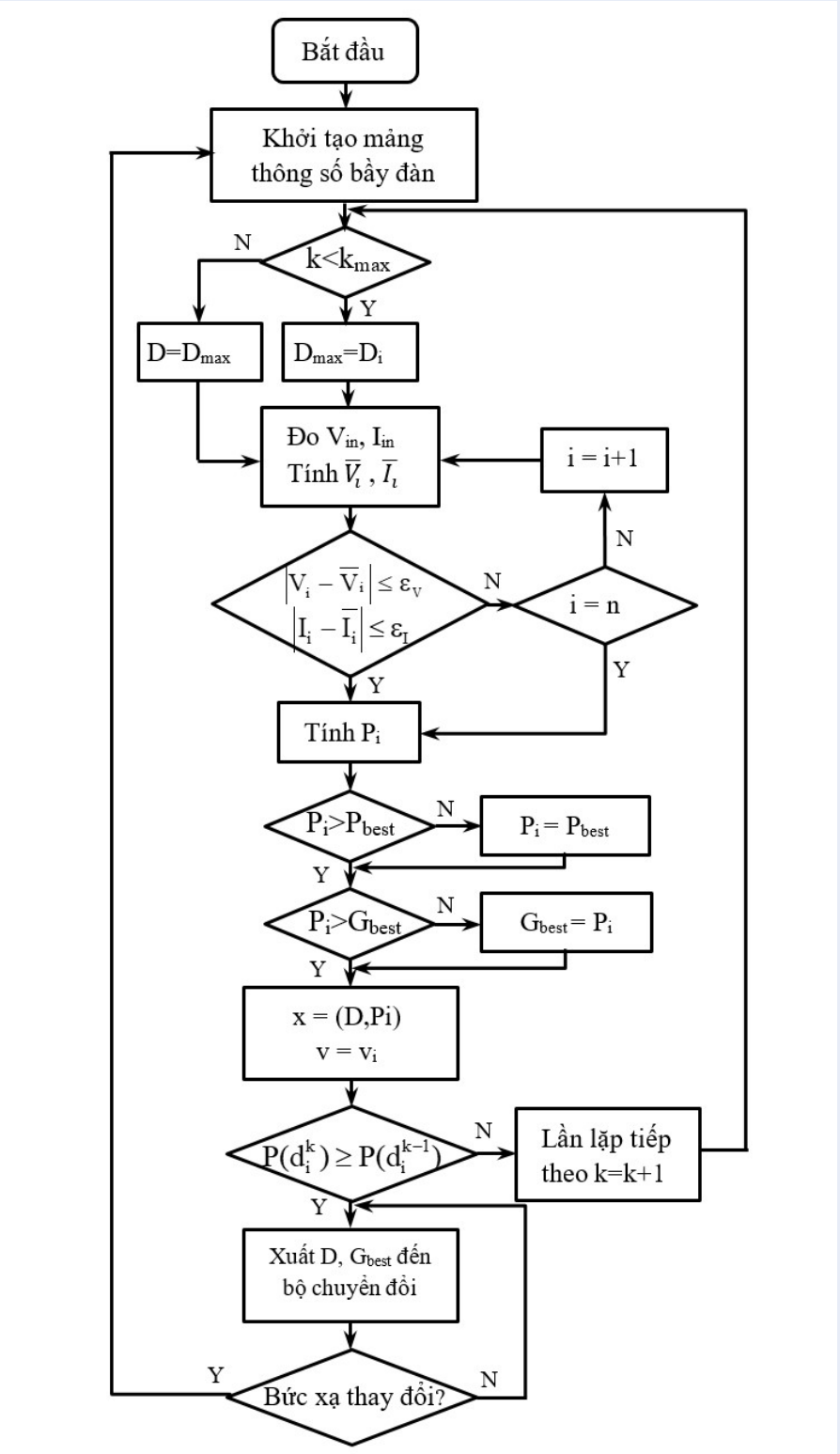

Hình 5: Lưu đồ giải thuật PSO đề xuất

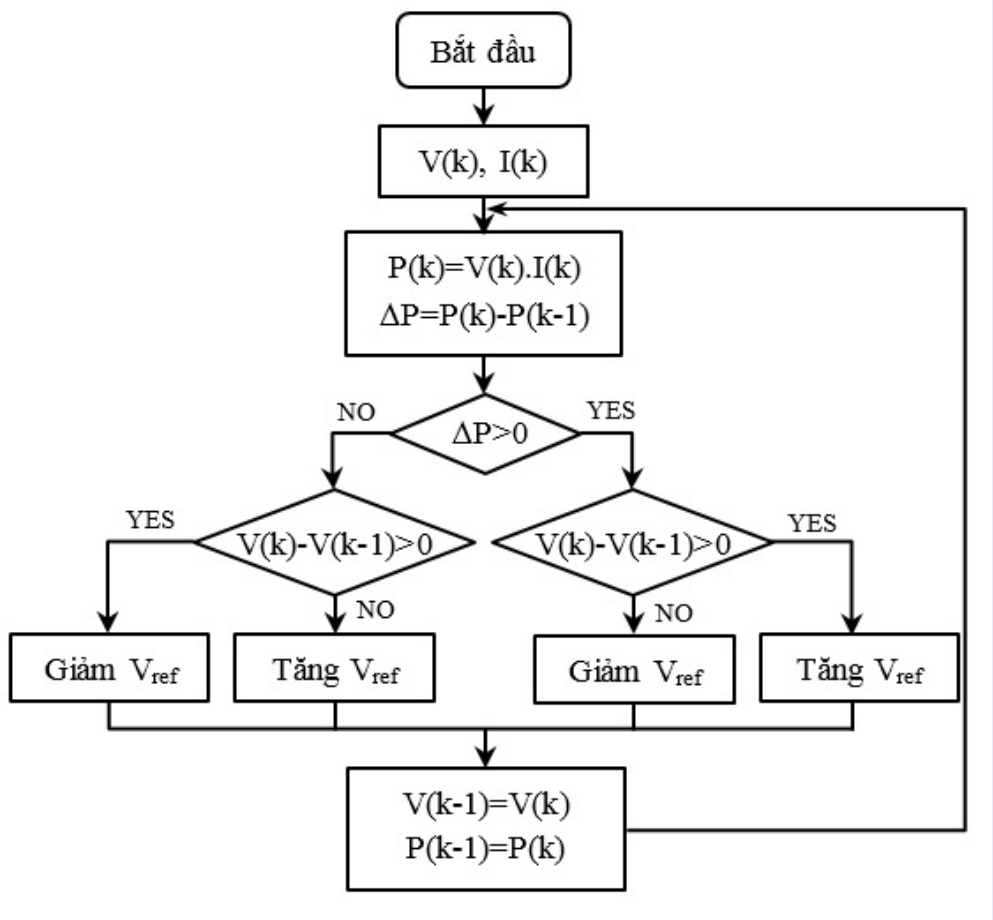

Hình 6: **Lưu đồ giải thuật P&O.**

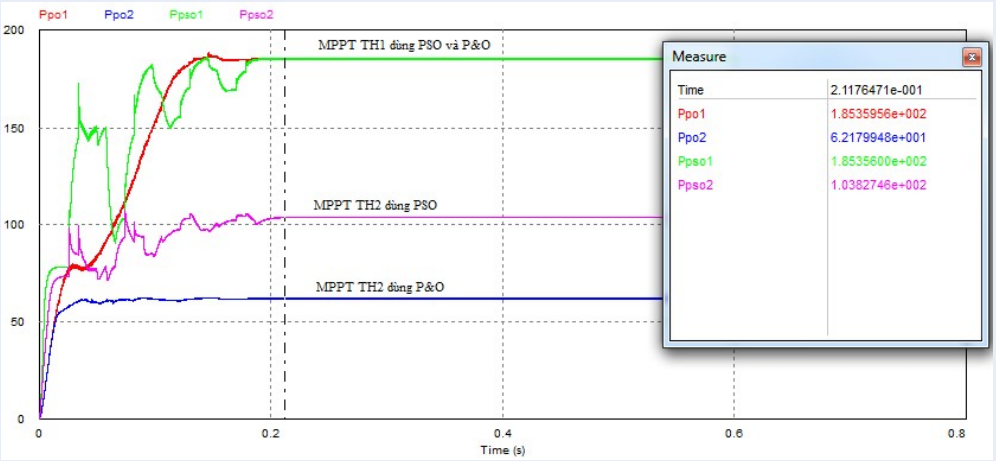

Hình 7: MPPT trong TH1và TH2.

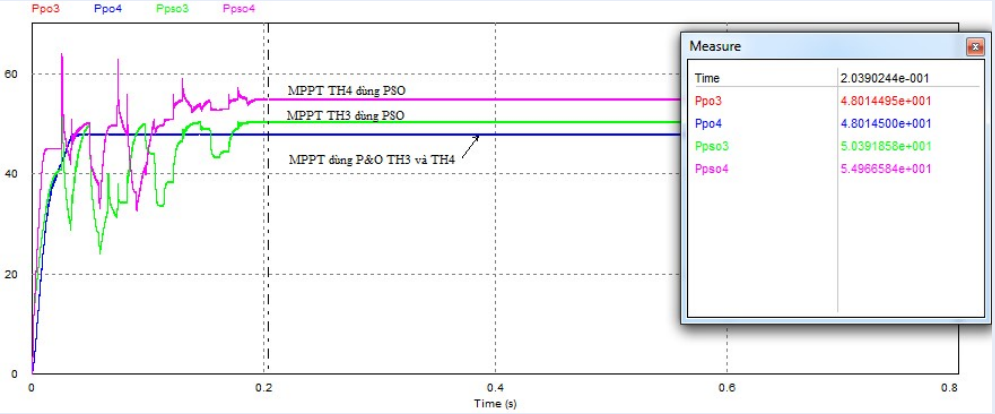

Hình 8: MPPT trong TH3 và TH4.

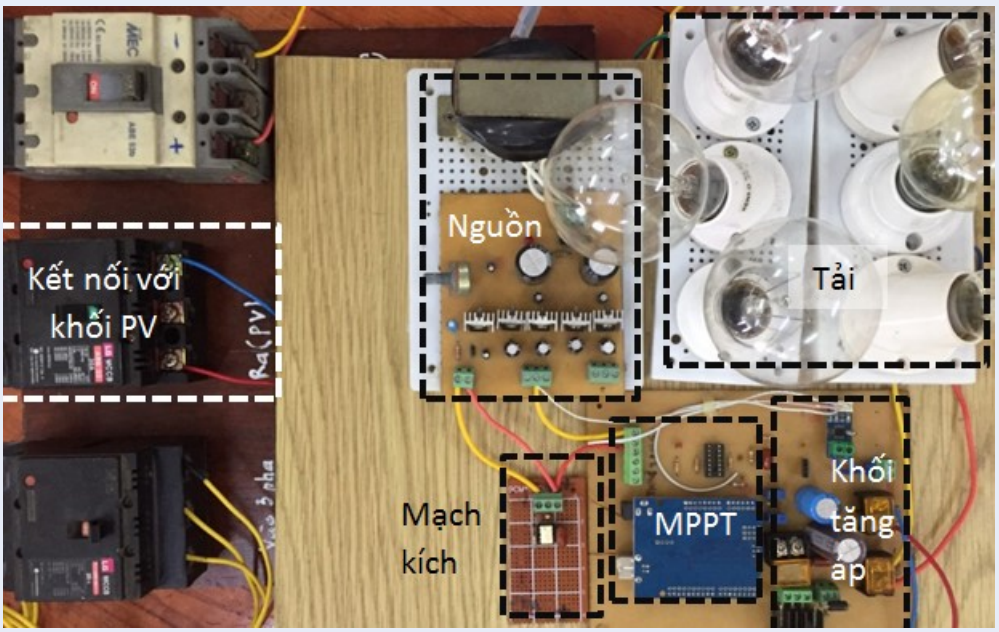

Hình 9: Sơ đồ kết nối mô hình thực nghiệm.

thay đổi ngẫu nhiên trong quá trình mô phỏng. Khi thay đổi trật tự các modul bị bóng che không làm ảnh hưởng đến đặc tuyến P-V và giá trị GMPP của hệ thống (**Hình 13**). Nó cũng cho thấy rằng tốc độ hội tụ của PSO luôn lớn hơn các giải thuật tối ưu khác (0,08s) với mức hiệu suất cao (554,78/556 = 0,9978) (**Hình 14**), trong khi P&O bị rơi vào LMPP khi bức xạ thay đổi liên tục

Những thông số trong **Bảng 5** cho thấy rằng: với các thuật toán tối ưu dựa trên nền tảng bầy đàn có chung một nhược điểm là tốc độ đáp ứng chậm. Bên cạnh đó, số lượng cá thể hạn chế sẽ không chắc chắn đảm bảo mọi lúc đều cho kết quả chính xác. Nhưng với việc chọn w_i, c_1 và c_2 hợp lý thì vấn đề định vị được GMPP bằng PSO có xác suất rất lớn. Điều này được thể hiện trong **Hình 14**, tại những thời điểm ban đầu 0s, 0,2s và 0,4s mặc dù các cá thể chưa có vị trí tốt nhất (G_{best}) nhưng với sự điều chỉnh thông số bầy đàn tích cực đã giảm đáng kể thời gian và không gian tìm kiếm. Như vậy, cho đến hiện tại, với các ví dụ mô phỏng trên hệ thống modul PV thì PSO chắc chắn sẽ tìm được GMPP. Nó cũng cho thấy tính linh hoạt và hiệu quả của giải pháp đề xuất.

Bảng 4: So sánh kết quả mô phỏng và thực nghiệm.

Thống kê theo công suất (W)						
TH	Kết quả mô phỏng			Kết quả thực nghiệm		
	Pmax (W)	P&O (W)	PSO (W)	Pmax (W)	P&O (W)	PSO (W)
1	190,07	185,36	185,35	182,6	178,4	179,3
2	106,51	62,18	103,83	108,2	94,49	107,9
3	51,05	48,01	50,39	48,53	48,43	48,23
4	55,79	48,01	54,96	55,04	48,23	55,03
Thống kê theo phần trăm (%)						
TH	Kết quả mô phỏng			Kết quả thực nghiệm		
	P&O (%)		PSO (%)	P&O (%)		PSO (%)
1	97,522		97,516	97,699		98,193
2	58,379		97,483	87,329		99,723
3	94,045		98,707	99,794		99,382
4	86,055		98,510	87,627		99,982

Bảng 5: So sánh các giải thuật tối ưu [14]

Giải thuật GMPPT	Độ phức tạp	Tốc độ hội tụ (s)	Hiệu suất (%)
PSO đề xuất	-	0,08	99,78
L_PSO [3]	Thấp	0,35	99,99
M-PSO [4]	Trung bình	1,3	98,92
ACO [5]	Thấp	1,1	100
BA [6]	Thấp	1,3	99,98
FFA [7]	Trung bình	1,3	99,8
FWA [8]	Thấp	-	-
GWO [9]	Cao	-	99,92
WHA [10]	Trung bình	4,6	99,99
INC-FFA [11]	Trung bình	0,38	99,99
FWA-P&O [12]	Trung bình	-	-
PSO-P&O [13]	Trung bình	0,9	-

Hình 10: Kết quả thực nghiệm trong TH2.

Hình 11: Kết quả thực nghiệm trong TH3.

KẾT LUẬN

Mô hình thí nghiệm được xây dựng trên nền PSIM và kiểm chứng thực nghiệm bằng Chroma 62050H nhằm nghiên cứu ảnh hưởng của bóng che một phần đến đặc tính làm việc của hệ thống PV và hiệu quả của giải thuật PSO trong việc xác định GMPP. Với kết quả thu được kể trên, nghiên cứu đã chỉ ra rằng.

- Trong điều kiện làm việc bình thường, việc xác định MPPT bằng PSO và P&O là như nhau. Điều này là do chỉ có một điểm MPP duy nhất khi bức xạ trên các modul PV đồng bộ.
- Khi có bóng che, số đỉnh MPP tăng lên khiến cho việc xác định GMPP phức tạp, giải thuật PSO đề xuất thể hiện tính hiệu quả vượt trội khi luôn bám sát GMPPT, khả năng hoạt động khá ổn định và linh hoạt trong quá trình mô phỏng cũng như thực nghiệm. Trong khi đó, giải thuật P&O kém ổn định hơn và bị bẫy vào LMPP. Điều này cho thấy PSO có thể đáp ứng tốt trong việc bám sát MPP trong những điều kiện vận hành phức tạp.

Kết quả nghiên cứu mở ra những hướng nghiên cứu mới như: cải tiến, ứng dụng PSO vào những cấu hình

Hình 12: Kết quả thực nghiệm trong TH4.

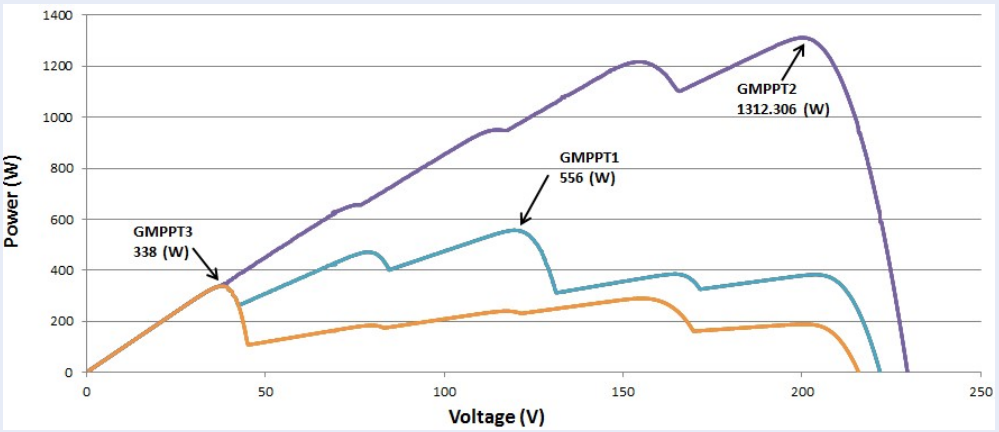

Hình 13: P_{max} của PV khi bức xạ thay đổi

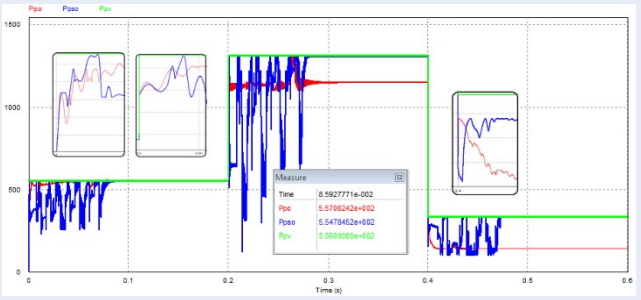

Hình 14: GMPPT khi bức xạ thay đổi liên tục

PV phức tạp hơn để nâng cao hiệu quả của hệ thống; nâng cao tốc độ dò tìm MPP của giải thuật để tránh lãng phí điện năng; thiết kế các mạch DC-DC công suất lớn đáp ứng nhu cầu nghịch lưu hòa lưới của hệ thống PV.

DANH MỤC CÁC TỪ VIẾT TẮT

ACO: tối ưu đàn kiến - Ant Colony Optimization
BA: thuật toán con dơi - Bat Algorithm
DC-DC: bộ biến đổi điện áp một chiều
FFA: thuật toán đom đóm - Firefly Algorithm
FWA: thuật toán pháo hoa - Firework Algorithm
GMPP: điểm phát công suất cực đại toàn cục – Global Maximum Power Point
GMPPT: theo dõi điểm phát công suất cực đại toàn cục – Global Maximum Power Point Tracking
GWO: thuật toán tối ưu hóa bầy sói xám - Grey Wolf Optimization
INC: phương pháp điện dẫn gia tăng - Incremental Conductance
LMPP: điểm phát công suất cực đại địa phương - Local Maximum Power Point
MPP: điểm phát công suất cực đại - Maximum Power Point
MPPT: theo dõi điểm phát công suất cực đại - Maximum Power Point Tracking
M-PSO: thuật toán tối ưu hóa bầy đàn hiệu chỉnh - Modified PSO
P&O: thuật toán nhiễu loạn và quan sát - Perturb and Observe
PGS: hệ thống nhà máy điện mặt trời - Photovoltaic Generation System
PSC: điều kiện bóng che một phần - Partially Shaded Condition
PSO: thuật toán tối ưu hóa bầy đàn - Particle Swarm Optimization
PV: pin quang điện - Photovoltaic
WOA: thuật toán cá voi - Whale Optimization Algorithm

XUNG ĐỘT LỢI ÍCH

Nhóm tác giả xin cam đoan rằng không có bất kỳ xung đột lợi ích nào trong công bố bài báo.

ĐÓNG GÓP CỦA TÁC GIẢ

Bùi Văn Hiền tham gia vào việc đưa ra ý tưởng bài viết, thu thập dữ liệu và xây dựng giải thuật cho nội dung bài viết.

Trương Việt Anh tham gia vào việc thiết kế, xây dựng mạch điều khiển cho mô hình thực nghiệm, kiểm tra các thông số thực nghiệm và hiệu chỉnh hình thức tổng quan bài viết.

Quách Thanh Hải tham gia quá trình thực nghiệm, mô phỏng so sánh và đưa ra kết luận, giải thích các dữ liệu và thông số kỹ thuật cũng như hiệu chỉnh nội dung bài viết.

TÀI LIỆU THAM KHẢO

1. Ehsanul, Kumar P, Sandeep, Adelodun AA, Kim KH. Solar energy: Potential and future prospects. Renewable and Sustainable Energy Reviews. 2018;82:894–900. Available from: https://doi.org/10.1016/j.rser.2017.09.094.
2. Al-Saidi M, Lahham N. Solar energy farming as a development innovation for vulnerable water basins. Development in Practice. 2019;Available from: https://doi.org/10.1080/09614524.2019.1600659.
3. Ram JP, Rajasekar N. A new robust, mutated and fast tracking LPSO method for solar PV maximum power point tracking under partial shaded conditions. Appl Energy. 2017;201:45–59. Available from: https://doi.org/10.1016/j.apenergy.2017.05.102.
4. Chao RM, Nasirudin A, Wang IK, Chen PL. Multicore PSO operation for maximum power point tracking of a distributed photovoltaic system under partially shading condition. Int J of Photoenergy 2016. 2016;p. 1–19. Available from: https://doi.org/10.1155/2016/9754514.
5. Titri S, Larbes C, Toumi KY, Benatchba K. A new MPPT controller based on the ant colony optimization algorithm for photovoltaic systems under partial shading conditions. Appl Soft Comput. 2017;58:465–479. Available from: https://doi.org/10.1016/j.asoc.2017.05.017.
6. Kaced K, Larbes C, Ramzan N, Bounabia M, Dahmane ZE. Bat algorithm based maximum power point tracking for photovoltaic system under partial shading conditions. Sol Energy. 2017;158:490–503. Available from: https://doi.org/10.1016/j.solener.2017.09.063.
7. Teshome DF, Lee CH, Lin YW, Lian KL. A modifiedfirefly algorithm for photovoltaic maximum power point tracking control under partial shading. IEEE J Emerg Sel Top Power Electron. 2017;5(2):661–671. Available from: https://doi.org/10.1109/JESTPE.2016.2581858.
8. Rajsekar N, Pabbewar A, Bhardwaj P, Verma M. Fireworks algorithm for MPPT. Int J Eng Res Technol. 2016;5(1):287–291. Available from: https://doi.org/10.17577/IJERTV5IS010295.
9. Mohanty S, Subudhi B, Ray PK. A new MPPT design using Grey Wolf optimization technique for photovoltaic system under partial shading conditions. IEEE Trans Sustain Energy. 2016;7(1):181–188. Available from: https://doi.org/10.1109/TSTE.2015.2482120.
10. Kumar CHS, Rao RSA. Novel global MPP tracking of photovoltaic system based on whale optimization algorithm. Int J Renew Energy Dev. 2016;5(3):225–232. Available from: https://doi.org/10.14710/ijred.5.3.225-232.
11. Shi JY, Ling LT, Xue F, Qin ZJ, Li YJ, Lai ZX, et al. Combining incremental con-ductance andfirefly algorithm for tracking the global MPP of PV arrays. J Renew Sustain Energy. 2017;9(2):1–19. Available from: https://doi.org/10.1063/1.4977213.
12. Chakkarapani M, Raman GP, Raman GR, Ganesan SI, Chilakapati N. Fireworks enriched P&O algorithm for GMPPT and detection of partial shading in PV systems. IEEE Trans Power Electron. 2017;32(6):4432–4443. Available from: https://doi.org/10.1109/TPEL.2016.2604279.
13. Hanafiah S, Ayad A, Hehn A, Kennel R. A hybrid MPPT for quasi-Z-source inverters in PV applications under partial shading condition. Proceedings of the 11th IEEE international conference on compatibility, power electronics and power engineering; 4-6 April 2017 ;Available from: https://doi.org/10.1109/CPE.2017.7915208.

14. Belhachat F, Larbes C. A review of global maximum power point tracking techniques of photovoltaic system under partial shading conditions. Renewable and Sustainable Energy Reviews. 2018;92:513–553. Available from: https://doi.org/10.1016/j.rser.2018.04.094.
15. Priyadarshi N, Padmanaban S, Popa LM, Blaabjerg F, Azam F. Maximum Power Point Tracking for Brushless DC Motor-Driven Photovoltaic Pumping Systems Using a Hybrid ANFIS-FLOWER . Pollination Optimization Algorithm. 2018;11(5):1–16. Available from: https://doi.org/10.3390/en11051067.
16. El-Helw HM, Magdy A, Marei MI. A hybrid maximum power point tracking technique for partially shaded photovoltaic arrays. IEEE Access. 2017;5:11900–11908. Available from: https://doi.org/10.1109/ACCESS.2017.2717540.
17. Chakkarapani M, Raman GP, Raman GR, Ganesan SI, Chilakapati N. Fireworks enriched P&O algorithm for GMPPT and detection of partial shading in PV systems. IEEE Trans Power Electron. 2017;32(6):4432–4443. Available from: https://doi.org/10.1109/TPEL.2016.2604279.
18. Mohanty S, Subudhi B, Ray PK. A Grey Wolf assisted perturb & observe MPPT algorithm for a PV system. IEEE Trans Energy Convers. 2016;32(1):340–347. Available from: https://doi.org/10.1109/TEC.2016.2633722.
19. Ramaprabha R, Mathur BL. AComprehensive Review and Analysis of Solar Photovoltaic Array Configurations under Partial Shaded Conditions. Hindawi Publishing Corporation. International Journal of Photoenergy. 2012;Available from: https://doi.org/10.1155/2012/120214.
20. Manna DL, Vigni VL, Sanseverinon ER, Dio VD, Romano P. Reconfigurable electrical interconnection strategies for photovoltaic arrays: A review. Renewable and Sustainable Energy Reviews. 2014;33. Available from: https://doi.org/10.1016/j.rser.2014.01.070.
21. del Valle Y, Hernandez JC, Venayagamoorthy GK, Harley RG. Multiple STATCOM Allocation and Sizing Using Using Particle Swarm Optimization. PSCE. 2006;p. 1884–1891. Available from: https://doi.org/10.1109/PSCE.2006.296200.

Science & Technology Development Journal – Engineering and Technology, 3(1):326-338

Open Access Full Text Article

Research Article

Optimization of the maximum power point of photovoltaic working under partial shading conditions

Hien Bui Van[1], Anh Truong Viet[2,*], Hai Quach Thanh[3]

Use your smartphone to scan this QR code and download this article

ABSTRACT

Photovoltaic is used to convert electricity from solar radiation. The working characteristics of photovoltaic depend on environmental conditions such as temperature, solar radiation intensity, and the surrounding environment. During operation, the photovoltaic generation system (PGS) can be partially or completely shaded due to natural phenomena such as clouds, buildings, dust, animals, electric pillars, trees ... these are changing the characteristics of the system's power output of PV. This paper proposes a maximum power point tracking algorithm for PGS operating under partially shaded condition (PSC) based on Particle Swarm Optimization (PSO) method, and a configuration comprises of three PV modules type PHM60W36 is used to simulate using PSIM software. The study focused on changing the working characteristics of the photovoltaic system when changing factors such as level, location of the photovoltaic module are shaded. The effectiveness of the proposed method is not only compared with the traditional Perturb and Observe (P&O) method but also compared with those proposed previously under the same operating conditions. In addition, an experimental model was developed to investigate the response of the proposed solution in the real environment with the Chroma-62050H simulator. The results show the superiority of the proposed solution in improving the performance MPPT and convergence speed of the system under complex operating conditions.

Key words: partial shading, photovoltaic (PV) cell, solar array, P-V characteristic

[1]*Ho Chi Minh City University of Food Industry, Viet Nam*

[2]*Ho Chi Minh City University of Technology and Education, Viet Nam*

[3]*Ho Chi Minh City University of Technology and Education, Viet Nam*

Correspondence

Anh Truong Viet, Ho Chi Minh City University of Technology and Education, Viet Nam

Email: anhtv@hcmute.edu.vn

History

- Received: 13/08/2019
- Accepted: 10/12/2019
- Published: 31/3/2020

DOI : 10.32508/stdjet.v3i1.544

Check for updates

VNU-HCM Press

Cite this article : Bui Van H, Truong Viet A, Quach Thanh H. **Optimization of the maximum power point of photovoltaic working under partial shading conditions**. *Sci. Tech. Dev. J. – Engineering and Technology;* 3(1):326-338.

Bài số 5:

Bùi Văn Hiền, Nguyễn Tùng Linh, Nguyễn Vũ Lân, Trương Việt Anh, Nguyễn Hồng Nguyên, *"Truy Xuất Điểm Phát Công Suất Cực Đại Của Hệ Thống Pin Quang Điện Trong Các Thiết Bị Di Chuyển",* Tạp chí Khoa học và Công nghệ Đại học Thái Nguyên 227(08), 2022: pp 131 – 139, https://doi.org/10.34238/tnu-jst.5471

MAXIMUM POWER POINT TRACKING OF PHOTOVOLTAIC SYSTEM IN MOVEMENT DEVICES

Bui Van Hien[1], Nguyen Tung Linh[2*], Nguyen Vu Lan[1], Truong Viet Anh[1*], Nguyen Hong Nguyen[3]
[1]Ho Chi Minh City University of Technology and Education, [2]Electric Power University
[3]Information and communication technology company of Vietnam Electricity

ARTICLE INFO

Received: 18/01/2022
Revised: 25/4/2022
Published: 26/4/2022

KEYWORDS

Modified Perturb & Observe algorithm (M_P&O)
Partial shading
Photovoltaic (PV) solar cell
Solar system
P-V characteristic

ABSTRACT

Photovoltaic (PV) systems used in moving equipment are frequently affected by the continuously changing operating environments. In general, the series connect (SC) configuration often have more extremes and can be neglected the energy of shaded PV panels under this condition. This is the cause of the unstable output voltage, making it difficult to access the maximum power point tracking (MPPT) and energy loss. This article introduces a solution to overcome the above disadvantages with a Series - Parallel connect (S-PC) configuration of PV arrays, which can significantly reduce the SC junction to simplify the characteristic curves. The proposed link combined with a buck-converter circuit and a modified perturbation and observation (M-P&O) algorithm has shown effective MPPT in all experimental operating conditions. The simulation results from the proposed solution are compared with the traditional P&O algorithm under the same operating conditions, pointed that it can be widely applied in displacement devices using PV systems.

TRUY XUẤT ĐIỂM PHÁT CÔNG SUẤT CỰC ĐẠI CỦA HỆ THỐNG PIN QUANG ĐIỆN TRONG CÁC THIẾT BỊ DI CHUYỂN

Bùi Văn Hiền[1], Nguyễn Tùng Linh[2*], Nguyễn Vũ Lân[1], Trương Việt Anh[1], Nguyễn Hồng Nguyên[3]
[1]Trường Đại học Sư phạm Kỹ thuật Thành phố Hồ Chí Minh, [2]Trường Đại học Điện lực
[3]Công ty Viễn thông Điện lực và Công nghệ thông tin – Tập Đoàn Điện lực Việt Nam

THÔNG TIN BÀI BÁO

Ngày nhận bài: 18/01/2022
Ngày hoàn thiện: 25/4/2022
Ngày đăng: 26/4/2022

TỪ KHÓA

Giải thuật nhiễu loạn và quan sát điều chỉnh (M_P&O)
Hiệu ứng bóng che
Tấm pin quang điện (PV)
Hệ thống pin mặt trời
Đặc tính P-V

TÓM TẮT

Các hệ thống pin quang điện (Photovoltaic – PV) được ứng dụng trong những thiết bị dịch chuyển thường xuyên bị ảnh hưởng do môi trường vận hành thay đổi liên tục. Nhìn chung, cấu hình liên kết nối tiếp (series connect – SC) thường sinh ra nhiều cực trị và có thể bỏ qua năng lượng của các tấm PV bị bóng che trong điều kiện này. Đây là nguyên nhân khiến điện áp ra kém ổn định, gây khó khăn cho việc truy xuất điểm phát công suất cực đại (Maximum Power Point Tracking – MPPT) và thất thoát năng lượng. Bài viết này giới thiệu một giải pháp khắc phục những nhược điểm trên bằng một cấu hình liên kết nối tiếp – song song (Series-Parallel connect – S-PC) các dãy pin quang điện (PV) nhằm hạn chế liên kết nối tiếp và đơn giản hóa các đường cong đặc tuyến. Cấu hình đề xuất kết hợp với mạch buck-converter cùng một giải thuật nhiễu loạn và quan sát (Modified Perturbation and Observation – M-P&O) điều chỉnh đã chứng tỏ được khả năng theo truy xuất điểm công suất cực đại hiệu quả trong mọi điều kiện vận hành thử nghiệm. Những kết quả thu được từ giải pháp đề xuất được so sánh với giải pháp P&O truyền thống trong cùng điều kiện vận hành cho thấy khả năng có thể ứng dụng rộng rãi trong các thiết bị dịch chuyển có sử dụng hệ thống pin quang điện.

DOI: https://doi.org/10.34238/tnu-jst.5471

* Corresponding author. *Email: linhnt@epu.edu.vn*

1. Giới thiệu

Trong các hệ thống pin quang điện (photovoltaic- PV) độc lập hoặc nối lưới, cấu trúc liên kết nối tiếp (series connect – SC) thường được chọn để đạt được mức điện áp và công suất mong muốn. Điốt bypass có thể hạn chế sự cố trong một số trường hợp bóng che một phần nhưng cũng làm giảm hiệu suất sinh điện của toàn dãy tấm pin do bỏ qua các tấm bị bóng che [1]. Hơn nữa, vấn đề sinh ra nhiều đỉnh cực trị trong các điều kiện vận hành không đồng nhất sẽ gây khó khăn cho việc truy xuất điểm phát công suất cực đại (Maximum Power Point Tracking – MPPT). Ngoài cấu trúc SC, môi trường này cũng có nhiều chọn lựa cho các kiểu liên kết khác nhau để tối ưu hóa khả năng sinh điện và giảm bớt tổn thất như: nối tiếp – song song (S-PC), liên kết cầu (BL), dạng tổ ong (HC) hay tổng liên kết chéo (TCT)... [2]-[6]. Tuy nhiên, hầu hết các cấu trúc này đều đòi hỏi số lượng lớn các PV trong hệ thống mới có thể hình thành liên kết và phát huy hiệu quả của các mối nối trong cấu trúc ngoại trừ S-PC [7]. Trong khi đó, việc ứng dụng PV vào các thiết bị dịch chuyển như: các thiết bị điện cầm tay, sản phẩm thời trang, hay các phương tiện giao thông ngày càng phổ biến. Đặc điểm chung trong lĩnh này là mức điện áp yêu cầu thấp, môi trường vận hành thay đổi liên tục và nhanh chóng do chúng thường xuyên dịch chuyển. Để ổn định các thông số ngõ ra và tốc độ MPPT hiệu quả đòi hỏi phải có một giải pháp đủ nhanh, mạnh và chính xác. Các nghiên cứu trong tài liệu [7]-[9] đã chỉ ra rằng liên kết kiểu PC luôn cho công suất lớn nhất và tổn thất công suất cũng ít nhất trong cùng điều kiện vận hành. Cấu hình này có điện áp ra thấp, tương đương điện áp của một PV trong hệ thống do cách liên kết. Nó khá phù hợp với những ứng dụng có yêu cầu về điện áp thấp và công suất nhỏ. Tuy nhiên, nhược điểm của nó là dòng điện ngõ ra lớn gây khó khăn cho việc thiết kế các khóa điều khiển [7]-[10]. Trong phạm vi ứng dụng của các thiết bị dịch chuyển, việc giới hạn số lượng PV của hệ thống không cho phép chọn lựa các cấu hình quá phức tạp. Trong khi đó, cấu hình SC lại có những bất lợi như đã phân tích ở trên. Đối với cấu hình kiểu S-PC thường được ứng dụng khá rộng rãi do khả năng thay đổi linh hoạt các PV trong các mối liên kết để tạo được mức dòng điện hay điện áp như mong muốn. Nó cũng cho thấy hai thông số này luôn ở khoảng giữa và ít dao động hơn so với SC và PC trong cùng tình trạng làm việc [7].

Tính khả thi của một giải pháp được thể hiện qua các tiêu chí như: cấu trúc đơn giản, khả năng phù hợp và có tính ứng dụng, tốc độ hội tụ và sự ổn định các thông số ngõ ra… Để giải quyết mục tiêu này, việc chọn một cấu hình phù hợp với phạm vi ứng dụng sẽ góp phần đáng kể vào việc chọn giải thuật MPPT cho hệ thống một cách hiệu quả. Tốc độ và hiệu suất MPPT bị ảnh hưởng nhiều bởi hình dạng đường cong đặc tuyến P-V của hệ thống. Trong môi trường đồng nhất, các đường cong đặc tuyến chỉ có một cực trị khi thay đổi điều kiện vận hành nên chỉ cần những thuật toán đơn giản cũng có thể đáp ứng được yêu cầu bài toán [7]. Tài liệu [10], nhóm tác giả đã cho thấy giá trị điện áp tại MPP (VMPP) xấp xỉ điện áp hở mạch Voc của hệ thống với một giá trị tương đương $V_{MPP} \approx k*Voc$ (k trong khoảng từ 0,71 đến 0,78). Ứng dụng thông số này, tài liệu [11] đã cải tiến giải thuật P&O truyền thống thông qua việc ước lượng các giá trị điện trở R_{PVmax}, R_{PVmin} và R_{PVavg} để điều chỉnh giá trị số gia ΔD cho tỷ số đóng điện D. Mặc dù giải pháp đã đạt được hiệu quả tối đa trên 97% nhưng phương pháp tính phức tạp đã khiến cho tốc độ MPPT lại là một nhược điểm của nó. Nội dung bài viết này đề xuất giải pháp tìm điểm MPPT cho hệ thống PV ứng dụng trong những thiết bị dịch chuyển nhằm nâng cao hiệu suất và tốc độ hội tụ, nhanh chóng ổn định các thông số ngõ ra trong môi trường vận hành thay đổi liên tục.

2. Ảnh hưởng của bức xạ và nhiệt độ lên đặc tính của PV

Hiệu suất của PV bị ảnh hưởng trực tiếp từ điều kiện vận hành, mà cụ thể là bức xạ mặt trời và nhiệt độ hoạt động trên bề mặt. Những nghiên cứu trước đây đã chỉ ra rằng, công suất phát của hệ thống PV đồng biến với bức xạ nhưng nghịch biến với nhiệt độ. Thực tế thì bức xạ khó đạt tới điều kiện tiêu chuẩn, trong khi đó nhiệt độ làm việc luôn cao hơn mức này là những nguyên nhân dẫn đến sụt giảm công suất phát của hệ thống PV [12].

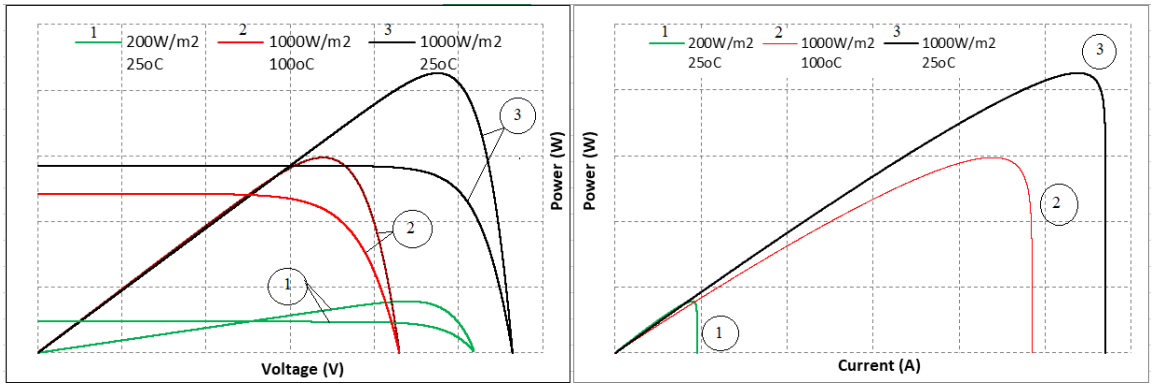

Hình 1. *Đặc tuyến P-V, I-V và P-I khi thay đổi bức xạ và nhiệt độ*

Trong hình 1 cho thấy mối quan hệ giữa công suất, dòng điện và điện áp tại các điều kiện làm việc khác nhau. Chúng ta có thể dễ dàng thấy rằng, khi thay đổi bức xạ, dòng điện tại các điểm MPP bị ảnh hưởng nhiều hơn so với điện áp. Ngược lại, nếu nhiệt độ vận hành của các PV bị thay đổi thì khả năng ổn định điện áp lại kém hơn so với dòng điện. Hơn nữa, khi thay đổi chỉ một thông số trong điều kiện vận hành thì họ các đường đặc tính luôn có tính quy luật (hình 2a). Điều này khiến cho việc ước lượng vùng hoạt động của các MPP trong hệ thống dễ thực hiện hơn. Vấn đề đặt ra trong điều kiện vận hành thực tế là khi tăng bức xạ bề mặt thì nhiệt độ làm việc của PV theo đó cũng gia tăng. Điều đó có nghĩa là cả hai thông số dòng điện và điện áp đều bị dao động dẫn đến điểm MPP của hệ thống PV cũng thay đổi khó nhận định hơn. Khi bức xạ gia tăng, lẽ ra công suất của hệ thống được cải thiện, nhưng do việc gia tăng nhiệt độ bề mặt của chúng mà dẫn đến mức tăng công suất không như mong muốn. Không những thế, vị trí của các MPP trong điều kiện thực tế không còn theo một quy luật cụ thể (hình 2b). Nó khiến cho khả năng dự đoán phạm vi hoạt động của các MPP trở nên khó khăn hơn. Thậm chí trong các liên kết SC khi bị bóng che một phần làm số đỉnh cực trị gia tăng thì vấn đề càng trở nên phức tạp hơn.

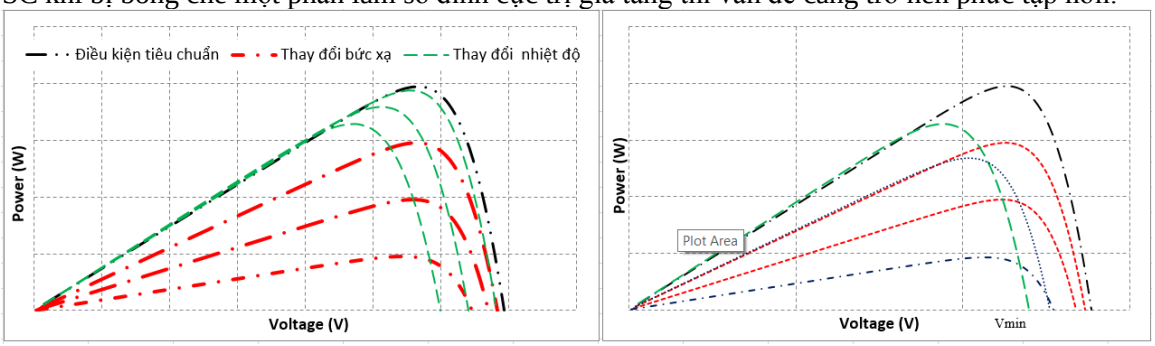

Hình 2. *Đặc tuyến P-V khi thay đổi: a: bức xạ hoặc nhiệt độ; b: cả bức xạ và nhiệt độ*

3. Đề xuất cải tiến thuật toán PO cho bài toán chuyển mạch trong tấm Pin mặt trời

3.1. Thuật toán P&O truyền thống

Đây là phương pháp cơ bản và thông dụng nhất với một thông số nhiễu loạn ΔV để quan sát sự thay đổi công suất ngõ ra ΔP trong quá trình MPPT dựa vào đường cong P-V của hệ thống.

Nguyên lý hoạt động của thuật toán dựa vào hai thông số đầu vào là điện áp VPV và dòng điện IPV của hệ thống PV với lưu đồ giải thuật P&O truyền thống được trình bày như hình 3. Các bước tính toán chi tiết của giải thuật này có thể được tìm thấy trong tài liệu [13], [14]. Thuật toán này khá hiệu quả trong những cấu hình đơn giản, điều kiện vận hành đồng nhất. Nhưng khi thay đổi đồng thời cả hai thông số như đã phân tích ở trên thì tốc độ MPPT và hiệu suất của giải thuật P&O truyền thống bị hạn chế. Với những ứng dụng ở mức điện áp thấp, một sự dao động

đủ nhỏ cũng ảnh hưởng đến chất lượng của toàn bộ hệ thống. Nó đòi hỏi phải có tốc độ hội tụ nhanh và khả năng ổn định các thông số cao hơn.

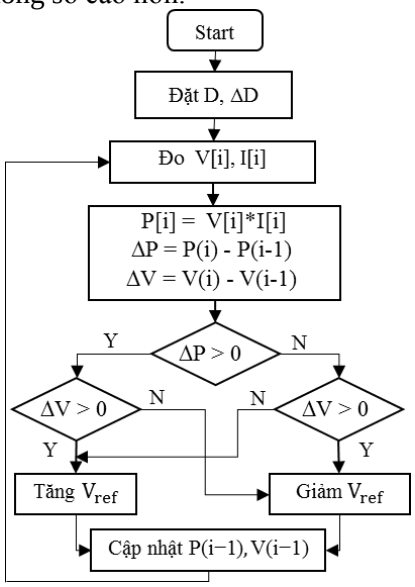

Hình 3. *Lưu đồ giải thuật P&O cho bài toán MPPT*

3.2. Đề xuất phương pháp cải tiến thuật toán

Những phân tích trên cho thấy đối với ứng dụng PV trong nội dung nghiên cứu, việc chọn giải pháp phù hợp sẽ cải thiện đáng kể hiệu suất sinh điện của hệ thống trong những điều kiện vận hành thay đổi liên tục và nhanh chóng. Tốc độ hội tụ và mức độ ổn định thông số đầu ra cũng cần được xem xét. Để giải quyết vấn đề này, bài viết đề xuất sử dụng cấu hình S-PC tối giản mối nối SC (hình 4) [7], [15] kết hợp giải pháp giới hạn vùng hoạt động của điện áp Voc [16] để cải tiến cho giải thuật P&O truyền thống giúp gia tăng tốc độ hội tụ và hiệu suất MPPT của hệ thống PV ứng dụng trong các phương tiện dịch chuyển.

Với số lượng PV không quá lớn thì đây được xem là sơ đồ tối ưu cho việc đáp ứng các thông số điều khiển và giải pháp MPPT. Nó cho thấy rằng, trong mọi điều kiện thay đổi bức xạ khác nhau, số lượng MPP luôn là thấp nhất so với các cấu hình khác [1], [7]. Hơn nữa, hầu hết các trường hợp bóng che theo hàng, cột, một góc, hai góc hay che một phần thì GMPP luôn lệch về phía điện áp cao. Chỉ duy nhất trường hợp tất cả các PV của một hàng có mức bức xạ nhỏ hơn 75% bức xạ lớn nhất của hàng còn lại (hình 4h) thì công suất của chúng sẽ bị bỏ qua. Khả năng này không thể không xảy ra nhưng trong thực tế xác suất là rất ít [15]. Cấu hình đề xuất được xây dựng trong môi trường PSIM liên kết với tải thông qua mạch Buck – converter như giới thiệu trong hình 5. Trong đó sử dụng mô hình PV loại PPS340P-72 có Isc = 9,22A; Voc = 47,5V, giá trị Vmpp = 38,2V và Impp = 9,22A

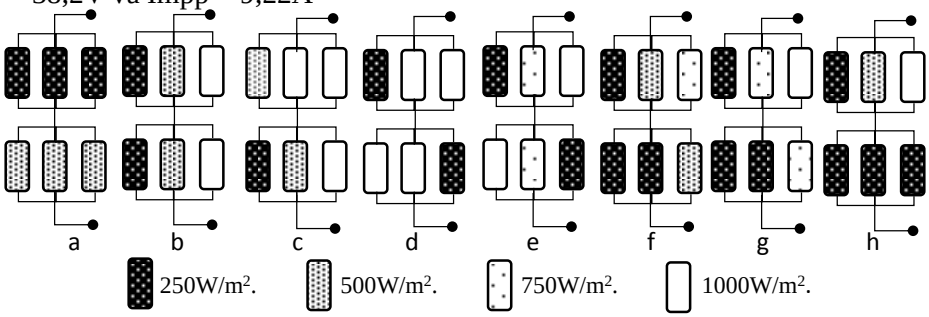

Hình 4. *Các kiểu bóng che theo: a: hàng; b: cột; c: một góc; d và e: đường chéo; f, g, h: một phần*

Với số lượng PV không quá lớn thì đây được xem là sơ đồ tối ưu cho việc đáp ứng các thông số điều khiển và giải pháp MPPT. Nó cho thấy rằng, trong mọi điều kiện thay đổi bức xạ khác nhau, số lượng MPP luôn là thấp nhất so với các cấu hình khác [7]. Hơn nữa, hầu hết các trường hợp bóng che theo hàng, cột, một góc, hai góc hay che một phần thì GMPP luôn lệch về phía điện áp cao. Chỉ duy nhất trường hợp tất cả các PV của một hàng có mức bức xạ nhỏ hơn 75% bức xạ lớn nhất của hàng còn lại (hình 4h) thì công suất của chúng sẽ bị bỏ qua. Khả năng này không thể không xảy ra nhưng trong thực tế xác suất là rất ít [12]. Cấu hình đề xuất được xây dựng trong môi trường PSIM liên kết với tải thông qua mạch Buck – converter như giới thiệu trong hình 5. Trong đó sử dụng mô hình PV loại 72cell-338W có Isc = 9,5A, Voc = 46,2V, giá trị Vmpp = 37,3V và Impp = 9,04A.

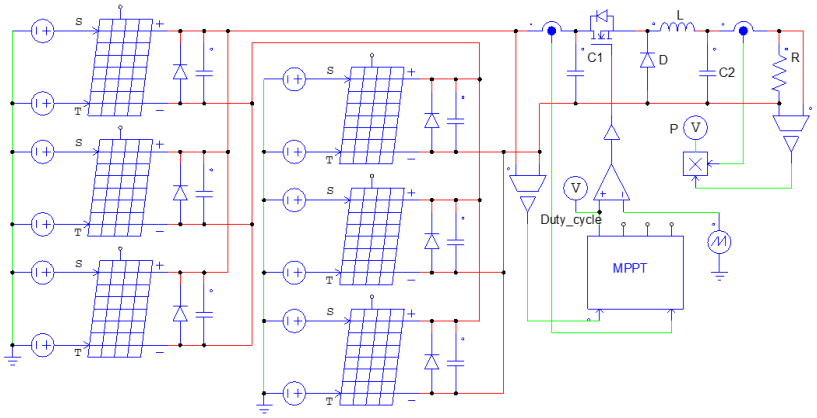

Hình 5. *Cấu trúc hệ thống mô phỏng trong PSIM*

Để gia tăng tốc độ hội tụ và khả năng ổn định các thông số ngõ ra của hệ thống. Lưu đồ giải thuật P&O truyền thống được cải tiến như hình 6.

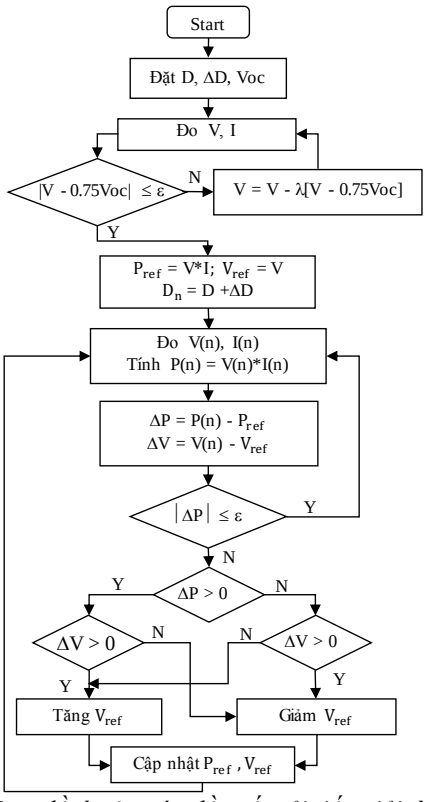

Hình 6. *Lưu đồ thuật toán đề xuất cải tiến giải thuật P&O*

Bước 1: Xác định điểm cực đại tiềm năng trên đường cong đặc tuyến P - V. Bằng việc lựa chọn giá trị duty cycle D = 0,1 và bước điều chỉnh ΔD = 0,01 hệ thống sẽ xác định được hai thông số V và I. Giá trị Voc được chọn tương ứng với điều kiện vận hành thấp nhất (bằng V_{min} – hình 2b). Trong nội dung nghiên cứu này là 100W/m^2 và 70^{o}C – điều kiện thực mà PV còn có thể sinh điện. Giá trị này nhằm thỏa mãn mọi trường hợp vận hành hệ thống sẽ luôn tìm được MPPT mà không bị trôi ra ngoài vùng tìm kiếm.

Bước 2: Kiểm tra điểm MPPT tiềm năng. Thông qua giá trị D để điều chỉnh điểm làm việc tiệm cận tới giá trị Vmpp tiềm năng bằng một hệ số k = 0,75. Hệ số λ được thêm vào như một số gia cho mỗi bước lặp nhằm gia tăng tốc độ đạt đến giá trị hội tụ. Trong trường hợp này chọn giá trị của λ = 0,3.

Bước 3: Xác định điểm khởi đầu cho giải thuật tìm kiếm P&O. Ngay khi điều kiện hội tụ của bước 2 thỏa mãn, các giá trị công suất, điện áp và tỷ số đóng điện được chọn làm các thông số tham chiếu cho việc MPPT của hệ thống

Bước 4: Xác định độ sai lệch công suất ΔP và điện áp ΔV. Bộ điều khiển MPPT sẽ đo các giá trị V(n), I(n) sau đó tính sai số công suất và điện áp so với giá trị tham chiếu ở bước trước đó.

Bước 5: Kiểm tra hội tụ của giải thuật. Nếu sai số công suất nhỏ hơn giá trị cho phép thì giải thuật không thay đổi giá trị tham chiếu ở các bước sau đó. Ngược lại, nếu có sự khác biệt sẽ tiến hành kiểm tra điều chỉnh theo nguyên tắc:

- Nếu ΔP.ΔV > 0 thì tăng giá trị điện áp tham chiếu Vref.
- Nếu ΔP.ΔV < 0 thì giảm giá trị điện áp tham chiếu Vref.

Sau khi thay đổi giá trị điện áp sẽ cập nhật lại giá trị tham chiếu và thực hiện các phép đo cho những chu kỳ tiếp theo.

4. Kiểm tra kết quả mô phỏng

Tính khả thi của giải pháp đề xuất không những được kiểm tra trong môi trường vận hành tiêu chuẩn, thay đổi bức xạ liên tục mà còn trong điều kiện thay đổi cả bức xạ và nhiệt độ. Ngoài ra, nó cũng được so sánh trực tiếp với giải pháp nguyên thủy trong cùng điều kiện vận hành để đánh giá tốc độ và khả năng bám MPP, giảm tổn thất công suất và ổn định ngõ ra của hệ thống PV. Những dạng sóng công suất P, điện áp V và tỷ số đóng điện D mô phỏng MPPT cho các kiểu bóng che đề xuất như hình 4 được thể hiện trong hình 7. Nó cho thấy tốc độ hội tụ của giải pháp đề xuất khá ấn tượng trong khoảng 0,25 ÷ 0,35s và hiệu suất trên 90%. Khi bức xạ lớn nhất giữa hai hàng khác nhau có độ chênh lệch không quá lớn thì hiệu suất của giải pháp vẫn có thể đạt trên 99%. Trong trường hợp xấu nhất (hình 4h), sự sụt giảm công suất ngõ ra được biết đến như khả năng hoạt động của diode bypass nhằm cách ly hàng bị bóng che để duy trì công suất phát của hệ thống không bị gián đoạn. Điều này cũng được tổng hợp thể hiện trong bảng 1.

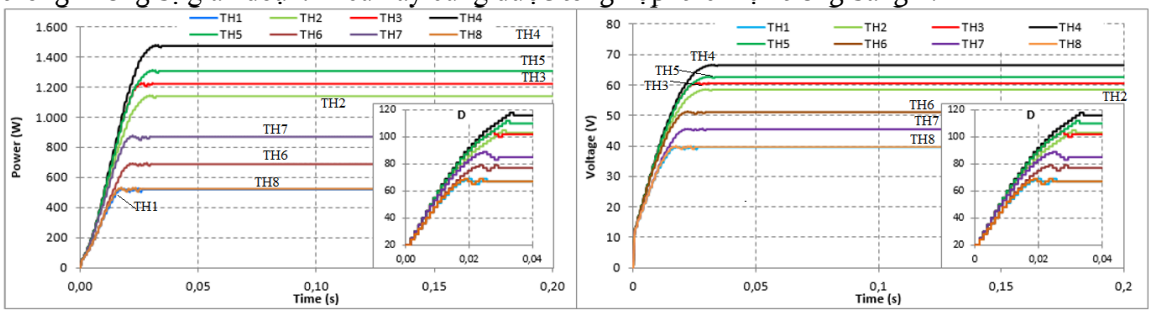

Hình 7. *Dạng sóng P, V và D khi MPPT trong các trường hợp bóng che*

Khi so sánh khả năng MPPT với giải thuật P&O truyền thống trong điều kiện tiêu chuẩn, kết quả trình bày trong hình 8 cho thấy: Tốc độ hội tụ của giải pháp đề xuất đã giảm hơn 50% so với khi chưa được cải tiến. Các giá trị tương ứng là 0,021s và 0,046s. Sở dĩ đạt được điều này là nhờ điều chỉnh giá trị λ cho các bước lặp ban đầu sao cho điện áp điểm làm việc tiến nhanh đến điểm

k*Voc. Khi khoảng cách càng xa điểm MPP tiềm năng thì bước điều chỉnh càng lớn để gia tăng tốc độ và ngược lại (thể hiện tại sóng D hình 8). Ở đó, tại những bước lặp đầu tiên, giá trị D khá lớn nên giảm bớt bước lặp đáng kể so với bản gốc. Khi tiệm cận đến gần MPP thì bước lặp được điều chỉnh về bằng với giá trị nguyên mẫu. Như vậy, thay vì phải mất 35 bước điều chỉnh thì giải pháp đề xuất chỉ còn 16 bước điều chỉnh để hội tụ. Nó cũng cho thấy khả năng ổn định dạng sóng công suất ngõ ra sớm hơn, trong khi giải pháp truyền thống vẫn bị dao động cho tới tận thời điểm 0,052s mới ổn định.

Bảng 1. *Kết quả MPPT của giải pháp đề xuất cho các kiểu bóng che*

Trường hợp	Bóng che kiểu	Pmax (W)	Pout (W)	Hiệu suất	Tốc độ (s)
1	4a	521,63	521,14	99,91	0,026
2	4b	1140,04	1138,4	99,86	0,032
3	4c	1222,74	1220,56	99,82	0,031
4	4d	1473,68	1472,4	99,91	0,035
5	4e	1307,78	1305,91	99,86	0,033
6	4f	689,86	688,02	99,73	0,029
7	4g	872,96	870,21	99,68	0,030
8	4h	558,46	523,85	93,80	0,025

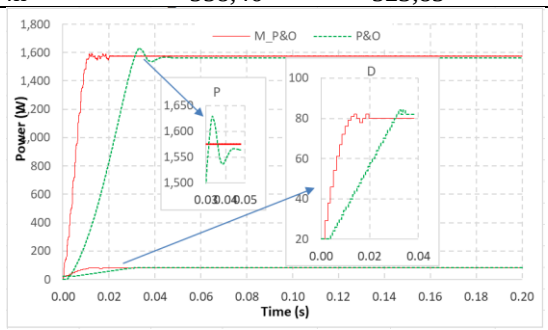

Hình 8. *So sánh hai giải pháp MPPT trong điều kiện tiêu chuẩn*

Trong một kịch bản khác, hệ thống giải định có sự thay đổi bức xạ đột ngột từ 800W/m^2 xuống còn 250W/m^2 tại thời điểm 0,15s. Những kết quả thể hiện trong hình 9 cho thấy, chỉ sau 8 bước điều chỉnh (tại thời điểm 0,162s) là hệ thống đã có thể bắt kịp tốc độ thay đổi của công suất ngõ ra khi bức xạ giảm sâu.

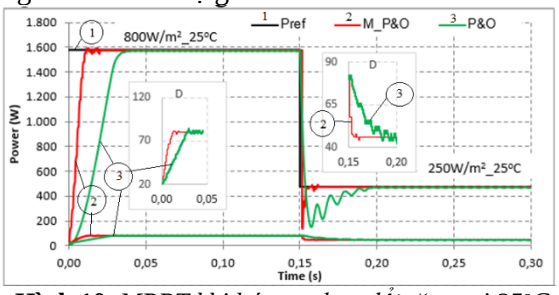

Hình 10. *MPPT khi bức xạ thay đổi tăng tại 25ºC*

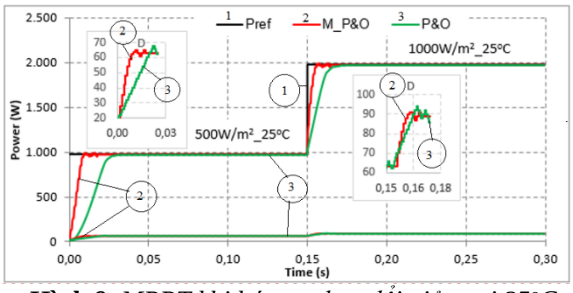

Hình 9. *MPPT khi bức xạ thay đổi giảm tại 25ºC*

Trong khi đó, giải thuật truyền thống phải mất 47 bước điều chỉnh (tại thời điểm 0,198s) mới bám đuổi kịp tốc độ thay đổi này. Nó cũng cho thấy tốc độ được cải thiện đáng kể chỉ thông qua 2 bước điều chỉnh giá trị D, hệ thống đã gần như xác định được vùng hoạt động mới (hình 9). Tương tự ở mức bức xạ 800W/m^2 tốc độ MPPT của giải pháp đề xuất cũng chỉ mất 16 bước điều chỉnh so với 38 bước của phương pháp truyền thống. Hơn nữa, dữ liệu trong hình 9 cũng cho thấy dạng sóng ra của giải pháp đề xuất ít dao động hơn nhiều trong cùng điều kiện vận hành. Điều này có thể được giải thích như sau: mặc dù xuất phát từ cùng một giá trị ban đầu nhưng giải pháp truyền thống với những bước lặp cố định nên dẫn tới sai số tiếp cận với điểm làm việc lý tưởng lớn hơn. Trong khi đó, nhờ có hệ số điều chỉnh λ phụ thuộc vào độ chênh lệch điện áp ở

mỗi bước khiến cho phạm vi điều chỉnh các giá trị D linh hoạt hơn, dễ tiếp cận với điểm làm việc lý tưởng hơn.

Trong trường hợp thay đổi bức xạ tăng như giới thiệu ở hình 10. Giải pháp cũng cho thấy khả năng MPPT với hiệu suất cao hơn, ít dao động hơn, từ đó giảm tổn thất năng lượng và gia tăng khả năng ổn định công suất phát của hệ thống. Ở mức bức xạ 500W/m^2, công suất và tốc độ hội tụ tương ứng là 975W và 0,017s, trong khi đó giải pháp truyền thống có số liệu tương ứng là 970W và 0,025s nhưng kém ổn định hơn. Tại thời điểm 0,15s bức xạ thay đổi đột ngột lên 1000W/m^2, các thông số tương ứng của hai giải pháp là 1975W/0,015s và 1970W/0,025s. Qua đó cho thấy, khi bức xạ thay đổi tăng hay giảm thì hệ thống luôn có tốc độ MPPT nhanh hơn và ổn định hơn nhiều so với giải pháp chưa được cải tiến, tính khả thi của giải pháp còn được kiểm chứng trong điều kiện thay đổi hai thông số là nhiệt độ và bức xạ. Như đã phân tích ở trên, trạng thái này có các giá trị dòng điện và điện áp biến động nhiều hơn và không theo quy luật khiến cho tọa độ MPP khó xác định hơn. Giả sử hệ thống đang hoạt động ở điều kiện 500W/m^2 và nhiệt độ trên bề mặt làm việc là 40^{o}C. Tại thời điểm t = 0,12s bức xạ giảm xuống còn 250W/m^2 nên nhiệt độ trên các PV cũng theo đó giảm xuống còn 30^{o}C. Kết quả MPP được thể hiện trong hình 11 đã cho thấy giải pháp đề xuất đã hội tụ tại t = 0,129s nhanh hơn 0,018s so với phương pháp truyền thống. Ngay sau đó, tại thời điểm t = 0,24s điều kiện vận hành lại thay đổi lên 800W/m^2 và 60^{o}C thì cả hai giải pháp đều hội tụ với 0,03s (tại thời điểm xấp xỉ 0,27s).

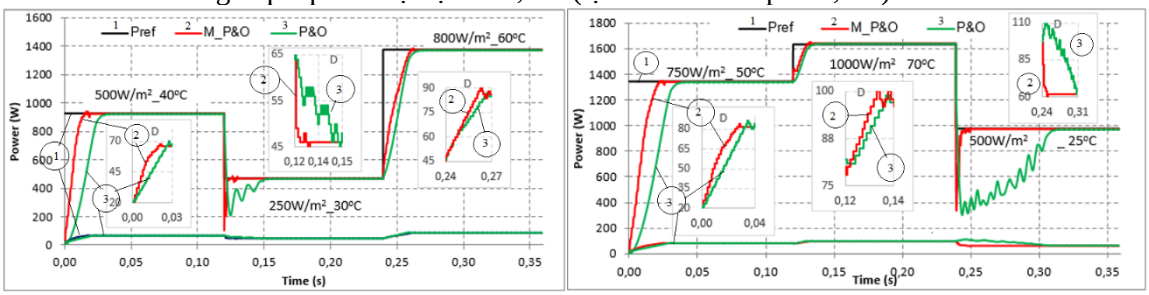

Hình 11. *So sánh MPPT khi thay đổi cả bức xạ và nhiệt độ*

Khi bức xạ và nhiệt độ thay đổi từ mức 750W/m^2 và 50^{o}C lên 1000W/m^2 và 70^{o}C, sau đó lại giảm xuống còn 500W/m^2 và 25^{o}C. Kết quả mô phỏng (hình 11) cũng chỉ ra rằng giải pháp đề xuất có khả năng ổn định vượt trội hơn so với phương pháp truyền thống. Dữ liệu thu thập trong các hình 9 đến hình 11 được tổng hợp so sánh trong biểu đồ hình 12 cho thấy, khi thay đổi theo chiều hướng giảm công suất từ điểm làm việc hiện tại thì giải pháp đề xuất có tốc độ luôn vượt xa so với khi chưa được điều chỉnh. Trong khi đó, công suất ngõ ra cũng ít dao động hơn nhiều mặc dù giá trị khá tương đương nhau. Trường hợp thay đổi tăng công suất thì tốc độ và hiệu suất có sự chênh lệch ít hơn. Tóm lại, tốc độ hội tụ của M_P&O nhanh hơn rất nhiều so với P&O truyền thống trong hầu hết các trường hợp (hình 12a). Nó phụ thuộc nhiều vào số bước lặp (hình 12b) và khả năng điều chỉnh kích thước cho các vòng lặp. Thông qua việc gia tăng kích thước D khi vị trí tìm kiếm cách xa điểm tiềm năng, giải pháp đã thu hẹp khoảng cách và giảm số lần lặp đáng kể nhằm gia tăng tốc độ hội tụ, sớm ổn định trạng thái hoạt động của hệ thống PV.

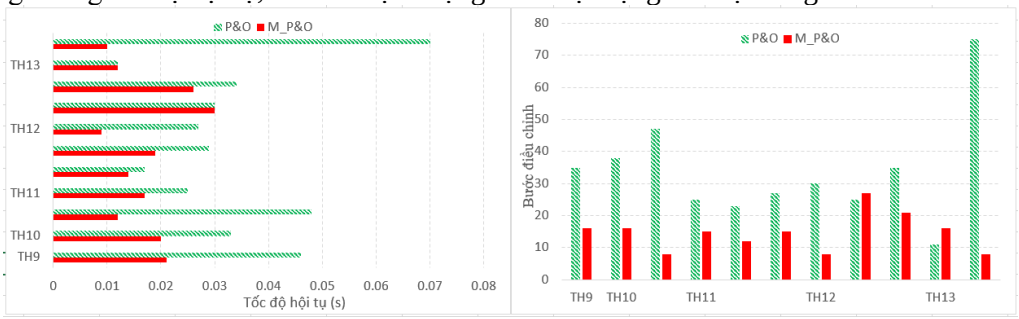

Hình 12. *So sánh hai giải pháp về a. tốc độ MPPT và b. số lượng các bước lặp*

5. Kết luận

Kết quả nghiên cứu của phương pháp đề xuất nhằm mục tiêu cải tiến phương pháp P&O truyền thống bằng cách điều chỉnh M_P&O như trong hình 6 cho thấy phương pháp đề xuất phù hợp với các điều kiện thực tế khi tấm Pin bị che phủ thay đổi liên tục và khả năng tìm điểm MPPT nhanh hơn so với phương pháp cổ điển. Kết quả mô phỏng đã chứng minh với những ứng dụng yêu cầu mức công suất và điện áp không quá lớn, việc chọn từng cấu hình phù hợp cho giải pháp đề xuất sẽ mang lại hiệu quả. Cụ thể, trong phạm vi nghiên cứu, tốc độ hội tụ đã giảm hơn một nửa so với trước khi có sự hiệu chỉnh. Nó rất quan trọng trong việc ổn định thông số ngõ ra của hệ thống khi phải làm việc trong môi trường thay đổi liên tục và nhanh chóng.

TÀI LIỆU THAM KHẢO/ REFERENCES

[1] L. Gao *et al.*, "Parallel – connected Solar PV System to Address Partial and Rapidly Fluctuating Shadow Conditions," *IEEE Transactions On Industrial Electronics*, vol. 56, no. 5, pp. 1548-1556, May 2009.

[2] K. S. Parlak, "PV array reconfiguration method under partial shading conditions," *Electrical Power and Energy Systems*, vol. 63, pp. 713-721, 2014.

[3] VILLA *et al.*, "Maximizing the power output of partially shaded photovoltaic plants through optimization," *IEEE Journal of photovoltaics*, vol. 2, no. 2, pp. 154-163, 2012.

[4] Bidram *et al.*, "Control and circuit techniques to mitigate partial shading effects in photovoltaic arrays," *IEEE journal of photovoltaics*, vol. 2, no. 4, pp. 532-546, 2012.

[5] M. Jazayeri *et al.*, "A Comparative Study on Different Photovoltaic Array Topologies under Partial Shading Conditions," 2014 IEEE PES T&D Conference and Exposition, pp. 978-1-4799-3656-April, 2014.

[6] M. Z. Shams El-Dein *et al.*, ""Optimal Photovoltaic Array Reconfiguration to Reduce Partial Shading Losses," *IEEE transactions on sustainable energy*, vol. 4, no. 1, pp. 145-153, 2013.

[7] V. A. Truong, V. H. Bui, T. L. Duong, and X. T. Luong, "Evaluation of the impact of shading on the working performance of solar cell connection configurations," *Journal of Science and Technology - Industrial University of HCMC*, vol. 21, pp. 136-146, July 2021.

[8] R. Ramaprabha and B. L.Mathur, "A Comprehensive Review and Analysis of Solar Photovoltaic Array Configurations under Partial Shaded Conditions," *International Journal of Photoenergy*, vol. 2012, 2012, Art. no. 120214, doi:10.1155/2012/120214.

[9] F. Belhachat and C. Larbes, "Modeling, analysis and comparison of solar photovoltaic aray configurations under partial shading conditions," *Solar energy*, vol. 120, pp. 399-428, 2015, doi: 10.1016/j.solener.2015.07.039.

[10] R. Alik, T. Sutikno, and A. Jusoh, "A Review on Perturb and Observe Maximum Power Point Tracking in Photovoltaic System," *TELKOMNIKA*, vol. 13, no. 3, pp. 745-751, 2015, doi: 10.12928/TELKOMNIKA.v13i3.1439.

[11] Y. J. Wang and P. C. Hsu, "An Investigation on Partial Shading of PV Modules with Different Connection Configurations of PV Cells," *Energy*, vol. 36, pp. 3069-3078, 2011, doi: 10.1016/j.energy.2011.02.052.

[12] V. H. Bui, V. A. Truong, and T. H. Quach, "Optimizing the peak capacity development point of photovoltaic cells working in shaded conditions," *Journal of Science and Technology - Industrial University of HCMC*, vol. 3, no. 1, pp. 326-338, 2020.

[13] A. Jusoh *et al.*, "A Review on Favourable Maximum Power Point Tracking Systems in Solar Energy Application," *TELKOMNIKA (Telecommunication Computing Electronics and Control)*, vol. 12, no. 1, p. 622, 2014.

[14] B. Yang, T. Zhu *et al.*, "Comprehensive overview of maximum power point tracking algorithms of PV systems under partial shading condition," *Journal of Cleaner Production*, vol. 268, pp. 121983-122002, 2020, doi: 10.1016/ j. jclepro. 2020.121983.

[15] V. Di Dio, D. La Cascia, R. Miceli, and C. Rando, "A Mathematical Model to Determine the Electrical Energy Production in Photovoltaic Fields Under Mismatch Effect," *International Conference on Clean Electrical Power*, Capri, Italy, 9-11 June 2009, pp. 46-51.

[16] M. H. Moradi and A. R. Reisi, "A hybrid maximum power point tracking method for photovoltaic systems," *Solar Energy*, vol. 85, pp. 2965-2976, 2011.

Bài số 6:

Trương Việt Anh, **Bùi Văn Hiền**, Nguyễn Tùng Linh, Nguyễn Vũ Lân, Quách Thanh Hải, *"Đề Xuất Giải Pháp Tìm Điểm Phát Công Suất Cực Đại Của Hệ Thống PV Dựa Vào Dự Đoán Giá Trị I_{sc} Và V_{oc}",* Tạp chí Khoa học và Công nghệ Đại học Thái Nguyên 227(11):2022, pp 77-86. https://doi.org/10.34238/tnu-jst.6088.

PROPOSE A METHOD TO FIND THE MAXIMUM POWER GENERATOR OF PV SYSTEM BASED ON I_{SC} AND V_{OC} VALUE FORECAST

Truong Viet Anh[1], Bui Van Hien[1,2], Nguyen Tung Linh[3*], Nguyen Vu Lan[1], Quach Thanh Hai[1]
[1]Ho Chi Minh City University of Technology and Education,
[2]School of Engineering and Technology, Van Lang University, [3]Electric Power University

ARTICLE INFO

Received: 31/5/2022
Revised: 14/7/2022
Published: 14/7/2022

KEYWORDS

Photovoltaic cell
Algorithm P&O
PV Parallel
Open circuit voltage
Maximum Power Point Tracker

ABSTRACT

The maximum power point (MPP) of the photovoltaic cell system is related to the value of the open-circuit voltage (V_{oc}) and the short-circuit current (I_{sc}) according to the fill factor. Consequently, knowing these two parameters will be able to approximate the optimal working position of the system. This can significantly reduce the search area for Maximum Power Point Tracking (MPPT) solutions to increase convergence speed and performance. The content of this paper introduces a solution that applies two parameters V_{oc} and I_{sc} combined with the traditional perturbation and observation (P&O) algorithm to solve the above problem. The proposed solution is simulated in a PSIM environment to compare the performance and speed of MPPT with the traditional P&O algorithm under the same experimental operating conditions. The obtained results show that it has faster convergence speed, higher efficiency, and stable output waveform compared to the unimproved solution.

ĐỀ XUẤT PHƯƠNG PHÁP TÌM ĐIỂM PHÁT CÔNG SUẤT CỰC ĐẠI CỦA HỆ THỐNG PV DỰA VÀO DỰ ĐOÁN GIÁ TRỊ I_{SC} VÀ V_{OC}

Trương Việt Anh[1], Bùi Văn Hiền[1,2], Nguyễn Tùng Linh[3*], Nguyễn Vũ Lân[1], Quách Thanh Hải[1]
[1]Trường Đại học Sư phạm Kỹ thuật Thành phố Hồ Chí Minh, [2]Trường Kỹ thuật và Công nghệ, Đại học Văn Lang,
[3]Trường Đại học Điện lực

THÔNG TIN BÀI BÁO

Ngày nhận bài: 31/5/2022
Ngày hoàn thiện: 14/7/2022
Ngày đăng: 14/7/2022

TỪ KHÓA

Pin quang điện
Giải thuật P&O
PV song song
Điện áp hở mạch
Điểm phát công suất cực đại

TÓM TẮT

Điểm phát công suất cực đại (Maximum Power Point - MPP) của hệ thống pin quang điện có mối quan hệ với giá trị điện áp hở mạch (open-circuit Voltage - V_{oc}) và dòng điện ngắn mạch (short-circuit current - I_{sc}) theo hệ số lấp đầy (fill factor – FF). Nghĩa là khi biết được hai thông số này sẽ có thể ước lượng được tương đối vị trí làm việc tối ưu của hệ thống. Từ đó có thể giới hạn phạm vi tìm kiếm cho các giải pháp truy xuất điểm phát công suất cực đại (Maximum Power Point Tracking - MPPT) nhằm gia tăng tốc độ hội tụ và nâng cao hiệu suất. Nội dung bài viết này giới thiệu một giải pháp ứng dụng hai thông số V_{oc} và I_{sc} kết hợp với giải thuật nhiễu loạn và quan sát (Perturbation and Observation - P&O) truyền thống để giải quyết bài toán trên. Giải pháp đề xuất được mô phỏng trong môi trường PSIM để so sánh hiệu suất và tốc độ MPPT với giải thuật P&O truyền thống trong cùng điều kiện vận hành thử nghiệm. Những kết quả đạt được cho thấy tốc độ hội tụ nhanh hơn, hiệu suất cao hơn và ổn định dạng sóng ngõ ra so với giải pháp chưa được cải tiến.

DOI: https://doi.org/10.34238/tnu-jst.6088

* Corresponding author. *Email: linhnt@epu.edu.vn*

1. Giới thiệu

Năng lượng điện mặt trời ngày càng được ứng dụng rộng rãi trong những lĩnh vực có yêu cầu mức công suất vừa và nhỏ như điện mặt trời áp mái, tưới tiêu, đèn giao thông, thiết bị dịch chuyển [1]. Một trong những trở ngại lớn nhất là điều khiển hệ thống PV vận hành tại MPP để thu được hiệu suất lớn nhất trong khi điều kiện làm việc thay đổi liên tục. Có nhiều kỹ thuật MPPT đã được giới thiệu nhằm giải quyết vấn đề này có thể phân chia thành các nhóm như: nhóm giải thuật truyền thống, nhóm giải thuật tối ưu cơ bản, nhóm giải pháp kết hợp, và nhóm các giải pháp khác [2], [3].

Nhóm giải pháp truyền thống có cấu trúc đơn giản, dễ thực hiện nhưng kém hiệu quả trong những điều kiện thay đổi [4]. Trong khi đó, nhóm giải pháp tối ưu có hiệu suất cao hơn nhưng lại kém linh hoạt và tốc độ hội tụ phụ thuộc vào các thông số thiết kế ban đầu [5]. Sự kết hợp ưu điểm của hai hay nhiều giải thuật giúp nâng cao hiệu suất và tốc độ MPPT, giảm dao động quanh vị trí MPP nhưng kèm theo nó là mức độ phức tạp và gia tăng chi phí.

Tài liệu [6] đã đề xuất giải pháp điện áp xấp xỉ $0,8*V_{oc}$ kết hợp với giải thuật P&O để nâng cao hiệu suất MPPT nhưng tốc độ chưa được cải thiện. Hơn nữa, việc chỉ sử dụng một thông số V_{oc} cố định sẽ kém chính xác hơn khi có sự thay đổi điều kiện vận hành của hệ thống. Bên cạnh đó, trong bài viết [7] kết hợp sử dụng đồng thời hai thông số V_{oc} và I_{sc} lại cho thấy khả năng tính toán phức tạp, chi phí cao và sai số gia tăng nếu không cập nhật V_{oc} theo thời gian. Trong nội dung nghiên cứu này, hai thông số V_{oc} và I_{sc} được kiểm tra liên tục và đóng vai trò như những tham số đầu vào nhằm giảm không gian tìm kiếm cho giải thuật P&O. Giải pháp đề xuất đã cho thấy hiệu suất có thể đạt 100% và tốc độ vượt trội hơn hẳn so với các giải pháp cải tiến được giới thiệu gần đây. Những kết quả đạt được qua mô phỏng so sánh đã cho thấy: thay vì chọn giá trị khởi động cố định, việc ước lượng giá trị độ rộng xung tùy thuộc vào điều kiện vận hành giúp cho các giải pháp truyền thống đơn giản nâng cao hiệu quả hơn cả các giải thuật tối ưu.

2. Ảnh hưởng của môi trường đến đặc tính PV

Mô hình hóa tế bào quang điện trình bày như hình 1 với giá trị dòng điện ngõ ra được tính theo công thức sau [8], [9]:

$$I_{PV} = I_{ph} - I_0\left\{e^{\frac{q\left(V+I_{pv}.R_S\right)}{nkT_c}} - 1\right\} - \frac{V + I_{pv}.R_S}{R_{sh}} \quad (1)$$

Trong đó: V điện áp ra của PV (V), I_{pv} dòng điện ra của PV (A), I_{ph} dòng quang điện (A), I_0 dòng điện bão hòa ngược (A), q điện tích của electron ($1,602\times10^{-19}$C), k hằng số Boltzman ($1,381\times10^{-23}$J/K), T nhiệt độ lớp tiếp xúc (K), n hệ số lý tưởng của diode, R_S và R_{sh} điện trở nối tiếp và song song (Ω),

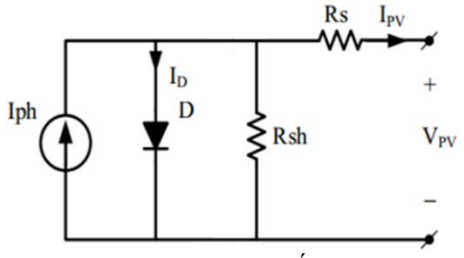

Hình 1. *Mô hình toán của tế bào quang điện*

Mặt khác, dòng quang điện I_{ph} phụ thuộc vào bức xạ mặt trời và nhiệt độ làm việc của nó theo biểu thức [9].

$$I_{ph} = \left[I_{sc} + K_I\left(T_c - T_{ref}\right)\right]S \quad (2)$$

Trong đó: I_{sc} dòng ngắn mạch của PV ở 25^0C (A), K_I hệ số nhiệt độ của dòng ngắn mạch, T_c nhiệt độ làm việc của PV, T_{ref} nhiệt độ tham chiếu, S bức xạ mặt trời (kW/m^2).

Hệ thống PV gồm nhiều tấm PV liên kết với nhau để đạt được công suất ra như mong đợi. Mối liên hệ giữa dòng điện, điện áp của một hệ thống gồm N_s tấm PV mắc nối tiếp và N_p chuỗi nối tiếp mắc song song được biểu diễn theo phương trình sau [9].

$$I = N_p I_{SC} - N_p I_0 \left\{ e^{\frac{q(V+N_s IR_S)}{N_s kT}} - 1 \right\} - \frac{V + N_s IR_S}{N_s R_P} \quad (3)$$

Tuy nhiên MPP của hệ thống PV thay đổi tùy thuộc vào môi trường làm việc và thông thường thì nó có hiệu suất thấp hơn so với điều kiện làm việc tiêu chuẩn 1000W/m^2 và 25^{o}C. Hình 2 mô tả đặc tuyến P-V và I-V trong những điều kiện bức xạ khác nhau [1], [5]. Trong đó hai thông số I_{sc} và V_{oc} cũng thay đổi tùy thuộc vào bức xạ mặt trời chiếu trên bề mặt PV.

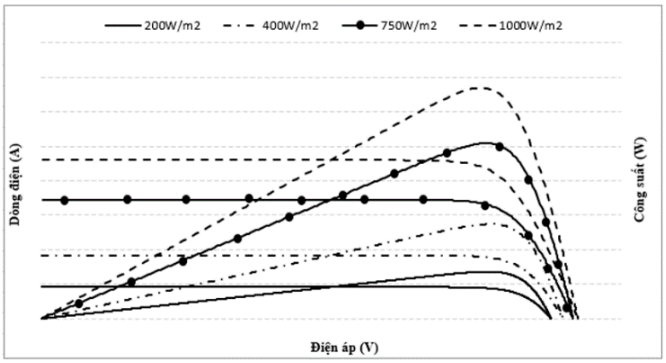

Hình 2. *Đặc tuyến I-V và P-V khi thay đổi bức xạ*

3. Giải pháp đề xuất

3.1. Cấu hình PV

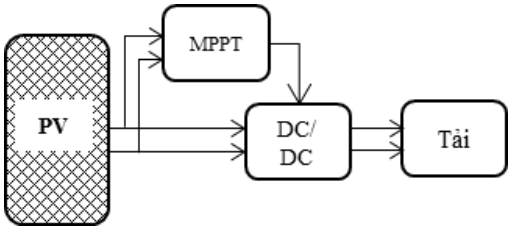

Hình 3. *Cấu hình hệ thống PV đề xuất.*

Bảng 1. *Thông số của PV sử dụng trong nghiên cứu*

Thông số	Giá trị
Số lượng cell	36
Công suất cực đại (P_{max})	60 (W)
Điện trở nối tiếp (R_s)	0.018 (Ω)
Điện trở song song (R_{sh})	1100 (Ω)
Dòng điện ngắn mạch (I_{sc})	3.7 (A)
Điện áp hở mạch (V_{oc})	21.6 (V)
Điện áp tại P_{max} (V_{mpp})	17.8 (V)
Dòng điện tại P_{max} (I_{mpp})	3.37 (A)

Có rất nhiều kiểu liên kết PV khác nhau và mỗi cấu hình đều có những đặc điểm về dòng điện và điện áp phù hợp với những ứng dụng khác nhau [10]. Đặc điểm chung mà chúng được nghiên cứu giới thiệu là nhằm khai thác tối đa hiệu suất của hệ thống PV. Trong đó, cấu hình liên kết

kiểu song song luôn cho hiệu suất tốt nhất trong mọi điều kiện vận hành [9], [10]. Do đó, với những ứng dụng trong nghiên cứu này, giải pháp đề xuất sử dụng cấu hình liên kết song song có các thông số của một tấm PV được liệt kê trong bảng 1. Với cấu hình này, hệ thống sẽ có ít cực trị nhất trong điều kiện vận hành thay đổi tạo thuận lợi cho giải pháp MPPT gia tăng hiệu suất và tốc độ hội tụ. Công suất phát của nó được cung cấp cho một tải thông qua mạch chuyển đổi Buck-boost và bộ MPPT có cấu trúc như hình 3.

3.2. DC/DC converter

Phạm vi ứng dụng của hệ thống PV công suất thấp khá rộng nên cần điều chỉnh điện áp cho phù hợp trong từng điều kiện. Điều này được thực hiện thông qua các mạch chuyển đổi DC/DC kết nối giữa nguồn PV và tải. Điện áp ngõ ra (V_{out}) được điều khiển theo điện áp vào (V_{in}) thông qua một độ rộng xung D có giá trị trong khoảng từ ($0 \le D \le 1$).

Trong nội dung nghiên cứu này thì bộ buck-boost converter được xem là một giải pháp hữu hiệu cho việc ổn định công suất đầu ra của hệ thống PV. Cấu trúc và các thông số mạch có thể được tìm thấy trong tài liệu [11]. Nó là sự kết hợp của hai mạch buck và boost nên quan hệ điện áp được biểu diễn theo biểu thức:

$$V_{out} = \frac{D}{1-D} V_{in} \tag{4}$$

Khi $D < 0,5$ thì $V_{in} > V_{out}$, ngược lại $D > 0,5$ thì $V_{in} < V_{out}$, trong khi đó nếu $D = 0,5$ thì $V_{in} = V_{out}$.

3.3. Giải pháp đề xuất

Tốc độ và hiệu suất MPPT phụ thuộc nhiều vào vị trí khởi tạo độ rộng xung D ước lượng tại MPP. Trong khi đó, tọa độ ước lượng này phụ thuộc vào hai thông số I_{sc} và V_{oc} của hệ thống PV. Trong nội dung nghiên cứu này, chúng được xác định thông qua độ rộng xung D theo trình tự sau:

Cài đặt độ rộng xung D_1 và D_2 có giá trị lần lượt là 0,80 và 0,78 để xác định các thông số dòng điện I, điện áp V và công suất P tương ứng của chúng. Đối với PV module sử dụng trong nghiên cứu này thì hai giá trị I_1 và I_2 (tương ứng với D_1 và D_2) sẽ nằm trong vùng tuyến tính ($I_1 \approx I_2$). Như vậy từ tọa độ của hai điểm phát công suất trên có thể xác định được phương trình đường thẳng qua chúng như sau:

$$I = \frac{I_2 - I_1}{V_2 - V_1} V + \left[I_1 - \frac{I_2 - I_1}{V_2 - V_1} V_1 \right] \tag{5}$$

Đồng thời xác định được điện trở nội của PV dựa vào giá trị dòng điện và điện áp tại D_1 là:

$$R_1 = \frac{V_1}{I_1} \tag{6}$$

Từ biểu thức (5) tính được giá trị I_{sc} (ứng với $V = 0$) là:

$$I_{sc} = I_1 - \frac{I_2 - I_1}{V_2 - V_1} V_1 \tag{7}$$

Giá trị dòng điện ước lượng tại điểm phát công suất cực đại là

$$I_{mpp} = k_I \times I_{sc} \tag{8}$$

Tiếp tục cài đặt giá trị $D_3 = 0,1$ để xác định điện áp V_3. Với giá trị D khá nhỏ thì có thể xem như $V_{oc} \approx V_3$ và thông qua đó có thể ước lượng điện áp tại MPP như sau:

$$V_{mpp} = k_v \times V_{oc} \tag{9}$$

Hai giá trị k_I và k_v trong nghiên cứu này được chọn phụ thuộc vào đặc tính của tấm PV (bảng 1) và được xác định như sau:

$$k_I = \frac{I_{mpp}}{I_{sc}} = \frac{3.37}{3.7} = 0.91, \; k_v = \frac{V_{mpp}}{V_{oc}} = \frac{17.8}{21.6} = 0.82 \tag{10}$$

Tọa độ điểm MPP được ước lượng một cách tương đối là P_{mpp}= (0,82×V_3; 0,91×I_{sc}). Với giá trị này, các thông số điện trở và độ rộng xung D của nó lần lượt được xác định và dùng làm giá trị tham chiếu cho giải pháp MPPT. Ưu điểm của việc tính toán hai tham số I_{sc} và V_{oc} so với việc chọn chúng cố định là có thể ước lượng linh hoạt hơn trong những điều kiện vận hành khác nhau. Do đó, giải pháp đề xuất có thể giảm sai số đáng kể ngay cả khi đường cong đặc tuyến bị thay đổi do suy hao theo tuổi thọ.

Điện trở nội PV tại điểm MPP ước lượng được tính toán theo biểu thức sau

$$R_{mpp} = \frac{V_{mpp}}{I_{mpp}} \tag{11}$$

Điện trở R_1 trong biểu thức (6) và điện trở tải thông qua mạch Buck-Boost có mối quan hệ theo phương trình sau:

$$R_{out} = \left(\frac{D_1}{1-D_1}\right)^2 R_1 \tag{12}$$

Tương tự, giá trị R_{mpp} có mối quan hệ với R_{out} qua độ rộng xung D_{tt} theo biểu thức sau:

$$R_{out} = \left(\frac{D_{tt}}{1-D_{tt}}\right)^2 R_{mpp} \tag{13}$$

Từ biểu thức (12) và (13) có thể tính được độ rộng xung D_{tt} như sau:

$$\left(\frac{D_1}{1-D_1}\right)^2 R_1 = \left(\frac{D_{tt}}{1-D_{tt}}\right)^2 R_{mpp} \tag{14}$$

$$D_{tt} = 1 - \frac{1}{1 + \frac{D_1}{1-D_1}\sqrt{\frac{R_1}{R_{mpp}}}} \tag{15}$$

Với giải pháp P&O truyền thống, để tránh bỏ sót điểm cực trị thì giá trị khởi động D thường khá nhỏ và cách xa D_{mpp} tại điểm MPP. Vì thế nó cần nhiều bước lặp mới có thể đạt tới giá trị tối ưu. Để gia tăng tốc độ hội tụ, giải pháp này thường cần có bước điều chỉnh lớn. Nhưng kết quả là hiệu suất của giải pháp không cao. Ngược lại, với các bước điều chỉnh nhỏ nhằm gia tăng hiệu suất thì tốc độ hội tụ giảm đáng kể. Các bước tính toán và lưu đồ giải thuật P&O truyền thống có thể được tìm thấy trong tài liệu [12].

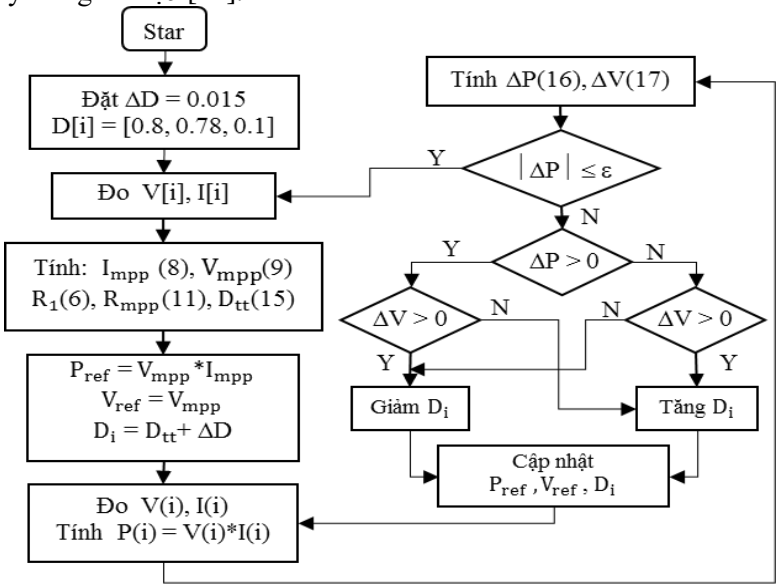

Hình 4. *Lưu đồ giải thuật đề xuất*

Từ giá trị D_{tt} tính được trong biểu thức (15) cùng với dòng điện, điện áp và công suất liên quan đến nó được dùng làm giá trị tham chiếu khởi tạo cho giải thuật P&O trong quá trình tìm kiếm cực trị. Giá trị D_{tt} này gần với độ rộng xung D_{mpp} nên cần ít bước lặp hơn để hội tụ. Việc thay đổi một lượng số gia ΔD để quan sát những thay đổi về công suất và điện áp so với giá trị tham chiếu để tìm điểm MPP. Giải pháp được xem là hội tụ khi thỏa mãn điều kiện sau:

$$\left|\Delta P\right| = \frac{P_{i+1} - P_i}{P_i} \times 100\% \le \varepsilon \quad (16)$$

Ngược lại nếu giải pháp không thỏa mãn hàm mục tiêu (16) thì kiểm tra sai số điện áp để điều chỉnh các thông số tương ứng.

$$\Delta V = \frac{V_{i+1} - V_i}{V_i} \times 100\% \quad (17)$$

Nếu ΔV×ΔP > 0 thì giảm D để tăng V.

Nếu ΔV×ΔP < 0 thì tăng D để giảm V.

Như vậy, lưu đồ giải thuật của giải pháp đề xuất được trình bày như hình 4.

4. Kết quả mô phỏng và đánh giá

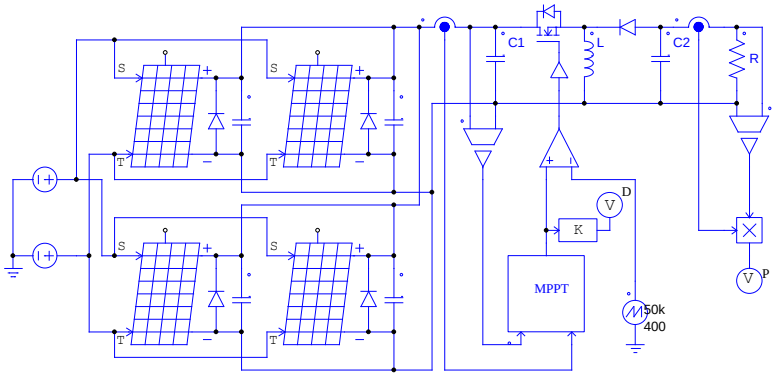

Hình 5. *Sơ đồ hệ thống đề xuất trong môi trường PSIM*

Từ những phân tích trong mục 3.1 cho thấy: cấu hình PV đề xuất sử dụng trong nghiên cứu này có tính ổn định về đường cong đặc tuyến trong mọi trạng thái bóng che. Sơ đồ hệ thống đề xuất mô phỏng trong môi trường PSIM có cấu trúc như hình 5. Tính hiệu quả của phương pháp MPPT được kiểm chứng trong các điều kiện vận hành có bức xạ thay đổi, nhiệt độ thay đổi và thay đổi cả hai thông số (bảng 2). Những kết quả đạt được qua mô phỏng trong môi trường PSIM được so sánh trực tiếp với giải thuật P&O truyền thống trong cùng điều kiện vận hành. Các thông số của hai giải thuật có thể được tìm thấy trong bảng 3.

Bảng 2. *Các trường hợp khảo sát vận hành hệ thống đề xuất*

No.	Bức xạ (W/m^2)	Nhiệt độ (^oC)	P_{max} (W)
1	200		47,73
2	500	25	122,31
3	850		205,51
4		20	244,89
5	1000	45	217,47
6		60	201,09
7	250	20	61,02
8	450	35	105,43
9	600	40	136,92
10	900	55	187,55

Bảng 3. *Các thông số của các phương pháp MPPT trong nghiên cứu*

Thông số	P&O	Giải pháp đề xuất
Giá trị khởi tạo D	0,1	D theo (15)
Số gia ΔD	0,015	0,015

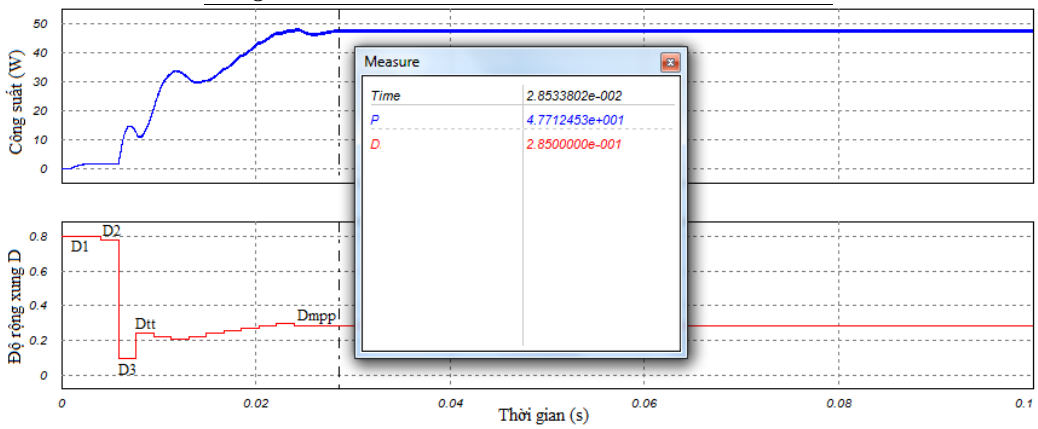

Hình 6. *Dạng sóng P và D khi mô phỏng cho trường hợp 1*

Khi mô phỏng trong điều kiện nhiệt độ tiêu chuẩn và bức xạ 200W/m^2 (No.1), kết quả thu được về khả năng MPPT chỉ ra trong hình 6 cho thấy: độ rộng xung ước lượng của giải pháp thông qua việc tính toán bằng biểu thức (15) là D_{tt} = 0,24. Từ vị trí tính toán này, các bước lặp P&O được triển khai để tìm đến MPP của hệ thống. Dữ liệu cũng cho thấy sau 9 bước điều chỉnh (từ giá trị D_{tt}), hệ thống đã có thể ổn định với độ rộng xung dừng lại ở giá trị D_{mpp} = 0,285 với công suất tương ứng là 47,71W đạt hiệu suất 99,96%. Những tình huống tiếp theo sau đó được thử nghiệm bao gồm: thay đổi bức xạ trên hệ thống trong khi giữ nguyên điều kiện nhiệt độ (No.1 đến No.3); Giữ nguyên bức xạ nhưng thay đổi nhiệt độ (No.4 đến No.6) và cuối cùng là thay đổi cả hai thông số bức xạ và nhiệt độ cho các trường hợp còn lại. Những kết quả đạt được cho các trường hợp đề xuất mô phỏng được trình bày trong bảng 4. Từ số liệu cho thấy giá trị D_{tt} ước lượng có thể lớn hơn hoặc nhỏ hơn D_{mpp} tùy thuộc vào điều kiện vận hành. Tuy nhiên hiệu suất của tất cả các trường hợp khi mô phỏng luôn đạt trên 99% và có thể đạt 100% trong một vài trường hợp. Kết quả này cho thấy giá trị D_{tt} gần với D_{mpp} nên để giảm bớt vùng tìm kiếm từ đó gia tăng tốc độ hội tụ và hiệu suất của giải thuật.

Bảng 4. *Kết quả mô phỏng MPPT cho các trường hợp*

No.	P_{mpp}	η (%) $= \frac{P_{mpp}}{P_{max}}100\%$	D_{mpp}	D_{tt}	T (s)	$P_{p\&o}$ W)	$\eta_{p\&o}$ (%) $= \frac{P_{p\&o}}{P_{max}}100\%$	$T_{p\&o}$ (s)
1	47,71	99,96	0,2850	0,2400	0,028	47,40	99,31	0,028
2	121,76	99,55	0,3900	0,3600	0,026	120,62	98,62	0,040
3	204,09	99,31	0,4375	0,4675	0,022	202,83	98,70	0,057
4	244,21	99,72	0,4700	0,5000	0,018	240,93	98,38	0,052
5	217,46	100,00	0,4825	0,5125	0,020	214,91	98,82	0,054
6	200,52	99,72	0,4870	0,5175	0,021	200,26	99,59	0,056
7	60,70	99,48	0,3000	0,2850	0,021	59,81	98,02	0,031
8	104,89	99,49	0,3800	0,3200	0,026	103,16	97,85	0,041
9	136,90	99,99	0,4175	0,3275	0,032	135,14	98,70	0,047
10	187,11	99,77	0,4750	0,3700	0,032	186,18	99,27	0,054

Bên cạnh đó, hình 7 trình bày kết quả so sánh khả năng MPPT của giải pháp đề xuất với phương pháp P&O truyền thống ở cùng điều kiện vận hành (No.3). Giải pháp đề xuất đạt mức công suất ra cực đại tại 0,022s là 204,09W tương đương với 99,31%. Trong khi đó P&O phải mất khoảng thời gian 0,05s mới tiếp cận được MPP. Một nhược điểm dễ thấy nữa là công suất ngõ ra bị dao động quanh vị trí MPP. Điều này được thể hiện ở cả hai dạng sóng công suất $P_{p\&o}$ và độ rộng xung D. Cũng từ dạng sóng D trong hình 7 cho thấy, giải pháp đề xuất đạt được tốc độ hội tụ nhanh như vậy là nhờ khả năng ước lượng D_{tt} = 0,4675 xấp xỉ với giá trị D_{mpp} = 0,4375. Qua đó nó chỉ mất 5 bước điều chỉnh xuống là có thể hội tụ tại điểm phát công suất mục tiêu. Cùng xuất phát từ giá trị D = 0,1 nhưng giải pháp P&O truyền thống mất khá nhiều thời gian để tiếp cận tới D_{mpp} và cũng bị dao động quanh vị trí này.

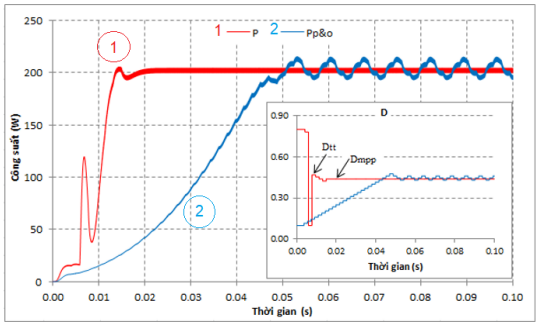

Hình 7. *So sánh MPPT trường hợp No.3*

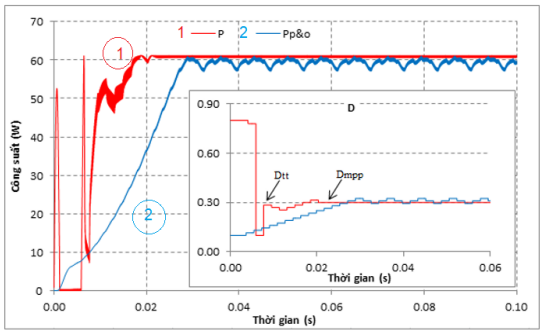

Hình 8. *So sánh MPPT điều kiện thay đổi cả bức xạ và nhiệt độ (No.7)*

Khi cả hai thông số bức xạ và nhiệt độ thay đổi khác với điều kiện tiêu chuẩn (No.7), kết quả mô phỏng trong hình 8 cho thấy rằng: giải pháp đề xuất vẫn duy trì khả năng MPPT hiệu quả khi hội tụ tại 0,021s so với phương pháp truyền thống là 0,029s. Dạng sóng công suất ra của nó cũng ổn định hơn và đạt giá trị 60,70W tương đương 99,48%, cao hơn so với P&O truyền thống ở mức 59,81W (tương đương 98,02%). Hơn nữa, cả hai dạng sóng công suất $P_{p\&o}$ và độ rộng xung D của phương pháp truyền thống đều bị dao động khá nhiều so với giải pháp đã được cải tiến.

Trong khi thay đổi đột ngột điều kiện vận hành theo xu hướng tăng cả bức xạ và nhiệt độ làm việc (hình 9) hoặc giảm bức xạ nhưng tăng nhiệt độ (hình 10). Những kết quả so sánh khả năng MPPT của hai giải pháp trong những trường hợp mô phỏng đề xuất đều cho thấy: giải pháp đề xuất luôn có tốc độ hội tụ nhanh hơn rất nhiều so với phương pháp truyền thống. Dạng sóng công suất ra của nó cũng ổn định hơn và có hiệu suất cao hơn hẳn. Kết quả khả quan này là nhờ khả năng tính toán nhanh giá trị D_{tt} để tiệm cận giá trị D_{mpp} tối ưu. Trong khi đó, để tìm được tới giá trị này thì giải pháp P&O truyền thống phải trải qua nhiều bước lặp nhằm kiểm tra toàn bộ không gian tìm kiếm. Vì thế tốc độ MPPT của nó chậm hơn mặc dù có cùng điểm xuất phát và cùng giá trị ΔD như nhau.

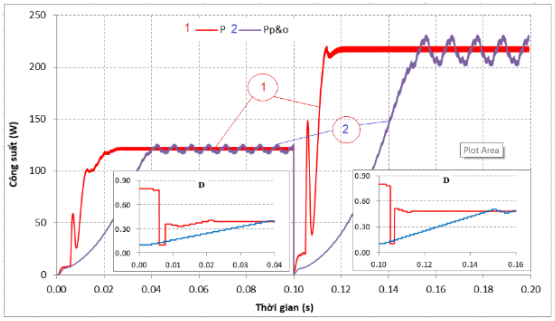

Hình 9. *So sánh MPPT thay đổi từ No.2 sang No.5.*

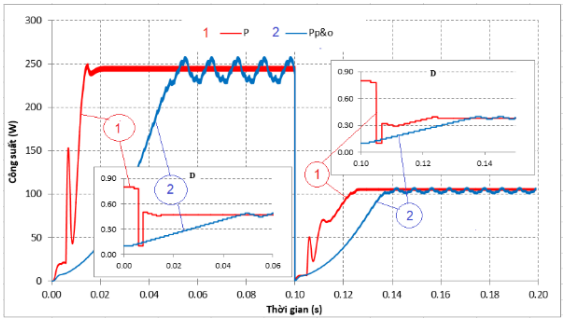

Hình 10. *So sánh MPPT thay đổi từ No.4 sang No.8*

Tổng hợp so sánh các trường hợp vận hành mô phỏng của giải pháp đề xuất so với phương pháp P&O truyền thống được trình bày trong bảng 4. Những kết quả đạt được cho thấy tốc độ hội tụ của giải pháp đề xuất trong khoảng từ 0,018s đến 0,032s nhanh hơn hẳn so với phương pháp P&O truyền thống ở mức 0,028 đến 0,057s. Đối với phương pháp P&O truyền thống, khi bức xạ càng lớn thì thời gian hội tụ gia tăng do khoảng cách từ điểm khởi động đến vị trí MPP lớn hơn. Trong khi đó, ở mọi điều kiện thì giá trị D_{tt} của giải pháp đề xuất đều dự đoán xấp xỉ giá trị D_{mpp} nên không có sự chênh lệch khá nhiều về các giá trị cho các điều kiện vận hành khác nhau.

Hình 11 trình bày kết quả so sánh hiệu suất và tốc độ MPPT của giải pháp đề xuất so với phương pháp P&O truyền thống. Biểu đồ được thành lập dựa trên thông số kết quả trong bảng 4. Trong đó, giải pháp đề xuất luôn đạt được hiệu suất cao hơn trong mọi trường hợp mô phỏng. Đặc biệt hai trường hợp No.7 và No.8 có sự chênh lệch đáng kể về hiệu suất MPPT. Bên cạnh đó, tốc độ hội tụ cũng là một ưu điểm vượt trội so với phương pháp P&O truyền thống khi mà thời gian MPPT chỉ bằng 34,62% trong trường hợp No.4 (0,018s so với 0,052s). Những số liệu thống kê so sánh đã cho thấy rằng, giải pháp đề xuất có thể cải thiện tốc độ và hiệu suất MPPT đáng kể so với phương pháp truyền thống.

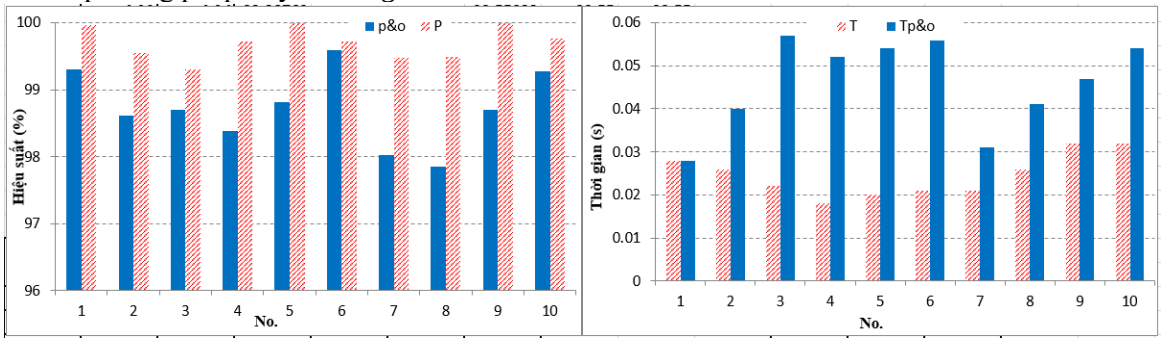

a. b.

Hình 11. *So sánh MPPT của hai giải pháp về a. hiệu suất và b. tốc độ*

5. Kết luận

Phương pháp đề xuất đã sử dụng giải pháp ước lượng hai thông số V_{oc} và I_{sc} để cải tiến tham số khởi động giải thuật P&O truyền thống nhằm nâng cao hiệu suất và tốc hộ MPPT. Những kết quả thu được qua mô phỏng trong môi trường PSIM đã cho thấy so với việc chỉ sử dụng một thông số đầu vào V_{oc} cố định, thậm chí là hai thông số I_{sc} và V_{oc} cố định thì cách tiếp cận này đã đạt được hiệu suất và tốc độ hội tụ vượt trội. Bằng cách tính toán hai thông số này thông qua phép ngoại suy nên giải pháp đề xuất sẽ tự động cập nhật và điều chỉnh tham số theo điều kiện vận hành hoặc suy hao sau thời gian sử dụng. Bên cạnh đó, hiệu suất trung bình luôn đạt trên 99% giá trị công suất cực đại mà hệ thống có thể cung cấp. Ngoài ra, tốc độ hội tụ của giải pháp đề xuất chỉ bằng 34,62% so với giải pháp truyền thống trong cùng điều kiện vận hành. Những kết quả này cho thấy tiềm năng ứng dụng của giải pháp đề xuất vào các lĩnh vực có yêu cầu điện áp và công suất thấp là đáng tin cậy.

Lời cảm ơn

Các tác giả chân thành cảm ơn sự hỗ trợ của Trường Đại học Điện lực, Công ty Điện lực và Công nghệ thông tin - Tập đoàn Điện lực Việt Nam, Trường Đại học Văn Lang và Trường Đại học Sư phạm Kỹ thuật Thành phố Hồ Chí Minh, đơn vị chủ trì đề tài nghiên cứu cấp Bộ B2019-SPK-10 và T2021-64TĐ.

TÀI LIỆU THAM KHẢO/ REFERENCES

[1] V. R. Kota and M. N. Bhukya, "A novel linear tangents based P&O scheme for MPPT of a PV system," *Renewable and Sustainable Energy Reviews*, vol. 71, pp. 257-267, May 2017, doi: 10.1016/j.rser.2016.12.054.

[2] M. H. Zafar, N. M. Khan, A. F. Mirza, and M. Mansoor, "Bio-inspired optimization algorithms based maximum power point tracking technique for photovoltaic systems under partial shading and complex partial shading conditions," *Journal of Cleaner Production*, vol. 309, August 2021, Art. no. 127279, doi: 10.1016/j.jclepro.2021.127279.

[3] F. Belhachat and C. Larbes, "A review of global maximum power point tracking techniques of photovoltaic system under partial shading conditions," *Renewable and Sustainable Energy Reviews*, vol. 92, pp. 513-553, September 2018, doi: 10.1016/j.rser.2018.04.094.

[4] A. O. Baba, G. Liu, and X. Chen, "Classification and Evaluation Review of Maximum Power Point Tracking Methods," *Renewable and Sustainable Energy Reviews*, vol. 19, no. 4, pp.433-443, doi: 10.1016/j.sftr.2020.100020.

[5] R. John, S. S. Mohammed, and R. Zachariah, "Variable step size Perturb and observe MPPT algorithm for standalone solar photovoltaic system," *IEEE International Conference on Intelligent Techniques in Control*, Srivilliputtur, India 2017, doi: 10.1109/ITCOSP.2017.8303163.

[6] M. E. Başoğlu and B. Çakır, "Hybrid global maximum power point tracking approach for photovoltaic power optimisers," *IET renewable Power Generation*, vol. 12, no. 8, pp. 875-882, June 2018, doi: 10.1049/iet-rpg.2018.0029.

[7] Y. Wang, Y. Li, and X. Ruan, "High Accuracy and Fast Speed MPPT Methods for PV String Under Partially Shaded Conditions," *IEEE Transactions on Industrial Electronics*, vol. 63, no. 1, pp. 235-245, Jan. 2016, doi: 10.1109/TIE.2015.2465897.

[8] H. M. A. Alhussain and N. Yasin, "Modeling and simulation of solar PV module for comparison of two MPPT algorithms (P&O & INC) in MATLAB/Simulink," *Indonesian Journal of Electrical Engineering and Computer Science*, vol. 18, no. 2, pp. 666-677, May 2020, doi: 10.11591/ijeecs.v18.i2.pp666-677.

[9] R. -H. Josean, U. Irantzu, M. O.-G. Jose, F.-G. Unai, M. Amaia and Z. Ekaitz, "Temperature based maximum power point tracking for photovoltaic modules," *Sci. Rep.*, vol. 10, 2020, Art. no. 12476, doi: 10.1038/s41598-020-69365-5.

[10] S. Vijayalekshmy, S. Rama Iyer, and B. Beevi, "Comparative Analysis on the Performance of a Short String of Series-Connected and Parallel-Connected Photovoltaic Array Under Partial Shading," *Journal of The Institution of Engineers (India)*, Series B, vol. 96, no. 3, pp. 217-226, January 2014, doi: 10.1007/s40031-014-0143-7.

[11] A. D. Martina, J. R. Vazqueza, and J. M. Cano, "MPPT in PV systems under partial shading conditions using artificial vision," *Electric Power Systems Research*, vol. 162, pp. 89-98, September 2018, doi: 10.1016/j.epsr.2018.05.005.

[12] B. Yang, T. Zhu, Y. Wang, H. Shu, T. Yu, X. Zhang, W. Yao, and L. Sun, "Comprehensive overview of maximum power point tracking algorithms of PV systems under partial shading condition," *Journal of Cleaner Production*, vol. 268, pp. 121983-122002, 2020, doi: 10.1016/j.jclepro.2020.121983.

Bài số 7:

X. T. Luong, **V. H. Bui**, D. T. Do, T. H. Quach and V. A. Truong, *"An Improvement of Maximum Power Point Tracking Algorithm Based on Particle Swarm Optimization Method for Photovoltaic System"*. 2020 5th International Conference on Green Technology and Sustainable Development (GTSD), Ho Chi Minh City, Vietnam, 2020, pp. 53-58. DOI: 10.1109/GTSD50082.2020.9303110

An Improvement of Maximum Power Point Tracking Algorithm Based on Particle Swarm Optimization Method for Photovoltaic System

Xuan Truong Luong
Department of Electrical and Electronics Engineering
Ho Chi Minh City University of Technology and Education
Ho Chi Minh City, Viet Nam
xuantruongpdl@gmail.com

Van Hien Bui[1,2]
[1]*Department of Electrical and Electronics Engineering*
Ho Chi Minh City University of Food Industry
[2]*Research student at HCMC University of Technology and Education*
Ho Chi Minh City, Viet Nam
hienbv.ncs@hcmute.edu.vn or buivanhientb@gmail.com

Duc Tri Do
Department of Electrical and Electronics Engineering
Ho Chi Minh City University of Technology and Education
Ho Chi Minh City, Viet Nam
tridd@hcmute.edu.vn

Thanh Hai Quach
Department of Electrical and Electronics Engineering
Ho Chi Minh City University of Technology and Education
Ho Chi Minh City, Viet Nam
haiqt@hcmute.edu.vn

Viet Anh Truong
Department of Electrical and Electronics Engineering
Ho Chi Minh City University of Technology and Education
Ho Chi Minh City, Viet Nam
anhtv@hcmute.edu.vn

***Abstract*— Partial shading is the cause of the reduction of the output power of the photovoltaic (PV) system due to changes in its P-V characteristic curve. Global Maximum Power Point Tracking (GMPPT) in more complex and multiple peaks conditions is the biggest challenge for current MPPT techniques to improve the performance of the system. This article introduces an improved method based on the traditional Particle Swarm Optimization (I_PSO) algorithm to increase the convergence speed in a constantly changing and complex environment. The study not only considers the influence of the best location of the individual and the swarm but also focuses on the experience of the neighboring individuals with a better position to avoid the local extreme trap. In addition to that, a boost converter uses to simulate the proposed algorithm applying PSIM software. The simulating results with those previously under the same operating conditions showed the superiority of the proposed approach in improving the efficiency of the photovoltaic system.**

Keywords—partial shading, photovoltaic system, global maximum power point tracking, solar array.

I. INTRODUCTION

In general, solar energy has been becoming a useful alternative fuel source for world energy security in recent years. The use of photovoltaic systems increases significantly because of its outstanding advantages such as low fuel and maintenance costs, environmentally friendly, and almost endless energy sources [1,2]. However, the expense of a PV plant and conversion equipment to reach the limit of the electricity system is a significant challenge in the development and use of them. Besides that, the PV characteristic curves depend on operating environment conditions as solar radiation and temperature, which can occur due to multiple reasons such as buildings, trees, or passing clouds, birds, and dust deposition…called partial shading. They are causes of energy losses in PV power generators. The traditional MPPT techniques such as P&O (Perturb and Observation), InC (Incremental Conductance) are significantly effective under uniform conditions but inaccurate under partial shading conditions [3]. To overcome these drawbacks and improve the performance in MPPT control techniques. The improvement methods based on two algorithms also introduced recently as I_InC (Improved Incremental Conductance) [4-6], VSSP&O (Variable Step Size Perturb and Observe) [7]. The optimization algorithms and their improvements based on the natural behavior of the swarm such as PSO (Particle Swarm Optimization), OD_PSO (Differential Particle Swarm Optimization), LPSO (Leader Particle Swarm Optimization), EL_PSO (Enhanced Leader Particle Swarm Optimization), MPSO (Multicore Particle Swarm Optimization) [8-12]. Another group is using hybrid methods that have emerged by combining two or more approaches in a solution to further enhance the performances as PSO-OCC (Particle Swarm Optimization Combined with one Cycle Control), SA-PSO (Simulated Annealing with Particle Swarm Optimization), INC-FFA (Firefly Algorithm with Incremental Conductance), PSO-P&O (Particle Swarm Optimization with Perturb and Observation), PSO-SFLA (Particle Swarm Optimization with Shuffled Frog Leaping Algorithm), and ABC-P&O (Artificial Bee Colony) [13-18]. These algorithms have achieved significant effects in solving the multi-peak GMPPT problem. However, the convergence speed, performance, applicability, and complexity are still barriers to the above solutions.

This paper proposes an improved method based on PSO to increase the convergence speed in GMPPT under continuously changing and complicated operation conditions. Compared to other MPPT techniques, the proposed algorithm has faster convergence speed, lower control cost, and greater efficiency by adding influence coefficients from neighboring particles with a better position. The remainder of this paper is as follows. Section II discusses the mathematical modeling of Solar PV and the effect of partial shading on the performance of the PV array. Section III proposed the I_PSO algorithm and how to use it for improving the MPPT performance. In section IV, the simulating results show and compare with

978-1-7281-9982-5/20/$31.00 ©2020 IEEE

other algorithms. Finally, Section 5 presents the conclusion of the work.

II. PV Simulation Model And The Effect Of Partial Shading On Its Characteristics

A. PV Simulation Model.

The equivalent circuit for a photovoltaic cell introduced in Fig. 1 consists of a current source driven by sunlight in parallel with a real diode and both parallel and series resistances R_P, R_S [19-22].

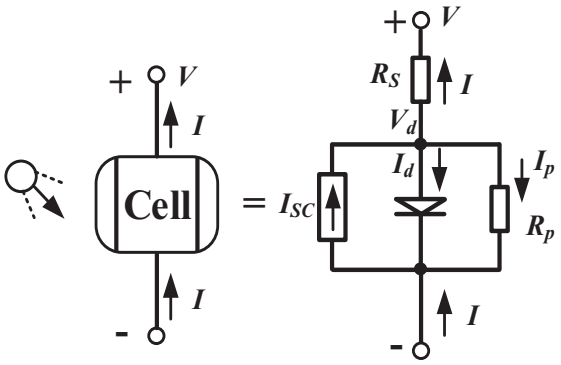

Fig. 1. PV cell equivalent circuit.

The current output of PV cell is:

$$I = I_{SC} - I_0\left\{e^{\frac{q(V+I.R_S)}{kT}} - 1\right\} - \frac{V + I.R_S}{R_P} \quad (1)$$

Where: V, I are output voltage (V) and current (A) of PV, respectively; I_{SC} is short circuit current (A); I_0 is the reverse saturation current of diode (A); q = 1,602.10^{-19} (C); k =1,381.10^{-23} (J/K); T (^{0}K); R_S, R_P (Ω).

B. Effect of partial shading on the PV system.

The simulation and discussion in the article base on a series connection of 5 PV modules type PHM60W36 with its parameters are 37.5 (V), 33.3 (A), and 330 (W) at MPPT under operating conditions (1000W/m^2 at 25^{o}C).

Previous studies have shown that, under uniform conditions, the P-V and I-V Characteristics Curves of the PV system are not different from those of a PV cell. Conversely, when the PV module operated under heterogeneous conditions like for partial shading cases caused by natural phenomena will increase multiple local maxima in the array's PV characteristics, which are capable of making it complex to determine GMPP and affect the system' output power (Fig. 2). Accordingly, the use of MPPT algorithms is necessary in this case [23].

The configuration of the proposed system simulates under partial shading conditions while only one case operates under a uniform environment. The data for changing solar radiation on the PV system shows in Table 1. When the irradiance is uniform, there is only an MPP (with maximum output power) exists on the P-V characteristic (Fig. 2). Meanwhile, the remaining cases have lower output power. It' characteristic curves also exhibit more LMPP. These show that the PV output power is affected by the level of shading on the modules. In other words, the radiation value received by modules will determine the whole system's output power. On the other hand, accurately determine GMPP under multiple-peaks conditions is the biggest challenge for MPPT algorithms to improve the operating efficiency of the PV system. Because of under partial shading conditions as well as instantaneous environmental changes, it requires more efficient algorithms and higher convergence speed.

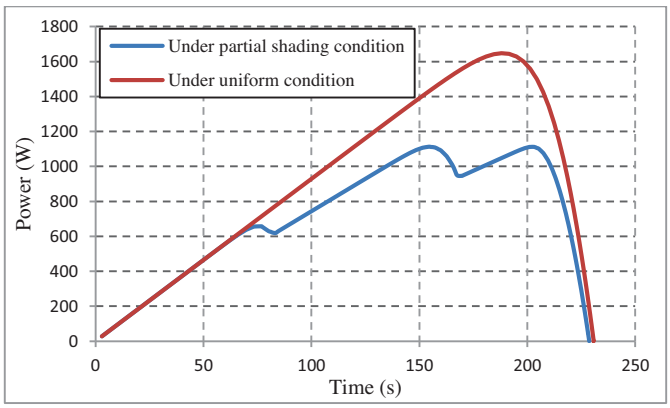

Fig. 2. P-V characteristic under different conditions.

TABLE I. THE PROPOSED CASES SIMULATE THE SYSTEM.

Case	Radiation Values Per Modules (×100 W/m2)				
	1	*2*	*3*	*4*	*5*
1	10	10	10	10	10
2	10	9	8	7	6
3	5	4	3	2	10
4	9	8	7	6	5
5	4	3	2	10	9
6	8	7	6	5	4
7	3	2	10	9	8
8	7	6	5	4	3
9	2	10	9	8	7
10	6	5	4	3	2

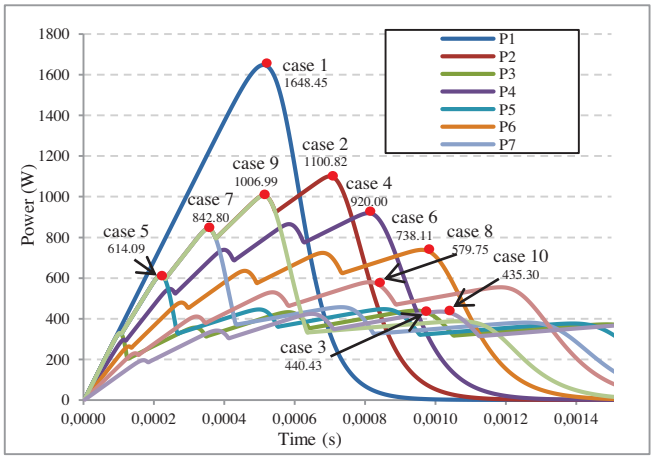

Fig. 3. GMPP under partial shading conditions

III. The Proposed Solution

A. DC/DC Converter.

A boost converter links between the PV array and the load to control the system working at the MPP is a DC/DC power converter. It is a class of switched-mode power supply containing at least two semiconductors (a diode and a transistor) and at least one energy storage element: a capacitor, inductor, or both in combination. It' diagram presents in Fig. 4, which is characterized by its duty

cycle D ($0 \le D \le 1$) that gives the ratio between the input and the output voltage when the conduction is continuous [24].

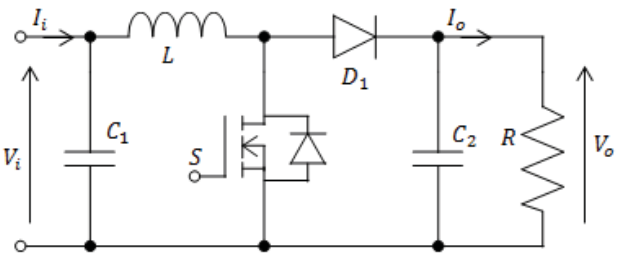

Fig. 4. Boost converter

The relationship between the input and output voltage depends on D is expressed by the following equation:

$$V_i = (1 - D)V_o \tag{2}$$

Where D, V_i, V_o are respectively the duty cycle, PV input voltage, and the output voltage of the Boost converter.

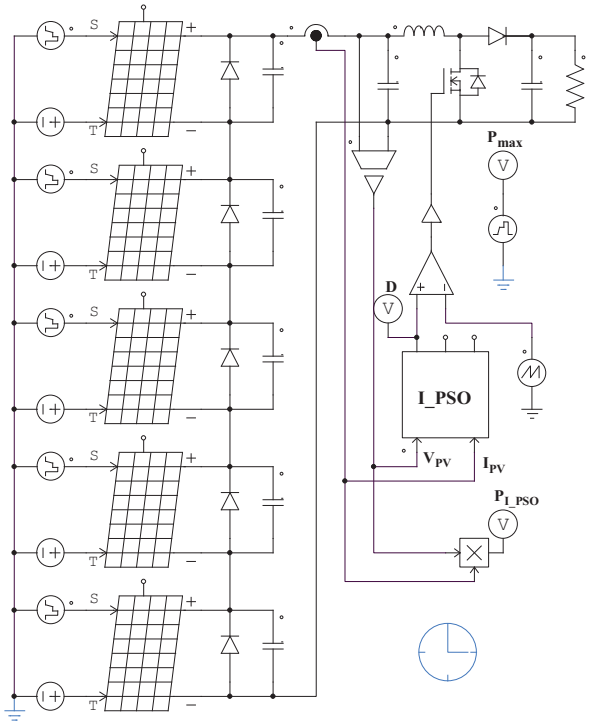

Fig. 5. Simulation model of the proposed system

With a load value is R = 120Ω, maximum input voltage V_i = 200V, switching frequency f = 50kHz, and a duty cycle is between 20-80% to ensure that it does not exceed the limit of the semiconductor switch. The determining of inductor value according to the continuous and discontinuous conduction modes by the following equation:

$$L = \frac{DV_i}{2I_m f} \tag{3}$$

Where I_m is the maximum power current of the PV system.

The output capacitor value to decrease output voltage ripple is:

$$C = \frac{D}{Rfr} \tag{4}$$

Where: output voltage ripple r is 1%.

Therefore, the inductors and capacitors' value for boost converter used for the proposed method, and other parameters lists in Table 2. The system is simulated in the PSIM environment and has the configuration shown in Fig. 5

TABLE II. THE SPECIFICATIONS OF THE IMPLEMENTED BOOST CONVERTER

The parameters	Set value
Input voltage	V_i = 80 - 200V
Output voltage	V_o = 400V
Output current	I_o = 5A
Output power	P_o = 2kW
Switching frequency	f = 50kHz
Output voltage ripple	$r \le 1\%$

B. I_PSO Implemented for MPPT.

PSO is a swarm intelligence optimization algorithm based on two main principles, i.e., to follow the best performing particle (G_{best}), and to move towards the best conditions found by the particle itself (P_{best}) [25, 26]. The I_PSO introduced in this article is also an improved version, in which the particles can avoid LMPP traps to give better positioning in the search space and faster convergence speed. The proposed study not only considers the influence from the best location of the individual (P_{best}), overall experience (G_{best}), and the present movement of the particles but also focused on the effect of the neighboring individuals with a better position (P_e), which used to decide their next values in the search space to avoid the local extreme trap.

Mathematically, the concepts of I_PSO can be expressed as follows:

$$v_i^{k+1} = w_i v_i^k + c_1 r_1 (P_{best,i} - x_i^k) + c_2 r_2 (G_{best} - x_i^k) + c_3 r_3 (P_e - x_i^k) \tag{5}$$

$$x_i^{k+1} = x_i^k + v_i^{k+1} \tag{6}$$

Where x_i, v_i are the position and velocity of i particle; k denotes the iteration number; w_i is the inertia weight; r_1 and r_2 are random variables uniformly distributed within [0, 1]; and c_1, c_2 are the cognitive and social coefficient, respectively. The P_{best_i} variable uses to store the best position that a particle has found so far (i_th), while the G_{best} is the best position of all the particles.

The significant difference in Eq. (5) is the influence coefficient c_3 and a randomly-generated random number r_3 between 0 and 1. Whereas, P_e represents the best position of an expert partial, which is better than P_{best} but not equal to G_{best}. Under this condition, when the G_{best} value of the swarm is determined, it is also its P_{best} local, which is likely reaching a velocity value equal to zero (v = 0) when added in the update function. As a result, the survey range will reduce because this position does not change in the next cycle. The addition of third-place effects out of Pbest and Gbest parameters is necessary to ensure that it will survey all of the swarm.

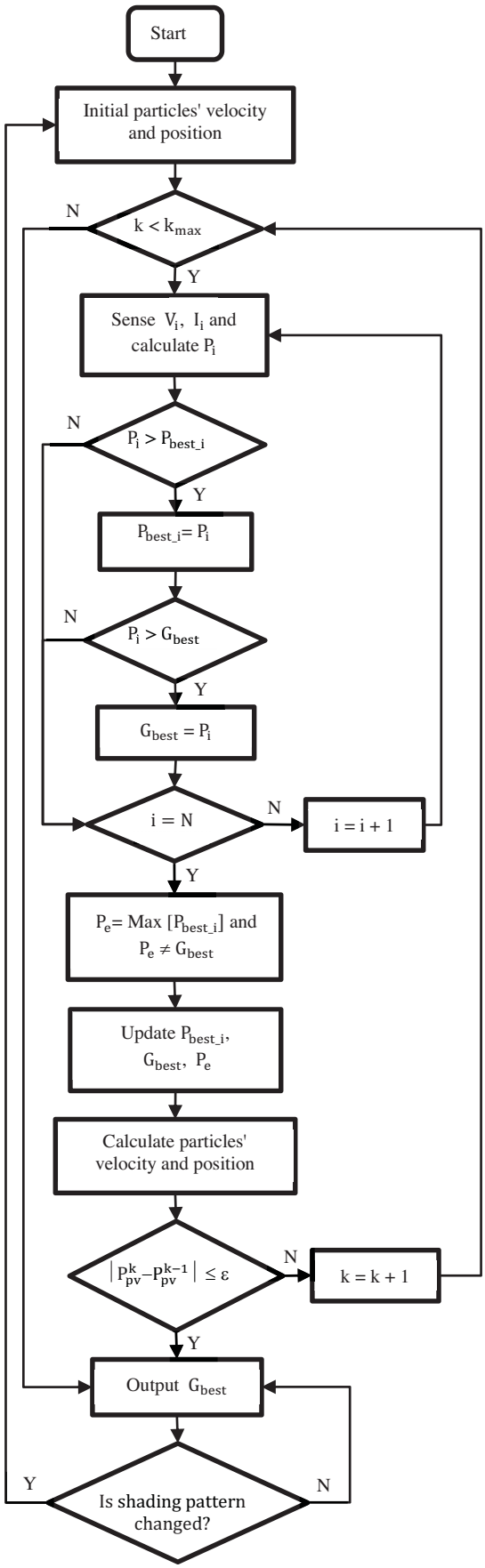

Fig. 6. Flowchart of the proposed algorithm

The complete flowchart of the proposed method illustrated in Fig. 6, the main blocks are described in detail as follows:

Step 1: In the proposed system, the selecting duty cycle *D* and delta *D* values of the DC-DC converter like the particle' position and velocity in the search space, respectively. Meanwhile, the fitness value evaluation function sets as the generated power of the whole system P_{PV}. The number of swarms in this paper is equal to six may be increased convergence time. However, the probability of overcome local extremes will significantly higher.

Step 2: Although particles can be placed on fixed positions or in the space randomly. In this paper, the particles' initialization value is permanent, which limits between 0.2 and 0.8 the search space with equal distances. It means that this is a region with the highest GMPP potential and also within the boost converter's operating range.

Step 3: After the digital controller output the PWM command according to the position of the i_th particle, which represents the duty cycle command, the voltage $V_{PV,}$ and current I_{PV} are defined. These values are the basis of calculating the fitness evaluation of the i_th particle.

Step 4: If the fitness value of the i_th particle is better the previous the best value (P_{best_i}), sets the current value as the new P_{best_i}. And then, this value can be utilized as a new G_{best} if it is greater than the G_{best} value, which is the best fitness value of all the particles in history (or not).

Step 5: Select Pe value as the expert particle, which is the best value of all P_{best_i} without G_{best} after each loop. Then, update all P_{best_i}, G_{best}, and P_e values.

Step 6: Update velocity and position of all the particles in the swarm by using Eq. (5) and (6).

Step 7: When the algorithm reaches the maximum number of iterations, or as soon as the output power of the PV system is not significantly different between two consecutive loops, it will stop and output the G_{best} solution. Convergence criteria determine according to Eq. (7) then it is utilized to detect the insolation change and shading pattern changes.

$$\left| P_{pv}^{k} - P_{pv}^{k-1} \right| \le \varepsilon \tag{7}$$

IV. Simulation Results And Discussion

The parameter selection in the method to achieve the best simulating results plays an important role. According to the characteristics of the PV system uses in this study, the setting values of the proposed algorithm listed in Table 3, while Table 1 shows the simulation cases under partial shade conditions.

In the PSIM environment, the PV panel can be implemented using the physical model of the solar cell in the renewable energy package and structured in Fig. 5. The MPPT simulation results for the proposed system summarized in Fig. 7, which is known as the measured output power waveform of the PV system when treated by the proposed algorithm in the PSIM environment. Meanwhile, Fig. 8 shows the result of the generated output power waveforms when the irradiance changes. The MPPT simulation results using the proposed algorithm compared

with the maximum available power of the PV module under a continuous shading pattern, which is extracted from Fig. 3 to determine the tracking effectiveness of this algorithm. Besides that, Figs 9 and 10 show a comparison of the maximum power point tracking speed and performance of the proposed algorithm compared with traditional PSO. Meanwhile, Table 4 introduces the MPPT convergence speed and performance of all the cases presented above.

From Fig. 7, the proposed algorithm always extracts GMPPT under different partial shading conditions with convergence time between 0.22s and 0.39s in cases 9 and 10, respectively. Even though under simulation conditions changed instantaneously, the system is still capable of MPPT quickly with significant performance (Fig. 8). The aggregated results in Table 5 also show two vital issues: Firstly, the proposed algorithm can reach maximum efficiency of 100% in a few cases, but the average efficiency is always greater than 99%. Therefore, the proposed algorithm is as effective as the other optimal algorithms introduced recently. Secondly, the convergence speed of the algorithm is 0.22s when the measured MPPT tracking efficiency is 99.95% in the case of 9, which is a remarkable advantage compared to other modified and improved versions. The obtained simulation results in this paper are compared with other MPPT techniques under the same operating conditions and presented in Table 5. These positives show the superiority of the proposed method compared with previous techniques in both convergence speed and GMPPT tracking efficiency. Last but not least, although the convergence speed of the proposed algorithm significantly improved, the MPPT performance is not decreased, which listed in Figs 9 and 10, respectively.

TABLE III. THE I_PSO ALGORITHM PARAMETERS

The parameters	Set value
Population sizes (N)	6
Maximum iteration (k_{max})	100
Acceleration factors (c_1; c_2)	0.1; 0.5
Influence coefficient (c_3)	0.35
Inertia weight (w_i)	0.07
Random variables (r_1, r_2, r_3)	[0 1]
Sampling time	0.2 (s)

TABLE IV. THE MPPT PERFORMANCE AND CONVERGENCE SPEED

Case	Pmax (W)	Pi_pso (W)	η (%)	T (s)
1	1648.45	1648.40	100.00	0.22
2	1100.82	1100.73	99.99	0.30
3	440.43	440.39	99.99	0.31
4	920.00	917.93	99.78	0.31
5	614.09	613.39	99.89	0.29
6	738.11	737.75	99.95	0.31
7	842.80	842.70	99.99	0.28
8	579.75	579.73	100.00	0.38
9	1006.99	1006.51	99.95	0.22
10	435.30	434.89	99.91	0.39

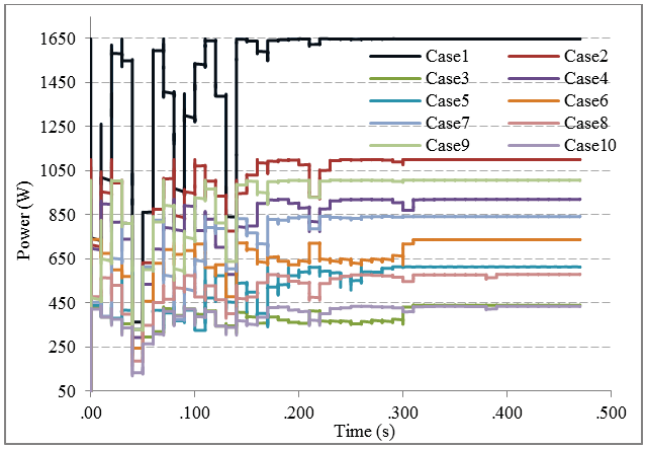

Fig. 7. Measured PV power waveforms under MPPT process.

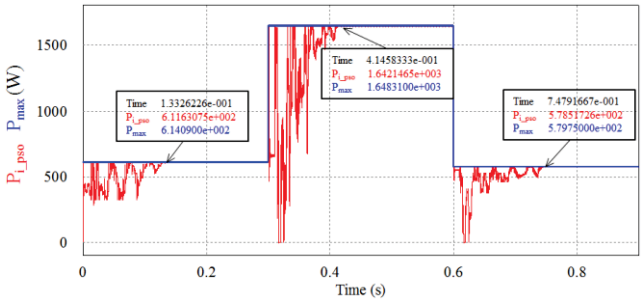

Fig 8. PV power waveforms when the irradiance changes

TABLE 5. COMPARISON OF GMPPT TECHNIQUES

MPPT Technique	η (%)	T (s)	MPPT Technique	η (%)	T (s)
I_PSO	100	0.22	L_PSO [10]	99.99	0.35
OD_PSO [9]	97.74	1.86	INC_FFA [15]	99.99	0.38
MPSO [12]	98.92	1.3	SA_PSO [14]	-	0.13
PSO [10]	99.83	0.85	PSO_P&O [16]	-	0.9
PSO_SFLA [17]	-	3.15	P&O [10]	99.95	0.52
ABC_P&O [18]	99.93	0.08	PSO_OCC [13]	100	1.2

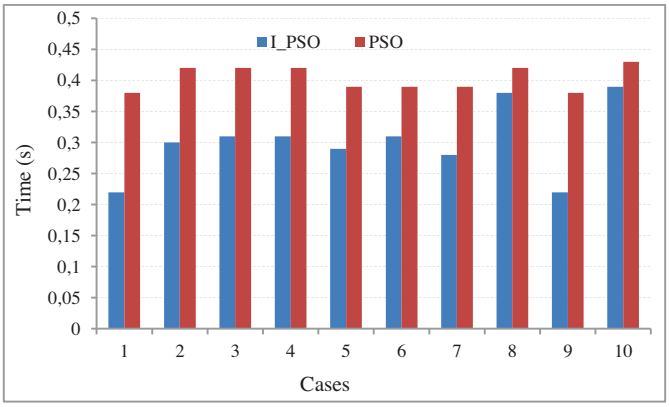

Fig 9. Comparison of convergence speed with and without c_3 coefficients

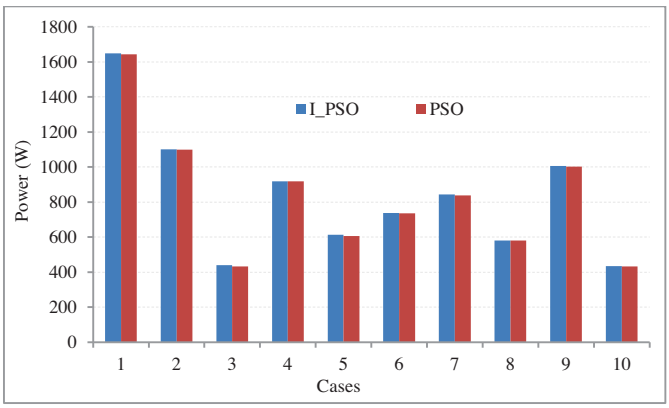

Fig 10. Comparison of MPPT performance with and without c_3 coefficients

V. Conclusion

I_PSO is an improved version based on the traditional PSO algorithm introduced in this article, which not only has a fast convergence speed but also has an outstanding MPPT tracking efficiency under different operating conditions. The simulation results show that the performance of the proposed algorithm is likely reaching 100% at 0.22s, which are higher than previous improvements to the traditional PSO algorithm. It is due to the addition of an influencing factor in the velocity equation of the classical PSO algorithm to improve the operating efficiency of the PV system. Conclusion, I_PSO is a simple and efficient technique, which is capable of escaping from LMPP traps and extracting the optimization power at high speed under partial shading condition as well as instantaneous environmental changes.

References

[1] Ehsanul, Pawan Kumar, Sandeep, Adedeji A. Adelodun, Ki-Hyun Kim, Solar energy: Potential and future prospects, Renewable and Sustainable Energy Reviews 82 (2018) 894–900.

[2] Al-Saidi, M., & Lahham, N. Solar energy farming as a development innovation for vulnerable water basins. Development in Practice, (2019).

[3] Saleh Elkelani Babaa, Matthew Armstrong, Volker Pickert: Overview of Maximum Power Point Tracking Control Methods for PV Systems, Journal of Power and Energy Engineering, 2014, 2, 59-72.

[4] Duy C. Huynh: An Improved Incremental Conductance Maximum Power Point Tracking Algorithm for Solar Photovoltaic Panels, International Journal of Science and Research, Volume 3 Issue 10, October 2014.

[5] Nazih Moubayed, Ali El-Ali, Rachid Outbib: A comparison of two MPPT techniques for PV system, WSEAS Transactions on Environment and Development, Issue 12, Volume 5, December 2009.

[6] Tawfik Radjai, Lazhar Rahmani, Saad Mekhilef, Jean Paul Gaubert; Implementation of a modified incremental conductance MPPT algorithm with direct control based on a fuzzy duty cycle change estimator using dSPACE, Solar Energy 110 (2014) 325–337

[7] Riby John, Sheik Mohammed S, Richu Zachariah, Variable Step Size Perturb and Observe MPPT Algorithm for Standalone Solar Photovoltaic System, IEEE International Conference On Intelligent Techniques In Control,Optimization And Signal Processing, 2017

[8] Chun-Liang Liu, Yi-Feng Luo, Jia-Wei Huang, Yi-Hua Liu: A PSO-based MPPT Algorithm for Photovoltaic Systems Subject to Inhomogeneous Insolation, SCIS-ISIS 2012, Kobe, Japan, November 20-24, 2012

[9] Li, H., Yang, D., Su, W., Lü, J., Yu, X., 2018b. An overall distribution particle swarm optimization MPPT algorithm for photovoltaic system under partial shading. IEEE Trans. Ind. Electron. 66 (1), 265–275

[10] Ram JP, Rajasekar N. A new robust, mutated and fast tracking LPSO method for solar PV maximum power point tracking under partial shaded conditions. Appl Energy 2017;201:45–59

[11] Pratik Shantaram Gavhane, Smriti Krishnamurthy, RidhimaDixet, J.Prasanth Ram, N.Rajasekar; EL-PSO based MPPT for Solar PV under Partial Shaded Condition, Energy Procedia 117 (2017) 1047-1053.

[12] Chao RM, Nasirudin A, Wang IK, Chen PL. Multicore PSO operation for maximum power point tracking of a distributed photovoltaic system under partially shading condition. Int J of Photoenergy (2016) 1–19.

[13] Anoop, K., Nandakumar, M., A novel maximum power point tracking method based on particle swarm optimization combined with one cycle control. Proceedings of the International Conference on Power, Instrumentation, Control and Computing (PICC). Thrissur 2018.

[14] Guan T, Zhuo F. An improved SA-PSO global maximum power point tracking method of photovoltaic system under partial shading conditions. In: Proceedings of the IEEE conference on environment and electrical engineering. Italy; 2017

[15] Shi JY, Ling LT, Xue F, Qin ZJ, Li YJ, Lai ZX, et al. Combining incremental con-ductance andfirefly algorithm for tracking the global MPP of PV arrays. J Renew Sustain Energy 2017;9(2):1–19.

[16] Hanafiah S, Ayad A, Hehn A, Kennel R. A hybrid MPPT for quasi-Z-source inverters in PV applications under partial shading condition. In: Proceedings of the 11th IEEE international conference on compatibility, power electronics and power engineering; 4–6 April 2017.

[17] Nie X, Nie H. MPPT control strategy of PV based on improved shuffled frog leaping algorithm under complex environments. J Control Sci Eng 2017;2017:1–12

[18] Pilakkat, D., Kanthalakshmi, S., An improved P&O algorithm integrated with ar-tificial bee colony for photovoltaic systems under partial shading conditions. Sol. Energy 178, 37–47, 2019.

[19] Neeraj Priyadarshi, Sanjeevikumar Padmanaban, Lucian Mihet Popa, Frede Blaabjerg and Farooque Azam, Maximum Power Point Tracking for Brushless DC Motor-Driven Photovoltaic Pumping Systems Using a Hybrid ANFIS-FLOWER Pollination Optimization Algorithm, (2018), 11(5), 1-16

[20] El-Helw HM, Magdy A, Marei MI. A hybrid maximum power point tracking technique for partially shaded photovoltaic arrays. IEEE Access 2017;5:11900–8.

[21] Chakkarapani M, Raman GP, Raman GR, Ganesan SI, Chilakapati N. Fireworks enriched P&O algorithm for GMPPT and detection of partial shading in PV systems. IEEE Trans Power Electron 2017;32(6):4432–43.

[22] Mohanty S, Subudhi B, Ray PK. A Grey Wolf assisted perturb & observe MPPT algorithm for a PV system. IEEE Trans Energy Convers 2016;32(1):340–7.

[23] Faiza Belhachat, Cherif Larbes, A review of global maximum power point tracking techniques of photovoltaic system under partial shading conditions, Renewable and Sustainable Energy Reviews 92 (2018) 513–553.

[24] Preti Tyagi, V.C. Kotak, V. P. Sunder Singh, Design High Gain DC-DC Boost Converter with Couplinginductor and Simulation in PSIM, International Journal of Research in Engineering and Technology, Volume: 03 Issue: 04,Apr-2014

[25] Vapnik, V.N. 1995. The Nature of Statistical Learning Theory. 2nd ed.; Springer-Verlag, New York.

[26] Kennedy, J., Eberhart, R.C., Shi, Y. 2001. Swarm Intelligence, Morgan Kaufmann, San Francisco, USA.

Bài số 8:

Trinh Trong Chuong, Nguyen Duc Minh, **Bui Van Hien**, Fan Yang, Truong Viet Anh (2021). *"Optimizing the Performance of the Photovoltaic System using the Micro DC-DC Converter*". 2021 3rd International Conference on Smart Power & Internet Energy Systems (SPIES) 978-1-6654-3879-7/21/$31.00 ©2021 IEEE, DOI: 10.1109/SPIES52282.2021.9633791

Optimizing the Performance of the Photovoltaic System using the Micro DC-DC Converter

Trinh Trong Chuong
Faculty of Electrical Engineering
Ha Noi University of Industry
Hanoi, Viet Nam
chuongtt@haui.edu.vn

Nguyen Duc Minh
Institute of Energy Science
Vietnam Academy of Science and Technology
Hanoi, Viet Nam
ducminhies@gmail.com

Bui Van Hien
Faculty of Electrical and Electronics Engineering
Ho Chi Minh city University of Food Industry
HCM City, VietNam
hienbv.ncs@hcmute.edu.vn

Fan Yang
College of Electrical Engineering
University of Shanghai Electric Power
Shanghai, China
yangfan@shiep.edu.cn

Truong Viet Anh
Faculty of Electrical and Electronics Engineering
Ho Chi Minh City University of Technology and Education
HCM City, VietNam
anhtv@hcmute.edu.vn

2021 3rd International Conference on Smart Power & Internet Energy Systems (SPIES) | 978-1-6654-3879-7/21/$31.00 ©2021 IEEE | DOI: 10.1109/SPIES52282.2021.9633791

***Abstract*—The generating capacity of photovoltaic (PV) systems depends on the operating environment and the modular topology. The previous research results showed that; with conventional types of coupling such as series (SC), parallel (PC), or series-parallel (SPC) when operating under uniform conditions, the characteristics curves do not change in shape. But when the working environment is heterogeneous due to partial shading conditions (PSC) the global maximum power point tracking (GMPPT) meet more difficulties due to having multiple extremes and easy to be trapped in local extremes (LMPP). To effectively solve this problem, the optimal algorithms for MPPT have strongly developed in recent years. This article introduces a Micro DC-DC converter incorporating an innovative MPPT solution for PV systems under PSC. The research results in the article have shown that: the proposed solution not only has a simple configuration, compact structure but also has high convergence speed and outstanding performance.**

Keywords—Partial shading, Micro DC-DC converter, solar photovoltaic system, P-V characteristic curve

List of Abbreviations

Abbreviation	Definition	Abbreviation	Definition
PV	Photovoltaic	PSC	Partial Shading Conditions
SC	Serial Configuration	GMPPT	Global Maximum Power Point Tracking
PC	Parallel Configuration	LMPPT	Local Maximum Power Point Tracking
SPC	Serial-Parallel Configuration	MPPT	Maximum Power Point Tracking
TCT	Total Cross Tied	BL	Bridge linked
HC	Honeycomb Configuration	PSO	Particle Swarm Optimization

Lists of Symbols

Symbol	Definition	Symbol	Definition
I_0	dark saturation current of diode (A)	k	Boltzman's constant ($1{,}381.10^{-23}$J/K)
q	absolute value of electron charge ($1{,}602.10^{-19}$C)	T	Absolute temperature (K)
I	output current of PV (A)	I_{SC}	short-circuit current PV (A)

I. INTRODUCTION

Solar power installations are increasing rapidly around the world [1, 2, 3]. Simultaneously, there has been large-scale research that studied solutions to improve solar PV panel output and enhance the efficiency of grid-connected PV systems [2], [3]. In the structure of grid-connected PV systems, multiple PV modules are linked together into a large system. As a result, practical issues to be considered in the design of grid-connected PV system include selecting connection configurations to achieve optimal performance, reducing capital investment costs, maintaining simple operation, and maximizing operating efficiency of the system.

Previous studies have shown that the parallel connection (PC) in Figure 1.b of PV panels will produce higher efficiency compared to series wiring (SC) in Figure 1.a under similar operating conditions [4-7]. The parallel wiring also generates a minimum number of maximum power point tracking. However, the PC design produces low output voltage and large current, which requires thicker wires to be utilized in voltage and current control circuits for power converters. On the other hand, SC produces lower efficiency and creates many extremes, but it offers higher output voltage with lower current, which is quite safe for power circuits. A series - parallel (SPC) configuration (Figure 1.c) wires PV modules in series connection to reach the desired voltage within safe limits. Then, they are connected in parallel to form an array to increase the output power.

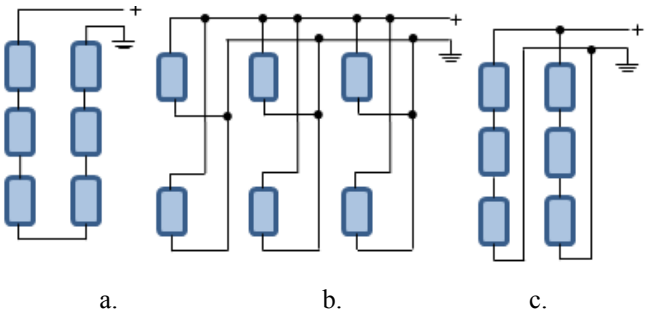

Fig. 1. Connection configurations of PV modules: a. SC, b. PC, c. SPC

Past studies on SPC configuration pointed out that this design could be used in sectors with higher demand of

energy, as the configuration allows for flexible number of PV modules connected in the series as well as number of PV arrays wired in system to deliver desired power output. However, for the same number of PV modules, SPC's current is larger than SC's but lower than PC's current. Voltage of SPC, on the other hand, is higher than PC's and lower than SC's and not stable under abnormal operating conditions. Moreover, connected modules in the array have similar disadvantages as the SC configuration under this condition, which could lead to the disruption of power supply (if no protection mechanism is available) or the loss of power (in case the system is protected by a bypass-diode). To address these issues, some upgraded configurations have been proposed, such as: Total Cross Tied - TCT, Bridge linked - BL, HoneyComb – HC [8], [9], [10], [11]. In theory, these configurations have overcome some drawbacks of traditional connection configurations. However, these solutions require extra modules to achieve the connection designs and deliver output as expected. It also generates many redundant connections under normal operating conditions, causing losses, increased costs, and is not feasible in actual testing. In fact, these complexed configurations are only suitable in software simulation. It is also not suitable for small and medium-sized projects with a limited number of modules as system resources are restricted to accommodate the designated topologies [12].

It is challenging to conduct experiments involving large amount of PV modules in partial shade conditions. This article proposes a solution to apply the cascaded DC/DC converter structure combined with the improved MPPT algorithm to enhance the efficiency and tracking speed of the PV system. The proposed system uses PV type HTM330PA-72, controlled by variable radiation conditions. This structure offers the advantages of small scale, low cost, high performance, and high convergence speed to meet the requirements of laboratory tests as well as practical operation. These results are simulated in the PSIM environment and compared with the bypass-diode solution in terms of speed and MPPT performance, clearly showing the superior performance compared to other topologies [13, 14].

II. Characteristic of PV Cell

A. Under Identical Operating Conditions

In identical operating conditions, radiation power and temperature affecting PV modules are uniform. Characteristics curves such as power - voltage curve P - V and current – voltage curve I - V of the system follows the modelled curves of each module across all configurations. This implies that there is only one maximum available, thus the GMPP tracking process is straight-forward. The relationship between power current and output voltage of a PV is illustrated in Equation (1).

$$I = I_{SC} - I_0 \left\{ e^{\frac{q(V+I.R_S)}{kT}} - 1 \right\} - \frac{V+I.R_S}{R_P} \quad (1)$$

As being mentioned, the power output of each PV module is limited and relatively low. To achieve high power levels, PV modules are wired in SPC configuration to form arrays in one system. There is no variation between the modelled characteristic curves and characteristic curves of a PV module in this topology. The relationship between the current and the voltage of a system consisting of Ns of modules wired in a series and Np of parallel chains is given in Equation 2.

$$I = N_P I_{SC} - N_P I_0 \left\{ e^{\frac{q(V+N_S R_S)}{N_S.kT}} - 1 \right\} - \frac{V+N_S R_S}{N_S R_P} \quad (2)$$

In short, under homogeneous environmental conditions, all connection configurations have the same curve characteristic but differ in the maximum value. Notably, there is only one extreme available in this case, so there is no need to apply highly complexed algorithms in GMPPT. Figure 2 presents the output characteristic curves of different configurations under uniform environmental conditions.

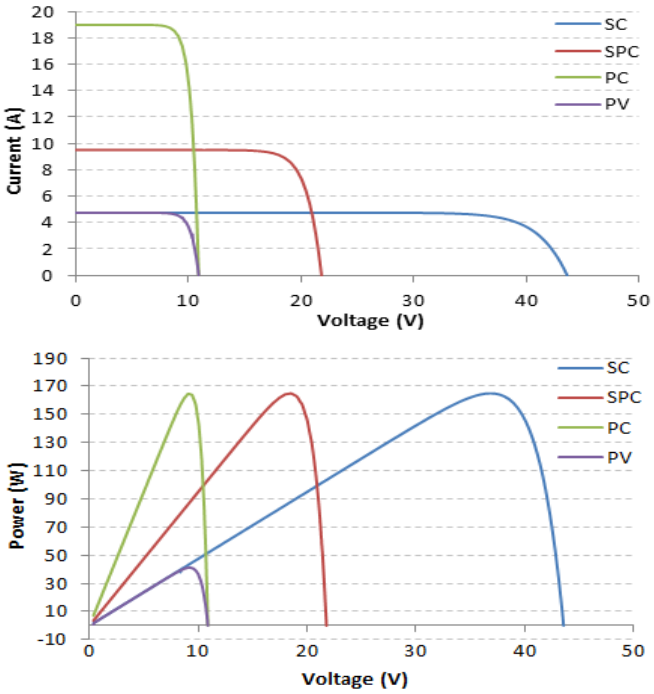

Fig. 2. Characteristic curves I-V and P-V of various configurations in identical operating conditions

B. Under Partial Shading Conditions

In normal operating environment, a PV plant is subject to radiative changes on modules due to PSC. Consequently, the power generation capacity of each PV module changes depending on the active surface temperature and solar radiation. This leads to a loss of synchronization in current, voltage and output power (Figure 3). It is also the cause of changing the shape of the overall characteristic curves, introducing multiple MPPTs, making it difficult to accurately determine the GMPPT.

The analysis shows that although PC configuration produces the fewest maximum values, which facilitates a smoother GMPPT process, low output voltage makes it difficult to design large power DC/DC circuits. Furthermore, this type of connection has a large output current that requires more system control keys. This leads to significant power loss on PV system with PC configuration. The SPC diagram consists of many series connected arrays, wired together in parallel.

Therefore, its number of maximum values is equivalent to the number of extremes produced by a series connection with the same number of modules. In this topology, the system output voltage is equal to the voltage across the series connected PV arrays, while the output current is equal to the sum of the currents through each series. As a result, SPC's output current always lies in between the two basic types of connection configurations analyzed above.

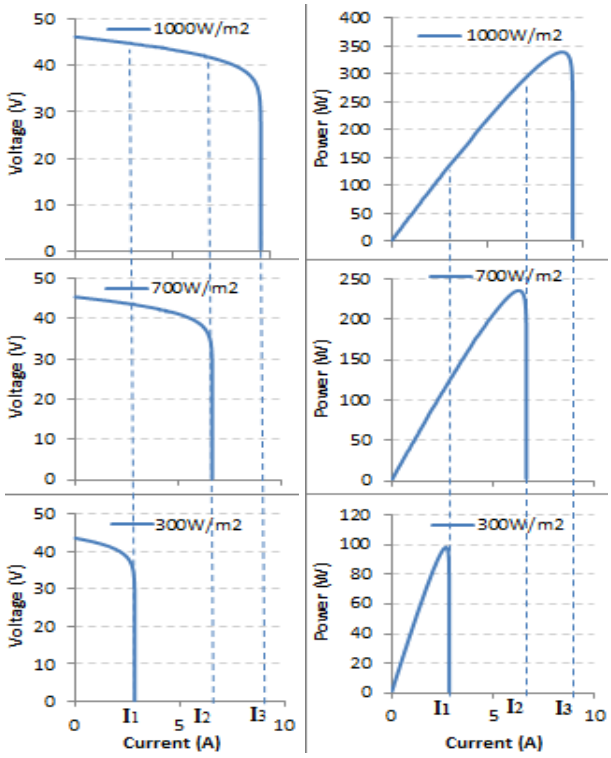

Fig. 3. Characteristic curves V-I, P-I as solar radiation levels vary

On the other hand, SC configuration offers large output voltage and small current, facilitating an easier DC-DC circuit designing process. Nevertheless, it creates many MPPTs and power loss when using bypass-diode for protection, which is a disadvantage compared to other types of configurations. In conclusion, the mixed operating environment induces higher number of MPPTs across all types of connection configurations, so simple algorithms are prone to be trapped in LMPPT, compromising the power generation efficiency. In addition, the GMPP tracking speed of classic solutions is also a drawback when operating PV systems under PSC conditions.

Although temperature also affects the characteristic curve of a PV system, the rate of change of temperature is slower than that of shading radiation. The natural shading phenomena occurs quickly, causing the temperature difference on the surface of the modules to occur slowly or change but uniformly. Furthermore, a solution that is fast, robust, and accurate enough in cases of immediate and rapid environmental change will be able to respond to slower changes. Therefore, in this paper, we do not consider the effect of temperature on the power generation capacity of the system.

C. Proposing a New System Design

The above analysis indicates the need of a GMPPT solution to generate high system performance, to accelerate convergence speed, and to ensure reasonable investment cost. Recent GMPPT optimization algorithms are quite effective in all operating conditions. At the same time, these advanced algorithms require many iterations, thus reducing the convergence speed. Consequently, the system faces higher risk to fail to respond when PSC changes rapidly. Moreover, when the radiation level in the system widely varies, the power output of the modules that receive the least radiation level might be excluded from the system output.

Meanwhile, traditional algorithms with simpler designs, are only effective in an identical operating environment, in which, the characteristic curves are equivalent to an independent PV module. Another disadvantage of these algorithms is that they easily fall into the local extreme trap in multi-extreme conditions. As a result, the system performance is reduced, and the convergence time increases. Magnitude of the effect depends on the input of the initialization value I_0 for the algorithm. This problem is explained in detail in Figure 4, assuming there are three serial-connected modules. If starting with a small initial value of I_0 to ensure capturing the power of all PV modules, the maximum power generated by PV modules exposed to highest level of radiation will be ignored. Moreover, with a low initial value, the search time is increased by going through many iteration steps to obtain high performance value. In this case, the enhancement of the convergence speed by expanding the interval between iterations leads to lower MPPT efficiency. Conversely, with a large initial value I_0, the power capacity of the modules receiving less radiation level will be left out. Therefore, both scenarios lead to the possibility of large power loss and compromised system efficiency.

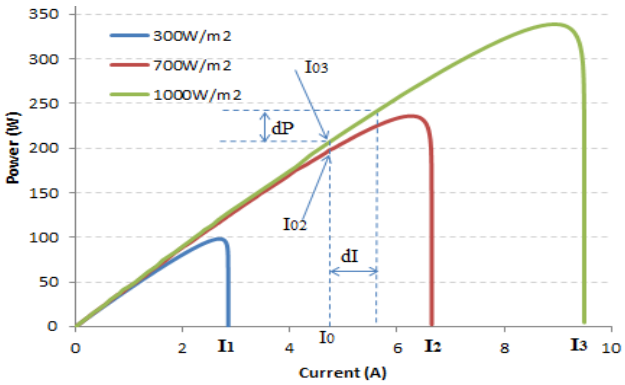

Fig. 4. Characteristic curve P-I of a PV module PV under various conditions

TABLE I. LIST OF SIMULATION CASES

No.	Radiation level/module (%)			P_{Total}, (W)
	PV_1	PV_2	PV_3	
1	100	40	20	521.632
2	200	500	800	488.758
3	750	600	400	572.205
4	500	1000	250	571.701
5	600	500	400	488.398
6	200	800	1000	655.681
7	750	400	200	438.516
8	800	1000	500	755.806
9	750	800	1000	839.613
10	1000	250	200	471.576
11	800	500	400	555.335

The above analysis shows that to increase convergence speed and GMPPT algorithm efficiency, it is required to simplify the characteristic curves to a minimal form so that it produces one extreme under all operating conditions, which allows the search algorithm to perform in the environment with one extreme available. To facilitate this target, we proposed a multistage DC/DC structure. The diagram of this structure is illustrated in Figure 5, and 11 scenarios as shown in Table I. The values of inductor L and capacitor C used in the paper are selected so that the output power of the system is stable and has the highest efficiency. That is, the values of L and C depend on the acceptable

values of the current and voltage ripples respectively. If small ripple is selected, the output values are stable but the efficiency is low, if high efficiency is selected, the ripple is large and the output values are unstable. Therefore, the selection of parameters for the circuit is calculated according to the condition [2, 14] with ripple values of current and voltage of 0.3% and 1% respectively. Subsequently, an improved MPPT algorithm is also proposed to support this connection configuration.

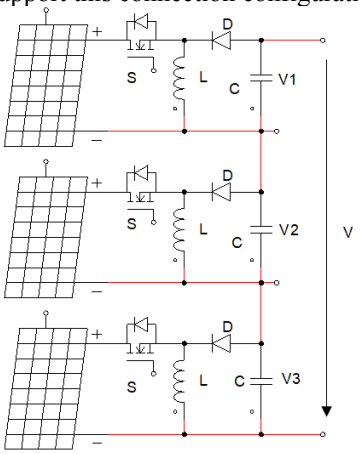

Fig. 5. Connection configuration of DC-DC converter

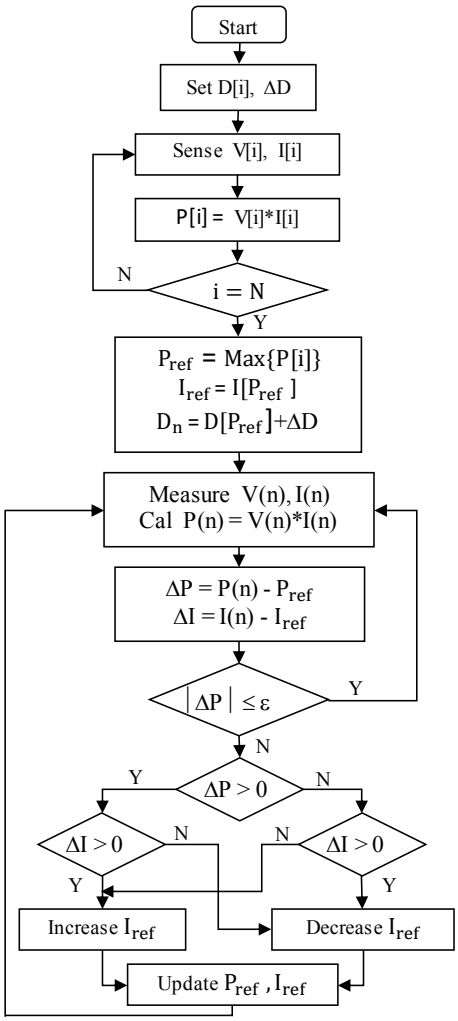

Fig. 6. Proposed algorithm flowchart

From the proposed solution, it can be seen that: the current parameter is used because it is more stable than electricity when the radiation changes. The current value is adjusted through an increment of the energizing ratio ΔD. This helps to increase convergence speed and MPPT performance. Furthermore, the use of a multistage DC-DC converter will reduce the number of extremes to the problem of the proposed solution because it is the cause of power loss if trapped in the LMPP value. The proposed solution is simulated in PSIM software with PV system with parameters as shown in Table II.

TABLE II. PARAMETERS OF A PV MODULE

HT Solar type HTM330PA-72 (STC 1000W/m^2; 20^{o}C)	
Module type	HTM330PA-72
Rated maximum power	330W
Voltage at Pmax (Vmp)	37.52V
Current at Pmax (Imp)	8.80A
Open-circuit Voltage (Voc)	45.95V
Short-curcuit Crrrent (Isc)	9.29A
Normal Operating Cell Tempeerature (NOCT)	45±2^{o}C

The proposed algorithm presented in Figure 6 consists of two components:

- The first component aims to limit the scope of search by determining the optimal initial value for the system:

• Step 1: check the points on the I-P curve. By setting the energy ratio D[i] randomly in the search range, the corresponding output power value will be determined by two factors V[i] and I[i]. The number of D[i] in this paper is set up as 4, corresponding to 4 output power values. This output value serves as the basis for the next step.

• Step 2: define the scope of search for MPPT. Once step 1 has generated an adequate number of samples P[i], comparing the values of these samples to pick out the maximum output power value. This maximum output power value then serves as the reference power for the next loop. This approach helps reducing the number of iterations required in comparison to the traditional approach to set this input value from 0. Additionally, the current value and its energy ratio are also selected as the reference and initialization values for the next loop. Each iteration step is incrementally adjusted by a corresponding amount of ΔD.

- Component 2 - Principles for determining GMPPT:

• Step 3: determine power deviation ΔP and current deviation ΔI. MPPT controller will measure the values V(n), I(n), and then calculate the error of power and current compared to the reference value in the previous step.

• Step 4: check the convergence results of the algorithm. If the power error is less than a predefined range, the algorithm does not change the reference value in the following steps. On the contrary, if the error is significant, an adjustment check will be conducted following the principle as below:

- If ΔP.ΔI > 0 then increase value of reference current I_{ref}.
- If ΔP.ΔI < 0 then decrease value of reference current I_{ref}.

After the adjustment check, new reference current value will be updated and be carried on for calculation in subsequent iteration rounds.

III. RESULTS AND DISCUSSIONS

To test the effectiveness of the proposed solution, the PV system was set up in three different configurations and operated under the conditions specified in Table I, including:

i) PV modules independently affect the process of identifying maximum output power the system could provide (P_{total})

ii) PV cells are wired in series connection, attached with bypass-diode for protection of performance in PSC (P_{SC});

iii) Set up PV module's connection according to recommended configuration to determine systemic MPPT (P_{mppt}).

iv) Serial connection configuration with bypass-diode, while utilizing the improved PSO algorithm introduced in previous research.

When simulated in a PSIM environment, the proposed solution is set up as being illustrated in Figure 7.

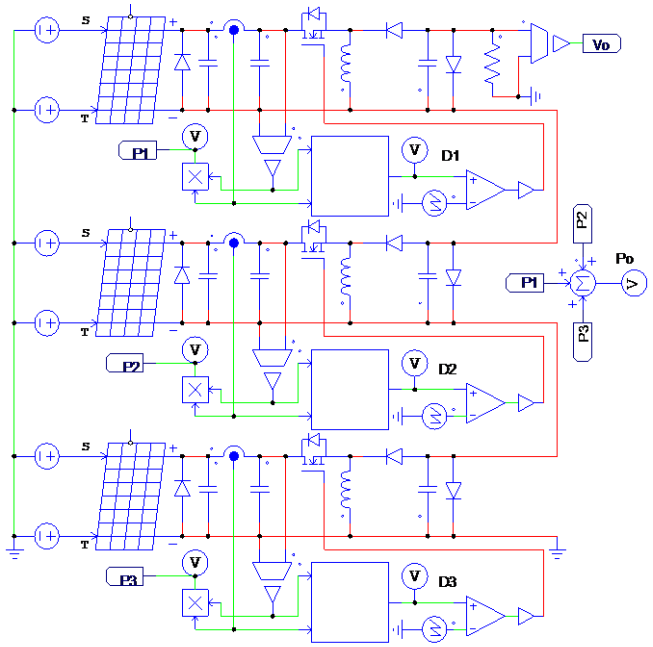

Fig. 7. Configuration structure in PSIM

Table III presents the output power values obtained via simulating the above connection configurations in standard conditions of 20^0C and 1.5atm. It also summarizes the MPPT speed and performance parameters of the solutions under specific circumstances. It is worth noting that the test results are robust and consistent, demonstrating outstanding GMPPT performance with remarkable speed across scenarios. In extreme cases involving large radiation difference (scenario 4, 7 and 10), the GMPPT point deviates towards the beginning or end of the curve – a position where the DC-DC converter is prone to under- or over-range. Nevertheless, test results show that GMPPT performance are robust. Figure 8 illustrate the GMPPT speed and performance for scenario 1.

TABLE III. OUTPUT POWER RECORED IN VARIOUS SCENARIOS

No	Power (W)		Efficiency rate (%)		Speed (s)
	P_{SC}	P_{mppt}	η_{SC}	η_{mppt}	
1	328.093	518.152	62.90	99.33	0.0058
2	351.627	481.643	71.94	98.54	0.0074
3	433.507	558.900	75.76	97.67	0.0063
4	356.518	527.774	62.36	92.32	0.0052
5	423.859	481.096	86.79	98.50	0.0067
6	555.347	637.982	84.70	97.30	0.0151
7	282.208	431.899	64.36	98.49	0.0067
8	555.347	755.805	73.48	100.00	0.0067
9	785.362	839.214	93.54	99.95	0.0141
10	328.093	428.655	69.57	90.90	0.0051
11	429.922	550.025	77.42	99.04	0.0065

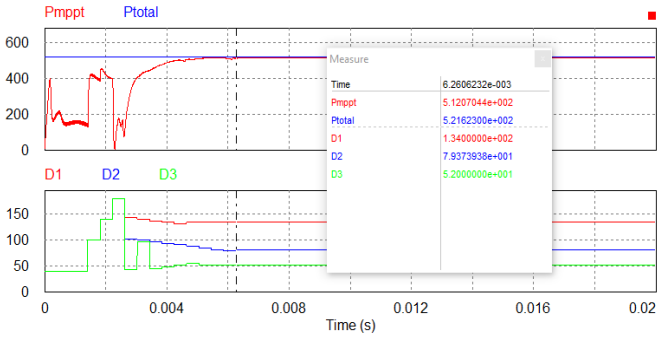

Fig. 8. Output results for scenario 1

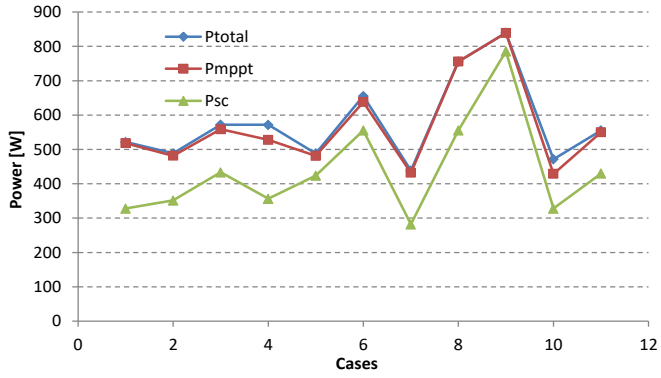

Fig. 9. Comparing the performance of GMPPT

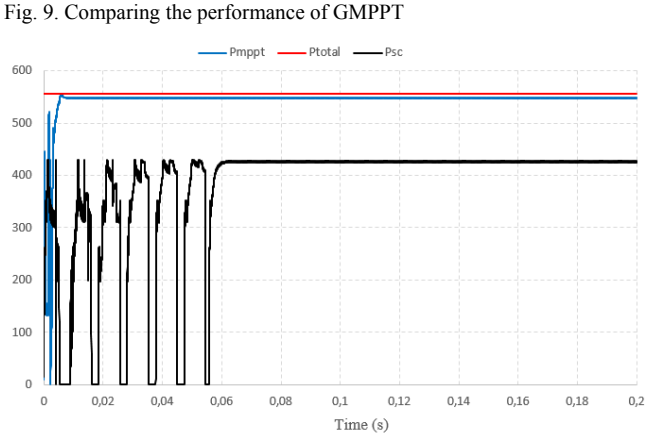

Fig. 10. Compare the speed and MPPT performance of the proposed algorithm with the PSO method (scenario 11)

In addition, the proposed solution also allows for customizing the initial values of the energy ratio D for each module when the level of radiation exposed to the module varies. Figure 9 compares the GMPPT performance of the proposed solution against the bypass-diode serial configuration across all tested scenarios. The solution displays higher efficiency with much smaller power loss than the traditional method. Test results highlights that:

- The GMPPT efficiency of the proposed solution can reach 100% and is always above 90% in all simulation cases. Although scenarios with larger radiation difference (case 4 and case 10) makes it difficult for the modules that receive the least solar radiation level to power the system, it proves to be much more efficient than the traditional method under the same conditions.

- Convergence speed is also an advantage of the solution as most cases show that MPPT tracking period takes only a few milliseconds. As being seen in Figure 8, by comparing the initial D values to find the most potential location, the number of unnecessary iterations is substantially cut down, which fasten the convergence speed. Figure 8 also points out that it only takes up to 10 iterations to find the optimal position for the whole system.
- Figure 8 also illustrates the possibility to choose different initial values for modules with different solar radiance levels. This significantly reduces the search time required compared to the traditional method when all modules are pegged to a fixed reference value. Problems that cause system power loss due to some modules with less radiation exposure is not addressed in this paper.
- Figure 9 clearly showcases the outstanding GMPPT performance of the proposed solution, ensuring accuracy of the search as well as efficiency compared to traditional diode-bypass solutions.
- Figure 10 reflects the comparison between MPPT performance of the proposed solution and the improved PSO algorithm in one of our previous studies. Under the same operating conditions, the improved PSO only reached 0.06s speed, compared to 0.006s convergence speed of scenario 11. Indeed, the new algorithm proposed in this paper displays a significant convergence speed improvement.

In summary, the solution proposed in this paper is: using the current value as a control parameter to stabilize the output and increase the convergence speed. Another advantage compared to previous studies is that the system's GMPPT is referred to as the MPPT of each module. This leaves no system: if partially shaded it does not ignore the modules that receive the least power. Thereby contributing to reducing power loss and increasing the efficiency of power production of the solar panel system.

IV. CONCLUSION

The paper proposed a two-stage GMPPT solution including: limiting the search range and improving the traditional MPPT method to improve the performance and convergence speed of GMPPT algorithm. The obtained results have proven that the new solution can achieve 100% efficiency with the fastest delivery time of 0.0051s. Simulated results also show that, just by limiting the exact search scope, without resourcing to complicated algorithms, it is possible to improve the power generation efficiency of the system at a reasonable cost.

Furthermore, simulation results show the outstanding advantages of the solution compared to traditional approach using bypass-diode. It not only helps to improve the efficiency of solar power generation but also reduces operating costs, owing to its simple structure and reliable operation across various changes of environmental conditions. This is a reliable MPPT improvement solution that supports a stable and effective operation of PV systems under partial shading conditions.

ACKNOWLEDGMENT

The authors specially thank the HaNoi University of Industry for providing fund and creating favor in data collection during the implementation of the study.

REFERENCES

[1] Nguyen Duc Minh, Trinh Trong Chuong, Bui Van Huy, Quach Duc Cuong and Bui Dinh Thanh, Research and design of inverter applied in solar PV systems connected to Distribution Grid. Journal of Electrical Engineering. Vol 7, No 1, Jan.-Feb. 2019 (Serial Number 26).

[2] Nguyen Duc Minh, Do Nhu Y, Trinh Trong Chuong, Development of algorithm to indentify the global optimized piont of solar Photovoltaics panel under the Condition of non-uniform solar array on the surcafe. Journal of Science and Technology, Vol. 56, No. 6 (Dec. 2020).

[3] M. Sacli, O. Ayan, M. Silsupur, B. Empre turkay, Investigation of Power Quality Analysis of Single-Phase Inverter Topologies for Solar Energy Systems. International Conference on Condition Monitoring, Diagnosis and Maintenance. Bucharest, Romania, Sept. 2017.

[4] [4]. R. Ramaprabha and B. L. Mathur, A Comprehensive Review and Analysis of Solar Photovoltaic Array Configurations under Partial Shaded Conditions, International Journal of Photoenergy, Volume 2012, Article ID 120214, doi:10.1155/2012/122014.

[5] F. Belhachat and C. Larbes, Modeling, analysis and comparison of solar photovoltaic array configurations under partial shading conditions, Solar Energy 120 (2015) 399–418.

[6] Koray Sener Parlak, PV array reconfiguration method under partial shading conditions, Electrical Power and Energy Systems 63 (2014) 713–721.

[7] Villa et al., Maximizing the power output of partially shaded photovoltaic plants through optimization, Journal of Photovoltaics, Vol. 2, No. 2, April 2012, 154 – 163.

[8] Bidram et al., Control and circuit techniques to mitigate partial shading effects in photovoltaic arrays, Journal of Photovoltaics, Vol. 2, No. 4, October 2012, 532 – 546.

[9] Moein Jazayeri et al, A Comparative Study on Different Photovoltaic Array Topologies under Partial Shading Conditions, Conference: T&D Conference and Exposition, 2014 IEEE PES At: Chicago, IL, USA

[10] M. Z. Shams El-Dein et al., Optimal Photovoltaic Array Reconfiguration to Reduce Partial Shading Losses, EEE Trans. on Sustainable Energy, Vol: 4, Issue: 1, Jan. 2013, 145 – 153.

[11] M. Z. Shams El-Dein et al, Novel Configurations for Photovoltaic Farms to Reduce Partial Shading Losses, 978-1-4577-1002-5/11.

[12] Yaw-Juen Wang and Po-Chun Hsu, An investigation on partial shading of PV modules with different connection configurations of PV cells, Energy 36 (2011) 3069-3078.

[13] H. V. Bui, V. A. Truong, T. H. Quach, Optimizing the maximum power generation point of PV cells under shading conditions, Journal of Science and Technology Development, 3(1) (2020): 326-338.

[14] X. T. Luong, V. H. Bui, D. T. Do, T. H. Quach and V. A. Truong, "An Improvement of Maximum Power Point Tracking Algorithm Based on Particle Swarm Optimization Method for Photovoltaic System," 2020 5th International Conference on Green Technology and Sustainable Development, HCM City, Vietnam, 2020, pp. 53-58, doi: 10.1109/GTSD50082.2020.9303110.

Bài số 9:

Bui Van Hien, Truong Viet Anh, Nguyen Duc Minh, Trinh Trong Chuong, Y Do Nhu, Trieu Viet Phuong, *"Module Integrated Converters and Independent MPPT Technique"* International Conference on Engineering Research and Applications, 2022, 685-698, https://doi.org/10.1007/978-3-031-22200-9_73

Module Integrated Converters and Independent MPPT Technique

Bui Van Hien[1], Truong Viet Anh[2], Nguyen Duc Minh[3], Trinh Trong Chuong[4(✉)], Y. Do Nhu[5], and Trieu Viet Phuong[6]

[1] Faculty of Mechanical—Electrical and Computer Engineering, School of Engineering and Technology, Van Lang University, Ho Chi Minh City, Vietnam
[2] Faculty of Electronics and Electrical, HCMC University of Technology and Education, Ho Chi Minh City, Vietnam
[3] Institute of Energy Science, Vietnam Academy of Science and Technology, Hanoi, Vietnam
[4] Faculty of Electrical Engineering, Hanoi University of Industry, Hanoi, Vietnam
chuonghtd@haui.edu.vn
[5] Faculty of Electro—Mechanics, Hanoi University of Mining and Geology, Hanoi, Vietnam
[6] Vietnam Standards and Quality Institute, Hanoi, Vietnam

Abstract. As the irradiance changes, the current at the maximum power generating point (MPP) of the photovoltaic (PV) cell system fluctuates. But when the temperature changes, its voltage is affected more. In actual conditions when operating in a partial shade (PSC) condition, fluctuation of these two parameters makes it difficult to determine the global maximum power point tracking (GMPPT) accurately. The compatibility between the PV system topology and the algorithm plays an important role in improving the performance of the whole system. This paper proposes a PV module architecture combined with inverters and a standalone MPPT technique operating under non-uniform temperature and radiation conditions. A modified P and O algorithm with multiple inrush current values as an input parameter is simulated in the PSC. The research results in this paper have shown that the proposed solution not only has outstanding speed but also has the ability to significantly improve performance compared to published methods under the same operating conditions.

Keywords: Partial shade · Photovoltaic (PV) · P–V characteristics · Integrated inverter module · Standalone MPPT

Abbreviations

PV	Photovoltaic
SC	Serial Configuration
PC	Parallel Configuration
SPC	Serial–Parallel Configuration
PSC	Partial Shading Conditions

D. C. Nguyen et al. (Eds.): ICERA 2022, LNNS 602, pp. 685–698, 2023.
https://doi.org/10.1007/978-3-031-22200-9_73

GMPPT Global Maximum Power Point Tracking
LMPPT Local Maximum Power Point Tracking
MPPT Maximum PowerPoint Tracking
PSO Particle Swarm Optimization

1 Introduction

This paper is an extension of the work presented at the International Conference on Smart power and internet energy systems [1]. Which has been rated to deliver outstanding performance in non-uniform operating conditions compared to several recently proposed solutions. Its outstanding advantage is that it does not produce many extremes in PV strings under all working conditions. From there, it is easy to choose the MPPT solution to achieve the highest efficiency with significantly improved speed. This is also the main reason to improve the performance of PV systems in series strings. Practice shows that Series Connection (SC) gives us an advantage in voltage but limits current. Which causes the entire PV series to operate the same current value even when they receive different radiation levels. This is the main cause leading to the phenomenon of heating, reversing the working state in some positions, and even destroying the entire chain link [2, 3]. In addition, the Parallel Configuration (PC) will give a fairly stable voltage value, producing the least extremes in all operating conditions, but the disadvantage is that the output current value is quite large. It makes it difficult to design and select control keys and has high power losses [4, 5]. Meanwhile, the demand for the installation and use of grid-tied solar power systems is growing rapidly [6–8]. In order to achieve applied power values in these cases requires PV systems sufficient to generate the appropriate voltage and current.

Several publications have proposed PV interconnection configurations to improve efficiency, increase convergence speed, reduce costs and reduce losses under all operating conditions. However, most of them are still based on two basic types of links, SC and PC. Among them, the most widely used type is Serial–Parallel Configuration (SPC). Here, PV modules are linked together in series to achieve the desired voltage value. Then, the strings are connected in parallel to form an array to increase the system current [9]. In actual operation, when the radiation changes, the surface temperature of the PVs also fluctuates. It is one of two factors that make it difficult to GMPPT, which has not been mentioned in [1].

In this paper, a system of 3×3 PV modules linked in series–parallel configuration is proposed. It is operated not only under varying radiation conditions but also with varying operating temperatures. In which, shading patterns at all different positions are tested in PSIM platform. Simultaneous PSC scenarios are operated with the bypass-diode method and an improved optimization algorithm under the same operating conditions [10, 11]. The simulation results are compared with some of the most recently proposed methods [12, 16–19].

2 Environmental Influence on PV Properties

2.1 Photovoltaics

The model for each photovoltaic cell that can be found in [13] includes a light-controlled current source in parallel with a diode. A resistor in parallel has a fairly large value (R_p) and a resistor in series (R_s) has negligible resistance. The relationship between the output current and the voltage of the PV cell is shown by Eq. (1).

$$I = I_{SC} - I_0\left\{e^{\frac{q(V+I.R_s)}{kT}} - 1\right\} - \frac{V + I.R_s}{R_p} \tag{1}$$

A PV system includes a plurality of cells interconnected to achieve a desired voltage and current. At that, the output current of a system of N_s module in a sequence and N_p parallel sequences is presented in Eq. (2).

$$I = N_p I_{SC} - N_p I_0\left\{e^{\frac{q(V+N_s IR_s)}{N_s kT}} - 1\right\} - \frac{V + N_s IR_s}{N_s R_s} \tag{2}$$

2.2 Effect of Operating Conditions

PV plants spread over a fairly large area are often operated in a heterogeneous situation due to PSC. This is the cause of changing the shape of the overall characteristic curves, causing the appearance of many MPPs in the strings, making it difficult to accurately determine the GMPP. Figure 1 presents the P–V curve of the system under two different operating conditions.

Even if the working condition is uniform whole system, it is not possible to assure stability throughout the operation period. Published studies have shown that when irradiance varies—often below standard conditions, the MPP coordinates are greatly affected by fluctuations in the current. Meanwhile, if the surface temperature changes—usually higher than the standard condition temperature, then the voltage parameter will have more impact on the stability of the MPP (Fig. 2) [14, 15].

Under real conditions, when the radiation increases, the temperature also increases and vice versa. This causes the MPP coordinates to fluctuate and is affected by both current and voltage parameters. Moreover, when these two parameters change heterogeneously, it will be more difficult to determine the GMPP among many extremes. It can be explained in detail from Fig. 1 that if only the irradiance is fluctuating, then the GMPP will be equivalent to the MPP3 point. However, as the radiation on a module increases, so does its surface temperature. This makes the power increase undesirable and leads to a change in the structure of the curve. If the temperature fluctuations are more than the radiation then it is likely that the GMPP will move to the MPP2 position. It shows that the GMPPT in real conditions is much more complicated.

2.3 Proposed Solution

Operating conditions greatly affect the performance, speed and accuracy of MPPT solutions. To solve this problem, a system of 3 modules with three different irradiance levels is proposed. Their P–I characteristic curves are presented in Fig. 3.

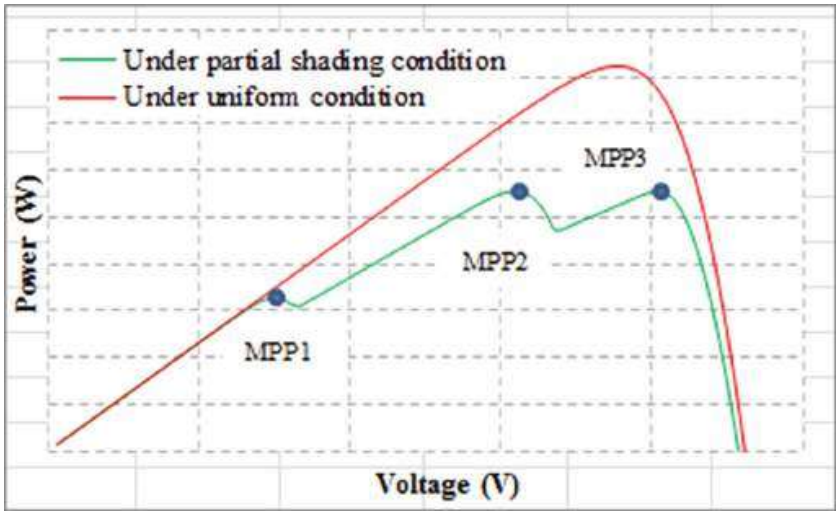

Fig. 1. P–V characteristics under operating conditions

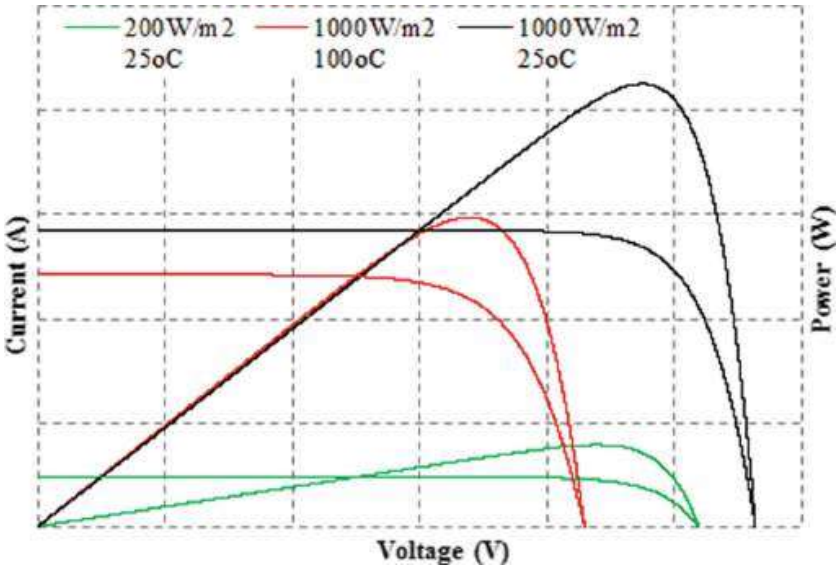

Fig. 2. Effect of radiation and temperature on the P–V and I–V curves

If the start current value I_0 is the same as the current position (Fig. 3), it means that only the two modules receiving the higher radiation are capable of emitting power. The module that receives the least energy will be ignored, so the performance is reduced. Moreover, at this boot site, the I_{03} series is quite far from its MPP so it takes a long time to converge. If the start value $I_0 > I_2$ is selected to increase the speed for the largest module in this case, the two modules corresponding to lines I_1 and I_2 will be ignored.

Conversely, if you want to obtain the full power of all three modules, the starting value $I_0 < I_1$. But with a low boot value will increase the system's MPPT search time. If the step size is increased to overcome this disadvantage, the system performance is reduced again.

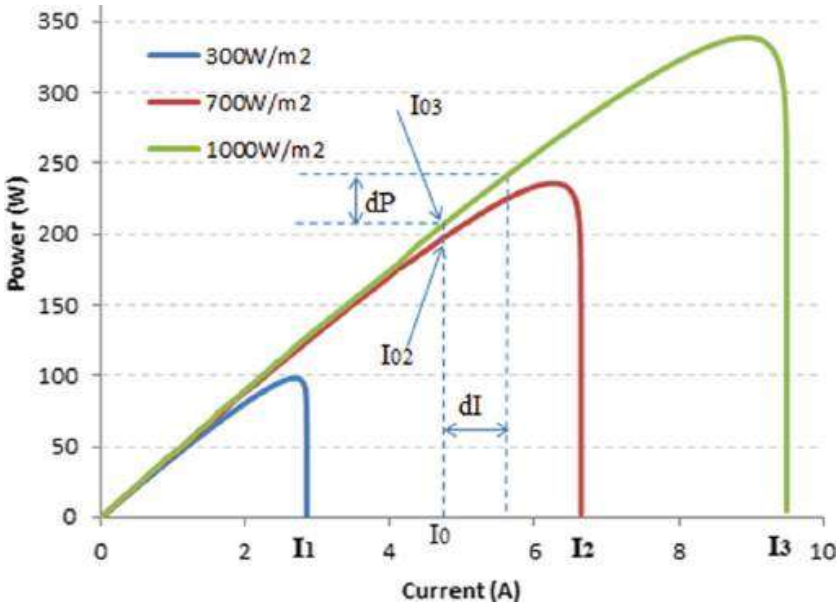

Fig. 3. P–I characteristics of PV module under different conditions

To resolve this difficulty, the article proposes a standalone MPPT solution for modules that simultaneously use multiple boot values at the same time in order to find the optimal value for each module and increase convergence speed. The structure of the proposed solution is presented in Figs. 4 and 5.

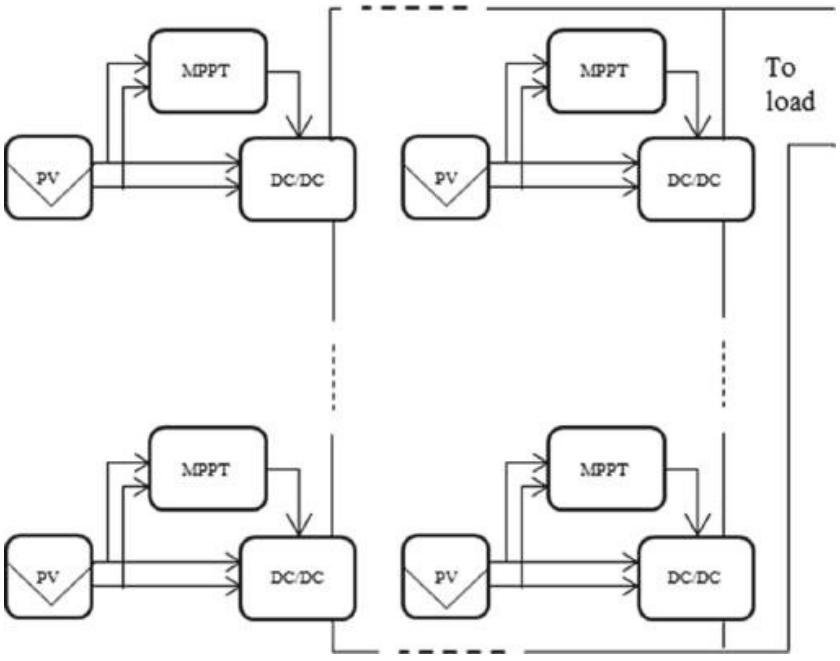

Fig. 4. Proposed solution structure

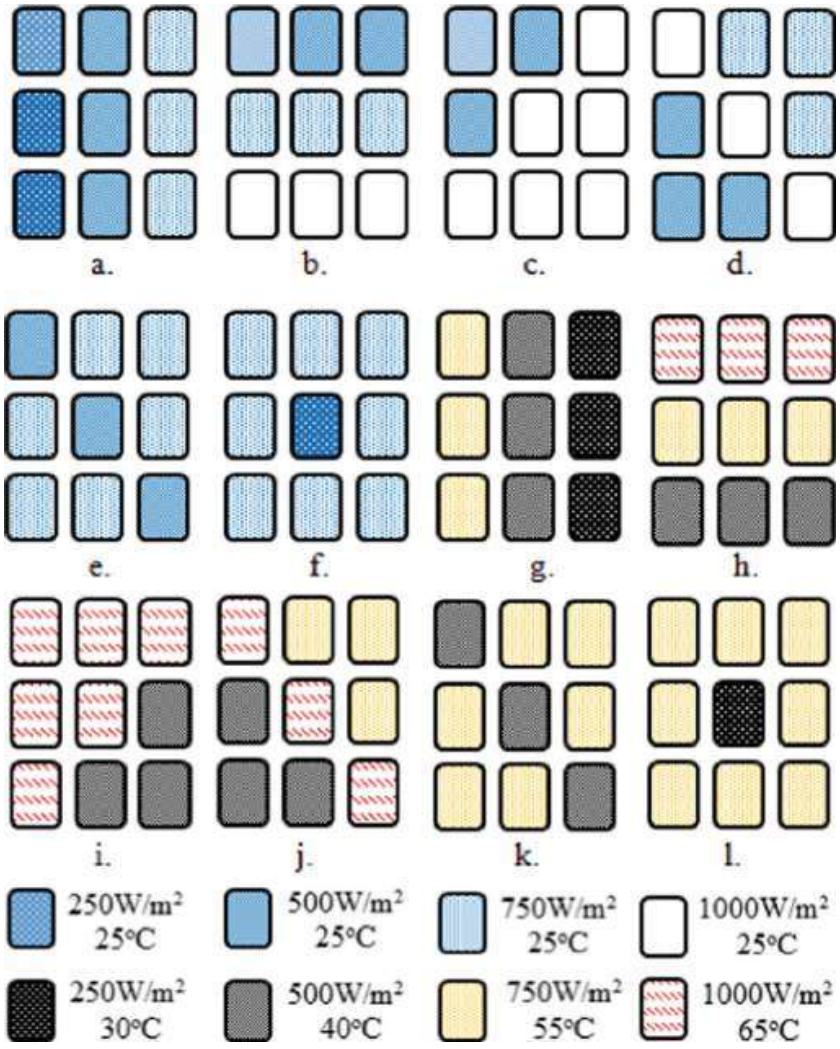

Fig. 5. Simulated shading states

The proposed solution consists of two parts; the first is to limit the search range through initialization values. Then there is the basic GMPPT part based on traditional P and O algorithm. The proposed solution flowchart shown in Fig. 6 includes the following steps:

- Step 1: Select 4 random D[i] start values in the search range. Thereby, the values of V[i] and I[i] are determined respectively.
- Step 2: define the MPP search scope. Calculate the power P[i] corresponding to the values D[i] in step 1. Select the largest value among the P[i] to be the reference value for the next iteration. The values D, V and I corresponding to this power level are also selected as reference values and initialized for the MPPT solution when changing a number of ΔD increments.
- Step 3: determine power deviation ΔP and current ΔI. The MPPT unit will measure the current and voltage values to calculate the power and current after having changed a quantity ΔD. Then calculate the power and current error compared to the reference value in step 2.

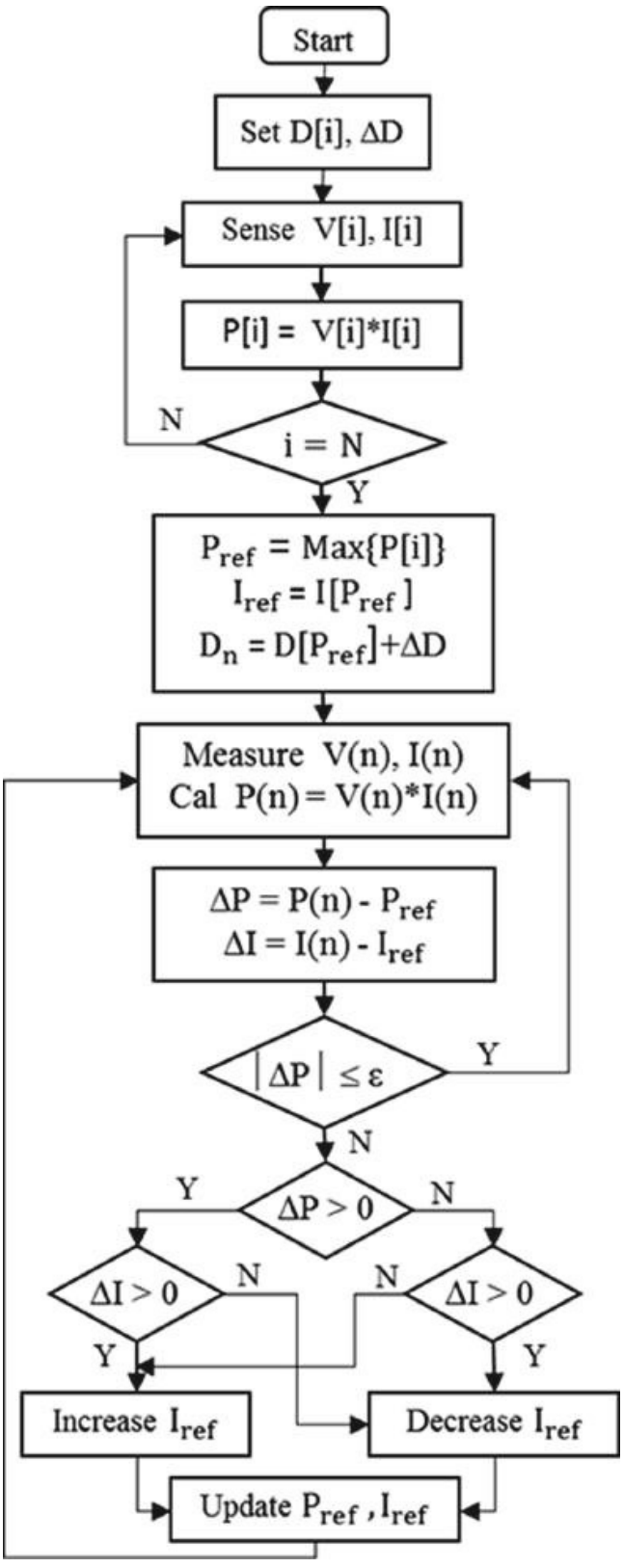

Fig. 6. Flowchart of the proposed algorithm

- Step 4: check the convergence of the algorithm. The solution is considered convergent when $P < \varepsilon$. Conversely, the reference current value will be adjusted via parameter adjustment D as follows.
- If $\Delta P.\Delta I > 0$, then increase the reference current value Iref.
- If $\Delta P.\Delta I < 0$, then reduce the reference current value I_{ref}.

Repeat the loops from step 3.

3 Results and Discussion

The proposed solution is tested on a configuration of 3×3 modules of type HTM330PA-72 (Fig. 4) with the following parameters: $I_{sc} = 9.29$ A, $V_{oc} = 46.15$ V, $I_{mpp} = 8.69$ A, $V_{mpp} = 37.89$ V. Shading states are listed in Fig. 5 from left to right and from top to bottom: column shading, row shading, corner shading, double corner shading, diagonal shading, and center shading. The first six cases only change irradiance when partially shaded. The scenario is repeated in the following cases but both radiation and temperature parameters are changed. With the performance shown in our previous study. Simulation states that will be performed on different structures to compare results include:

(i) Use bypass-diode for protection in cases of partial shade (PSC).
(ii) Use the proposed configuration to MPPT the system (P_{MPPT}).
(iii) Using bypass-diode and combined with the improved PSO algorithm in the proposed study introduced previously.

Table 1 presents the MPPT results when simulating the proposed configuration compared with the traditional method in the above cases. The obtained results show that in all working conditions, the proposed solution always proves to be capable of significantly improving power generation efficiency. Specifically, in the case of row shading (No. 2), it was possible to increase the efficiency by more than 28% compared to the traditional method. This can be explained as when shading in rows, the operating conditions of the modules in a chain will be different, so there are many extremes. Which directly affects the ability to generate electricity in the chain as well as the whole system. Likewise, in the case of variations in both irradiance and temperature in rows (No. 8), the performance improvement is also quite impressive.

This result is confirmed again when the improved performance of the diagonal shading case (No. 5 and No. 11) is 21.51% and 20.21%, respectively. This advantage has also been demonstrated in our previous study when considering SC in PSC. Meanwhile, the column shading cases (No. 1 and No. 7) have insignificant performance improvement. The cause of this result is that when shading in columns, the operating conditions of the modules in a series are identical, so both solutions can easily approach MPP equally. In addition, the data in Table 1 also shows that the convergence speed of the proposed solution is quite impressive at the fastest level of 0.006 s. The more complicated cases make the search time last in the range of 0.024 s (No. 11).

When comparing the performance of the proposed solution compared with the improved PSO method, the results obtained in Fig. 7 show that: when the operating

Table 1. MPPT results in cases

No	Power (W)		$\Delta P = \frac{P_{mppt} - P_{sc}}{P_{sc}} \times 100\%$	Speed (s)
	P_{sc}	Prompt		
1	1440.55	1441.45	00.06	0.008
2	1624.66	2083.26	28.23	0.007
3	2028.78	2275.44	12.16	0.013
4	1815.50	2144.42	18.12	0.013
5	1590.23	1932.29	21.51	0.007
6	1997.45	2022.41	01.25	0.006
7	1316.35	1317.21	00.07	0.008
8	1461.94	1795.49	22.82	0.020
9	1747.38	1993.17	14.07	0.020
10	1629.55	1787.99	09.72	0.023
11	1469.59	1766.54	20.21	0.024
12	1546.45	1774.34	14.74	0.006

conditions on each series are homogeneous (shading in columns), the solutions are quite different. The similarity in MPPT performance. They differ only in the speed of convergence. With three different strings, the proposed solution gives three representative results about the value of D. In the first group (column 1) the most shaded also corresponds to the longest search time ($D_1 = D_2 = D_3$) is 0.006 s. Meanwhile, the group that received the highest radiation (column 3) had the fastest convergence rate ($D_7 = D_8 = D_9$). With the same operating conditions, the solution using PSO shows that it takes more time to converge at 0.036 s.

In another scenario, when the operating conditions are more complex (No. 11), the results of comparing the MPPT capabilities of the solutions shown in Fig. 8 show that the proposed solution not only has convergence speed. Outstanding but also has quite impressive power generation efficiency. Its performance improvement over the traditional method is up to 20.21%. Although the energization ratio D stops at 0.008 s and the output stabilizes later at 0.024 s, it is still far ahead of the PSO solution when it converges at 0.037 s. In this case, the proposed solution has only two representative D values because this diagonal shading produces two extrema at each series. The values $D_1 = D_5 = D_{12}$, and the rest are equal to D_6.

When changing operating conditions continuously during the simulation, the results obtained in Figs. 9, 10 and 11 show that: the proposed solution always gives the performance greater than or equal to the other method. Its response speed is about 0.01 s on average, which is also a prominent advantage compared to 0.38 s for the improved PSO algorithm. Thereby, the proposed solution not only significantly improves the MPPT performance but also increases the convergence speed in the continuously changing and complex PSC.

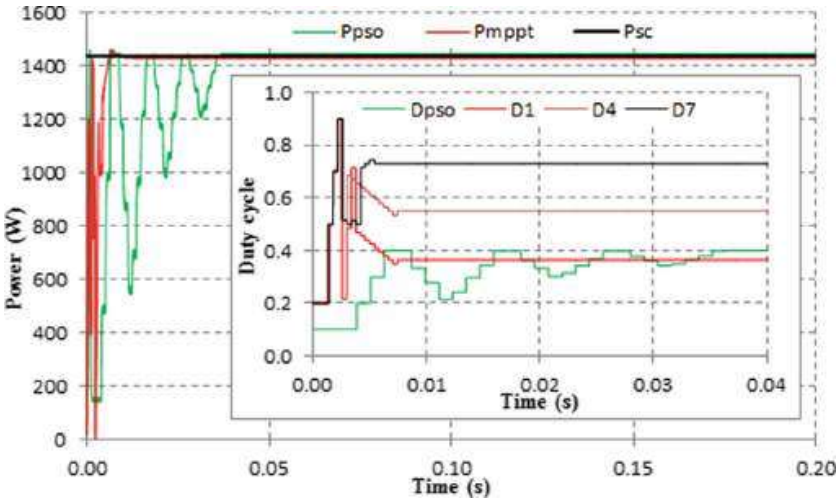

Fig. 7. Comparison of MPPT performance in No. 1

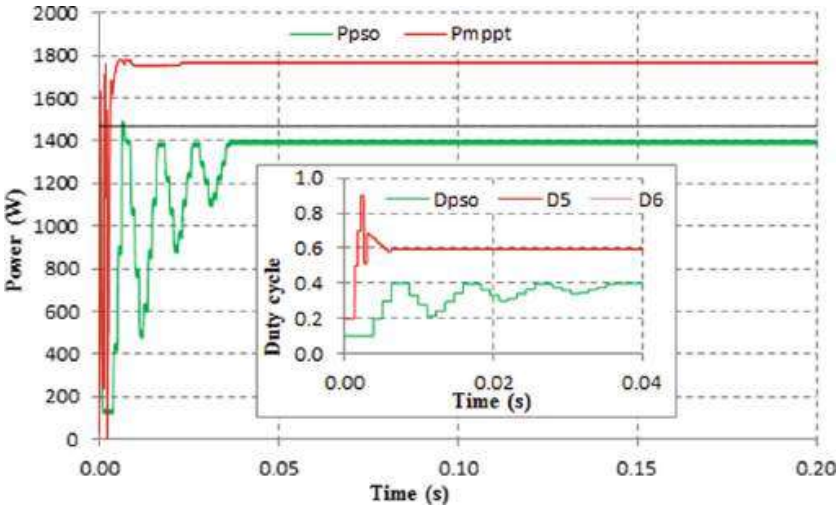

Fig. 8. Comparison of MPPT performance in No. 11

The MPPT efficiency of the solutions for all shading cases is presented in Fig. 12. From the column chart, it can be seen that: the proposed solution has superior power generation ability compared to the previously proposed methods in all operating conditions. Especially this ability is best demonstrated in the cases of shading in rows, corners, and diagonals. Which is 100% efficient in previous research when surveying on a series [1]. Meanwhile, under these conditions, the PSO algorithm proved to be less efficient. When operating conditions are uniform across the series, all solutions have the same power generation efficiency (No. 1 and No. 7) as analyzed above.

In addition, the performance, convergence speed, and convergence speed of the proposed solution are also compared with some optimized algorithms that have been improved recently. The figures shown in Table 2 show outstanding MPPT capability with impressive convergence time.

From the obtained simulation results, it is shown that:

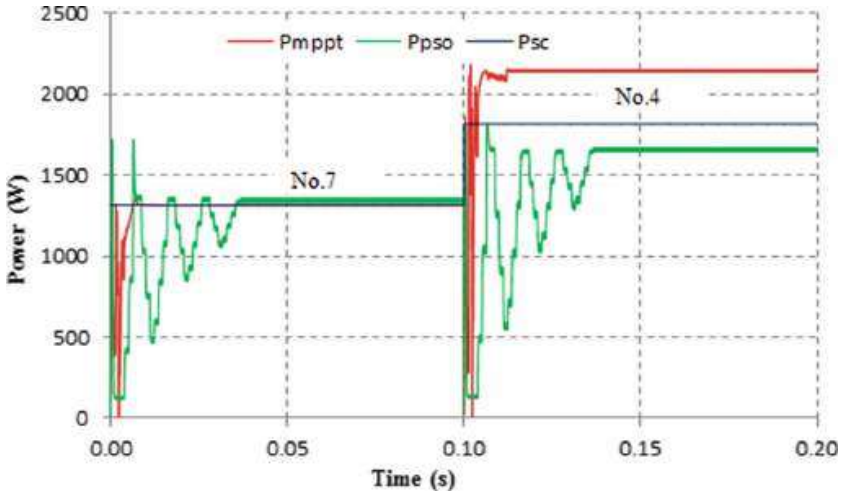

Fig. 9. Comparison of MPPT performance when changing from No. 7 to No. 4

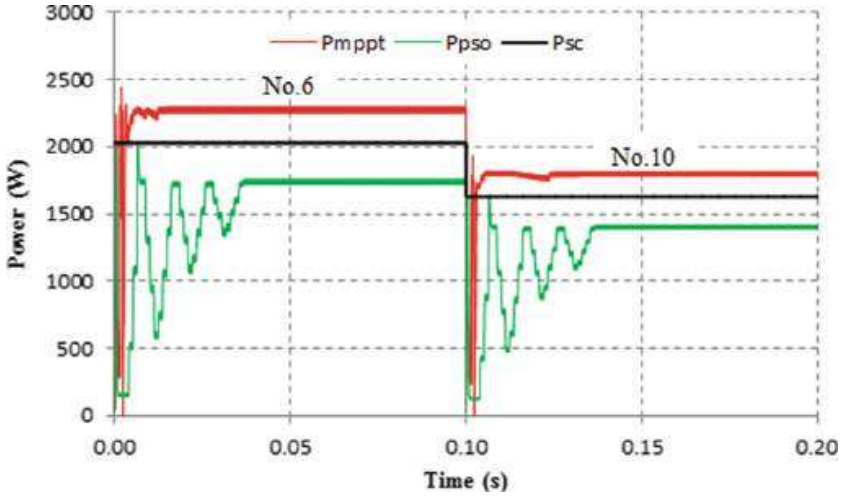

Fig. 10. Comparison of MPPT performance when changing from No. 6 to No. 10

- The GMPPT efficiency of the proposed solution can be improved by over 28% compared to the traditional method. Especially in complex shading states and changing operating conditions, both radiation and temperature parameters.
- Convergence speed is also an advantage of the solution as most cases show that MPPT takes only a few milliseconds. This can be explained from Figs. 7 and 8, that by comparing the initial D values to find the most potential location, the number of unnecessary iterations will be greatly reduced and the convergence speed will be greatly reduced. It also reflects the comparison results between the proposed solution and the improved PSO algorithm in one of our previous studies. Which proved to be quite effective when it reached 0.08 s. But when operating under the same conditions in this study, it only reached 0.036 s compared to 0.006 s (No. 1).

In addition, it also presents the possibility to choose different initialization values for modules with different solar irradiance. This greatly reduces the search time compared

Table 2. Comparison of the proposed solution with some other solutions

Algorithms	Converter type	Speed of tracking (s)	Efficiency (%)	Complexity
Proposed	Buck-boost	0.006	100	Simple
E P and O [12]	Boost	0.12	100	Simple
M INC [16]	Boost	0.05	–	Moderate
I GWO [17]	SEPIC	0.4	100	Complicated
N INC [18]	Boost	0.3	98	Moderate
M ABC [19]	Buck-boost	0.39	99.91	Complicated

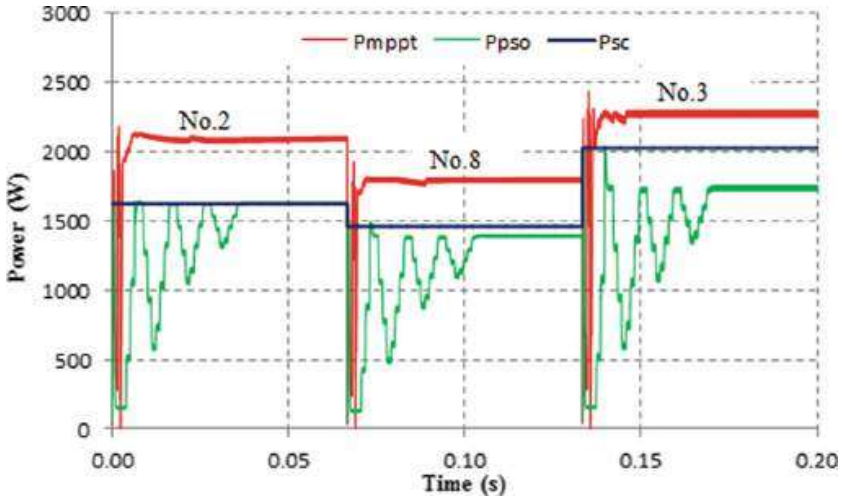

Fig. 11. Comparison of MPPT performance under continuous change

to the traditional method when all are selected for a fixed reference value. Which can cause a drop in system capacity by ignoring the capacity of some modules that receive less power.

4 Conclusion

The paper proposes a standalone GMPPT solution based on the improved traditional MPPT method to enhance the performance and convergence speed. The obtained results proved that the solution can increase the maximum efficiency by 28.23% and achieve the fastest convergence speed of 0.006 s. It also shows that simply by limiting the exact search scope without using complex algorithms, it is still possible to improve the system's power generation efficiency at a reasonable cost.

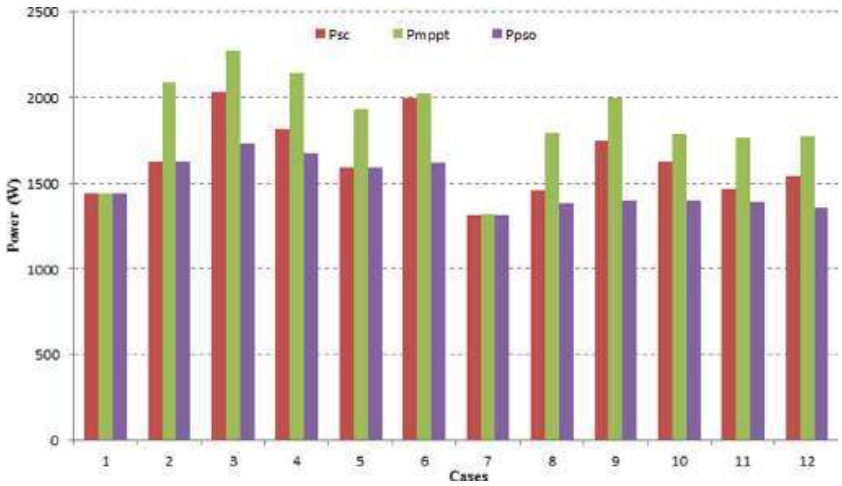

Fig. 12. Comparison of GMPPT performance

The obtained simulation results show the outstanding advantages of the proposed solution compared with some recently published solutions. It helps to improve the efficiency of solar power generation in more realistic conditions when both radiation and temperature parameters are considered. In short, this is a reliable MPPT improvement solution that helps the PV system operate stably and effectively in a non-uniform operating environment.

Acknowledgements. This research is funded by Van Lang University, website: https://www.vanlanguni.edu.vn. The authors would like to show their gratitude to the support from Van Lang University, Ho Chi Minh City University of Technology and Education, Vietnam, which coordinates the research project T2021-64TĐ.

Appendix

I_0—saturation current of the diode (a);
q—charge of the electron (1,602.10–19 C);
k—Boltzman constant (1,381.10–23 J/K);
T—contact layer temperature (K);
I—PV output current (A);
I_{SC}—PV short circuit current (A).

References

1. Chuong, T.T., Minh, N.D., Hien, B.V., Yang, G., Anh, T.V.: Optimizing the performance of the photovoltaic system using the micro DC–DC converter. In: 3rd International Conference on Smart Power and Internet Energy Systems, pp. 392–397 (2021)
2. Ramaprabha, R., Mathur, B.L.: A comprehensive review and analysis of solar photovoltaic array configurations under partial shaded conditions. Int. J. Photoenergy **2012**, 120214 (2012). https://doi.org/10.1155/2012/120214

3. Gao, L., et al.: Parallel—connected solar PV system to address partial and rapidly fluctuating shadow conditions. IEEE Trans. Ind. Electron. **56**(5), (2009)
4. Alik, R., Sutikno, T., Jusoh, A.: A review on perturb and observe maximum power point tracking in photovoltaic system. TELKOMNIKA **13**(3), 745–751 (2015). https://doi.org/10.12928/TELKOMNIKA.v13i3.1439
5. Belhachat, F., Larbes, C.: Modeling, analysis, and comparison of solar photovoltaic array configurations under partial shading conditions. Sol. Energy **120**(2015), 399–418 (2015)
6. Minh, N.D., Chuong, T.T., Huy, B.V., Cuong, Q.D., Thanh, B.D.: Research and design of inverter applied in solar PV systems connected to distribution grid. J. Electr. Eng. **7**(1), (2019) (Serial Number 26)
7. Minh, N.D., Do Nhu Y., Chuong, T.T.: Development of algorithm to identify the global optimized point of solar Photovoltaics panel under the condition of non-uniform solar array on the surface. J. Sci. Technol. **56**(6), (2020)
8. Sacli, M., Ayan, O., Silsupur, M., Empre turkay, B.: Investigation of power quality analysis of single-phase inverter topologies for solar energy systems. In: International Conference on Condition Monitoring, Diagnosis and Maintenance. Bucharest, Romania (2017)
9. Pachauri, R., Mahela, O.P., Sharma, A., Bai, J., Chauhan, Y.K., Khan, B., Alhelou, H.H.: Impact of partial shading on various PV array configurations and different modeling approaches: a comprehensive review. IEEE Access **8**, 181375–181403 (2020)
10. Bui, H.V., Truong, V.A., Quach, T.H.: Optimizing the maximum power generation point of PV cells under shading conditions. J. Sci. Technol. Dev. **3**(1), 326–338 (2020)
11. Luong, X.T., Bui, V.H., Do, D.T., Quach, T.H., Truong, V.A.: An improvement of maximum power point tracking algorithm based on particle swarm optimization method for photovoltaic system. In: 5th International Conference on Green Technology and Sustainable Development, HCM City, Vietnam, pp. 53–58 (2020). https://doi.org/10.1109/GTSD50082.2020.9303110
12. Mohammad, A.N.M., Radzi, M.A.M., Azis, N., Shafie, S., Zainuri, M.A.A.M.: An enhanced adaptive perturb and observe technique for efficient maximum power point tracking under partial shading conditions. Power Electron. Appl. Power Energy Syst., Sci. **10**(11), 3912 (2020)
13. Baba, A.O., Liu, G., Chen, X.: Classification and evaluation review of maximum power point tracking methods. Sustain. Futur. **2**, (2020)
14. Kadri, R., Andrei, H., Gaubert, J.-P., Ivanovici, T., Champenois, G., Andrei, P.: Modelling of the photovoltaic cell circuit parameters for optimum connection model and real-time emulator with partial shadow conditions. Energy **42**, 57–67 (2012)
15. John, R., Sheik Mohammed, S., Zachariah, R.: Variable step size Perturb and observe MPPT algorithm for standalone solar photovoltaic system. In: IEEE International Conference on Intelligent Techniques in Control, Srivilliputhur, India (2017)
16. Shang, L., Guo, H., Zhu, W.: An improved MPPT control strategy based on incremental conductance algorithm. Prot. Control Mod. Power Syst. **5**, 14 (2020)
17. Debnath, D., et al.: Improved grey wolf assists MPPT approach for solar photovoltaic system under partially shaded and gradually atmospheric changing condition. Int. Energy J. **20**, 87–100 (2020)
18. Xu, L., Cheng, R., Yang, J.: A new MPPT technique for fast and efficient tracking under fast varying solar irradiation and load resistance. Int. J. Photoenergy **2020**, (2020)
19. Li., N., et al.: Maximum power point tracking control based on modified ABC algorithm for shaded PV system. In: AEIT International Conference of Electrical and Electronic Technologies for Automotive, 2–4 July 2019, Turin, Italy (2019)